VIBRATION OF BANDSAWS

A THESIS

SUBMITTED IN PARTIAL FULFILMENT

OF THE REQUIREMENTS FOR THE DEGREE

OF

DOCTOR OF PHILOSOPHY IN MECHANICAL ENGINEERING

IN THE

UNIVERSITY OF CANTERBURY

by

Lan Lengoc

University of Canterbury

1990

Mến tặng Thu Hồng

Abstract

The aim of this thesis was to investigate the vibrational characteristics of wide band bandsaws.

Firstly, the vibration of bandsaw structures was considered.

A computer program was developed to predict the natural frequencies and mode shapes of three dimensional structures, consisting of beams, springs, viscous dampers, concentrated masses, and gyroscopic rotors. The method used was the *dynamic stiffness method.*

Some of the vibrational characteristics of the bandsaw structure were then established from experimental results and results obtained from the computer program. The gyroscopic effects on the bandsaw structure due to rotating pulleys were also examined.

Secondly, the dynamic stiffness method was used to solve the moving beam problem. The moving beam had been used previously to model the bandsaw blade. The dynamic stiffness method allowed complex problems to be analysed in a systematic manner.

A moving beam proved to be too crude a representation of a wide bandsaw blade at the level of detail being investigated. Therefore, attempts were made to model the dynamic behaviour of wide bandsaw blades with moving plates.

A general approach to the solution of the moving plate problem is presented in

this thesis, it uses the *extended Galerkin method* to discretise the partial differential equation of motion and the boundary conditions into a quadratic eigenvalue problem. The solutions for this problem were obtained by using a *linearisation* technique.

The effects of in-plane stresses on bandsaw blades are considered in this thesis. Three cases are examined; a linearly distributed stress across the width of the blade due to wheel-tilting and/or backcrowning, a parabolic distributed stress across the width of the blade due to prestressing, and stresses induced by tangential cutting forces.

Parametric instabilities due to fluctuating tension, and due to periodic tangential cutting forces were investigated. The *harmonic balance method* was used on the discretised form of the moving plate equation to obtain the required instability regions.

Finally, the dynamic instability of a moving plate due to a nonconservative component of the tangential cutting force was considered. The method of solving this nonconservative problem was the same as that used to solve the conservative case.

Contents

List of Tables

List of Figures

Chapter 1

INTRODUCTION

The main objectives of the saw milling industry are :

- To produce a straight, smooth cut at maximum speed and with a minimum loss of raw material, for a wide range of timber types and depths of cut.
- To spend as little as possible on the maintenance and down time costs of the machinery used.

The bandsaw has become a very important machine in the sawing process because :

- It has the thinnest blade among all the wood cutting machines, therefore minimizes the wastage of material.
- It operates at a very high cutting speed, allowing higher production rates than other types of saws.
- It is capable of handling a large range of log sizes.
- It usually operates at lower noise levels than other types of saws, such as the circular saw.

Transverse vibration of the bandsaw blade is a by-product from the interactions of the blade with the machine structure and the timber being cut. It increases the amount of saw dust produced, decreases the accuracy of the cut, decreases the production rate and decreases the life of the blade. In the last 25 years, engineers and foresters have been trying to reduce the vibration of the blade from experimental and theoretical studies. A vast knowledge on the behaviour of the moving bandsaw blade has been gained, however, many mysteries still remain in this area of research which have to be solved in order for the technology to advance in the future.

There have been complaints recently in New Zealand that the bandsaw structures inhere considerable vibrations, which cause annoyance to workers and increase the risk of machine failures. These complaints have initiated this project which proposed to look into the structural vibration of the bandsaw. A literature search showed that there has never been any consideration on the vibration of bandsaw structure, all previous reseach has been directed toward the cutting span of the saw blade.

The behaviour of the saw blade during sawing is another area of great interest, which needs a lot more attention in the future. This project, therefore, attempts to investigate the cause of instability of the blade during sawing. This area of research will become necessary in the development of automatic control of the timber cutting process.

1.1 Historical Background

The work to be presented in this thesis requires the materials in three different fields:

- Structural vibrations
- Dynamics of bandsaw blades
- Dynamics of plates

1.1.1 Structural Vibrations

Theoretical analysis of structural vibrations has been well documented in many vibration text books and taught in undergraduate vibration courses, however, there seems to be a lack of unification in the methods of solution. The advances in computer technology also have affected many of these methods, offering better methods of analysis, allowing more complex problems to be solved, and making some methods obsolete.

Bishop and Johnson (1956) [10] and McCallion (1973) [48] presented comprehensive backgrounds on the theory of beam vibrations. The method of analysis used in this thesis, the dynamic stiffness method, was developed by Kron (1939,1963) [40,41] and was reinterpreted into a more easily understood form by McCallion (1973) [48]. Other publications involving the use of the dynamic stiffness method include Rieger and McCallion (1965) [65,66], Henshell et.al. (1965)[29], Palmers and McCallion (1973) [61], Williams and Wittrick (1970) [92], Howson (1979) [33].

The mathematical algorithms to perform various numerical operations, such as calculating determinants of matrices, finding roots of equations etc. , are well presented in many numerical methods text book, notable is the *Numerical Recipes* (1986) [63]. Other cited references, relating to numerical methods, are [51,74].

The theory on the gyroscopic effects of rotors refers to the publications by Ware (1978) [90], McCallion (1973) [48] and Downham (1957) [21,22].

The experimental analysis of structural vibrations has been the subject of many researches in recent years because of the advances in electronics and computer technologies. A most up to date text book on this topic is the book written by Ewins (1984) [23] who is one of the leading experts in the field of modal analysis. Other references relating to this area of research, which had been cited for this thesis, were [28,69,30,31,18,70].

1.1.2 Dynamics of Bandsaw Blades

Most of the research on bandsaws was carried out in the last two decades. Ulsoy and Mote (1978) [85] published a comprehensive literature review which listed 115 publications in relation to the bandsaw problems. D'Angelo et.al. (1985) [16] provided a more recent list of research being carried out on circular and band saw vibration and stability.

This literature review will categorise some of the more relevant research, instead of attempting to list all the research relating to band saw problems.

The literature on bandsaws can be classified into 9 topics:

- General information on bandsaws.
- Experimental studies in the free vibration of saw blades.
- Experimental studies of the blade during sawing.
- Stresses in bandsaw blades
- Theoretical studies on the free vibration of moving materials.
- Theoretical studies on the stability and vibration of moving materials due to external and parametric excitations.
- Studies on the coupling between cutting span and non-cutting span of the saw blade.
- Nonlinearities in moving material.
- Saw guides

General information

The most informative text book on the subject of bandsaws is the book by Simmonds (1980) [71], which includes up to date technology in the *art of saw doctoring.* Other books, discussing the use of bandsaws, include [93,91]. The manufacturers also have a large amount of information on the design and operation of bandsaws.

This information is the prerequisite in any study on bandsaw. It forms a direct link between researchers and the industry.

Experimental Studies - Free vibration

There are many publications in this topic, but the most noteworthy works were by Kirbach and Bonac (1978) [37,38], and by Tanaka et.al. (1981) [80]. These publications provided the natural frequencies of bandsaw blades with various dimensions, velocities, and stresses.

Experimental Studies - During Sawing

The subject of bandsaw vibrations during sawing is slightly touched on in recent years, perhaps because it is rather costly and difficult to investigate the behaviour of the saw blade during sawing. There have not been any conclusive results in this area of research. Das (1982) [17] demonstrated the existence of instability during sawing, unfortunately, not enough information was given in the paper to draw any conclusion. Tanaka et.al. (1983) [81] also investigated the saw blade vibration during sawing, the results presented however, seemed to lack practical intuition, for example, one of the conclusions was that the timber being cut clamps the blade hence acts as a boundary support for the top part of the blade.

Stresses in bandsaw blades

This is a very important topic in the design of a saw blade. In-plane stresses dominate the stiffness of the blade and their effects on the vibration and stability of the blade are considerable. Pahlitzsch and Puttkammer (1972) [60] discussed the stresses occurred on the blade. A more comprehensive work on the same topic was presented by Allen (1985) [3], which suggested that by applying higher strain on the blade, the stability under cutting conditions was improved. The problem is that too much strain will cause failure of the blade, however, investigations of these stresses have only used basic theories of strength of materials or have been based on experimental measurements. A more comprehensive study is yet to be carried out so that a maximum strain can be put on the blade with confidence. Foschi (1975) [25] who investigated the technique of measuring residual stresses in bandsaw blades, concluded that the present method, the light gap technique, was not reliable, but did not suggest any alternatives.

Theoretical Studies - Free Vibration of Moving Materials

This topic provides the foundation for all the theoretical works on vibration and stability of the moving bandsaw blade.

The first investigation was dated back to 1897 when Skutch [73] studied the transverse vibration of an axially moving string. It was not until 1965 when the first study of the bandsaw blade was carried out by Mote [52,53], which considered the transverse vibration of a moving beam, using the exact method. Later, Anderson (1974) [6] looked at the same problem using a finite element method which allowed moving beams with more complex boundary conditions to be solved. Alspaugh (1967) [5] considered the torsional vibration, and in 1968, Soler [75] looked at the coupling between transverse and torsional vibration. Ulsoy and Mote (1980,1982)

[86,87] produced excellent works on the vibration of moving plates to represent wide saw blades.

Theoretical Studies - Parametric and Direct Excitations

An understanding of the behaviour of a moving saw blade under excitations is important in the design of the blade. Naguleswaran and Williams (1968) [58] investigated the stability of moving beam under fluctuating tension. This tension fluctuation is caused by pulley eccentricities, irregularities on the surface of pulleys and the surface of blade. Ariaratnam and Asokanthan (1988) extended the study to torsional vibration using the method of averaging. Soler (1968) [75] looked at a point load, perpendicular to the longitudinal direction of the blade, to approximate the cutting condition. Mote (1968) studied the divergence buckling of an edge loaded beam [55], the parametric instability of beams under fluctuating tension (similar to [58]), and the parametric instability of beams under periodic edge force. In 1986, Wu and Mote went back to this periodic edge loading on beams but also considered the coupling between transverse and torsional vibrations.

There has been no study in the area of parametric stability using a moving plate model to represent the wide saw blade. Ulsoy and Mote (1980) [86] briefly mentioned the effects of edge loadings on a moving plate but concluded that the magnitudes of these forces were small compared with other effects, such as tension on the blade.

Coupling between Cutting and Non-cutting Spans

This is a new area of research with the first experimental observations of the coupling in 1984 by Wu and Mote [94]. A full theoretical investigation of the coupling, using transverse vibration of moving beam, was carried out by Wang and Mote (1986) [88]. In 1987, Wang and Mote [89] looked at the vibration of the same coupling

system under impulsive excitation.

Nonlinear Vibration of Axially Moving Materials

Mote (1966) [54] discussed the nonlinear vibration of an axially moving string due to a large amplitude of vibration at high axial velocity and low tension. Thurman and Mote (1969, 1971) extended this to a moving beam, and showed that nonlinearities result in the coupling between transverse and longitudinal vibrations. Kim and Tabarrok (1972) [36] again investigated the nonlinear vibration of travelling strings, using a different approach based on the theory of fluid mechanics.

The above publications stated that this area of research was very significant. However, it has been ignored by recent research, perhaps because of its complexity, or perhaps because of its impracticability in the bandsaw blade case.

Saw Guides

This area of research was not considered in this thesis, but is mentioned here for the sake of completeness.

The effects of saw guides on the vibration of bandsaw blade are well observed in practice, however there is a lack of theoretical background on the guides. Only recently, Tan and Mote (1988) [79] treated the guides as hydrostatic bearings and investigated their effects on the vibration of saw blades.

1.1.3 Dynamics of Plates

The theory on plate stability and vibration are required in this thesis to model the wide bandsaw blade. A thorough understanding of the plate theory is necessary to develop a sound method of analysis for the moving plate.

The basis of plate theory is in many vibration text books [48, page 125], and

there are text books devoted entirely to plate theory [76,35]. Leissa (1969,1973) [45,46] provided an extensive study of the vibration of a rectangular plate under all combinations of boundary conditions, using the exact method where possible and the Ritz method for the remaining cases. Young (1950) [97] had already considered the rectangular plate problems using the Ritz method.

By using approximate methods, such as the Ritz method or the Galerkin method, shape functions which describe the deflections of the plate are required. The conventional shape functions are the separable beam functions for each direction [76, page 228]. Bassily and Dickinson (1975) [8] suggested the use of degenerated beam functions for plates involving free edges. More recently (1985,1986), orthogonal polynomials had been suggested as a better alternative for choosing shape functions for plates [9,19].

Zienkiewicz and Morgan (1983) [99] provided a powerful reference on the methods of approximation which has been used to solve the plate problems presented in this thesis.

Two types of dynamic stabilities had been considered in this study; parametric and nonconservative.

Takahashi and Konishi (1988) [78,72] considered the stability of a rectangular plate subjected to parametric excitation. References to the method of analysis, the harmonic balance method, are in [12,59,50,77,24,62].

The stability of rectangular plates subjected to nonconservative loadings has been studied by Leipholz (1982,1983) [43,44] using Galerkin method. The foundation for this area of research is the text book written in Russian by Bolotin (1961) and translated to English in 1963 [11]. Other related publications include [1,32].

1.2 Scope of the Project

The first part of the project was to study, experimentally and theoretically, the vibrational characteristics of the bandsaw structure. This work was aimed primarily at developing a technical knowledge in the field of vibrations, and secondly at viewing the practical aspects of the problem. The results found in this work could be used to reduce the vibration of the bandsaw structure or to see if they could affect the performance of the saw blade. An important effect to be investigated was the gyroscopic effect of the rotating pulleys.

A more powerful method of solution for the moving beam case has been developed in Chapter 6. Although there have been acceptable methods for this problem, the new method of analysis is believed to be simpler and can provide much more informative solutions than previous methods. Interactions between the blade and the structure can be investigated by this method.

Another method of analysing the moving plate problem was developed in Chapter 7, which can be extended from the usual vibration case to the more complicated stability problems. This method has been used to calculate the natural frequencies of bandsaw blades with various in-plane stresses.

Parametric excitations on a moving plate have been studied in this project, which are closely related to the moving beam case, but would offer much more accuracy and flexibility in the study of wide bandsaw blades.

A study of stability of a moving plate under nonconservative cutting forces is presented, for the first time, in this thesis. The results are very encouraging and an experimental study would be necessary in the future to back up these results.

Chapter 2

THE DESIGN OF A TYPICAL BANDSAW

2.1 General Assembly

There are many types and sizes of bandsaws used in the sawmilling industry today. The most common type is the vertical log bandsaw (Figure 1,2), and therefore, the structural vibration study will consider primarily this type of bandsaw. The blade behaviour would be the same whether the bandsaw was of the vertical or horizontal type.

The classification of a bandsaw is by the diameter of the saw pulleys – typical sizes are 48 in., 54 in., 60 in.. The bandsaw, selected for the experimental study, was a 60 in. bandsaw, manufactured by the Southern Cross Engineering Company and installed at the Waimakariri Sawmill (referred to as the Waimak bandsaw).

The main structures of the vertical bandsaw are best subdivided into three sections:

- Section below the base.

- Section above the base.
- The straining device.

The saw blade is an independent component of the bandsaw hence it is treated separately.

From now on, the front of the bandsaw refers to the cutting side of the saw as shown in Figure 1.

2.2 Section Below the Base

The base itself is usually bolted down to the foundation for maximum rigidity. A pit is, therefore, required for the portion of the bandsaw below the base. However, there are installations which raise the base above ground level. These bandsaws may have large vibrations at low natural frequencies, due to weak supports.

Figure 3 shows the back view of the bandsaw looking into the pit.

The section of the bandsaw below the base consists of

Bottom Pulley It is usually made of cast iron. The bottom pulley, being the driving pulley, is stronger (bigger spokes) and therefore heavier than the top pulley. The pulley of the Waimak bandsaw has a diameter of 60 in. (1.5 m), weighs about 550 kg. It has eight spokes, each about 0.1 m in diameter.

Shaft The bottom shaft is 1.6 m long and 0.1 m in diameter. The pulley is mounted close to one end of the shaft as in Figure 2. This asymmetrical mounting may produce some interesting phenomena.

Bearings Two '22222 K.H.L. H322 4in.' spherical-roller bearings are used to support the bottom shaft. The housing for each bearing is bolted to a bracket by

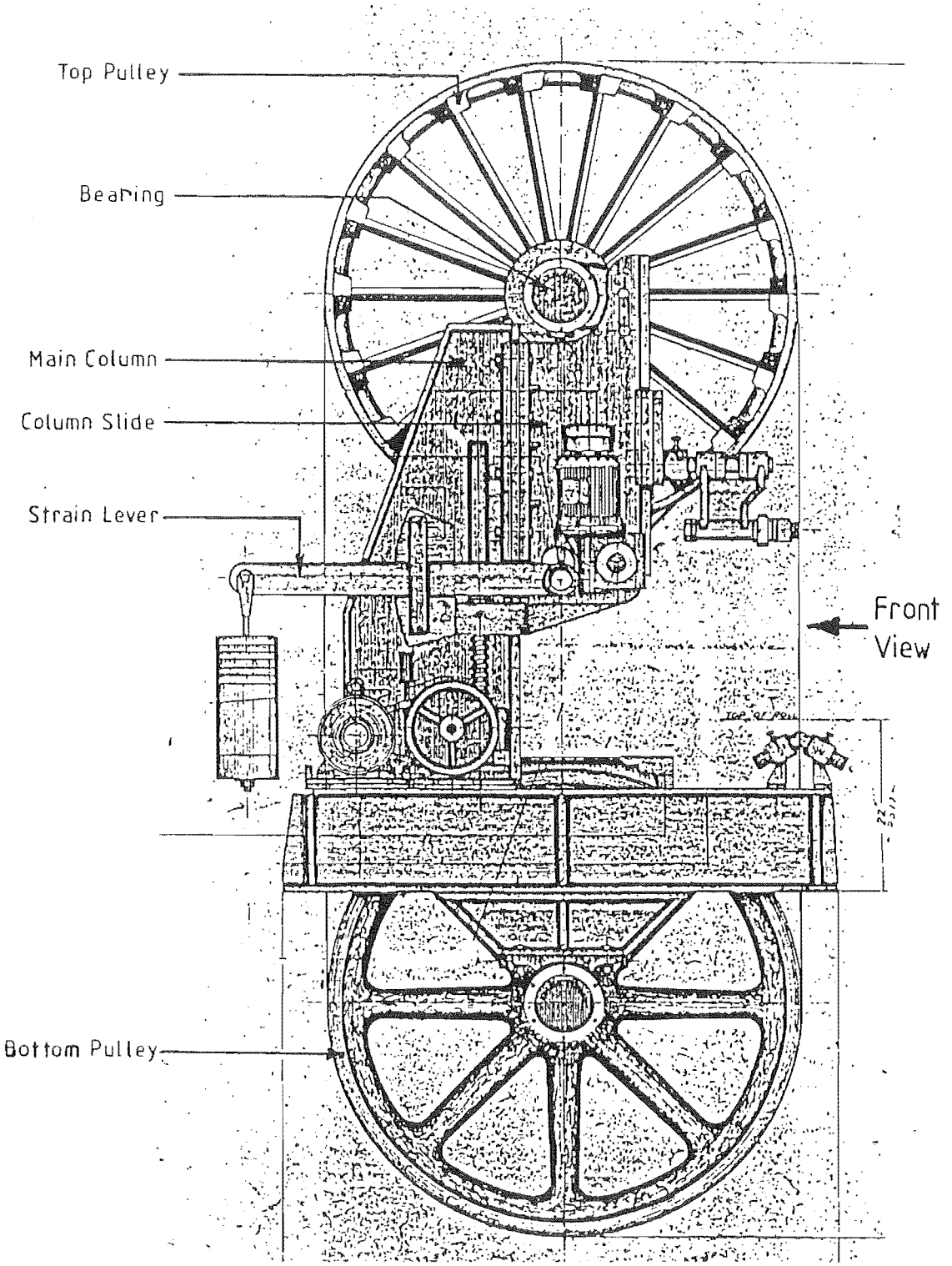

Figure 1: General assembly of a 60 in. band head rig. Right side view.

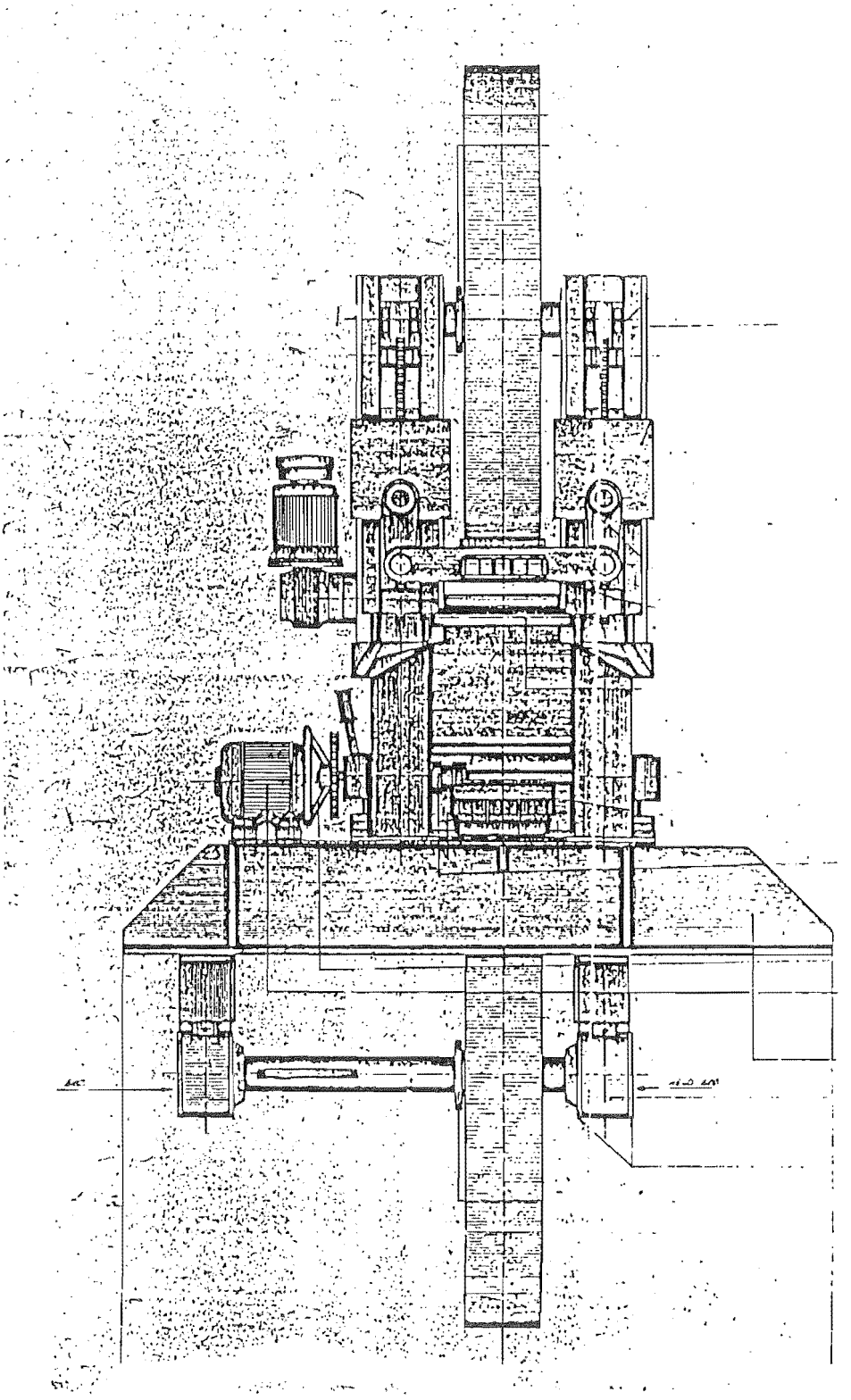

Figure 2: General assembly of a 60 in. band head rig. Front view.

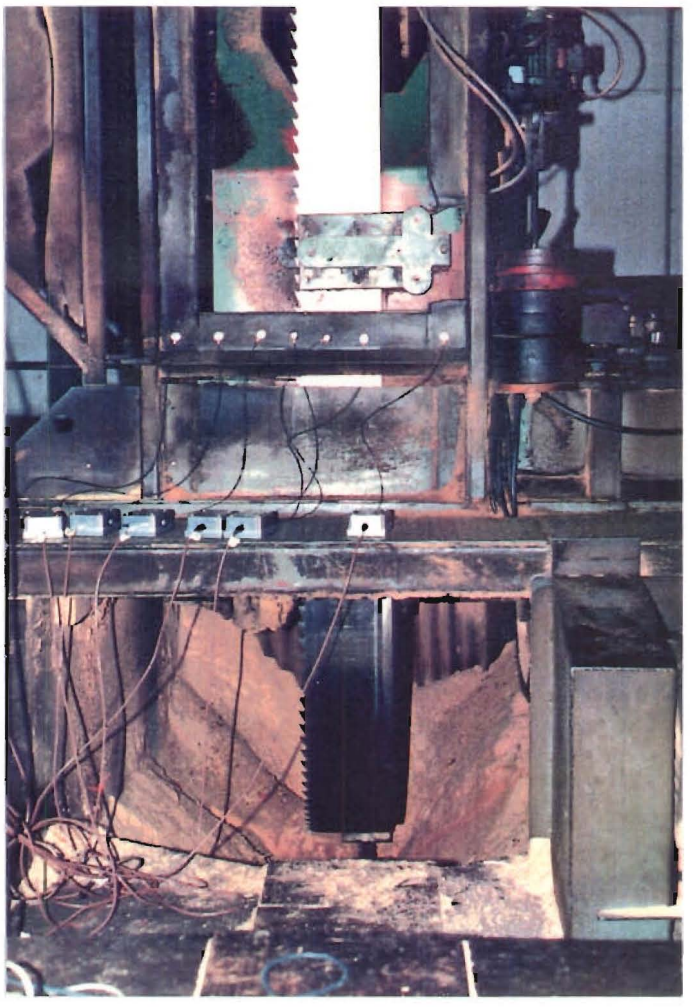

Figure 3: Back view of the Waimak bandsaw.

four 20 mm bolts. The bracket is fabricated from 20mm plate and is welded to the base.

Motor and Transmission The bandsaw is driven by an electric motor, and the transmission of power to the bottom pulley is by V-belts.

2.3 Section Above the Base

Figure 4 and Figure 5 show the left and the right views of the Waimak bandsaw respectively.

These figures show that the structure of the top section of the bandsaw is quite complicated. It is, therefore, expected that the theoretical calculations based on beam theory will not provide accurate values for the natural frequencies of the bandsaw. The beam model would still be important in understanding the general vibrational characteristics, and in explaining the experimental results.

The main components of the bandsaw are:

Main Column It is extended vertically from the base, and fabricated from mild steel plate. It provides the skeleton for the bandsaw.

Column Slides There are two column slides which are guided vertically by the main column. They can be driven up and down by two jack assemblies. Figure 6 shows a side view of the column slide. At the front of the column slide is another slider where the top saw guide is attached. The bearing housing is pinned to the top of the column slide.

Top Pulley The top pulley is mounted on the column slides so that it can be moved to tension the saw blade.

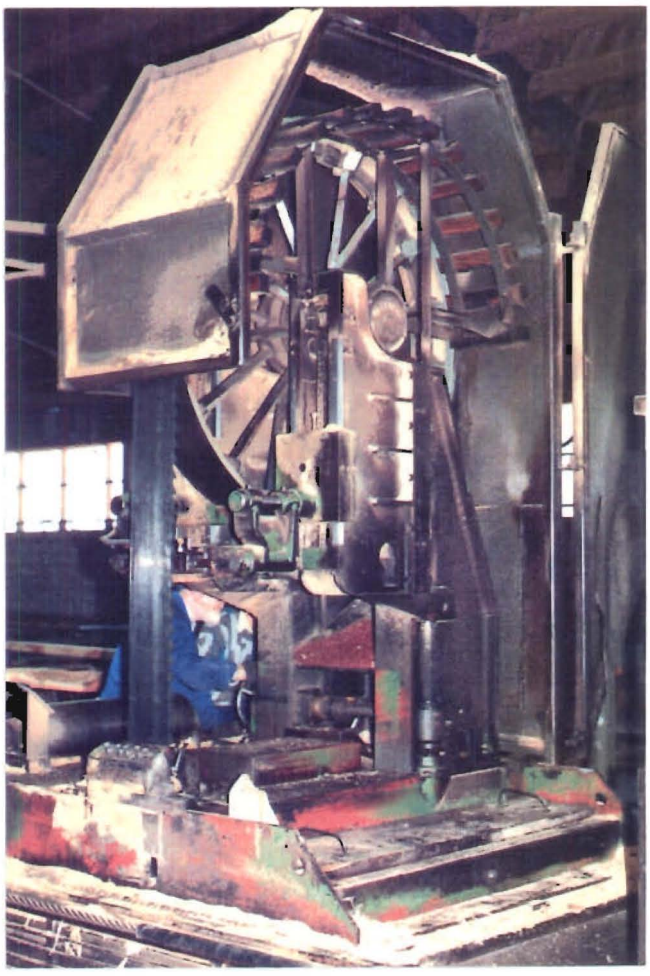

Figure 4: Left view of the Waimak bandsaw.

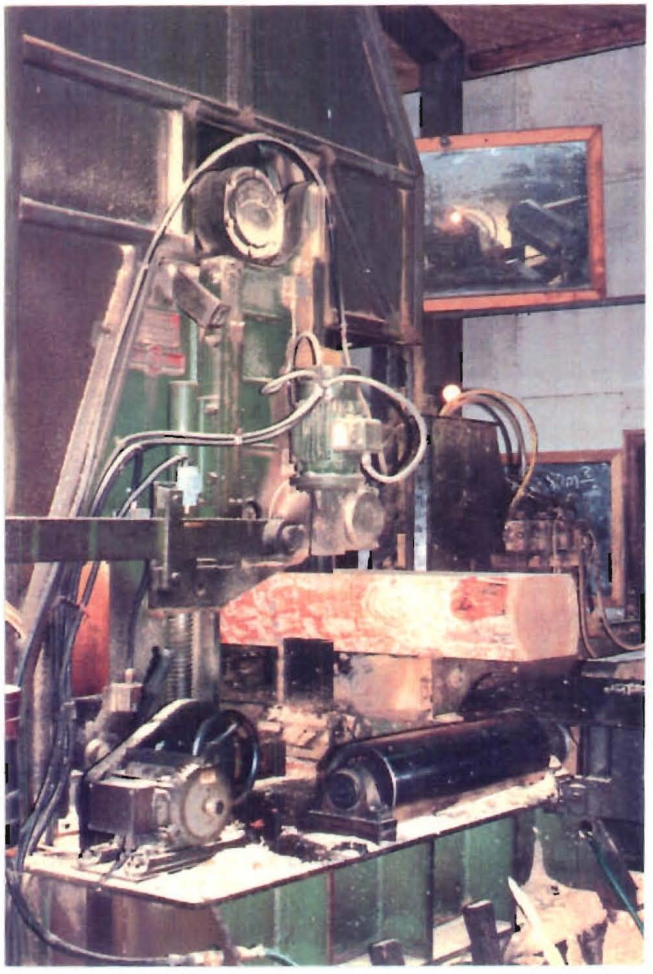

Figure 5: Right view of the Waimak bandsaw.

Bearings The bearings used to support the top pulley are identical to those for the bottom pulley. The column slides are locked in position after tensioning the saw blade. To prevent the tension on the blade changing excessively during starting-up or while cutting, there is a dead load straining mechanism. The bearing housings are pinned to the column slides so that they can be rotated relative to the fixed column slides.

Saw Guides Saw guides are used to reduce the vibration of the saw blade and hence increase the blade's stability. There are several types of saw guides but the most common type used in wide-band bandsaws is the pressure guide. The lower guide is fixed in place so that it supports the blade immediately below the work piece, see Figure 7 . Dense woods or synthetic materials are used for the packings. A 0.005 in. clearance between the packings and the saw blade is recommended. The upper guide, Figure 8, can be moved up and down to adjust for a range of depths of cuts. The pressure guide is pressed against one side of the blade. It was found that vibrations on the non-cutting span can be transmitted to the cutting span, and a damper is usually fitted to reduce the vibrations of the non-cutting span, Figure 9. The damper is also used as a cleaning device for the saw blade.

2.4 Straining Device

The most common straining device is the counterweight and lever mechanism. Figure 10 shows the components of the straining mechanism. The counterweight mechanism is analogous to the spring-mass system, where the blade behaves as an elastic spring and the counterweight is the mass.

In modern bandsaws, air strain devices are used because they have faster response

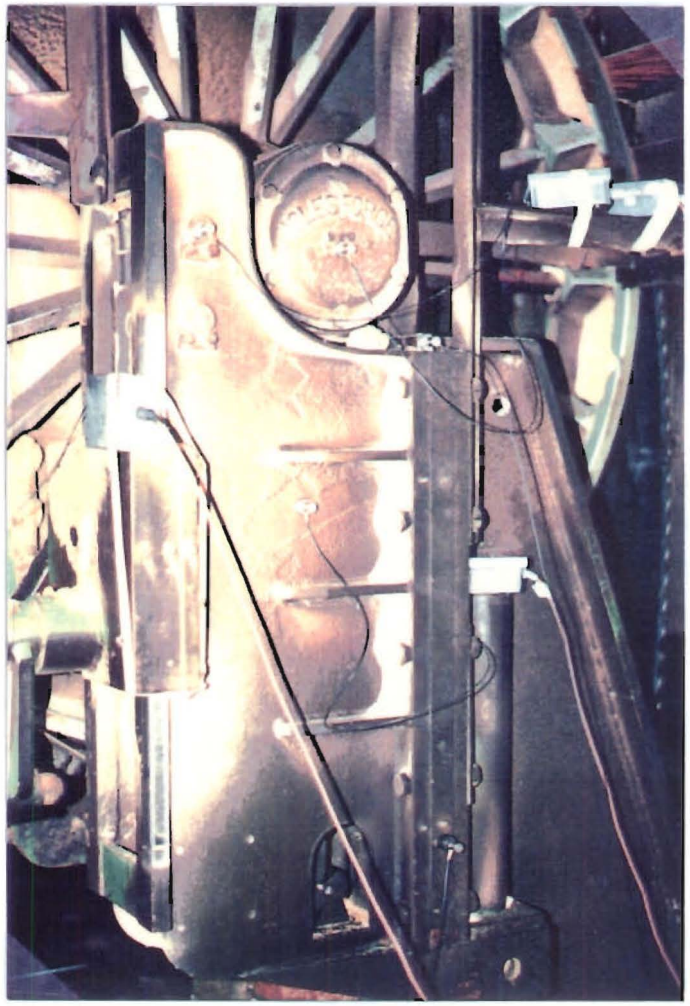

Figure 6: Column slide.

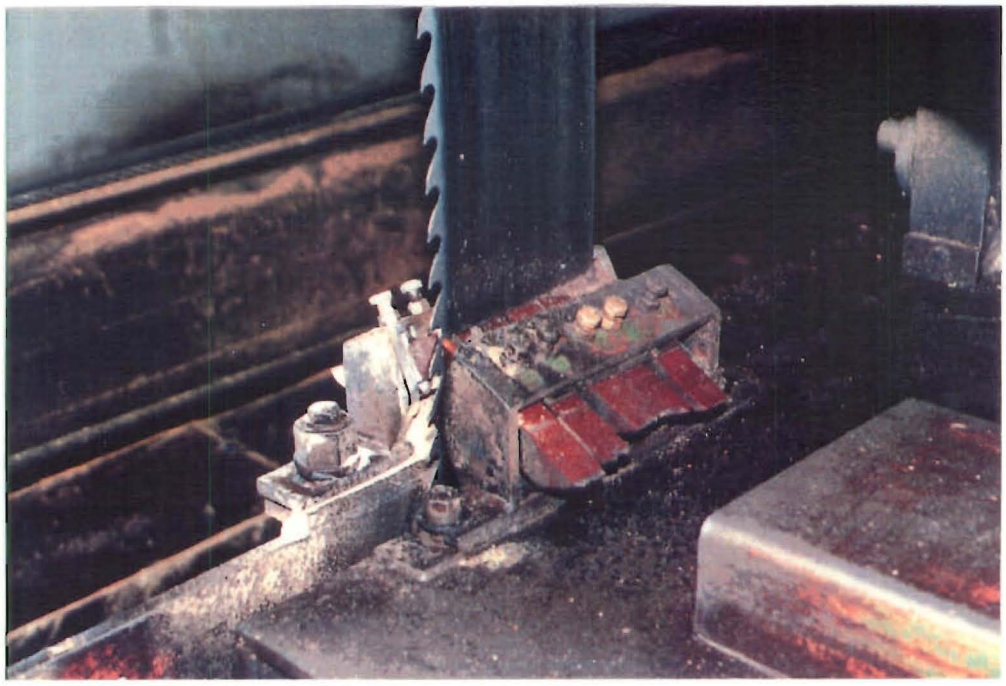

Figure 7: Lower saw guide.

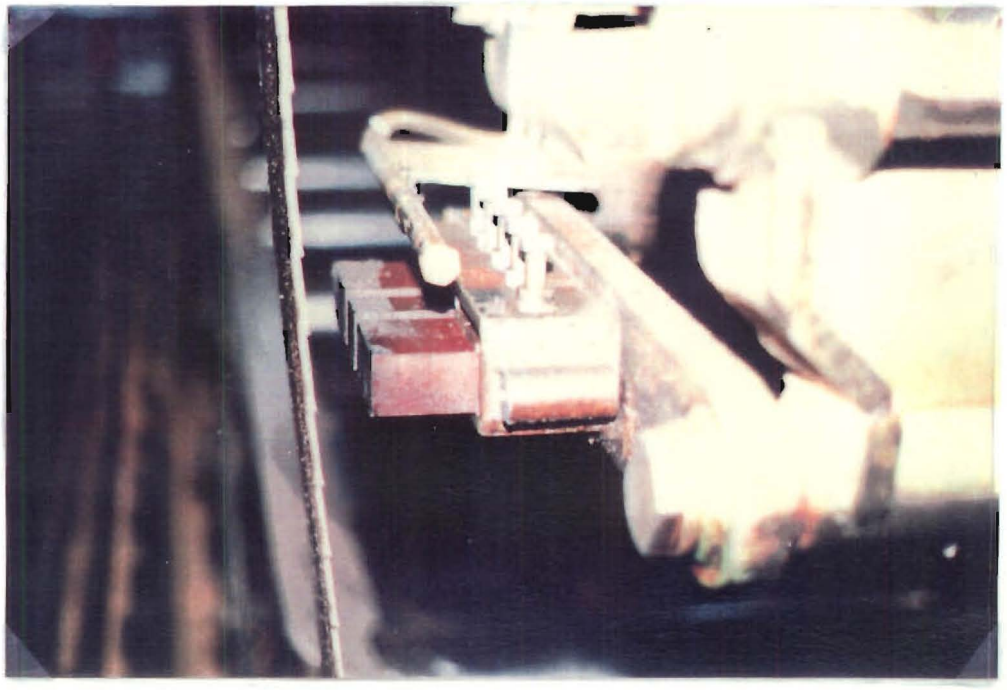

Figure 8: Upper saw guide.

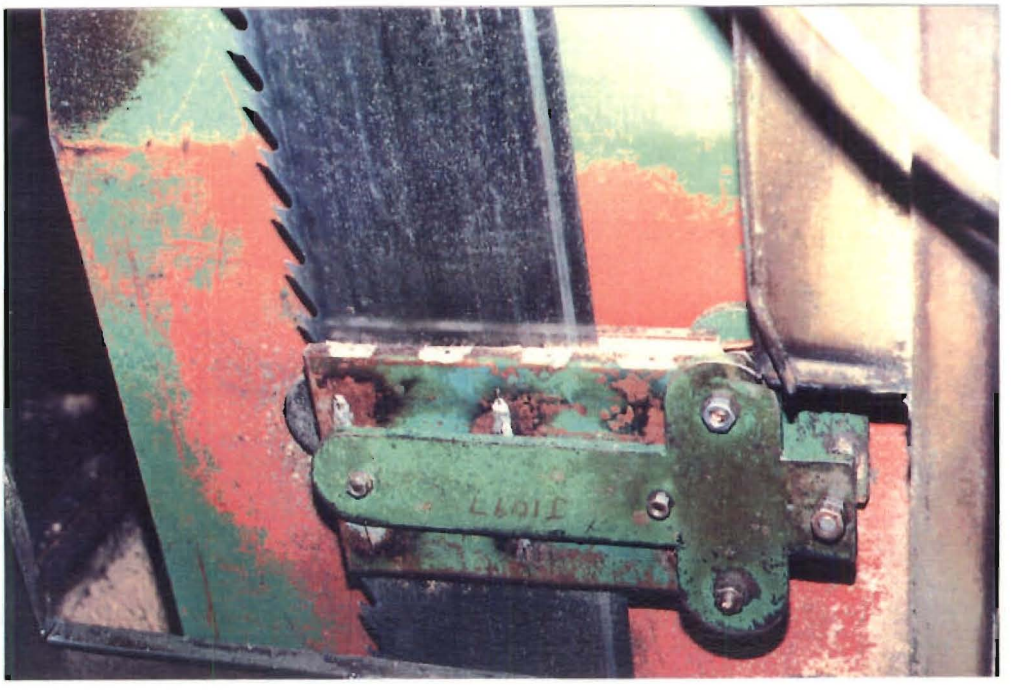

Figure 9: Non-cutting span damper.

times than the dead weight mechanism. However, there are still many bandsaws in operation today using the simple counterweight and lever device.

2.5 Saw Blade

From the definition given in [71], a wide bandsaw blade is any blade which has at least 76 mm in width. For the Waimak bandsaw, a 240 mm wide blade is used. This size of saw blade is also used in the experiments of Kirbach and Bonac [37,38]. The total length of the blade is about 9.75 m (32 ft), and the thickness is approximately 1.6 mm.

There are two types of tooth setting for saw blades; spring set and swage set. Spring set is when the teeth are bent alternatively on either sides of the blade, and swage set is when the tip of the tooth is made wider than the thickness of the blade to provide clearance for the cut (Figure 12).

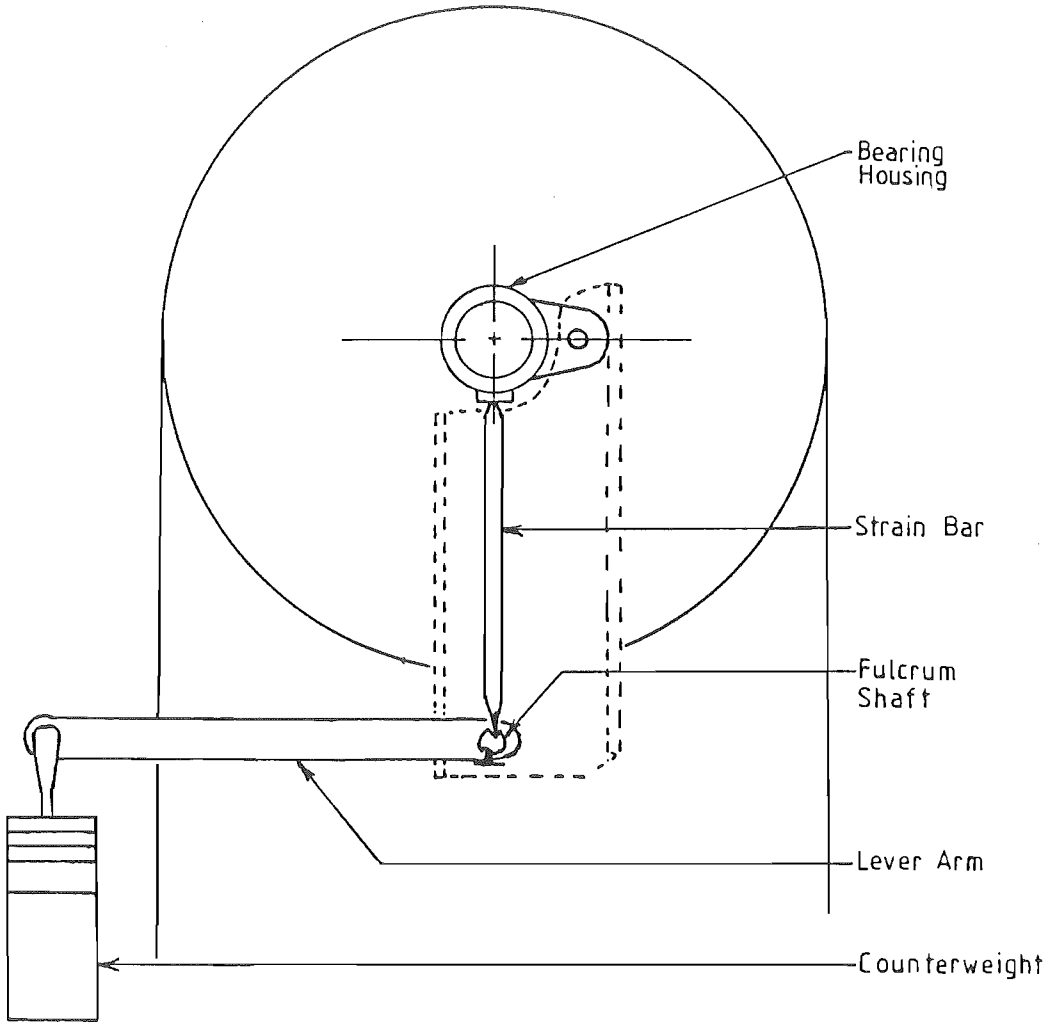

Figure 10: Counterweight straining mechanism.

Figure 11: End view of rocker shaft.

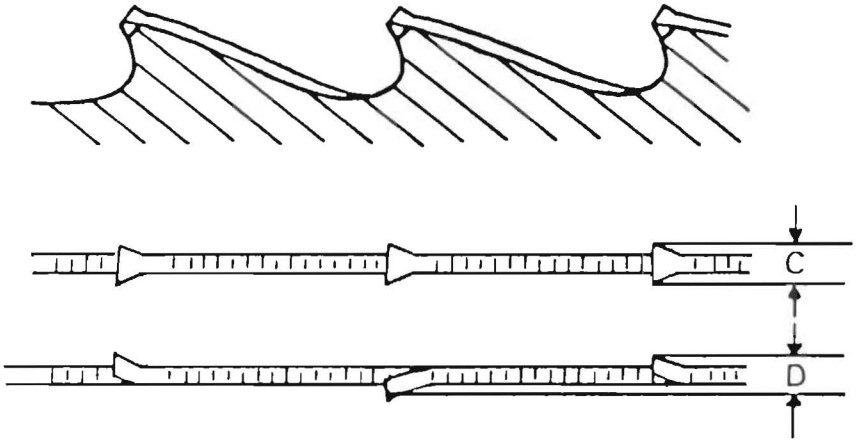

Figure 12: Spring and swage set.

Swage setting is now accepted as being the better method of the two and spring setting method is, therefore, becoming obsolete.

Dimensions and profile of the teeth on the blade used on the Waimak bandsaw are given in Figure 13.

The book, by Simmonds [71], provides full details of the manufacture and preparation of wide bandsaw blades. The two techniques, widely used in the preparation of saw blades to improve its performance, are the prestressing and the back crowning. Both alter the stress states of the blade and hence modify its dynamic characteristics. This thesis will consider theoretically the effects of both prestressing and back crowning, by using plate theory, because they cannot be predicted by beam analysis.

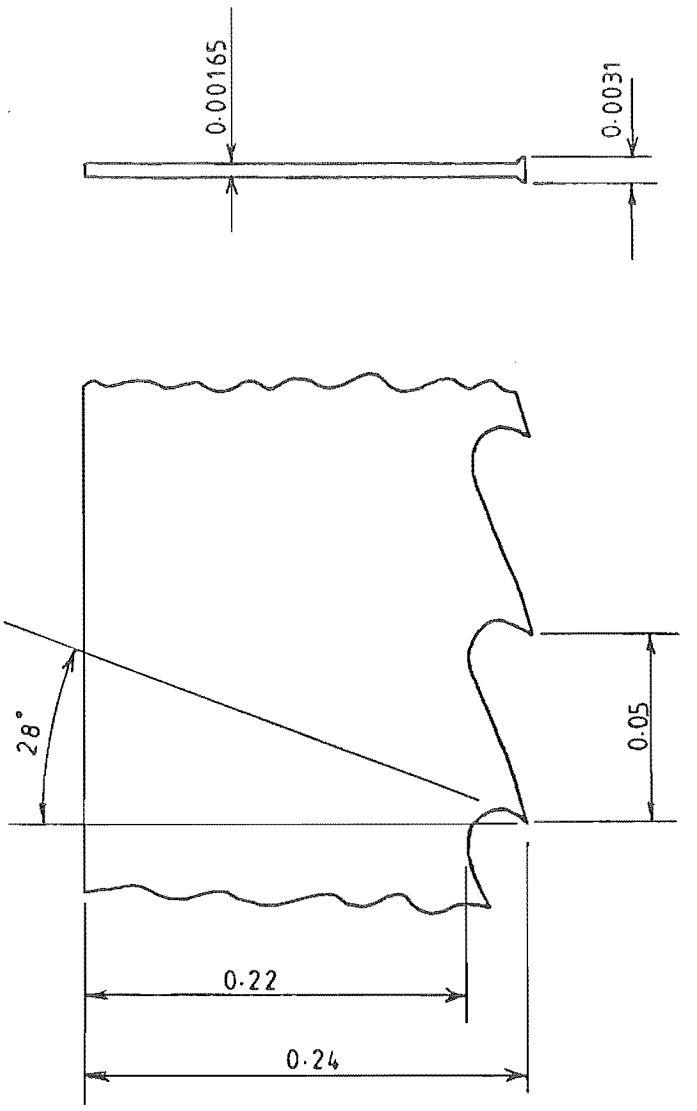

Figure 13: Dimensions of teeth.

Chapter 3

EXPERIMENTAL METHOD IN STRUCTURAL VIBRATIONS

3.1 Introduction

The two major objectives of vibration measurement, as stated by Ewins [23], are

- To determine the nature and extent of vibration response levels.
- To verify theoretical models and predictions.

These two objectives indicate the two types of test used in the experimental analysis. The first objective corresponds to the measurement of vibrations of the machine or structure under study during *operation*, and the second objective requires the measurement of vibrations with *known excitations*.

Both types of test were performed on the Waimak bandsaw. Experiments carried out on a prototype bandsaw in a laboratory would be ideal, unfortunately, such an arrangement was not available. Tests on real operational bandsaws are not as flexible but realistic results can be obtained.

3.2 General Procedure in Experimental Analysis

Vibration measurement of a machine during operation requires no special technique and can be performed with the equipment used in the vibration measurement with known excitations.

The vibrational characteristics of a structure, with known excitations, can be obtained in three stages. First the structure has to be excited, then the vibrations of the structure can be measured and recorded, and finally, the recorded data can be analysed.

3.2.1 Excitation of the Structure

The two types of excitations are continuous excitation such as sinusoidal, random etc. , and transient excitation such as pulse, chirp, impact.

Devices available for exciting the structure can be devided into two categories : contacting and non-contacting.

Contacting exciters remain attached to the structure throughout the test. Some commonly used contacting exciters are mechanical exciters (out-of-balance rotating masses), electromagnetic exciters (moving coil in magnetic field), and electrohydraulic exciters.

Non-contacting exciters include non-contacting electromagnets, and impactors which are only in contact for a short period.

The object of using the exciter is to excite the structure over a range of frequencies so that the frequency response characteristics of the structure can be determined. The best method is the sinusoidal excitation where the exciting frequency can be

controlled over the range of interest. However, the instruments for sinusoidal excitation can be expensive and impractical, especially for a large structure such as the bandsaw. Impact excitation is applicable in the low range of frequencies and no or very little preparation on the structure is needed before using the impactor. Small explosive charges had been successfully used as an impact exciter on structures where access to the structure was not possible during tests, such as aeroplane wings during flight. Other possible impactors are hammers, hanging masses or sudden release of statically deformed structures.

3.2.2 Measurement of the Vibrations and the Excitations

The vibration of the structure can be measured as displacement, velocity or acceleration, of which acceleration is the most popular and the most practical measurement. Acceleration is measured by accelerometers whereas the exciting force can be measured by force transducers. Both of these transducers are piezoelectric transducers which produce voltages for the vibratory motions or the exciting forces.

There are two types of vibration measurement techniques; those in which just one parameter is measured (usually the response), and those in which both input and output response are measured. If only the natural frequencies of the structure are of interest, then measurement of one parameter is sufficient, but if the levels of the vibrations are also important then measurement of two parameters would give much greater accuracy.

The voltage produced is very small and conditioning amplifiers are required to boost the signal up to a measurable amount. Voltage amplifiers and charge amplifiers are the two types of conditioning amplifiers available.

Measured data can be stored using a multi channels FM tape recorder. This data is then post-processed by using an analyser. Modern FFT analysers enable

the signals from the transducers to be processed instantanously and store on floppy disks, however, tape recordings are still useful in keeping a full real-time record of the response.

3.2.3 Analysis

The recorded vibration data needs to be processed into a more practical form. For the one parameter measurement technique, Fourier analysis transforms the data from the time domain to the frequency domain so that any natural frequencies of the structure at the point of measurement can be seen from the spectrum. The other technique, where both the vibratory motions and the excitations are measured, is analysed by obtaining the frequency response function of the structure. The methods available for plotting the frequency response function had been discussed in [23]. Modern analysers have built-in functions to produce plots of frequency response functions from the input and output data.

There are many problems associated with digital spectral analysis. Although modern FFT analysers are designed to take care of most of these problems, knowledge of them is necessary in interpreting the FFT results.

Alias is a problem caused by discrete sampling of the signal (Figure 14), where the FFT result does not represent the actual signal. To overcome this problem the sampling frequency must be more than two times the maximum frequency of interest; anti-alias filters are also required to screen out frequencies higher than the sampling frequency.

Leakage is a problem caused by the recording of the signal over a finite interval. Transient signals do not have leakaging problems, but periodic signals do. This problem is caused by an assumption in the FFT algorithm that the finite-time-record is repeated throughout time. This assumption can sometimes produce a distorted

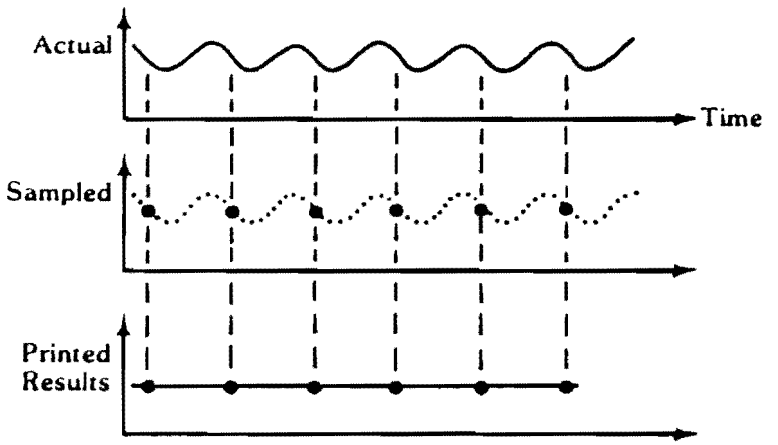

Figure 14: Aliasing effect in discrete sampling of signal.

waveform as illustrate in Figure 15. The effect of leakage in the frequency domain is to smear the energy throughout the frequency domain (Figure 16). Most of the problem seems to be at the edges of the time record, a method used to reduce the leakage is to multiply the record by a function which would reduce the magnitude of the record near the edges (Figure 16). This method is called windowing, and there are various types of windows for different purposes. Note that the windowing technique alters the actual signal, hence it is not expected to produce perfect results.

3.3 Instrumentation

3.3.1 Methods of Excitation

Due to having only limited time access to the bandsaw, contacting excitors were not practical. However, as only the low range of frequencies was of interest, non-contacting excitors proved to be a better choice. Amongst the non-contacting excitors, the impact hammer was chosen.

A 3kg sledge hammer was used to excite the bandsaw structure. A rubber block

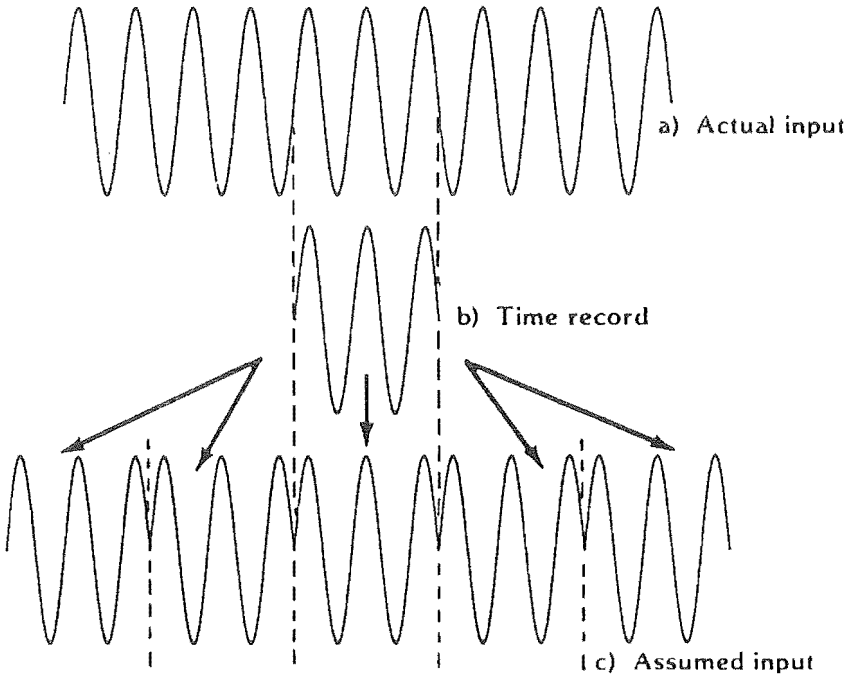

Figure 15: Actual signal and FFT assumed signal.

was glued to the hammer head to prevent damage to the bandsaw when impacting the structure. Because a force transducer was not available, an accelerometer was used instead, and the hammer was calibrated so that the readings from the accelerometer gave the amount of force applied.

Figure 17 shows a typical impulsive force pulse, it was approximately a half-sine wave. Fourier transformation of this pulse gave the frequency spectrum which was essentially flat up to a certain frequency, f_c. This f_c is the upper frequency range of the hammer. The sledge hammer used in this experiment was effective up to 350 Hz.

3.3.2 Vibration Measurement Techniques

Ten accelerometers were available for this experiment. Two Bruel & Kjael conditioning amplifiers and eight home-made charge amplifiers were used with these

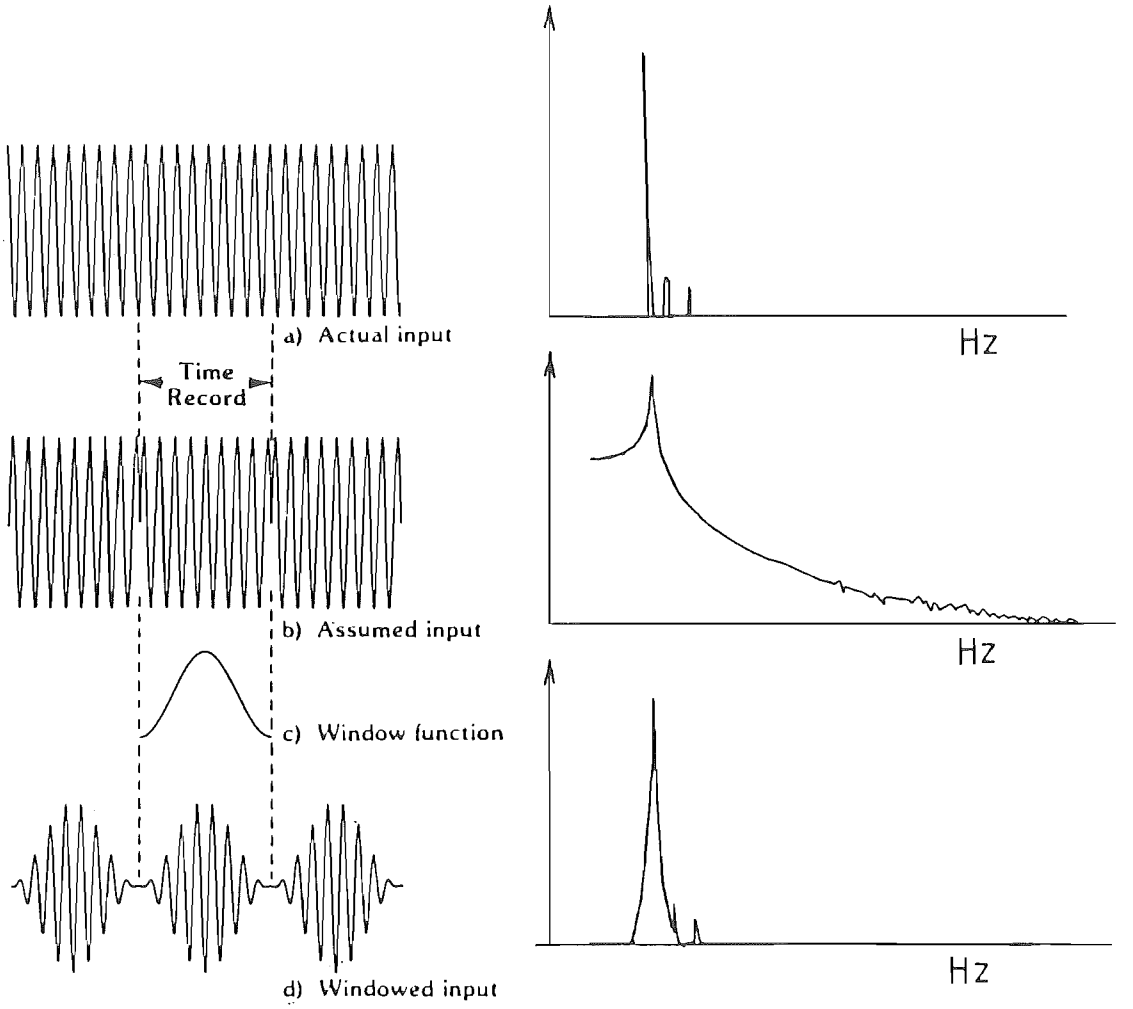

Figure 16: The effect of windowing.

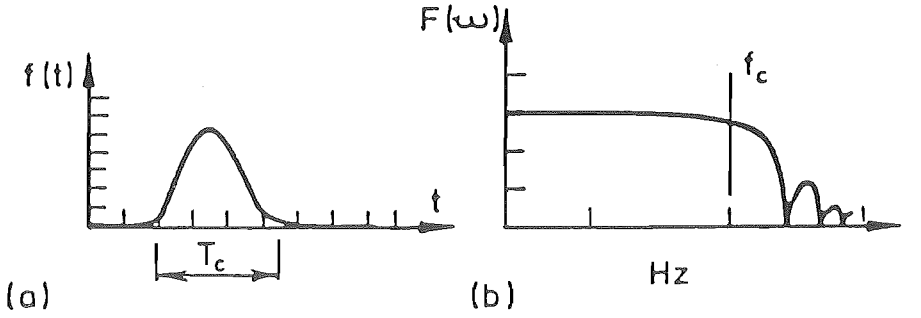

Figure 17: Typical impact force pulse and spectrum.

accelerometers.

There are several methods of attachment of accelerometer to the structure. Some of the common methods are threaded stud [which requires modification to the structure and was hence undesirable], cemented stud, thin layer of wax, and magnet. The choice of attachment method determines the range of frequency the accelerometer can measured. Magnetic attachment was used. It has low useful frequency range (0 Hz - 1000 Hz), but was acceptable for this experiment.

For experiments requiring multiple accelerometer readings instantaneously, the signals were recorded on an eight channels Hewlett-Packard tape recorder, and for those requiring only one or two inputs, the signals were read and recorded directly by the FFT analyser.

3.3.3 FFT Analyser

An Iwatsu SM-2701 FFT analyser was used for analysing the data. It had many built-in functions for vibration and sound analyses. For the bandsaw experiments, only three functions were used; the time domain measurement, the frequency domain measurement (Fourier transform of the time domain data), and the frequency response function measurement.

Even though, no major problems were encountered in using the FFT analyser, an experience user could have saved a lot of time in setting up the equipment, and producing and storing the required data.

Chapter 4

THEORETICAL METHOD IN STRUCTURAL VIBRATIONS

4.1 Modelling the Bandsaw Structure

It is impossible to predict accurately the vibrational characteristics of the bandsaw, because of its complexity. However a simple model would still be helpful in explaining some of the results from the experiments.

The major components of the bandsaw, to be considered in the vibration analysis, together with their theoretical representations are:

Main column and column slides Beam elements will be used to model the main column and the column slides. Although, these two components are far more complicated than the simple beam models, the beam models are adequate because only the displacements at the top of the column slides, where the bearing housings are supported, are of importance. Thick beam formulation should be used due to the aspect ratio of the two components.

Pulleys Because of the massive size and high rotating speed of the pulley, gyroscopic effects should be included in the analysis. The theory for gyroscopic rotors was, therefore, used in this study to represent the pulley.

Shafts The top shaft is very short, its stiffness is expected to be very high compared with other components, therefore, a non-rotating thick beam theory would be adequate for representing the top shaft. For the bottom shaft, a rotating beam model may be required because of its length, but it was not practical at this stage to add another complication to the model, so a non-rotating beam was assumed to be sufficient.

Miscellaneous Masses, springs and dampers can be easily incorporated into the analysis and would be very useful in modelling the bandsaw structure as well as many other applications.

4.2 Methods of Analysis

The advent of high speed computers has made the theoretical analysis of complicated systems relatively simple. One numerical method, the *finite elements method* (FEM), has become one of the most powerful method in many fields of engineering such as solid mechanics, fluid mechanics, vibrations. The biggest advantage in using FEM is that it can handle very complicated problems in a systematic way so that the theory can be kept simple. However, the FEM suffers a major disadvantage, the accuracies of the solutions are unknown unless they can be checked by some other method.

In the vibration analysis of beam structures, an exact method called the *dynamic stiffness method* uses the finite element concept to formulate the frequency equations of complicated beam structures. This method may be less computationally efficient

than the FEM, however, it is the exact method, therefore more insight can be gained from the solutions than the FEM. With the high speed computers available today, efficiency and speed are no longer the major factors in choosing the method of analysis. Another advantage of the dynamic stiffness method over the FEM is that only one element is required to represent one beam, whereas a single element of the FEM would give very inaccurate results. This means that the data required for the dynamic stiffness method would be much less than that required for the FEM. The dynamic stiffness method was, therefore, chosen for the study of bandsaw structural vibration.

4.3 A General Procedure in the Dynamic Stiffness Method

The dynamic stiffness method is described in [48, page 121]. In this method, the system under investigation is broken up into elements. The dynamic behaviour of each element can be described by relating the generalised forces, $\{F\}_e$ with the generalised displacements, $\{V\}_e$ by

$$\{F\}_e = [K]_e \{V\}_e \tag{1}$$

where $[K]_e$ is the elemental dynamic stiffness matrix.

These elemental dynamic stiffness matrices can be assembled into a global system dynamic stiffness matrix, $[K]_g$, by considering the relationship between the elemental coordinates, $\{V\}_e$, and the global coordinates, $\{V\}_g$. This phase of the analysis is identical to the assembly process of the FEM [14].

The natural frequencies of the system are the frequencies at which the determinant of the global dynamic stiffness matrix becomes zero, that is

$$\left|[K]_g\right| = 0 \tag{2}$$

The next step in the analysis is to obtain the modeshape associated with each frequency. This can be done by substituting a frequency into $[K]_g$ and letting one displacement to be unity. Equation

$$[K]_g \{V\}_g = \{0\} \tag{3}$$

can be rearranged to solve for the remaining displacements which describe the mode shape of the system at the given frequency. Care must be taken in choosing which displacement to be unity because a node (zero displacement) may occur in the mode shape at the chosen point.

4.4 Dynamic Stiffness Matrices

4.4.1 Transverse Vibration of Thin Beams

The formulation of the dynamic stiffness matrix can be found in [48, page 109].

The equation of motion for the transverse vibration of a thin beam is

$$EI\frac{\partial^4 v}{\partial x^4} + \rho A\frac{\partial^2 v}{\partial t^2} = 0 \tag{4}$$

The steady state solution is of the form

$$v = V(x)\, e^{i\omega t} \tag{5}$$

where ω is the angular frequency, t is time. Substitute Equation (5) into Equation (4) gives

$$\frac{d^4 V}{dx^4} - \frac{\rho A\omega^2}{EI}V = 0 \tag{6}$$

The solution for this equation is

$$V = B_1 \sin \lambda x + B_2 \cos \lambda x + B_3 \sinh \lambda x + B_4 \cosh \lambda x \tag{7}$$

where

$$\lambda^4 = \frac{\rho A \omega^2}{EI}$$

Referring to Figure 18, the boundary conditions are

$$\begin{aligned} N_1 e^{i\omega t} &= -EI \frac{\partial^2 v}{\partial x^2} \\ P_1 e^{i\omega t} &= EI \frac{\partial^3 v}{\partial x^4} \\ N_2 e^{i\omega t} &= EI \frac{\partial^2 v}{\partial x^2} \\ P_2 e^{i\omega t} &= -EI \frac{\partial^3 v}{\partial x^3} \end{aligned}$$

Substitute for v from Equation (5) and Equation (7) and express in the results in matrix forms to give

$$\begin{Bmatrix} P_1 \\ P_2 \\ N_1 \\ N_2 \end{Bmatrix} = EI \begin{bmatrix} -\lambda^3 & 0 & \lambda^3 & 0 \\ \lambda^3 \cos \lambda L & -\lambda^3 \sin \lambda L & -\lambda^3 \cosh \lambda L & -\lambda^3 \sinh \lambda L \\ 0 & \lambda^2 & 0 & -\lambda^2 \\ -\lambda^2 \sin \lambda L & -\lambda^2 \cos \lambda L & \lambda^2 \sinh \lambda L & \lambda^2 \cosh \lambda L \end{bmatrix} \begin{Bmatrix} B_1 \\ B_2 \\ B_3 \\ B_4 \end{Bmatrix}$$

That is

$$\{F\} = [D]\{B\} \tag{8}$$

The unknown coefficients B_i can also be expressed, in terms of the maximum end deflections and slopes, as

$$\begin{Bmatrix} V_1 \\ V_2 \\ \Theta_1 \\ \Theta_2 \end{Bmatrix} = \begin{bmatrix} 0 & 1 & 0 & 1 \\ \sin \lambda L & \cos \lambda L & \sinh \lambda L & \cosh \lambda L \\ \lambda & 0 & \lambda & 0 \\ \lambda \cos \lambda L & -\lambda \sin \lambda L & \lambda \cosh \lambda L & \lambda \sinh \lambda L \end{bmatrix} \begin{Bmatrix} B_1 \\ B_2 \\ B_3 \\ B_4 \end{Bmatrix}$$

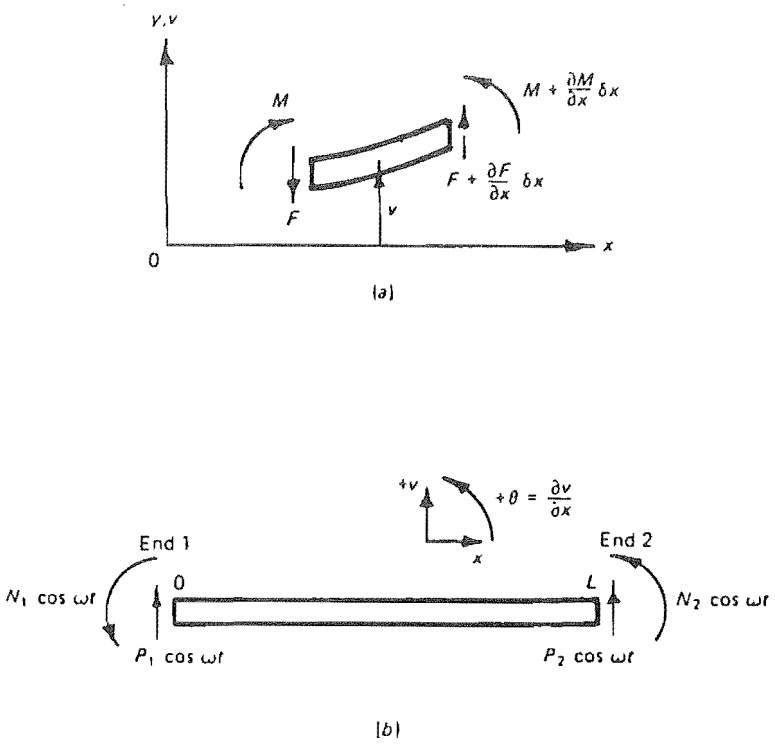

(*a*) Bending moment and shear force sign convention
(*b*) Positive directions for end forces and couples

Figure 18: Positive sign convention.

or

$$\{V\} = [C]\{B\} \tag{9}$$

therefore

$$\{B\} = [C]^{-1}\{V\} \tag{10}$$

The dynamic stiffness matrix for the thin beam element can be derived by combining Equation (8) and (10), to give

$$\{F\} = [D][C]^{-1}\{V\} = [K]\{V\} \tag{11}$$

$[K]$ is the dynamic stiffness matrix

$$[K] = \frac{EI\lambda^2}{F_3}\begin{bmatrix} -\lambda F_6 & \lambda F_7 & -F_1 & F_{10} \\ \lambda F_7 & -\lambda F_6 & -F_{10} & F_1 \\ -F_1 & -F_{10} & F_5/\lambda & F_8/\lambda \\ F_{10} & F_1 & F_8/\lambda & F_5/\lambda \end{bmatrix} \tag{12}$$

where

$$\begin{aligned} F_1 &= \sin\lambda L \sinh\lambda L \\ F_5 &= \cos\lambda L \sinh\lambda L - \sin\lambda L \cosh\lambda L \\ F_6 &= \cos\lambda L \sinh\lambda L + \sin\lambda L \cosh\lambda L \\ F_7 &= \sin\lambda L + \sinh\lambda L \\ F_8 &= \sin\lambda L - \sinh\lambda L \\ F_{10} &= \cos\lambda L - \cosh\lambda L \end{aligned}$$

L is the length of the beam.

4.4.2 Transverse Vibration of Thick Beams

When the depth of the beam becomes a significant proportion of its length, then a thick beam theory must be used, which takes into account the effect of shear

deformation and rotary inertia [48, page 113], [61], [29].

The equation of motion for a thick beam, sometimes referred to as Timoshenko's beam, is

$$EI\frac{\partial^4 v}{\partial x^4} - \rho I\left(\frac{E}{kG}+1\right)\frac{\partial^4 v}{\partial x^2 \partial t^2} + \rho A\frac{\partial^2 v}{\partial t^2} + \frac{\rho^2 I}{kG}\frac{\partial^4 v}{\partial t^4} = 0 \qquad (13)$$

where G is the shear modulus and k is the shear constant which is dependent on the cross section of the beam. Cowper (1966) [15] presented the formulations and numerical values of the shear constant for various cross-sections.

The elements of the dynamic stiffness matrix are given in [61,29], however there are many typographical mistakes in both papers, these elements are, therefore, provided in Appendix A.

4.4.3 Longitudinal and Torsional Vibration of Beams

The formulations for these two types of vibration are very similar. The displacement vector for longitudinal vibration is

$$\{V\}_{\text{long}} = \begin{Bmatrix} U_1 \\ U_2 \end{Bmatrix}$$

where U_1 and U_2 are the longitudinal displacements at the two ends of the beam as in Figure 19.

The displacement vector for torsional vibration of beam is

$$\{V\}_{\text{tor}} = \begin{Bmatrix} \phi_1 \\ \phi_2 \end{Bmatrix}$$

where ϕ_1 and ϕ_2 are the end angles of twist as in Figure 20.

The equation of motion for longitudinal vibration of a beam is

$$\frac{E}{\rho}\frac{\partial^2 u}{\partial x^2} - \frac{\partial^2 u}{\partial t^2} = 0 \qquad (14)$$

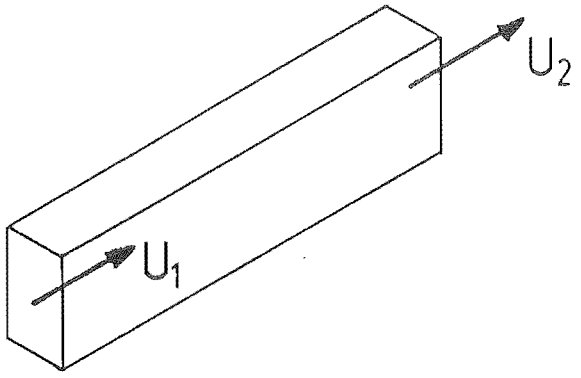

Figure 19: Generalised coordinates for longitudinal vibration.

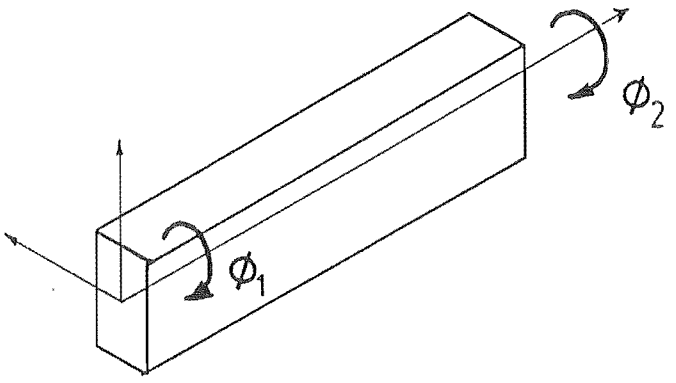

Figure 20: Generalised coordinates for torsional vibration.

The dynamic stiffness matrix for the longitudinal vibration can be derived in a similar manner as for the transverse vibration. It is

$$[K]_{\text{long}} = EA\alpha \begin{bmatrix} \cot \alpha L & -\csc \alpha L \\ -\csc \alpha L & \cot \alpha L \end{bmatrix} \tag{15}$$

where

$$\alpha^2 = \frac{\rho\omega^2}{E}$$

The equation of motion for the torsional vibration of a beam is

$$GJ\frac{\partial^2\phi}{\partial x^2} + I_p\rho\frac{\partial^2\phi}{\partial t^2} = 0 \tag{16}$$

where J is the Saint Venant torsional constant, and I_p is the polar moment of inertia.

The dynamic stiffness matrix for the torsional vibration is

$$[K]_{\text{tor}} = GJ\beta \begin{bmatrix} \cot \beta L & -\csc \beta L \\ -\csc \beta L & \cot \beta L \end{bmatrix} \tag{17}$$

where

$$\beta^2 = \frac{\rho I_p\omega^2}{GJ}$$

For a circular cross sectional beam, J is equal to I_p therefore $\beta^2 = \rho\omega^2/G$. When the cross section is not circular, J can be determined with other formulas [67].

4.4.4 3D Beam Elements

For a general three dimensional beam element, twelve generalised displacements are required to described the vibration, see Figure 21. The dynamic stiffness matrix for this 3D beam element is just simply an assemblage of the longitudinal, torsional and two transverse dynamic stiffness matrices. This is possible because of the assumption that these vibrations do not couple with each other, therefore, zeros can be filled into the dynamic stiffness matrix at the appropriate positions.

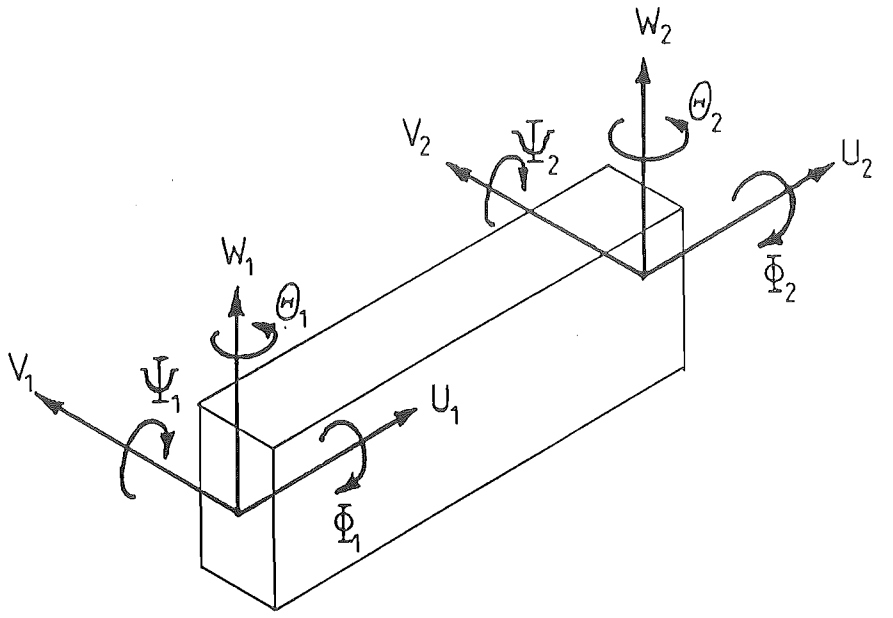

Figure 21: Generalised displacements for a 3D beam element.

4.4.5 Concentrated Masses

Concentrated mass is a very useful feature in many applications, and it is the easiest element to include in the analysis. The only contribution of a mass in the equation of motion is the inertial force, that is, mass times acceleration $\left(m\frac{d^2v}{dl^2}\right)$. For three dimensional analysis, the displacement vector is

$$\{V\}_{\text{mass}} = \begin{Bmatrix} U \\ V \\ W \end{Bmatrix}$$

The dynamic stiffness matrix is

$$[K]_{\text{mass}} = -m\omega^2 \begin{bmatrix} 1 & 0 & 0 \\ 0 & 1 & 0 \\ 0 & 0 & 1 \end{bmatrix} \tag{18}$$

This is in fact a mass matrix rather than a stiffness matrix, however, the dynamic stiffness matrix combines both stiffness and mass matrices into one, hence

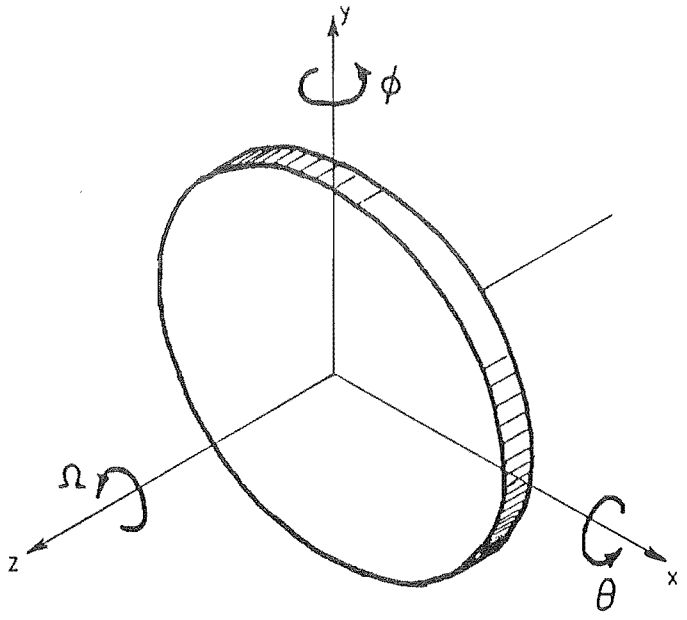

Figure 22: Angular displacements in a symmetrical rotor.

Equation (18) can be treated as a stiffness matrix and assembled into dynamic stiffness matrix the same way as other elements.

4.4.6 Gyroscopic Rotors

A rotor is simply an element with a large moment of inertia about its diameter and about its central axis. For a non-rotating rotor, its effect in the equation of motion is the inertial moments, which is analogous to the inertial force of the concentrated mass. For a rotating rotor, gyroscopic effects have to be considered in the vibratory motions. The gyroscopic effect couples two angular displacements θ, and ϕ (see Figure 22), because of the conservation in angular momentum. The theory for this gyroscopic effect is in [48, Chapter 8]. Small amplitude vibrations of a symmetrical rotor are much simpler to analyse than those of an asymmetrical rotor. Because of the geometry and the small amplitude of vibration of the bandsaw pulley, the theory for symmetrical rotors is used in this investigation.

The inertial moments, G_θ and G_ϕ are

$$\begin{Bmatrix} G_\theta \\ G_\phi \end{Bmatrix} = \begin{bmatrix} I_r D^2 & J_r \Omega D \\ -J_r \Omega D & I_r D^2 \end{bmatrix} \begin{Bmatrix} \theta \\ \phi \end{Bmatrix} \tag{19}$$

where D is the time differential operator, Ω is the speed of rotation about the central axis, I_r is the second moment of inertia about a diameter and J_r is the second moment of inertia about the central axis of the rotor.

Substitute a solution of the form

$$\begin{Bmatrix} \theta \\ \phi \end{Bmatrix} = e^{i\omega t} \begin{Bmatrix} \Theta \\ \Phi \end{Bmatrix} \tag{20}$$

into Equation (19), the dynamic stiffness matrix can be obtained as

$$[K]_{\text{gyro}} = \begin{bmatrix} -I_r \omega^2 & i J_r \Omega \omega \\ -i J_r \Omega \omega & -I_r \omega^2 \end{bmatrix} \tag{21}$$

The coupling terms involve the first time differential, therefore the dynamic stiffness matrix is skewed symmetric and the off-diagonal terms are complex. This fact will impose problems in the search for natural frequencies of a gyroscopic system. Fortunately, modern computer languages, such as FORTRAN 77, can deal with complex values and arithmetics easily and efficiently. Section 4.7 will discuss the method of searching for the complex roots of the determinant of the dynamic stiffness matrix.

4.4.7 Springs

There are two types of springs, linear and torsional. A spring element is considered to be acting in one direction only. Its effects in any other directions have to be treated as seperate elements.

For a linear spring with U_1 and U_2 as the end displacements, that is

$$\{V\} = \begin{Bmatrix} U_1 \\ U_2 \end{Bmatrix} \tag{22}$$

The stiffness matrix is

$$[K]_{\text{spring}} = \begin{bmatrix} k & -k \\ -k & k \end{bmatrix} \tag{23}$$

where k is the spring stiffness.

The torsional spring dynamic stiffness matrix is the same as Equation (23) with k as the torsional spring stiffness.

4.4.8 Dampers

A viscous damper does not have stiffness, however, it has a relationship between force and displacement, which can be treated as dynamic stiffness. The displacement vector, $\{V\}$ is the same as $\{V\}$ for the spring, and the dynamic stiffness matrix is given by

$$[K]_{\text{damp}} = \begin{bmatrix} i\omega c & -i\omega c \\ -i\omega c & i\omega c \end{bmatrix} \tag{24}$$

where c is the damping constant.

The dynamic stiffness matrix is complex, and can be analysed the same way as for a gyroscopic rotor. When damping exists, the amplitude of oscillation will decay. This decaying factor is included in the dynamic stiffness method as an imaginary part of the frequencies.

The usual notation for the solution, when damping is present, is $e^{\lambda t}\{V\}$ instead of $e^{i\omega t}\{V\}$, where $\{V\}$ is the amplitude vector, and λ is the complex eigenvalues of the dynamic stiffness matrix. The imaginary part of λ is the damped natural frequency and the real part represents the decaying part, while the real and imaginary

parts of the amplitude together define the amplitude and phase of the vibratory motion [90]. To be consistent with other dynamic stiffness matrices, $e^{i\omega t}\{V\}$ was used instead. ω is also complex but the real part represents the usual frequency and the imaginary part represents the decay when damping exist, that is $\lambda = i\omega$. The imaginary part is zero when there is no damping in the system.

4.5 Problem with the Infinite Magnitude of the Determinants

It is possible for the magnitude of the determinant of the dynamic stiffness matrix for a beam to be infinite, and sign changes of the determinants could occur at such infinities.

For a single beam element, the infinities occur at the natural frequencies of beams with the clamped-clamped boundary conditions, because the stiffness matrix is undefined for this case as there is zero generalised end displacement. This may be seen by inspection of the dynamic stiffness matrix for a thin beam, the process responsible for the infinite magnitudes of the determinant is the division by F_3 when $F_3 = 0$; F_3 is the frequency equation for the clamped-clamped beam. To eliminate this problem, an extra node is provided where the generalised displacements is non-zero.

For structures with two or more beams, the above problem is much less likely to happen, however, there are cases when the mode of vibration is such that there are zero displacements at all the generalised coordinates, and determinantal infinities are again encountered. An example of this is the third mode of the inplane vibration of a portal frame as in Figure 23. In this case, an extra node on any member of the frame will eliminate the problem.

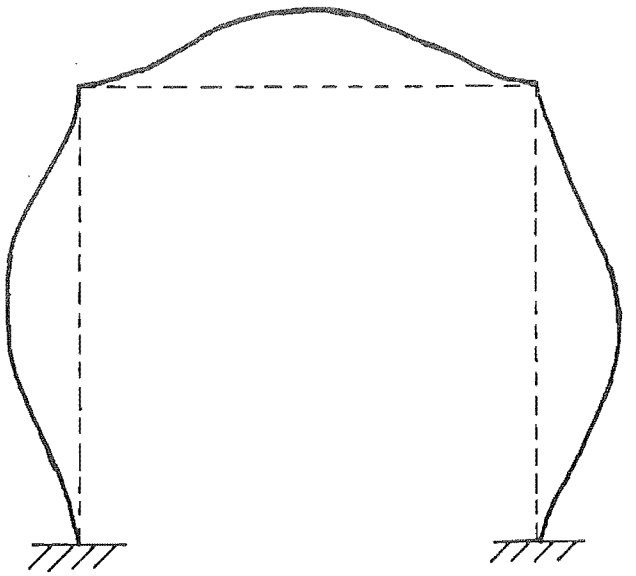

Figure 23: Third mode of a portal frame.

At the time of developing the computer program, the determinantal infinities was avoided by using three node beam elements, that is, an 18 by 18 dynamic stiffness matrix was obtained for a 3 dimensional beam element instead of a 12 by 12 matrix. This method was acceptable for analysing structures with a small number of beams, but, the inefficiency of the method was evident when analysing structures with more than five beam elements. A more efficient way of dealing with this problem would be to analyse the usual two node beam elements, for a check to be included in the program to detect the possible determinantal infinities and for it to report a message. An extra node could then be added manually into the structure to remove the infinities.

4.6 Coordinates System and Transformations

The process of assembling the global dynamic stiffness matrix involves two steps. The first step is the transformation of the dynamic stiffness matrix based on the local

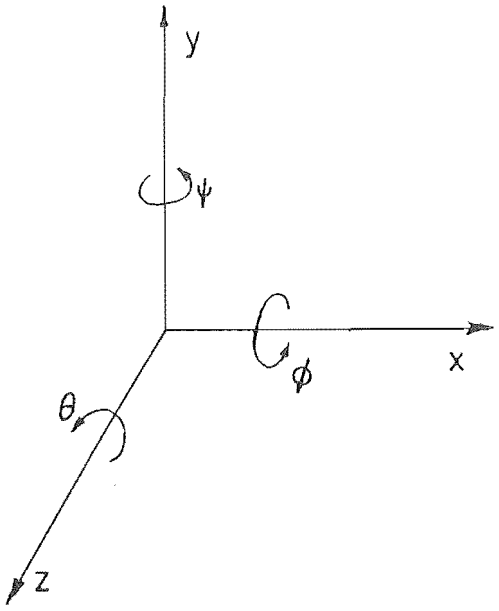

Figure 24: Global coordinates in three dimensions.

coordinates system, to the dynamic stiffness matrix based on the global coordinates system. The second step is the assembly of the transformed elemental dynamic stiffness matrices into a global dynamic stiffness matrix. This second step, in fact, imposes compatibility conditions on the model, or in other words, the assembly process links all the elements together to form the total system representation.

4.6.1 Coordinates System

The global coordinates system (x, y, z) is the coordinates system where the whole structure is referred to in space. The global degrees of freedom are the degrees of freedom of all the nodes of the structure in the directions of the global coordinates. In three dimensional space, each free node has six degrees of freedom, of which, there are three displacements and three rotations. A completely restraint node has zero degrees of freedom.

The local coordinates system (X, Y, Z) is the coordinates system defined on each

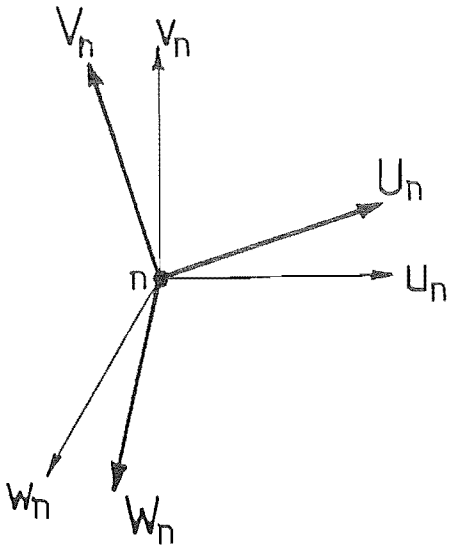

Figure 25: Local and global degrees of freedom of node n.

seperate element, and the local degrees of freedom are the degrees of freedom at each topology of the element in the directions of the local coordinates. For a beam element, the topologies are the two end nodes, and for a concentrated mass element, the topology is the node on which the mass is defined. For a three dimensional beam element, there are twelve local degrees of freedom as shown in Figure 21.

4.6.2 Transformation of Coordinates

The local dynamic stiffness matrix of an element, $[K]_E$, referring to the local degrees of freedom, must be transformed to a stiffness matrix, $[K]_e$, referring to the degrees of freedom in the directions of the global coordinates before it can be assembled into the global stiffness matrix, $[K]_g$.

For brevity, consider only the three displacements for the degrees of freedom at a node, that is, (U_n, V_n, W_n) for the local degrees of freedom and (u_n, v_n, w_n) for the global degrees of freedom at node n (Figure 25).

The transformation matrix, $[T]$, is the connection between the global and the

local coordinates.

$$\begin{Bmatrix} U_n \\ V_n \\ W_n \end{Bmatrix} = [T] \begin{Bmatrix} u_n \\ v_n \\ w_n \end{Bmatrix} \tag{25}$$

If U_n can be written in terms of u_n, v_n and w_n as

$$U_n = i_U u_n + j_U v_n + k_U w_n \tag{26}$$

and similarly

$$V_n = i_V u_n + j_V v_n + k_V w_n \tag{27}$$

$$W_n = i_W u_n + j_W v_n + k_W w_n \tag{28}$$

then the transformation matrix can be expressed as

$$[T] = \begin{bmatrix} i_U & j_U & k_U \\ i_V & j_V & k_V \\ i_W & j_W & k_W \end{bmatrix} \tag{29}$$

The same $[T]$ can be used to transform the three rotational degrees of freedom, Φ_n, Ψ_n, Θ_n to ϕ_n, ψ_n, θ_n.

For a three dimensional beam, the global positions of the two end nodes do not completely define the position of the beam. One of the methods used by the finite element scheme to define the local coordinates of a three dimensional beam is the *third node method*, where the coordinates of another point lying on the X-Y plane of the beam is provided (Figure 26).

If $(x_1, y_1, z_1), (x_2, y_2, z_2)$ and (x_3, y_3, z_3) are the global coordinates of node 1, node 2 and node 3, respectively, and L is the length of the beam, then i_U, j_U and k_U are give by

$$i_U = \frac{x_2 - x_1}{L}, \quad j_U = \frac{y_2 - y_1}{L}, \quad k_U = \frac{z_2 - z_1}{L} \tag{30}$$

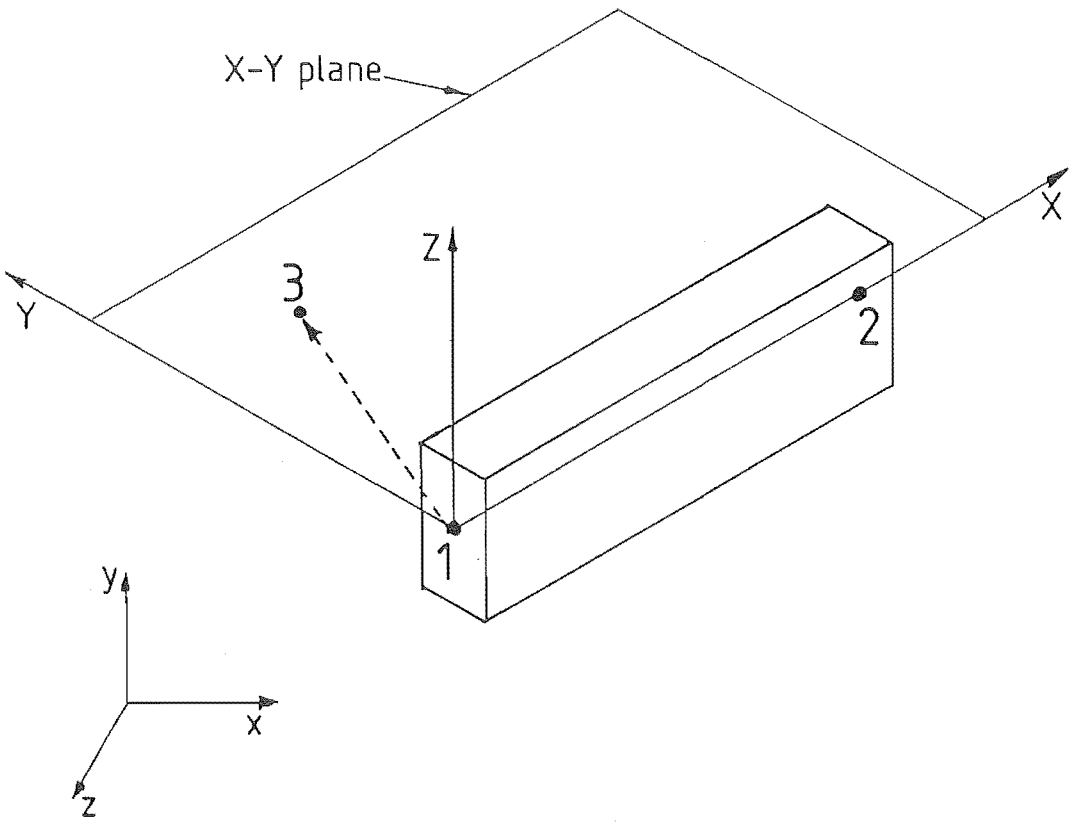

Figure 26: Third node of a beam element.

i_W, j_W and k_W define a vector perpendicular to the X-Y plane, hence

$$(i_W, j_W, k_W) = (i_U, j_U, k_U) \times \left(\frac{x_3 - x_1}{L_3}, \frac{y_3 - y_1}{L_3}, \frac{z_3 - z_1}{L_3}\right) \tag{31}$$

where

$$L_3 = \left((x_3 - x_1)^2 + (y_3 - y_1)^2 + (z_3 - z_1)^2\right)^{1/2}$$

Similarly, i_V, j_V and k_V define a vector perpendicular to the X-Z plane, therefore

$$(i_V, j_V, k_V) = (i_U, j_U, k_U) \times (i_W, j_W, k_W) \tag{32}$$

The stiffness matrix, $[K]_E$ can be transformed to $[K]_e$ by [48, page 72],[14, page 151]

$$[K]_e = [T]^T [K]_E [T] \tag{33}$$

4.6.3 Assemblying the Global Stiffness Matrix

The assembly process is merely the additions of the elements of the matrix $[K]_e$ to the appropriate rows and columns of the global matrix $[K]_g$, depending on the numbering scheme of the global degrees of freedom. More information on this process can be found in most FEM text books, such as [14].

4.7 Roots Finding Method

This step is very important in the analysis and probably the most difficult step.

For FEM, solution of the frequency equation of a system is a linear eigenvalue problem. All the eigenvalues can be found by a numerical algorithm [74]. The number of eigenvalues obtained is dependent on how many elements were chosen to approximate the problem.

With the dynamic stiffness method for a beam, solution of the frequency equation is a transcendental eigenvalue problem, hence there are an infinite number of

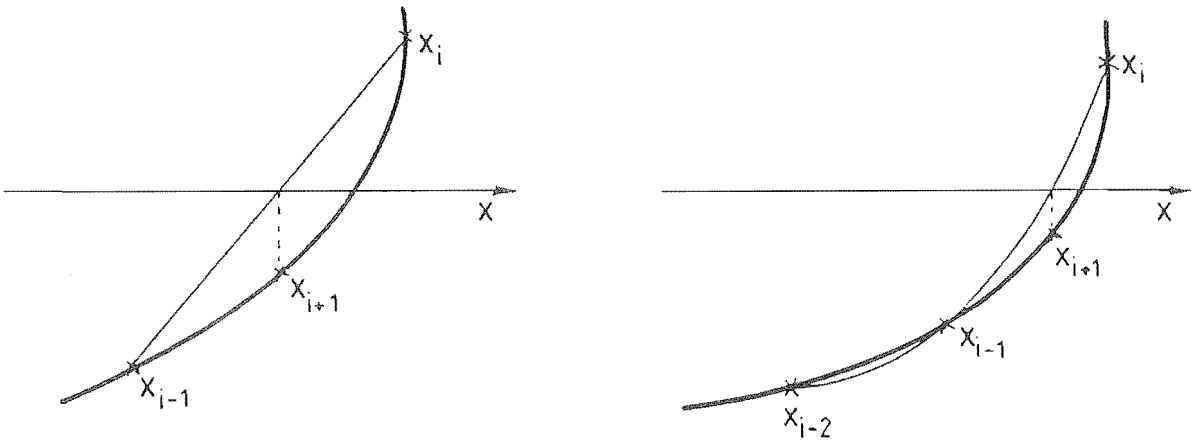

Figure 27: Secant's and Muller's methods.

frequencies, which is expected because there are infinite degrees of freedom. The only way to find the roots of a transcendental equation is to search for each frequency with a robust numerical scheme. Bisection method, regula falsi method, Secant method and Newton-Raphson method are a few popular methods for finding roots of a general equation. Williams and Wittrick [92] described an infallible method of finding all required natural frequencies of skeletal structures. However, these methods are for real roots only. There are very few methods that can handle complex equations and complex roots.

Text books on Numerical Analysis [63,13] suggested the Muller's method as a robust numerical algorithm for finding real and complex roots of a general equation.

Muller's method works on the same principle as the Secant method, but instead of using linear interpolation, Muller's method uses quadratic interpolation to find the next approximate point (Figure 27)

To find a root of a function $F(x)$, Muller's method requires three initial guesses, x_{i-2}, x_{i-1}, x_i. Then the next approximation x_{i+1} can be found as followed

$$q = \frac{(x_i - x_{i-1})}{(x_{i-1} - x_{i-2})}$$

$$
\begin{aligned}
A &= qF(x_i) - q(1+q)F(x_{i-1}) + q^2F(x_{i-2}) \\
B &= (2q+1)F(x_i) - (1+q)^2F(x_{i-1}) + q^2F(x_{i-2}) \\
C &= (1+q)F(x_i) \\
x_{i+1} &= x_i - (x_i - x_{i-1})\left[\frac{2C}{B \pm \sqrt{B^2 - 4AC}}\right]
\end{aligned}
$$

The sign $\pm$ in the denominator of the above equation is chosen to make its value as large as possible.

Because of the square root in the equation, a complex value for x_{i+1} is possible hence the method can converge to a complex root.

The Muller's method is believed to have almost global convergence, that is, it will converge to a root with any starting values. However, it is impossible to establish which particular root the method will converge to, hence some roots may be missed during a search.

The Muller's method was adequate for providing the solutions of this analysis. The mode shapes were plotted to check the validity of the roots found.

The algorithm given in [13, page 72] is more efficient and more stable than the above algorithm. It is

$$
\begin{aligned}
h_1 &= x_{i-1} - x_{i-2} \\
h_2 &= x_i - x_{i-1} \\
a_1 &= \frac{F(x_{i-1}) - F(x_{i-2})}{h_1} \\
a_2 &= \frac{F(x_i) - F(x_{i-1})}{h_2} \\
d &= \frac{a_2 - a_1}{h_2 + h_1} \\
b &= a_2 + h_2 d \\
D &= \sqrt{b_2 - 4F(x_i)\,d} \\
x_{i+1} &= x_i - \frac{2F(x_i)}{b \pm D}
\end{aligned}
$$

A computer subroutine based on this algorithm was written in FORTRAN 77, it was used to find the natural frequencies of the bandsaw structure.

4.8 Description of the Computer Program

A program to analyse two dimensional structural vibrations, VIB2, was written first to examine the practicability of the dynamic stiffness method, and also to provide test results for the full three dimensional vibration problems. Only transverse and longitudinal vibrations of thin beams were considered in VIB2.

VIB3 was written as a general computer program to analyse the vibrations of three dimensional structures consisting of thick beams, masses, springs, dampers and gyroscopic rotors.

4.8.1 Hierarchical Structure of VIB3

The program reads input data from a data file which fully defines the vibratory system. Three main tasks of the program are :

- To find the values of the determinant of the dynamic stiffness matrix for a given range of frequencies and step size.
- To find the natural frequencies of the system by using Muller's method to search for the roots of the function $F(\omega)$, where ω is the angular natural frequency and $F(\omega)$ returns the value of determinant of the dynamic stiffness matrix. The three initial starting points affect which frequencies the method will converge to, therefore care must be taken to find all required natural frequencies.

- To plot the mode shapes of the system at a given natural frequency. The task of visualising the mode shapes is as important as the task of finding the natural frequencies. There is a considerable amount of work involved in generating the mode shapes of complicated structures by hand. Fortunately, computer graphics can be used to automate this process.

Figure 28 shows the hierarchical structure of VIB3. The program is menu-driven to give the users more flexibility.

4.8.2 Input Data

The preparation of input data for VIB3 was designed to be similar to the input for PAFEC, the commercial finite element software.

VIB3 data is in modular form, each module begins with a header, hence the module can be placed in any order. There are eight modules available

MATERIAL defines the material and geometrical properties of the beams. Each set of properties is numbered so that it can be referred to in the program. Because of the complexity of calculating the geometrical properties of various cross sectional shapes (rectangular, I section, T section etc.), especially the shear coefficients [15], and the torsion constants [67], a computer program, PROP, was written to calculate all the geometrical properties of various cross-sectional geometries.

NODE defines the coordinates of all the nodes of the structure.

BEAM defines the topologies of the beams, directions of their principal planes, and the connections at their ends. At the moment, VIB3 considers only the rigid joints and the pinned joints, but elastic linkages can be included at a later stage [61].

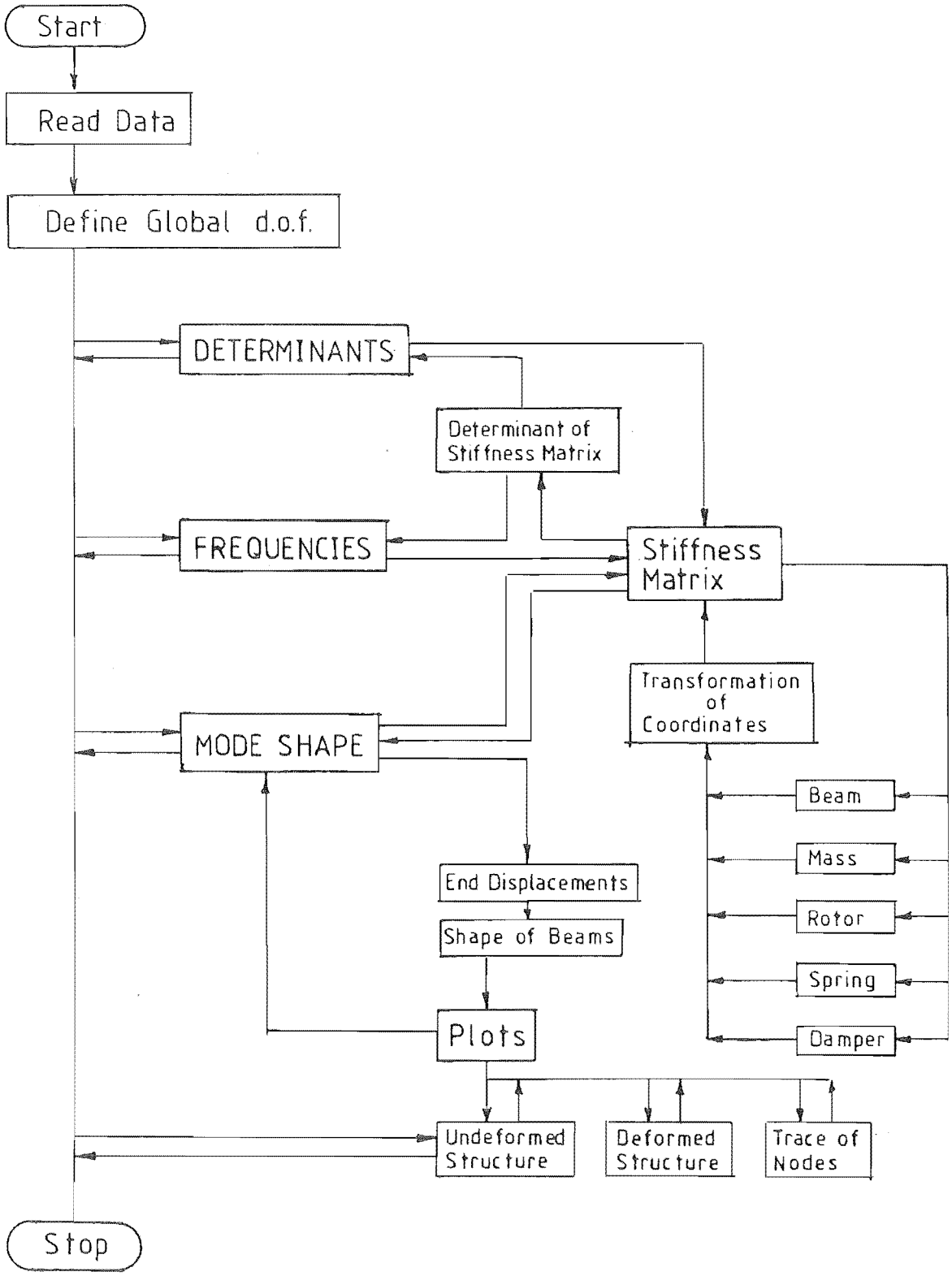

Figure 28: Hierachical structure of the program.

RESTRAINT defines the global boundary conditions.

MASS, ROTOR, SPRING and DAMPER are modules which define the properties and the topologies of the concentrated masses, gyroscopic rotors, linear springs, torsional springs, linear dampers and torsional dampers. The modules can be omitted if the elements are not present in the structure.

4.8.3 Output data

The output data is stored in a file and displayed on the screen.

The DETERMINANT option asks for a range of frequencies and the step size, then displays the frequencies with their corresponding values of the determinant of the stiffness matrix. Sign changes can be detected by visual inspection. This option can be used to give an indication of the location of natural frequencies. However, when the determinant has complex values as for the cases when gyroscopic rotors and dampers are included, it is impossible to infer the natural frequencies by visual inspection.

The FREQUENCIES option requires three starting values for the iteration, then uses Muller's method to search for a natural frequency. It is not possible to know which frequency the method will converge to, but usually it will converge to the roots closest to the three starting points.

Once a natural frequency has been detected, the MODE SHAPE option can be used to plot the mode shape. The program uses PLOT79 graphics package to generate three views of the structure and its mode of vibration. One isometric view of the structure gives the overall picture of the vibratory mode, however, it can be ambiguous, therefore, a plan and an elevation views are plotted to define it unambiguously.

Chapter 5

EXPERIMENTAL RESULTS AND THEORETICAL EXPLANATIONS OF THE WAIMAK BANDSAW VIBRATIONS

5.1 Introduction

About ten years ago, the Waimak bandsaw was reported as having problems with excessive vibration. Attempts to reduce the vibration, such as rebalancing the pulleys and bracing the structure to the ground, were unsuccessful. About a year ago, during a maintenance overhaul, one of the rolling contact bearings was found to be defective and was replaced. This appeared to reduce the vibration to an acceptable level, when the bracing was removed.

Although, this bandsaw had no vibration problem at the time of the experiments, problems have been reported on similar bandsaws in other saw mills in New Zealand. Also a better understanding of the vibrational characteristics of the Waimak bandsaw may help to explain the reasons for some of the vibration problems occurring on the other bandsaws.

The steps involved in the experiments and in the interpretations of results were not straight forward. The experimental anlysis had to be carried out in conjunction with the theoretical analysis, to explain the modes of vibration of the Waimak bandsaw.

The bandsaw structure was broken up into three sections as described in Chapter 2, and the assumption made was that the vibrations of these sections were uncoupled from each other, that is, each section could be analysed independently.

5.2 The Base

The base of the bandsaw is essentially a short cantilevered plate with masses attached to it. The programme VIB3 does not consider the plate model, but from practical intuition, the base is expected to be reasonably stiff compared with the other parts of the bandsaw.

The response of the base to an impact showed many peaks in the frequency spectrum. Some of the low amplitude peaks in the spectrum were related to the natural frequencies of other sections of the saw. By exciting and measuring the responses at different locations on the base, it was found that 168 Hz and 195 Hz were the dominant natural frequencies of the base. The 168 Hz had been identified as a transverse mode and the 195 Hz was a transverse-torsional mode, as shown in Figure 29. The coupling in the 195 Hz mode was due to the mass of the main column being situated on one side of the base, therefore it coupled the transverse

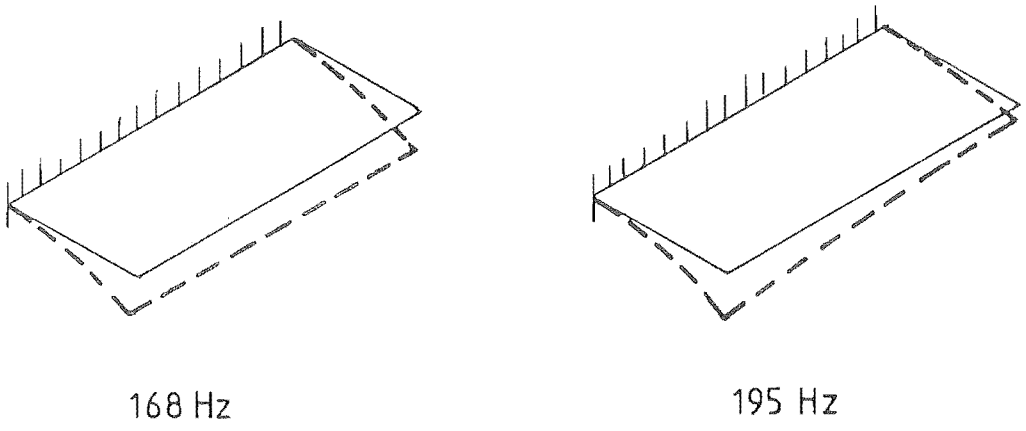

Figure 29: Mode shapes of the base.

mode with the torsional mode.

Although these results showed that the base was not rigid, its natural frequencies were high compared with the natural frequencies of the other sections, therefore, it was reasonable to assume that the dynamics of the section below the base would have very little influence on the dynamics of the section above it in the low frequency range, and vice versa.

5.3 Section Below the Base

This section was quite simple compared with the section above the base. Its basic components were the bottom pulley, the shaft and the brackets supporting the bearing housings (Figure 30).

5.3.1 Experimental Results and Interpretations

Figure 31 shows the spectrum of an accelerometer reading, which was placed on the bearing housing in the axial direction of the shaft.

Three natural frequencies shown in the spectrum were approximately 30 Hz,

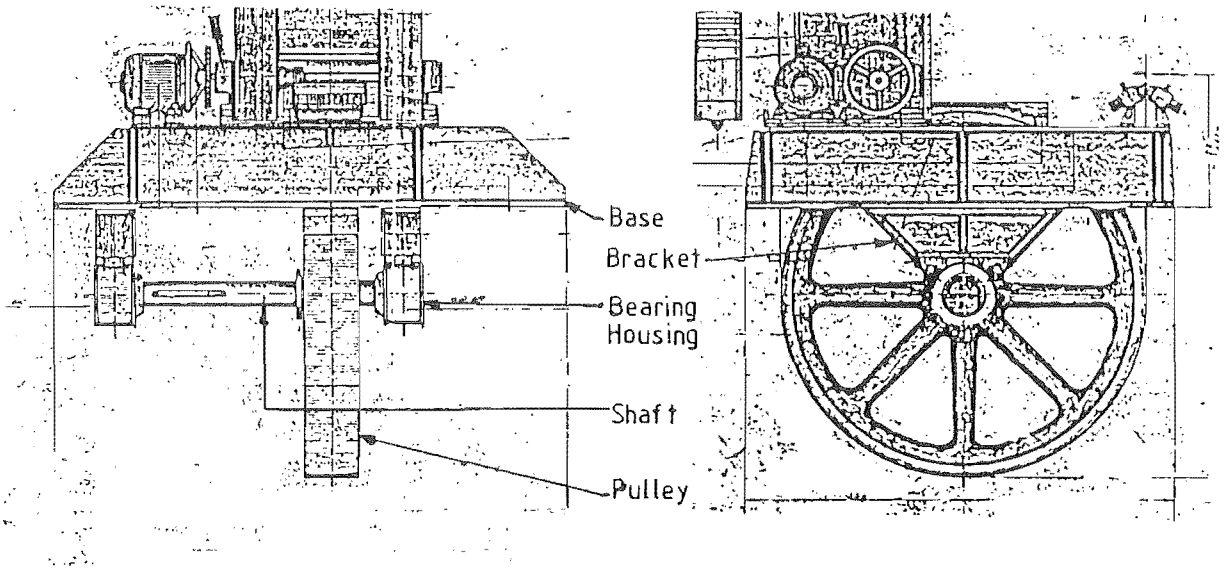

Figure 30: Section below the base.

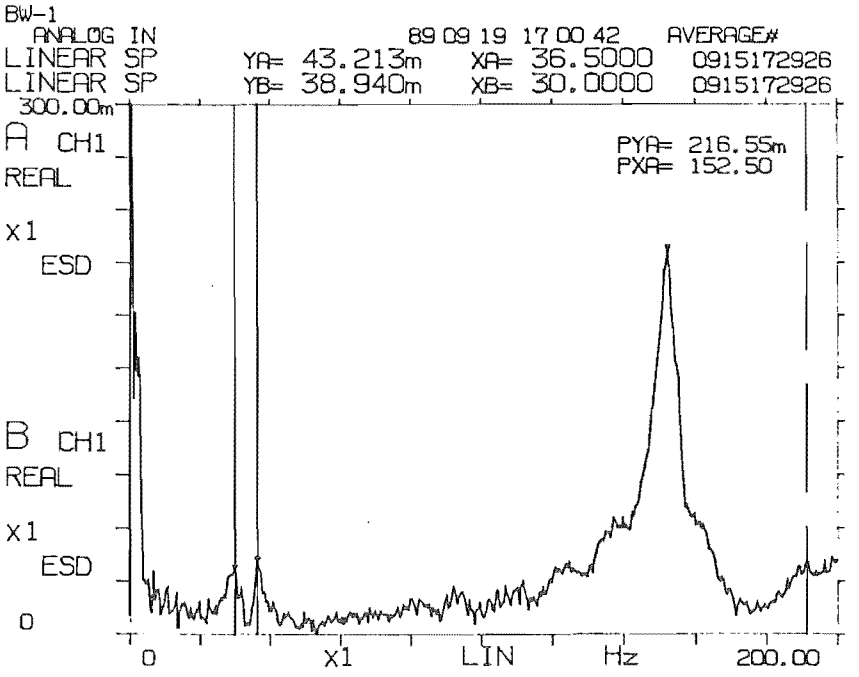

Figure 31: Frequency spectrum of a response of the section below the base.

36 Hz and 152 Hz.

The shaft alone would have had quite high natural frequencies, but the inertia of the pulley reduced the shaft frequencies considerably. This was analogous to a cantilever beam with a concentrated mass attached at the end.

The phases between two accelerometer readings at various positions on the rim of the bottom pulley revealed that the 30 Hz frequency was related to the first transverse mode of the shaft in the horizontal direction, the 36 Hz was related to the first transverse mode of the shaft in the vertical direction, and the 152 Hz was the swinging mode in the axial direction of the shaft. There were 90 Hz and 95 Hz natural frequencies present in the measurements on the rim of the pulley, however, their mode shapes were not identified during the experiments.

5.3.2 Theoretical Analysis

The programme VIB3 was used to obtain the first few natural frequencies and mode shapes of the section below the base of the bandsaw.

The model consisted of four beams and a rotor. The model mesh is shown in Figure 32.

It was assumed that the material properties for both the shaft and the brackets were those of mild steel, this was a reasonable assumption because the variations in the properties of different types of steel were small.

The plots of the first five modes are in Figures 33,34,35,36, and 37.

Although the natural frequencies differed from those obtained experimentally, the first, second and fifth mode shapes agreed with those found experimentally. The shapes of the third and fourth mode were identified as the second transverse modes of the shaft in the horizontal and vertical directions, respectively. They appeared to be the mode shapes of the 90 Hz and 95 Hz natural frequencies in the experiments.

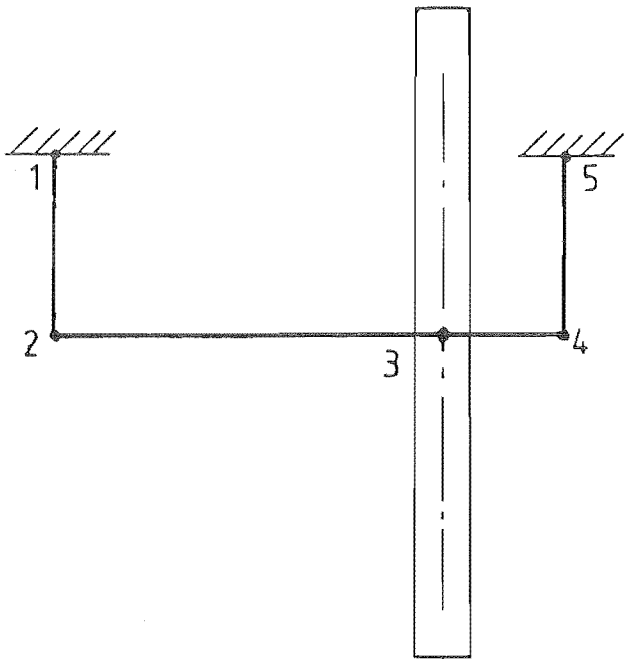

Figure 32: Model mesh.

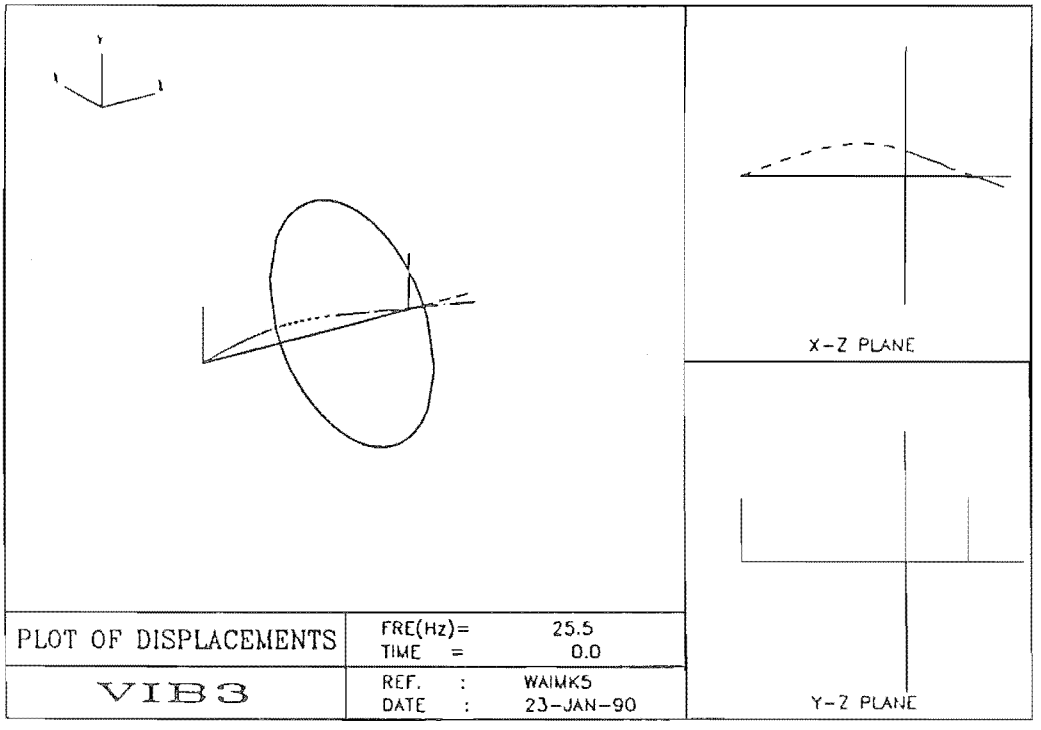

Figure 33: First mode.

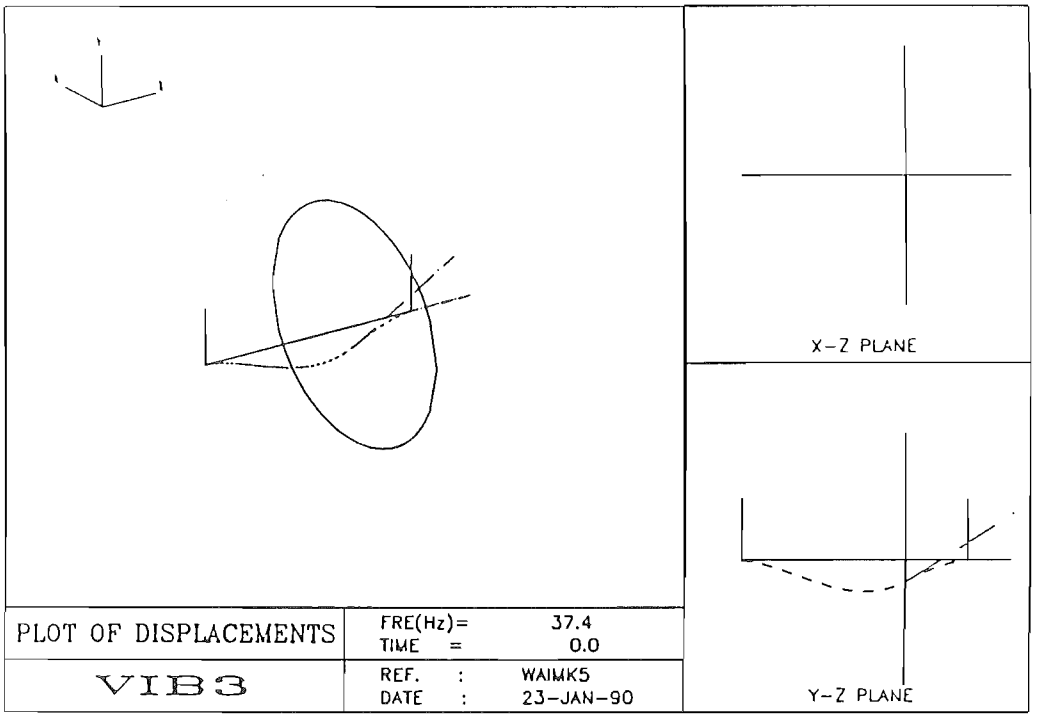

Figure 34: Second mode.

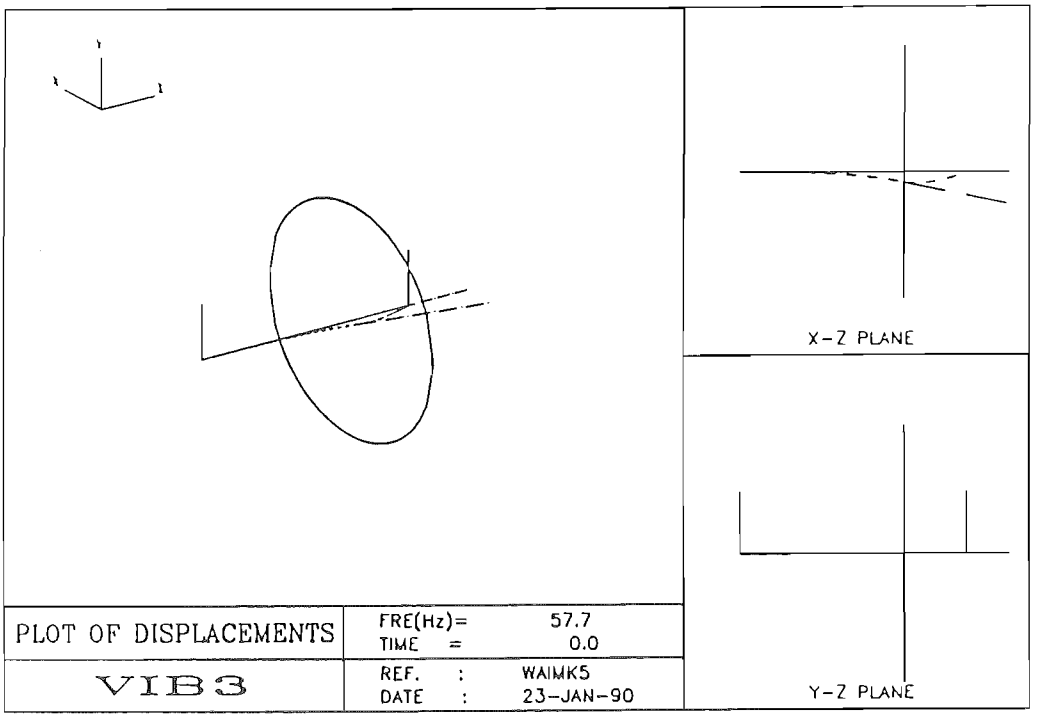

Figure 35: Third mode.

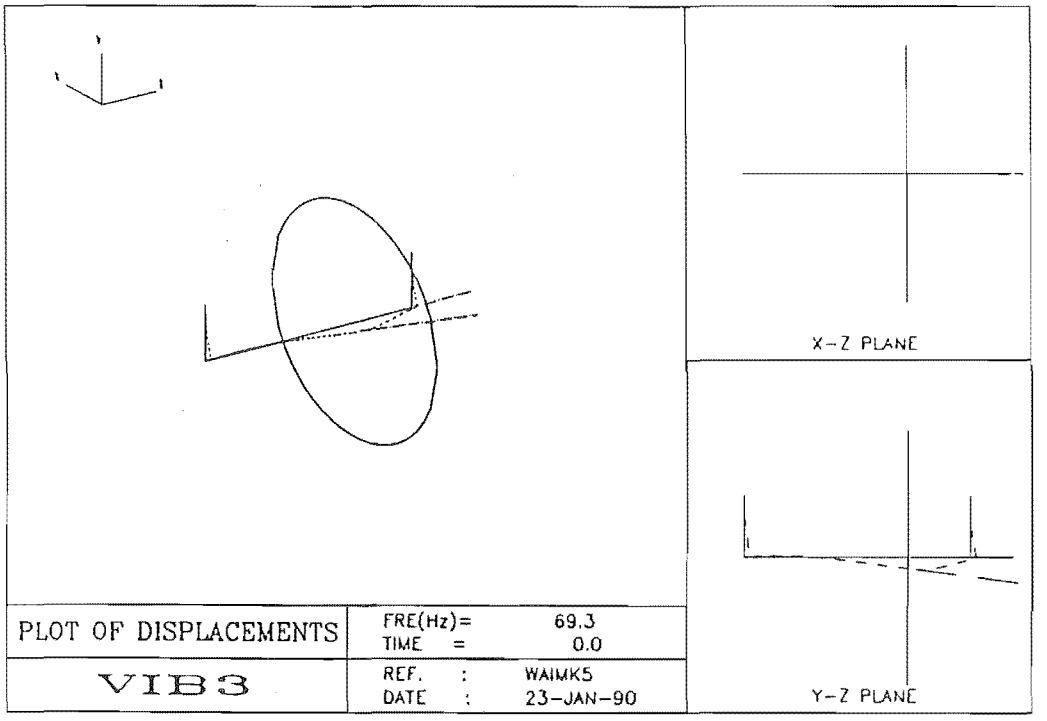

Figure 36: Fourth mode.

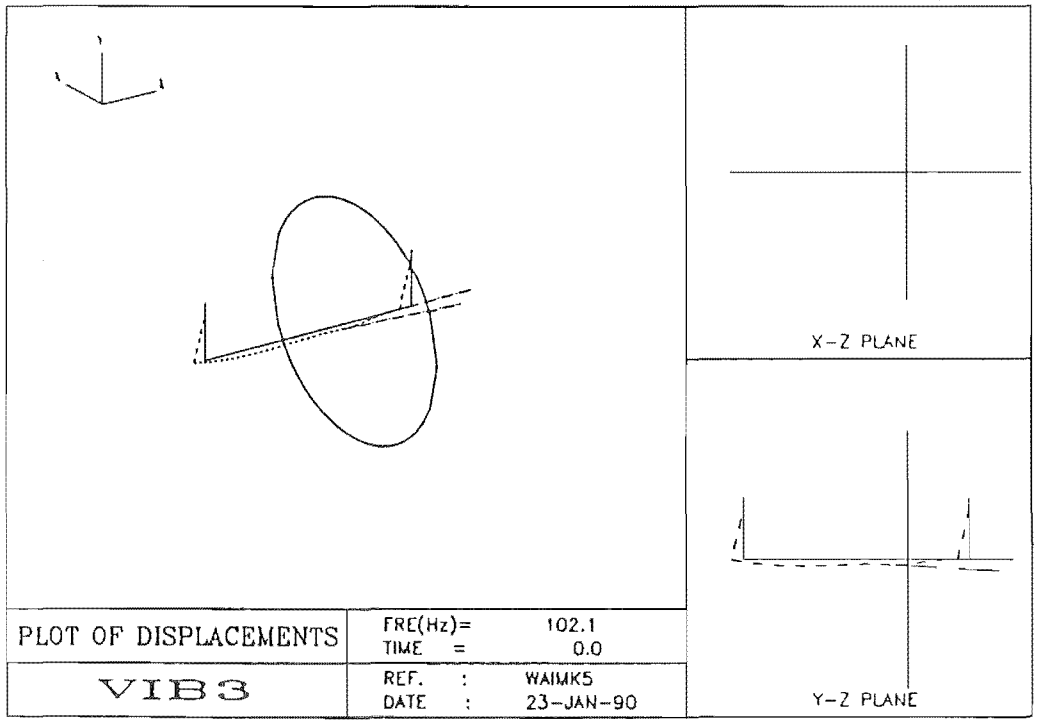

Figure 37: Fifth mode.

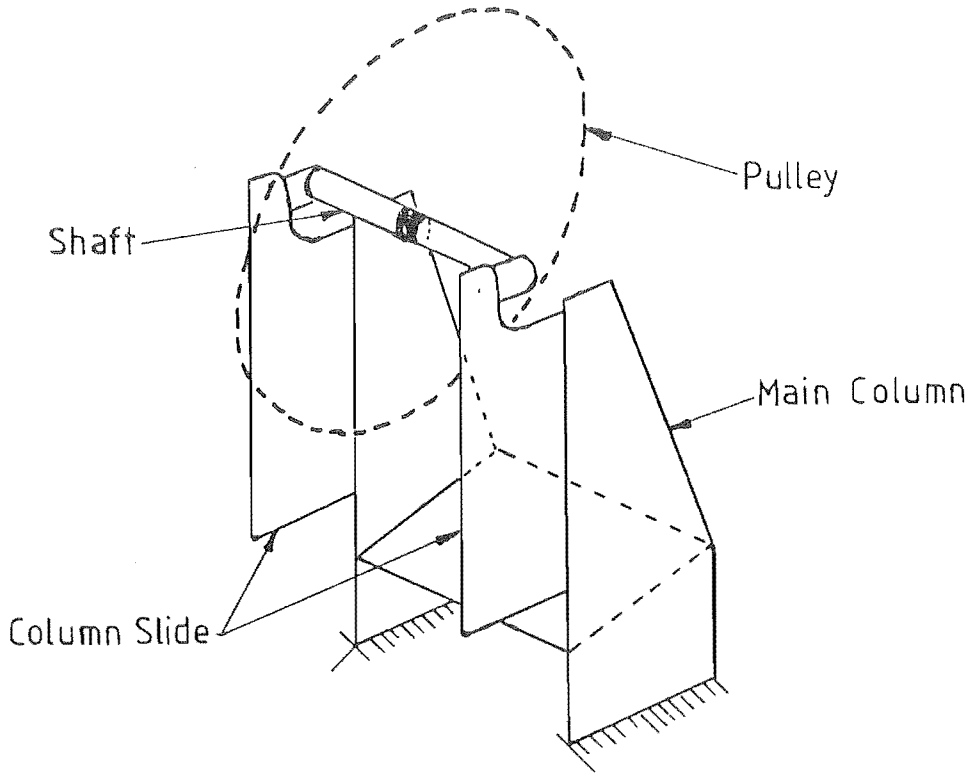

Figure 38: Main components of the section above the base.

5.4 Section Above the Base

As previously mentioned, this section of the bandsaw is far more complicated than a simple beam-structure. The programme VIB3 was, therefore, used only to explain some of the natural modes of the structure, the calculated natural frequencies were not expected to be close to the measured natural frequencies.

The main structural components of this section were the main column, the column slides, the top shaft, and the top pulley. Figure 38 simplifies the section above the base to only the main components of interest.

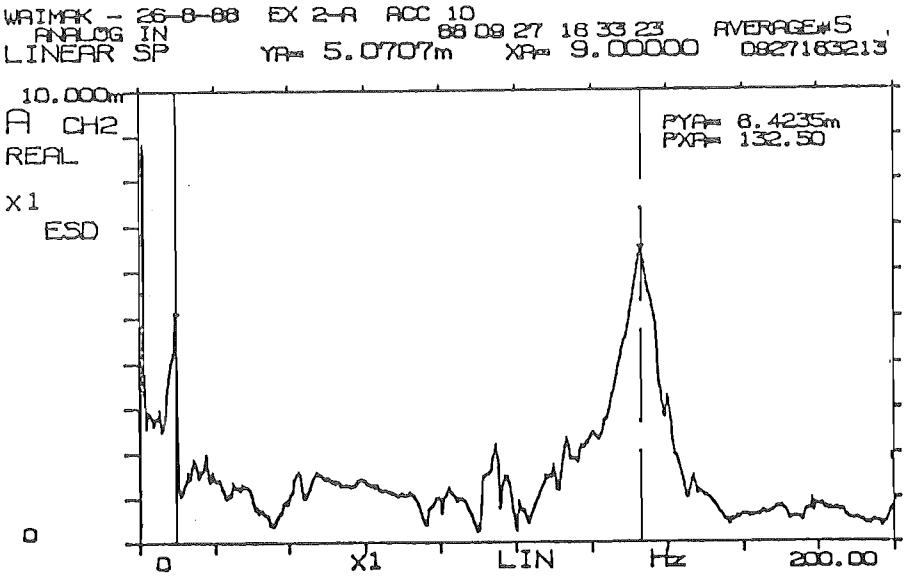

Figure 39: Frequency spectrum of the side-to-side transverse vibration.

5.4.1 Experimental Results

Frequency response functions were obtained for various positions of measurement and of excitation. These results were similar to those obtained from the frequency spectra of the transient response. This meant that the one parameter reading method was acceptable as the measurement method for these experiments. Figure 39 and Figure 40 show the frequency spectrum and the frequency response function measured on the left bearing housing in the axial direction of the shaft.

These plots show that the major natural frequencies, in the side to side vibrations, were the 9 Hz, 135 Hz, 260 Hz.

Figure 41 and Figure 42 show the frequency spectrum and the frequency response function measured in the to-and-fro transverse direction. These two graphs indicated that 21 Hz, 96 Hz and 157 Hz were the natural frequencies of the structure.

It was assumed that the stiffness of the column slides would not alter the flexural rigidity of the main column, because they were not rigidly attached to each other. Hence, the column slides were treated as masses only, which were attached to the

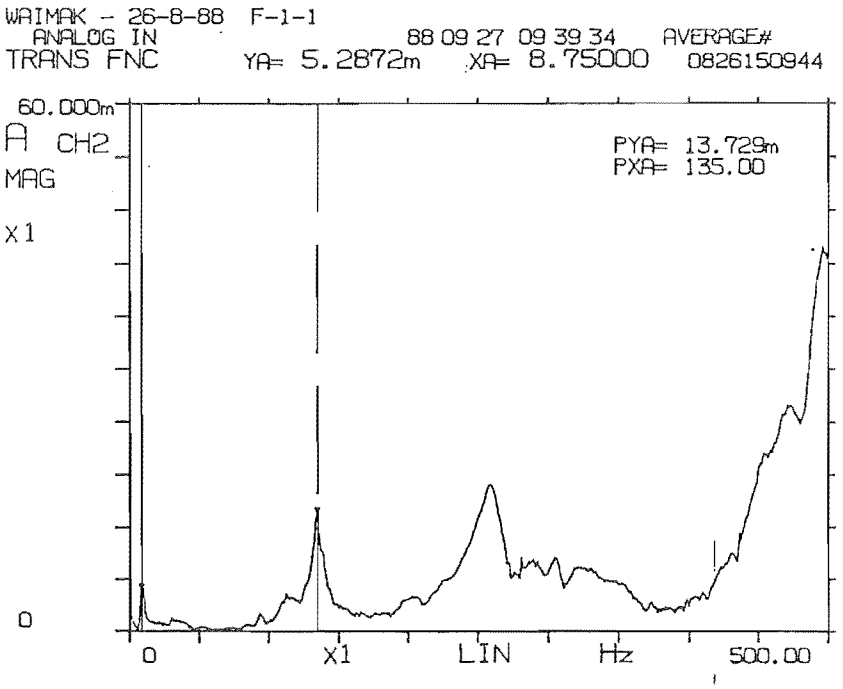

Figure 40: Frequency response function of the side-to-side transverse vibration.

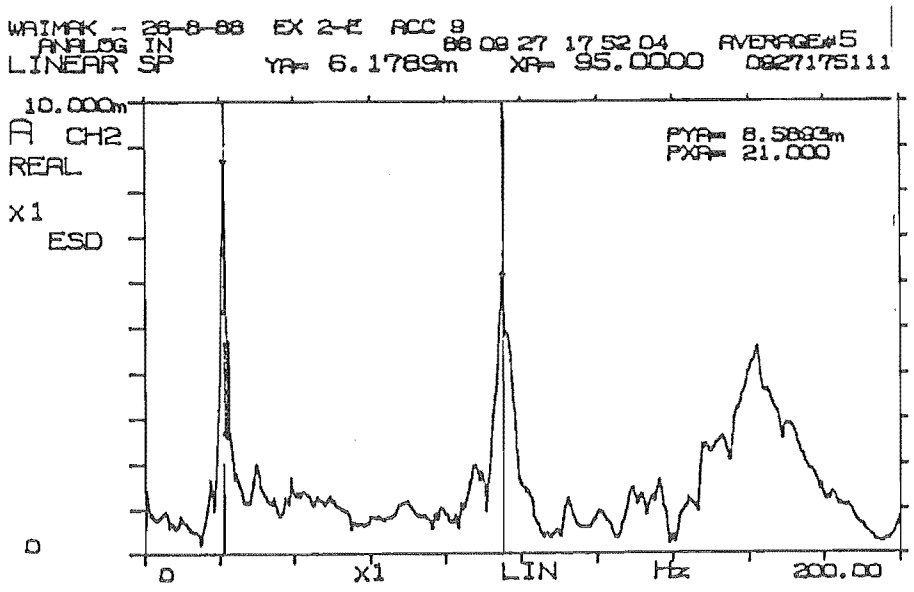

Figure 41: Frequency spectrum of the to-and-fro transverse vibration.

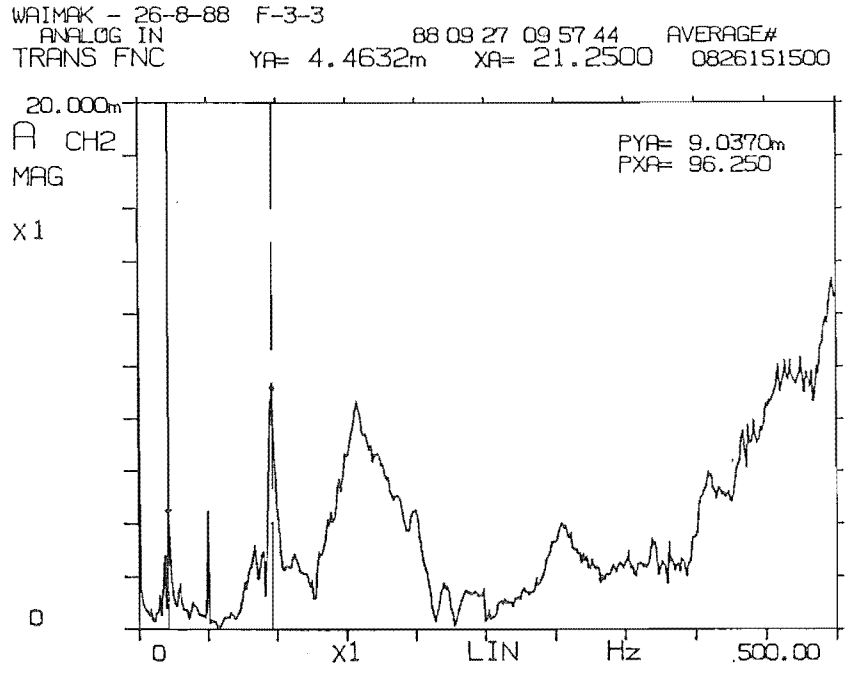

Figure 42: Frequency response function of the to-and-fro transverse vibration.

main column.

The most important natural frequency of this section was the 9 Hz frequency because it was very close to the 8 Hz rotational speed of the pulley.

For different measurement positions and excitation positions, the spectra showed many other minor peaks, which appeared to be due to the coupling effects of other attachments to bandsaw, such as the saw guide, the straining device.

The 9 Hz frequency was identified to be the torsional mode of the main column. The 20 Hz was an in-phase to-and-fro transverse vibration of the main column, while the 96 Hz was also a to-and-fro transverse motion, but the motion of the two vertical sections supporting the slider columns were 180 degrees out of phase with each other. The 135 Hz appeared to be a side-to-side transverse vibration.

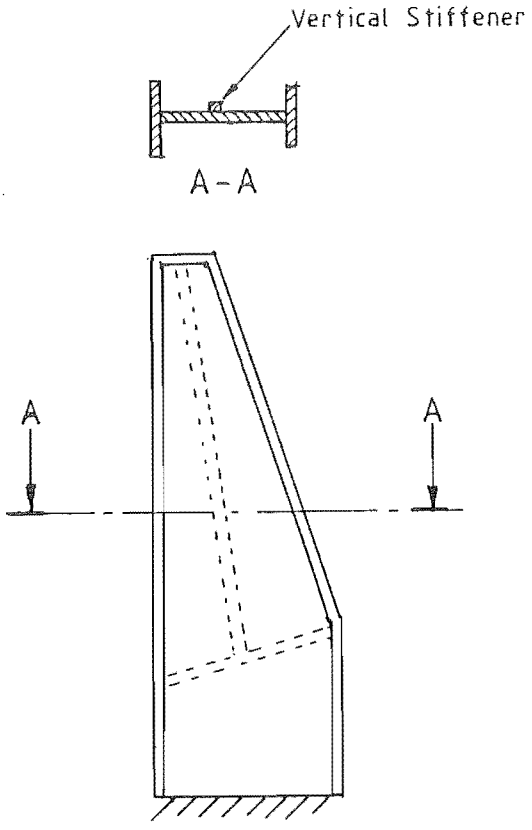

Figure 43: Main column.

5.4.2 Theoretical Analysis

A natural frequency of 9 Hz was very low for this structure, which meant that there was a very flexible component in the structure. Some considerations on the possible causes of this low natural frequency, by theoretical and experimental analyses, concluded that the most likely cause of this 9 Hz was the torsional vibration of the main column.

The main column consisted of two beams extending 1.5 m from the base, and a plate, which was welded between the two beams at about 0.5 m above the base, leaving 1 m free length on the beams (Figure 43). These two beams could be considered as tapered-I sections. The web thickness was only about .016 m.

As a preliminary test of the validity of the hypothesis of low torsional stiffness,

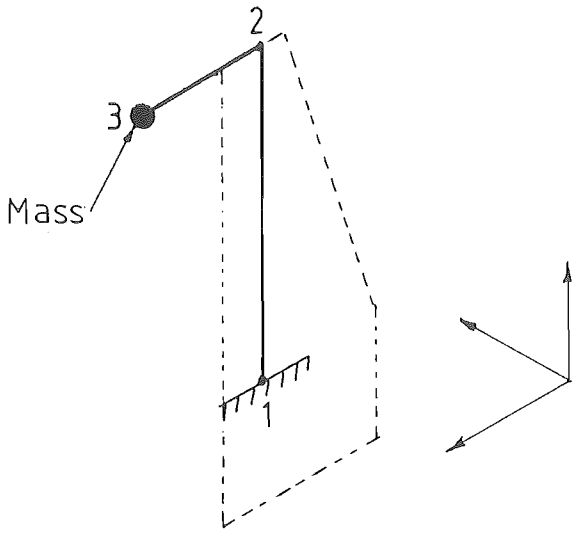

Figure 44: First model mesh.

a simple model of the main column was investigated. This simple model considered only one beam section of the main column. The mass of one slider column and half the mass of the top pulley was represented as a concentrated mass (Figure 44).

Figure 45,46, and 47 show the first three modes of this simple model. The first mode was, as expected, the torsional mode of the vertical beam, and the natural frequency was also very low. The second mode also matched with the second mode in the experiments, that is, the to-and-fro transverse mode. The 96 Hz obviously could not have been predicted by this model, because it would have required two beams to model the main column. The third mode in the theoretical analysis agreed with the 135 Hz in the experiments.

A more complete model of the structure was then analyzed, which took into account the whole structure of the main column and the inertia of the top pulley. The model mesh is shown in Figure 48 and the first five mode shapes are in Figures 49,50,51,52 and 53.

The first mode shape was again the torsional mode of the main column, and

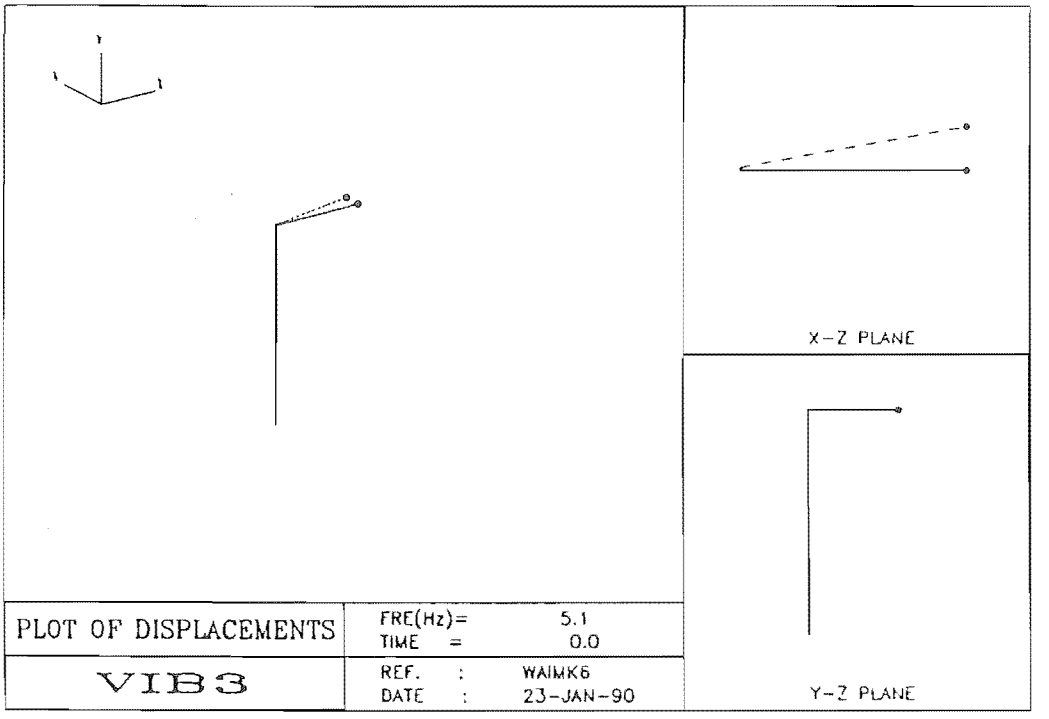

Figure 45: First mode shape of the first model.

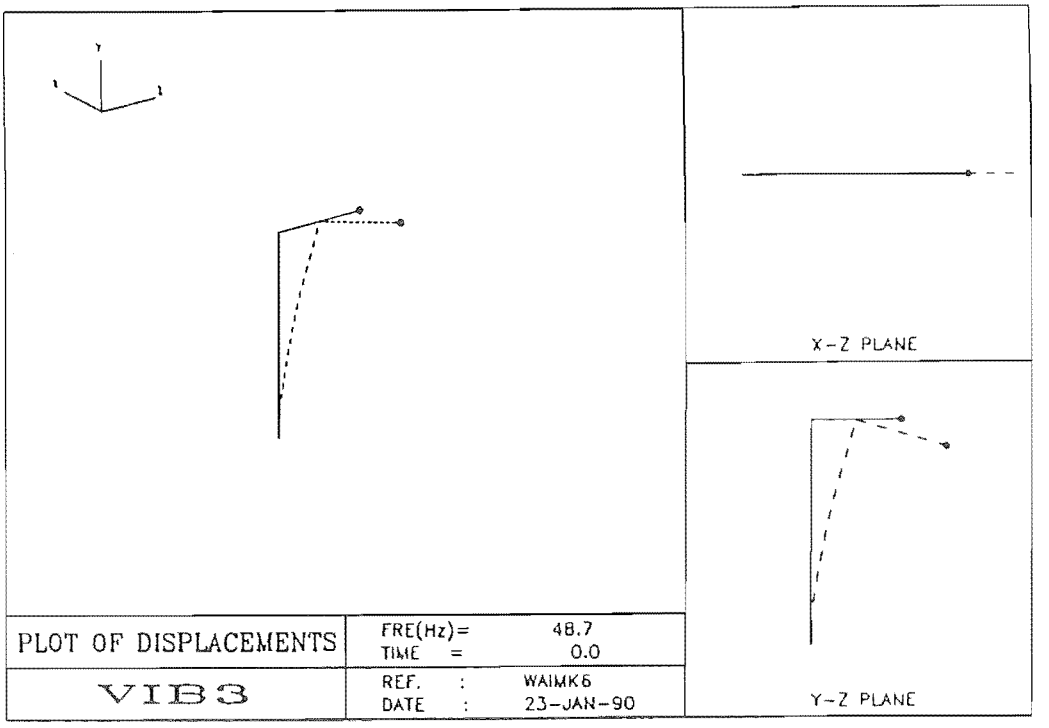

Figure 46: Second mode shape of the first model.

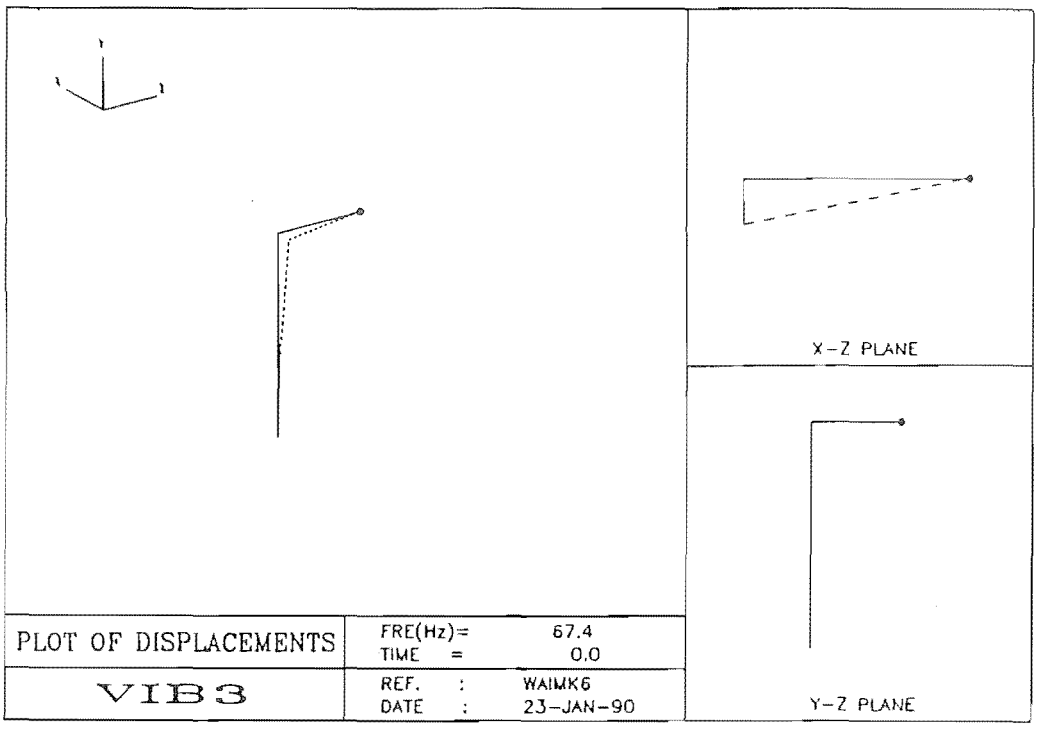

Figure 47: Third mode shape of the first model.

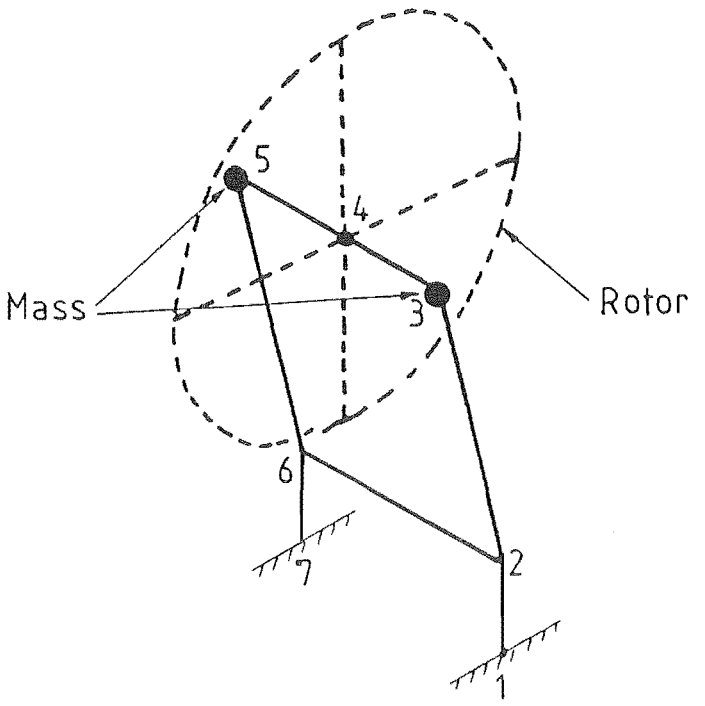

Figure 48: Second model mesh.

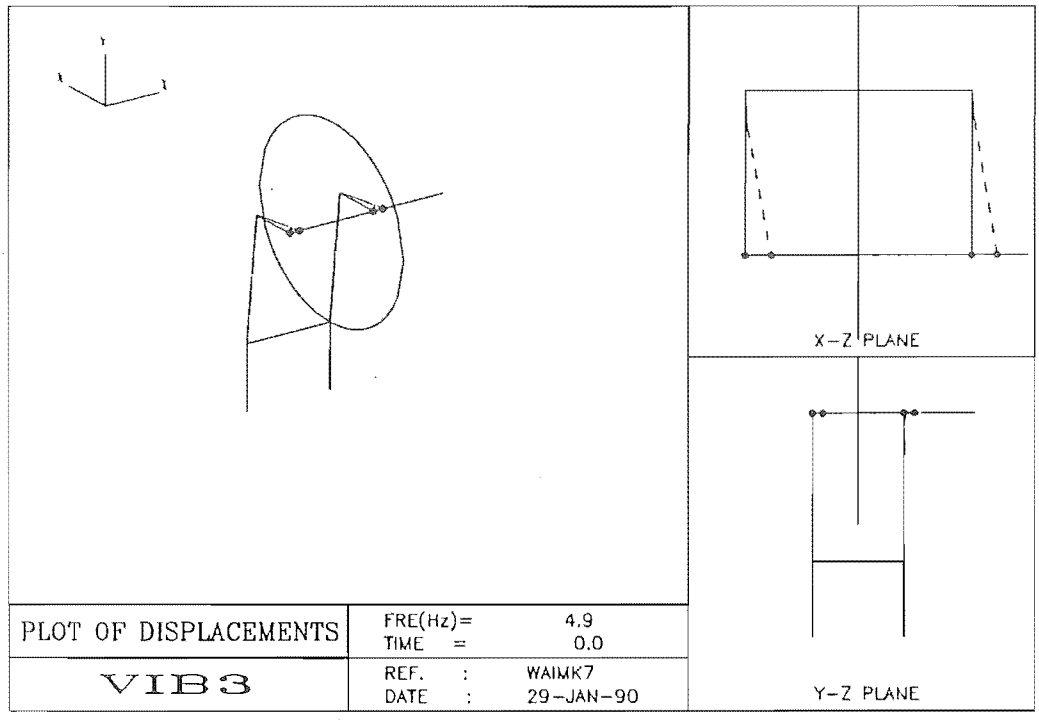

Figure 49: First mode shape of the second model.

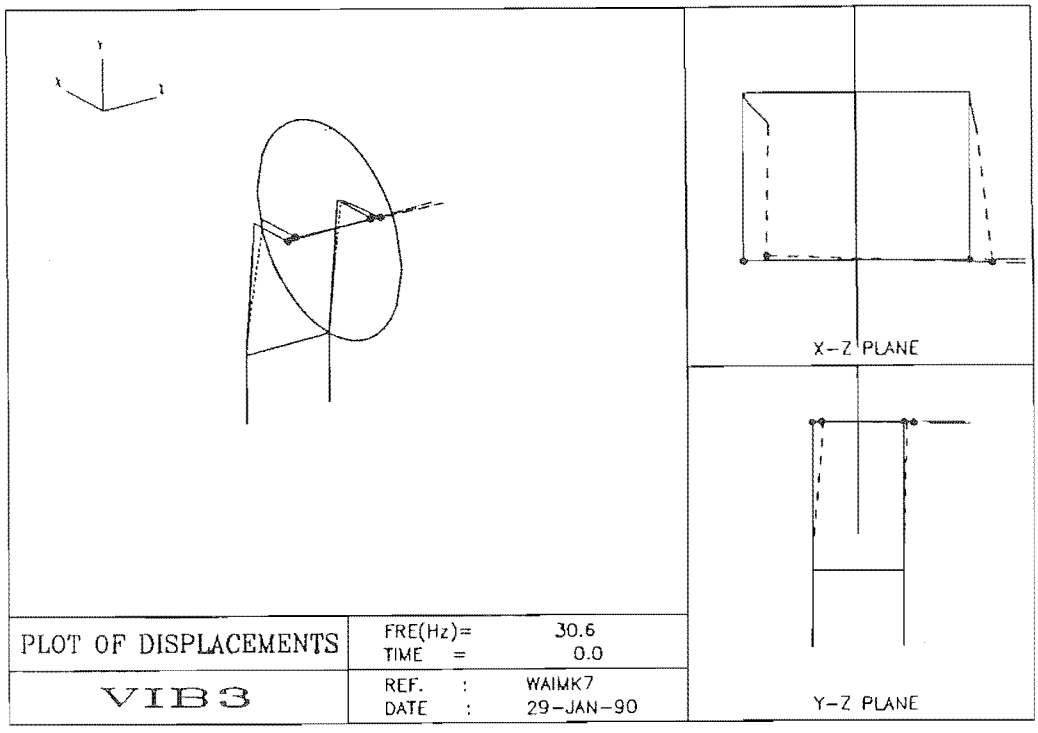

Figure 50: Second mode shape of the second model.

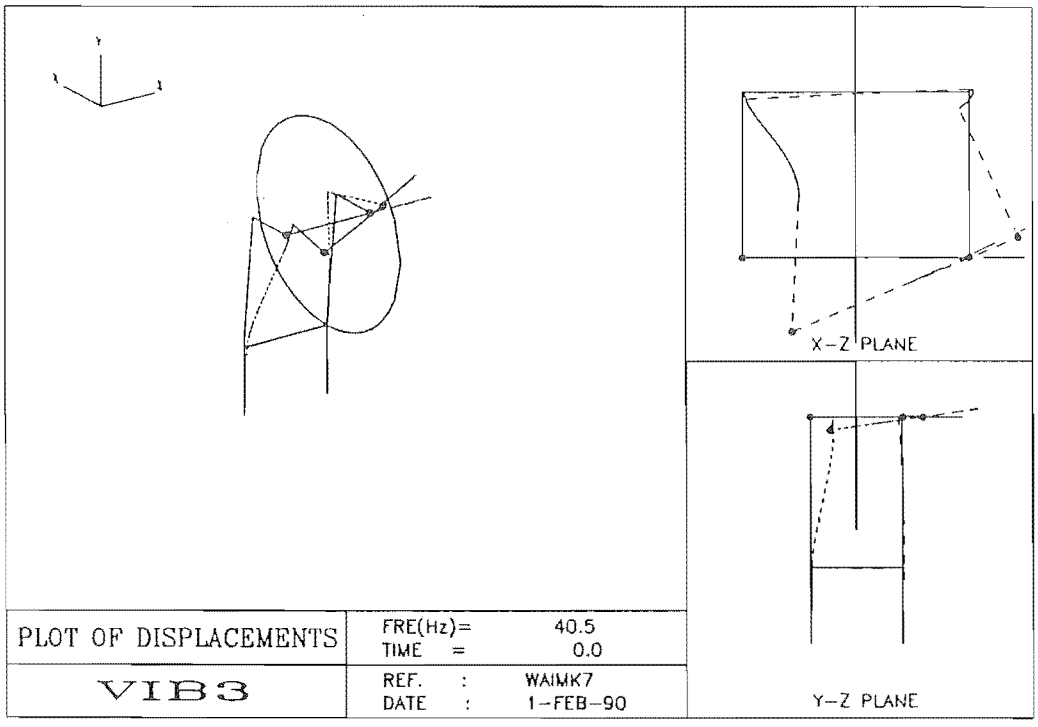

Figure 51: Third mode shape of the second model.

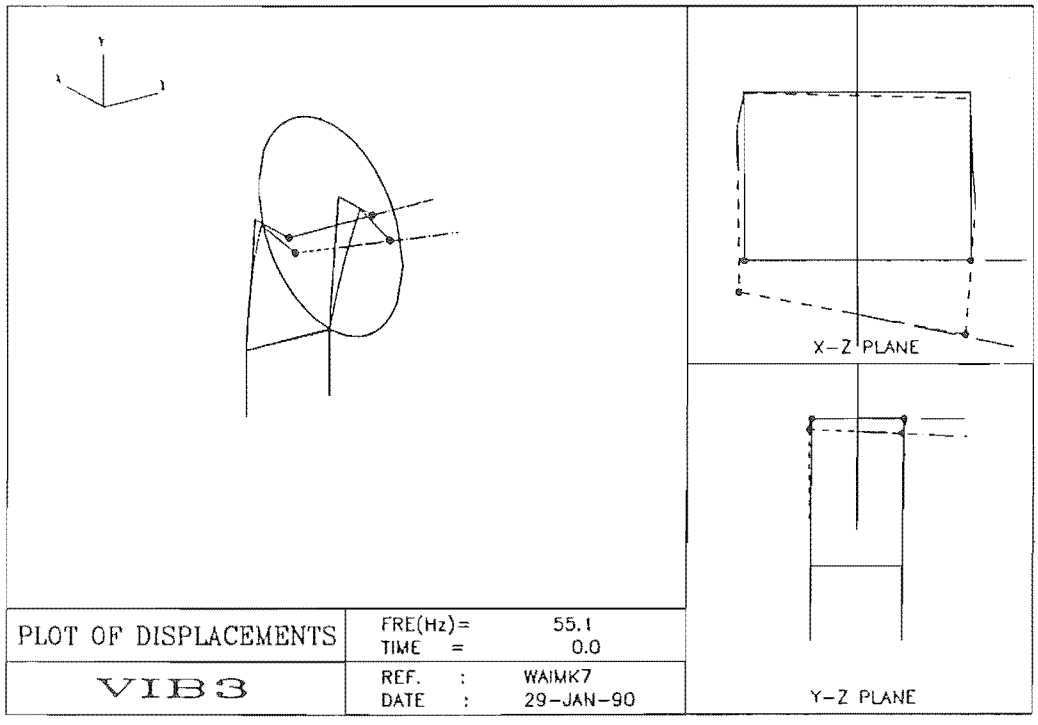

Figure 52: Fourth mode shape of the second model.

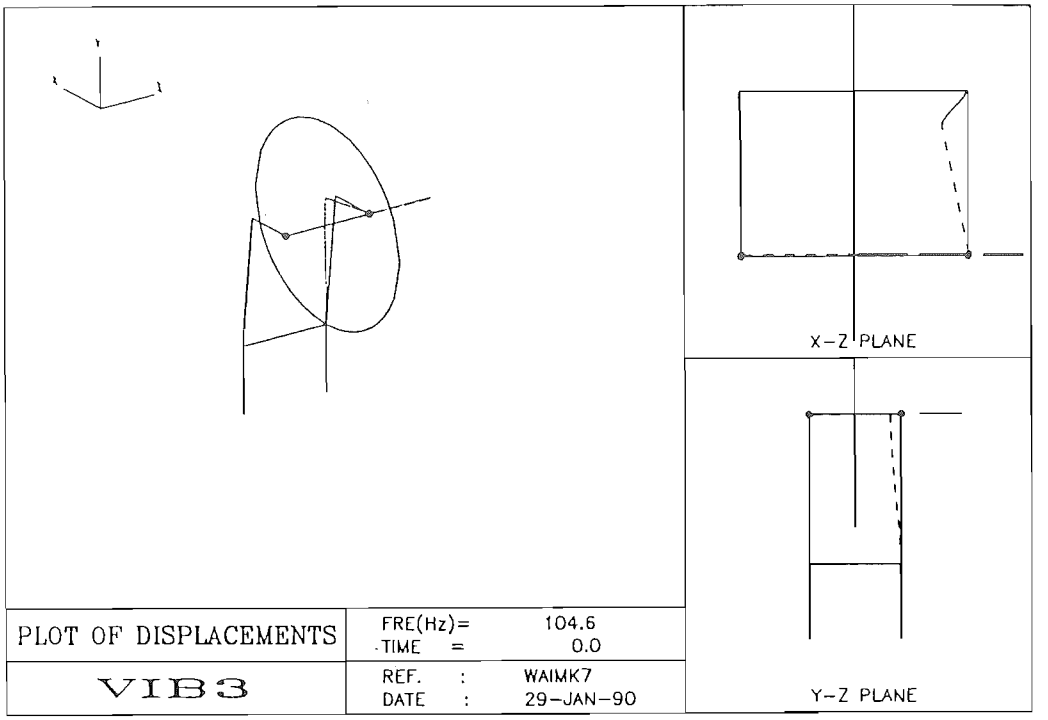

Figure 53: Fifth mode shape of the second model.

the associated natural frequency was 4.9 Hz. This mode shape was a very close representation of the 9 Hz measured natural frequency. The next natural frequency was at 30.6 Hz, which was a combination of the torsional mode on one vertical beam of the main column, and the transverse mode on the other. The third natural frequency was 40.5 Hz, with a coupled transverse-torsional mode. This mode shape appeared to match that of the measured 96 Hz natural frequency. The first to-and-fro transverse mode was at 55.1 Hz natural frequency, which related to the measured 21 Hz frequency. The fifth mode was the side-to-side transverse mode at 104.6 Hz frequency. The measured natural frequency for this mode was 136 Hz.

The theoretical model predicted all the modes of vibration observed on the Waimak bandsaw, and suggested one other, which was not realised at the time of the experiments. Although the third and fourth mode shapes were found in the experiments, their associated natural frequencies were quite different to those

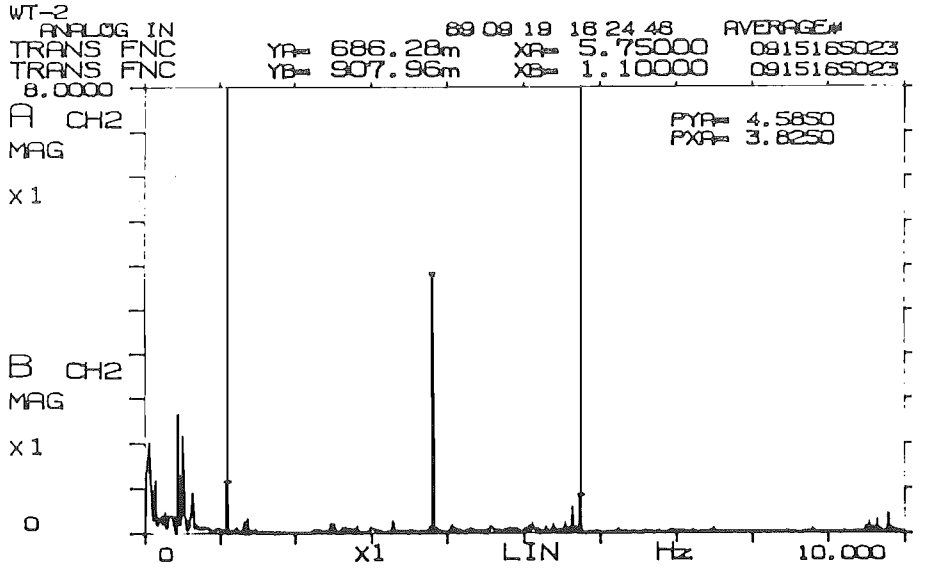

Figure 54: Frequency response function of the straining device, 0-10 Hz.

obtained experimentally.

5.5 Straining Device

The components of the straining device include the counterweight, the lever arm, the fulcrum shaft, and two compression rods. Figure 10 in Chapter 2 showed the assembly of a counterweight mechanism.

5.5.1 Experimental results

There was a low natural frequency, which related to the rigid body motion of the straining mechanism, that is, the vertical motion of the two top bearings. The stiffness was provided from the longitudinal stiffness of the saw blade, and the mass was a combination of the mass of the top pulley and the counterweight. Figure 54 showed that this oscillation was at 3.8 Hz and the width of the peak was very narrow which meant that there was little damping in the oscillation.

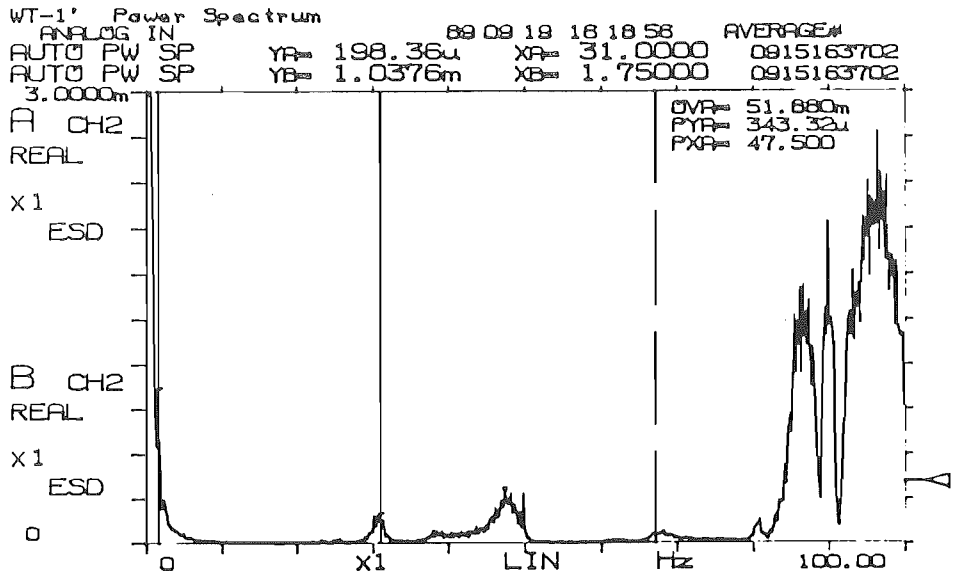

Figure 55: Frequency spectrum of the straining device, 0-100 Hz.

Figure 55 and Figure 56 show a frequency spectrum and a plot of the frequency response function of the vertical motion of the bearing housing for a range 0-100 Hz frequency. These two plots agreed that 31 Hz, 48 Hz, 87 Hz were the three dominant natural frequencies of the mechanism.

These vertical vibrations of the bearings would produce tension fluctuations in the saw blade, especially at 3.8 Hz because of large displacements. Other frequencies were also of interest because it was possible for the blade to become unstable at certain frequencies due to parametric excitation, as will be discussed in Chapter 10.

5.5.2 Theoretical Analysis

The low frequency vertical oscillation of the top pulley could be modelled accurately by representing the structure of the straining mechanism as a simple spring-mass system. The fulcrum shaft, the two compression rods and the top shaft could be assumed to be rigid for this low frequency oscillation, hence could be removed from the model. This assumption reduced the system to two masses and a spring as in

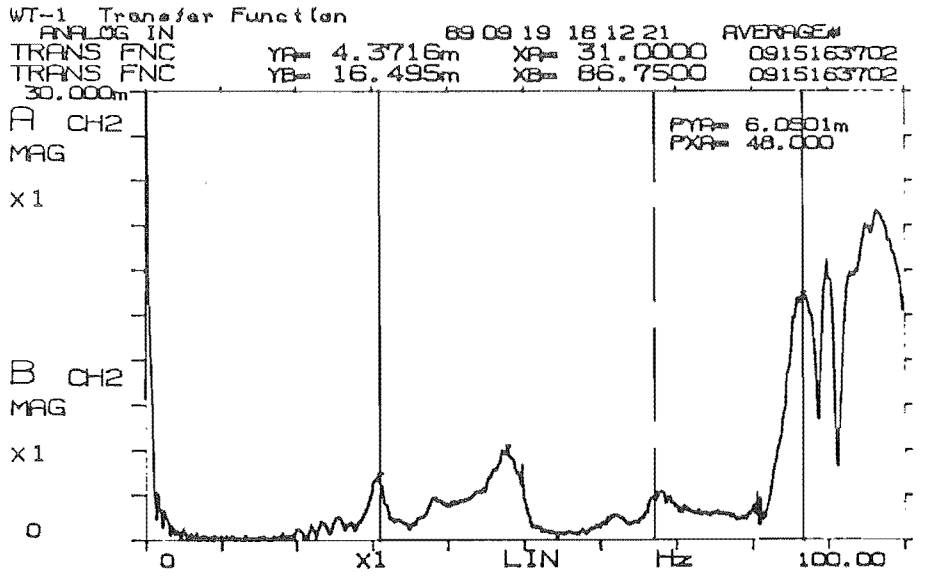

Figure 56: Frequency response function of the straining device, 0-100 Hz.

Figure 57. Mass m_1 was the mass of the counterweight (85 kg), mass m_2 was the mass of the top pulley, the shaft, the bearings and the bearing housings (approximately 600kg), and the spring stiffness could be approximated from the longitudinal stiffness of the non-cutting and cutting spans of the blade, $k = \frac{EA}{L}$, where E was the Young's modulus, A was the cross-sectional area of the blade and L was the length of the blade, and for this case

$$k = \frac{2 \times 200 \times 10^9 \times 0.22 \times 0.00165}{2.29} = 63.4 \times 10^6 \text{ N/m}$$

The natural frequency of the system, ω, was given as

$$\omega = \sqrt{\frac{k}{\left(\frac{a}{b}\right)^2 m_1 + m_2}} \tag{34}$$

For the Waimak bandsaw, $\frac{a}{b} = 42$, hence $\omega = 20.5$ rad/s, or 3.3 Hz. This was very close to the measured frequency of 3.8 Hz.

This analysis showed that the 3.8 Hz frequency of oscillation could be altered by choosing appropriate magnification ratio of the lever arm, $\frac{a}{b}$, and the mass of

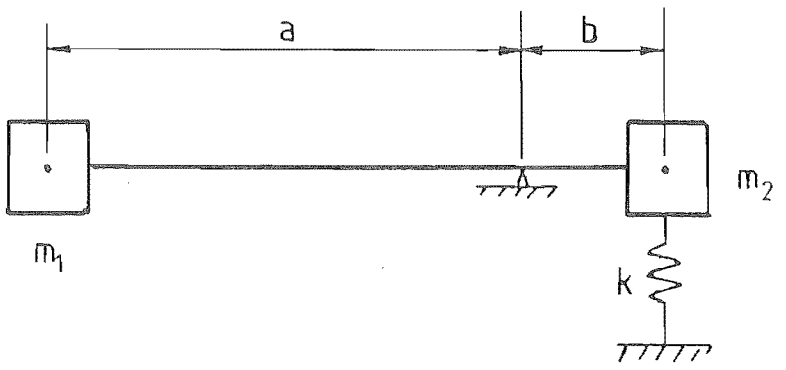

Figure 57: Model to represent the rigid body mode of the straining device.

the counterweight, m_1. For example, if $\frac{a}{b}$ was reduced to 21 instead of 42, then m_1 has to be 170 kg instead of 85 kg to produce the same amount of strain on the saw blade, and the natural frequency becomes 4.6 Hz instead of 3.3 Hz. Although this oscillation of the counterweight had not been under any investigation, it was possible that shifting the natural frequency could improve the cutting performance of the saw blade, and this could be achieved by a simple alteration to the existing bandsaw.

The other frequencies that appeared in the spectrum were related to the structural vibrations of the components in the mechanism. The programme VIB3 showed that the dynamics of the components of the straining mechanism were uncoupled, hence they could be considered individually.

For the lever arm, the calculated first natural frequency in the vertical direction was found to be 226 Hz (by considering it as a pinned-free beam with a mass at the free end). The first frequency of the lever arm in the horizontal direction was only about 4 Hz, however, this vibration would not affect the vertical motion of the bearings.

The torsional and transverse vibrations of the fulcrum shaft were also considered as possible causes of the vertical vibrations of the bearings. It was difficult to

establish the end conditions for the fulcrum shaft, but for various combinations of the end conditions, the first torsional frequency seemed to be always greater than 150 Hz. The calculated first transverse frequency of the fulcrum shaft was 196 Hz.

A simply-supported beam under constant longitudinal compression was used to model the transverse vibration of the strain bar, and the calculated first natural frequency was 88 Hz. The longitudinal vibration of the strain bar was also considered, however, the calculated first frequency was found to be greater than 120 Hz.

These considerations only explained the 87 Hz frequency in the experimental spectrum as the the first transverse frequency of the strain bar. At this stage, the cause of the 31 Hz and 48 Hz have not been found. However, the vibration of the column slide in the vertical direction, the connections between the bearing housings and the column slides, and the connection between the lever arm and the fulcrum shaft are suspected to be the possible causes of the 31 Hz and the 47 Hz frequencies.

5.6 Theoretical Study of the Gyroscopic Effects on Bandsaw Structure

Gyroscopic motion has always been a very interesting subject in the field of dynamics, and its effects are important in considerating the design of rotating machinery. In structural vibration problems, gyroscopic effects can couple flexural modes of vibration and hence alter the natural frequencies of the system.

The bandsaw consists of two gyroscopic systems; the top pulley and the bottom pulley. The previous sections have considered the structural natural frequencies of the Waimak bandsaw when both pulleys were stationary. Under idling condition, the gyroscopic effects of the pulleys on the structure may alter the vibrational characteristics of the bandsaw, hence they must be examined. The programme VIB3

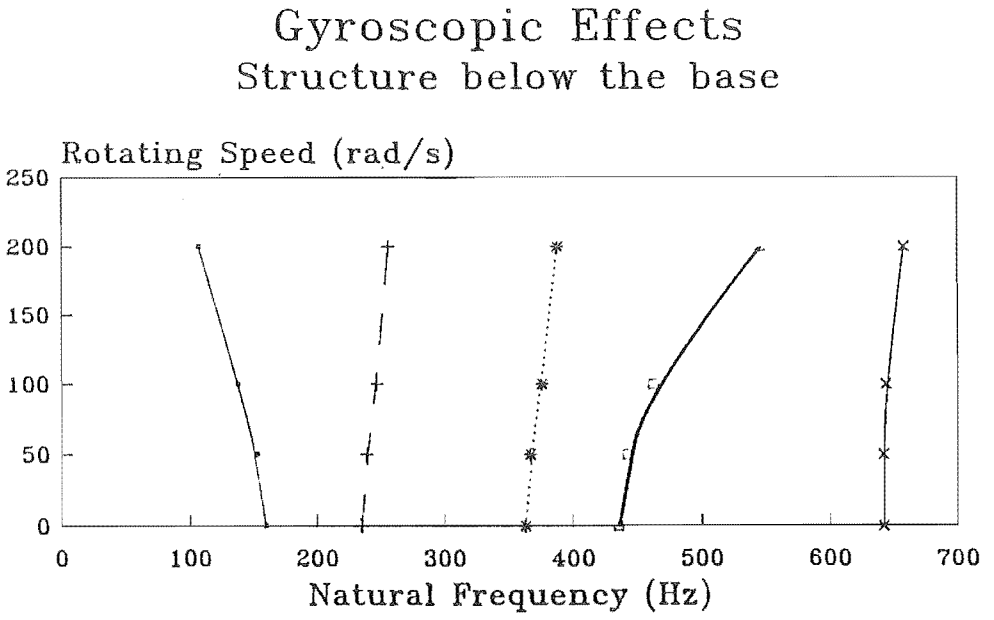

Figure 58: The variation of the natural frequencies, ω_i, of the bandsaw structure below the base, with pulley rotating velocity, Ω.

provided a useful analytical tool for this investigation.

5.6.1 Structure Below the Base

The model considered in Section 5.3.2 was used to see the effects on the natural frequencies of the structure below the base for various rotating speeds of the pulley. A graph showing the results is in Figure 58.

The graph shows that only the first natural frequency ω_1 decreases as the rotating speed Ω increases, which means that the gyroscopic effects soften the first mode and stiffen the remaining four modes of vibration. However, the actual idling speed of the Waimak bandsaw was about 50 rad/s (8 Hz), and the gyroscopic effects only alter the natural frequencies by 1 Hz or less, hence they can be considered as negligible.

5.6.2 Structure Above the Base

The main flexural component of the structure below the base was the shaft, which was parallel to the axis of rotation of the pulley. For the structure above the base, the main column was the main flexural component and was perpendicular to the axis of rotation of the top pulley. The behaviour of the structure above the base due to the rotating pulley was, therefore, expected to be different from the behaviour described in the previous section.

Figure 59 shows the effects of varying the rotating speed on the natural frequencies of the second model in Section 5.4.2. The second, third and fourth natural frequencies decreased as the rotating speed increased, the first natural frequency remained the same, and the fifth natural frequency increased as the speed increased. The rotating pulley did not affect the first mode because its motions did not produce any rotation of the spin axis about another axis, hence there was no gyroscopic coupling effect.

Again, at 50 rad/s rotating speed, the gyroscopic effects were very small, shifting the natural frequencies by less than 1 Hz.

5.7 Experimental Results of the Structural Vibrations of Bandsaw under Idling Conditions

The vibrations of the Waimak bandsaw during idling were measured to provide information about the nature of the bandsaw under normal operating condition. Only the top section of the bandsaw was considered in the experiment.

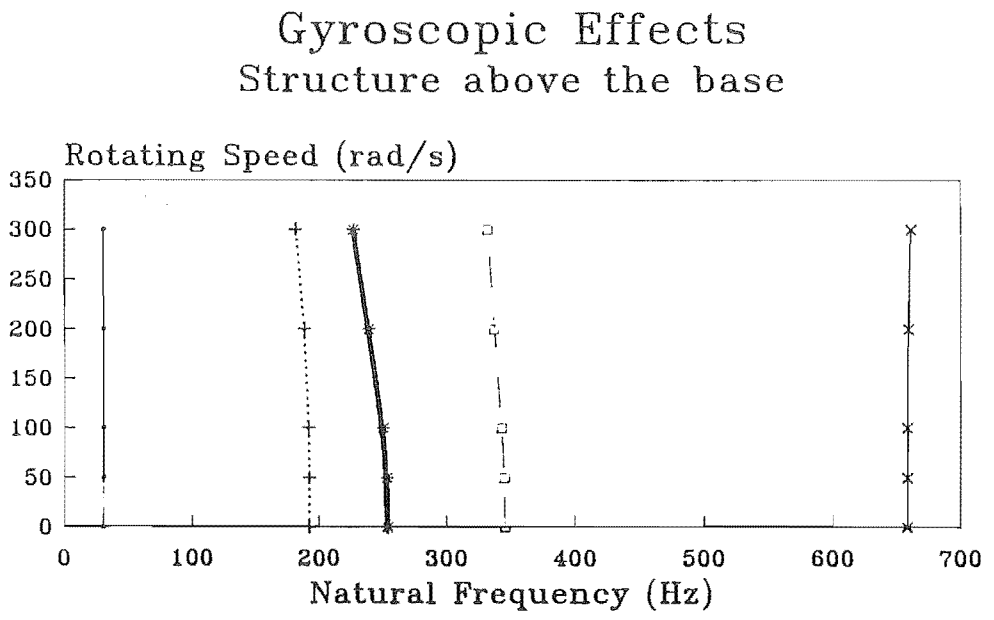

Figure 59: The variation of the natural frequencies, ω_i, of the bandsaw structure above the base, with pulley rotating velocity, Ω.

5.7.1 Results

The spectra of the vibration measurements at the top bearing in three directions are given in Figure 60,61, and 62.

All three spectra show the same characteristic, namely the presence of the 8 Hz frequency and its harmonics. However, the magnitudes of the harmonics were different in different directions. In the vertical direction the highest harmonic peak was at 47.5 Hz. The harmonic was at 47.5 Hz and not 48 Hz because the rotating speed of the pulley was not exactly 8 Hz, and the analyser could only resolve to 0.5 Hz in the 0 Hz-200 Hz frequency range. In the to-and-fro vibrations, the 23.5Hz frequency had the highest peak, and in the side-to-side vibrations, the 8 Hz was the dominant one. There were also high peaks at 50 Hz and 150 Hz, but they were probably mains frequency induced.

Obviously the forcing harmonic closest to a natural frequency of the structure

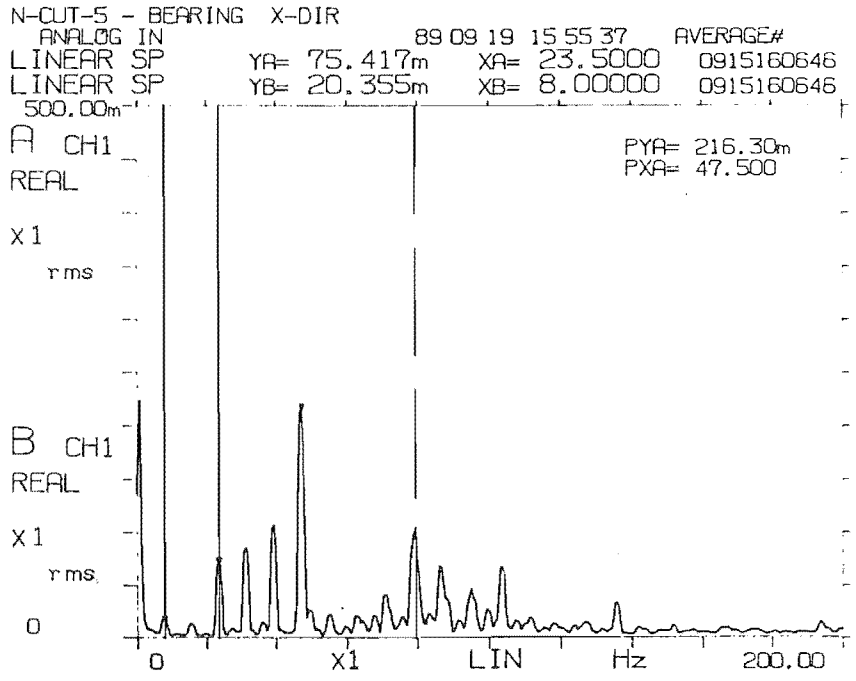

Figure 60: Spectrum of the vibration during idling in the vertical direction.

would excite a higher response amplitude than other harmonics. In the vertical direction 47 Hz had been identified as a natural frequency, which agreed with the 47.5 Hz highest harmonic. The 9 Hz side-to-side transverse natural frequency amplified the 8 Hz harmonic of the spectrum under idling condition, and the 21 Hz to-and-fro transverse natural frequency enhanced the 24 Hz harmonic.

5.7.2 Explanations

These spectra are typical of the vibrational characteristics of rotating machinery. There are many reasons for the the presence of the harmonics in the spectra, such as the imbalance of rotating parts, defects in the bearings, misalignment of shafts, and mechanical looseness [31, page 23].

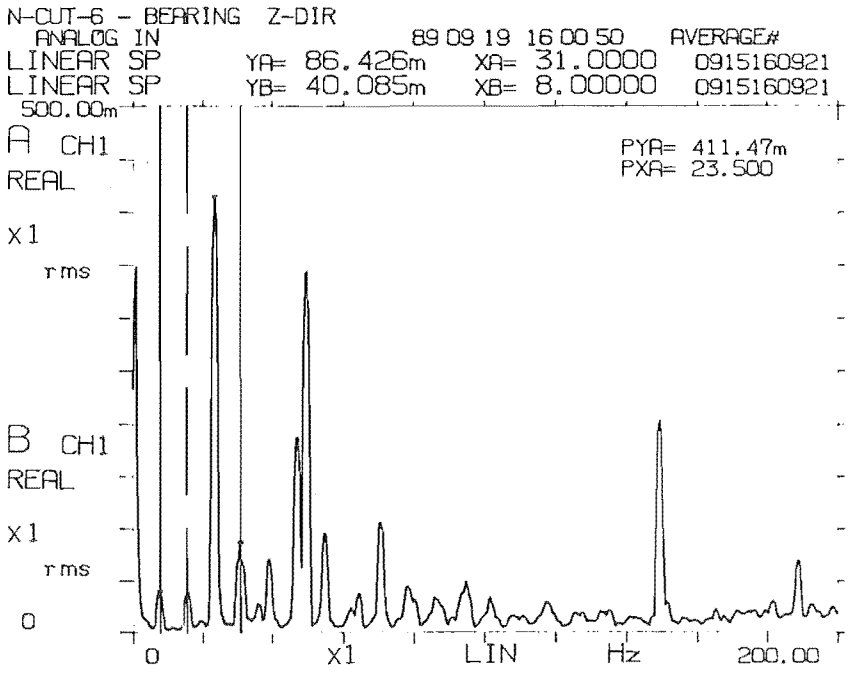

Figure 61: Spectrum of the vibration during idling in the to-and-fro direction.

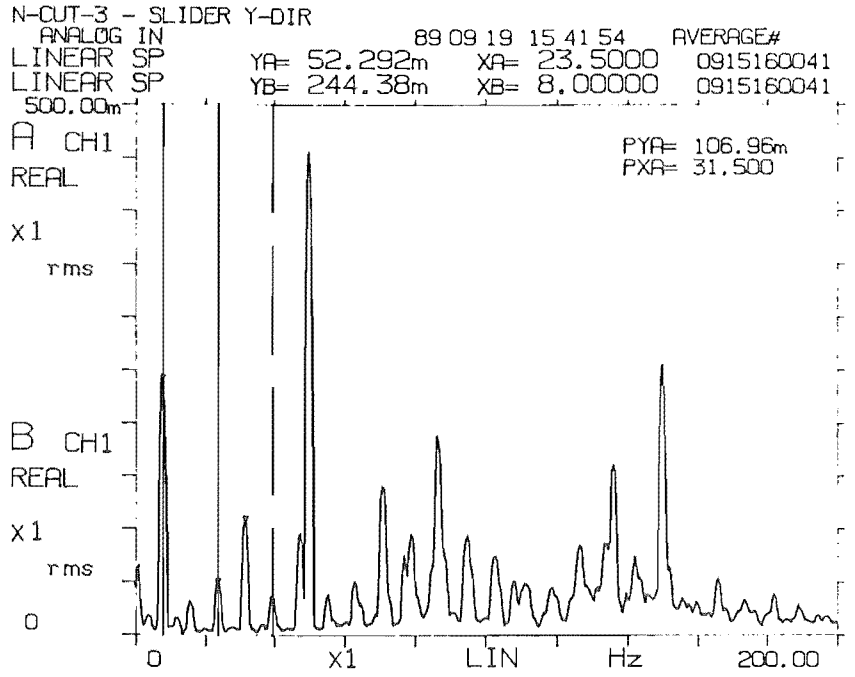

Figure 62: Spectrum of the vibration during idling in the side-to-side direction.

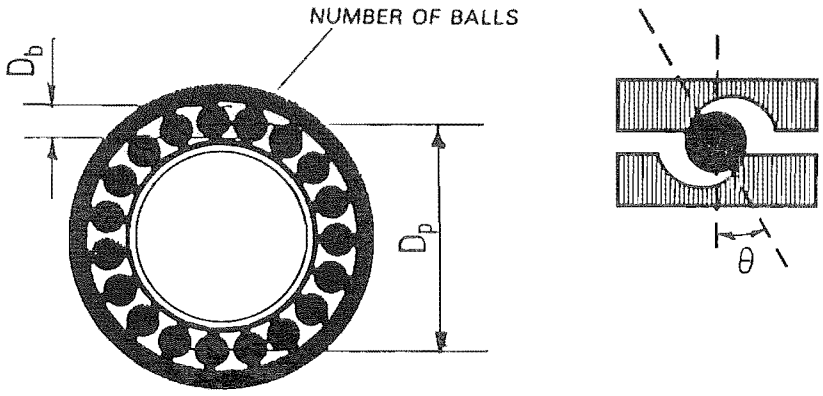

Figure 63: Bearing dimensions.

Imbalance

Imbalance of the pulley always exists to some degree in all bandsaws, and is characterised by sinusoidal vibration at the frequency of rotation, that is, the 8 Hz frequency for the Waimak bandsaw. The vibration caused by pure imbalance is sometimes accompanied by low-level harmonics but not the high-level harmonics. This fact rules out imbalance of the pulley as a fault in the Waimak bandsaw. Another reason for this conclusion is that the magnitudes of 8 Hz frequency in the vertical and to-and-fro directions were very low compared with the other harmonics.

Bearing Defects

The unique vibration characteristics of rolling element bearing defects make vibration analysis an effective tool for the detection of those defects.

The specific natural frequencies that result from bearing defects depend on the defect, the bearing geometry, and the speed of rotation. The required bearing dimensions are the number of balls N, the ball diameter D_b, the pitch diameter D_p and the contact angle θ (Figure 63).

For the '22222 K.H.L. h322' 200 mm spherical roller bearing used on the Waimak

bandsaw, there were 19 rollers around the circumference of the bearing, the diameter of the rollers was 22 mm, the pitch diameter was 150 mm and the contact angle could assumed to be 0 degrees.

The bearing characteristic frequencies were:

- The outer ball pass frequency f_o, which is the frequency caused by a defect on the outer race of the bearing

$$f_o = \frac{N}{2}\left(\frac{\Omega}{2\pi}\right)\left(1 - \frac{D_b}{D_p}\cos\theta\right) \tag{35}$$

  where Ω is the rotational velocity in rad/s.

- The inner ball pass frequency f_i, which was the frequency caused by a defect on the inner race of the bearing

$$f_i = \frac{N}{2}\left(\frac{\Omega}{2\pi}\right)\left(1 + \frac{D_b}{D_p}\cos\theta\right) \tag{36}$$

- The ball spin frequency f_b, which was the frequency caused by a defect on one of the balls or rollers

$$f_b = \frac{D_p}{2D_b}\left(\frac{\Omega}{2\pi}\right)\left(1 - \left(\frac{D_b}{D_p}\right)^2\cos^2\theta\right) \tag{37}$$

- The fundamental train frequency f_t, which occurs at a frequency lower than the rotation speed, and is usually caused by a severely worn cage

$$f_t = \frac{\Omega}{4\pi}\left(1 - \frac{D_b}{D_p}\cos\theta\right) \tag{38}$$

For the Waimak bandsaw, f_0 was 64.8 Hz, f_i was 87.2 Hz, f_b was 26.7 Hz and f_t was 3.4 Hz.

These frequencies did not appear in the spectra, hence bearing defects were not considered to be at fault in the Waimak bandsaw.

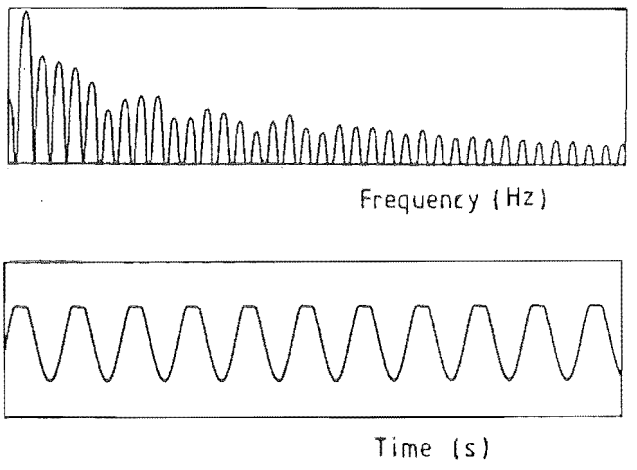

Figure 64: Frequency spectrum of a truncated sine wave.

Misalignment

Misalignment takes two basic forms, preload from a bent shaft or improperly seated bearing, and offset of the shaft centre lines of machines in the same train.

Vibration due to misalignment is usually characterised by a component at twice the running speed and a high level of axial vibrations. The spectra did not have a high 16 Hz component, and the levels of vibration in the axial direction (side-to-side motion) were similar to the other directions, therefore, misalignment could safely be dismissed as a fault of the Waimak bandsaw.

Mechanical Looseness

Mechanical looseness, generally referred to as nonlinearity, almost always results in a large number of harmonics in the vibration spectrum. The mechanism for producing harmonics is the truncation of the response caused by looseness. The Fourier transformation of a truncated sine wave is shown in Figure 64.

Mechanical looseness appeared to be the most practical explanation for the bandsaw harmonics. The slackness between the column slides and the main column, the

joints between the top bearing housings and the column slides, and the contacts between the top saw guide and the column slides are the prime suspects of the mechanical looseness on the Waimak bandsaw. However, more experimental work is needed to verify this point, and to suggest possible solutions to the troublesome vibration of the bandsaw.

Chapter 6

THEORETICAL ANALYSIS OF THE TRANSVERSE VIBBRATION OF A MOVING BANDSAW BLADE

6.1 Introduction

Excessive structural vibrations have detrimental effects on the bandsaw as a whole, however, the most significant impact of the vibrations is on the cutting process. The result of vibrations is poor cutting accuracy, wastage of raw material, and a decrease in the production rate. The main offender is the part of the bandsaw that has immediate contact with the timber, the cutting span of the saw blade. This, rightly enough, had been the only area of research on bandsaw vibrations for the last twenty-five years, but until now it had not been very well understood and as pointed out by Ulsoy and Mote in 1982 [87] that '*the performance criterion, relating*

band design, probably represented though the spectrum, to the band performance as a cutting tool remains unresolved'. One main reason for this is because the mechanism of cutting wood has not been thoroughly examined. Given the present technology, the wood cutting mechanism could be investigated in much more detail. A suggested method of analysis would be to model the tooth of the saw blade and the work piece independently, by using the FEM, then to analyse the case when the two models were moved into each other. This method has been mentioned by Grönlund in 1988 [26] but it was pointed out that *work with this model is at present far from complete.*

Until the wood cutting mechanism is well understood, then and only then, the design of a bandsaw blade as a cutting tool can be studied. The wood cutting mechanism is, therefore, a very important research area, unfortunately, it was realised quite late, hence out of the scope for this thesis. Instead, the effects of cutting on the stability of bandsaw blade was studied with fictitious cutting forces as in Section 9.6.

The cutting span of the saw blade has been modelled as a moving thin beam and as a moving plate. The two most popular techniques, used by saw blade designers to calculate the natural frequencies of the blade, are the flexible band approximation [52,53] and the FEM [6]. The flexible band approximation can be used for hand calculations but only for simply-supported beams. The FEM can handle more complicated boundary conditions but a computer is needed for the calculations. This chapter presents another method of analysis, the dynamic stiffness method. The advantages of this method over the FEM had been discussed in Chapter 4.

6.2 Dynamic Stiffness Method Applied to Moving Beams

Because the main objective of this chapter is to illustrate an alternative method of solution for the moving beam, the derivation of the problem is given in Appendix B. A full derivation of the moving plate problem will be presented in the following chapters and is analogous to the moving beam problem.

The equation of motion that described the transverse vibration of a moving thin beam under transport speed[1] dependent tension is

$$EI\frac{\partial^4 v}{\partial x^4} + \rho A\frac{\partial^2 v}{\partial t^2} + 2\rho Ac\frac{\partial^2 v}{\partial x \partial t} + \left((1-\eta)\rho Ac^2 - R_0\right)\frac{\partial^2 v}{\partial x^2} = 0 \tag{39}$$

and the boundary conditions are

$$v = 0 \quad \text{or} \quad EI\frac{\partial^3 v}{\partial x^3} + \left((1-\eta)\rho Ac^2 - R_0\right)\frac{\partial v}{\partial x} + \rho Ac\frac{\partial v}{\partial t} = 0 \tag{40}$$

$$\frac{\partial v}{\partial x} = 0 \quad \text{or} \quad EI\frac{\partial^2 v}{\partial x^2} = 0 \tag{41}$$

where v, x, t, E, I, ρ, A are the usual symbols for beam transverse vibration, c is the transport speed of the beam and η is a constant denoting the type of straining device.

The reasons for the terms containing c will be discussed in Chapter 8, and for the term containing η is in Chapter 9.

Now, assume a separable solution of the form

$$v(x,t) = V(x)\, e^{i\omega t} \tag{42}$$

and substitute into Equation (39) to give

$$EI\frac{d^4 V}{dx^4} - \rho A\omega^2 V + 2\rho Ac(i\omega)\frac{dV}{dx} + \left((1-\eta)\rho Ac^2 - R_0\right)\frac{d^2 V}{dx^2} = 0 \tag{43}$$

[1] Axial speed of a moving beam

The solution of this fourth order differential equation is

$$V = Be^{i\alpha x} \tag{44}$$

substitute this into Equation (43) to give

$$EI\alpha^4 - \rho A\omega^2 - 2\rho Ac\omega\alpha - \left((1-\eta)\,\rho Ac^2 - R_0\right)\alpha^2 = 0 \tag{45}$$

This characteristic equation is a fourth order polynomial in α. In the case of a stationary beam, an expression for α can be written down explicitly, however, for the moving beam, because of the mixed derivative term in the equation of motion, the solutions for α are very complicated (though not impossible). An easy way to overcome this problem is to find the four values of α by using a numerical root finding algorithm. These four values can then be used in the formation of the dynamic stiffness matrix.

There are many robust algorithm for finding roots of polynomials. Laguerre's method was recommended as the most straight forward and robust technique [63], and a subroutine was also available, which could be incorporated easily into the computer program for calculating the natural frequencies and mode shapes of the moving beams.

The usual procedure for obtaining the dynamic stiffness matrix can now be carried out numerically.

The complete solution is

$$V = B_1e^{i\alpha_1 x} + B_2e^{i\alpha_2 x} + B_3e^{i\alpha_3 x} + B_4e^{i\alpha_4 x} \tag{46}$$

Referring again to Figure 18 for the positive sign convention adopted, the boundary conditions are

$$N_1e^{i\omega t} = -EI\frac{\partial^2 v}{\partial x^2}$$

$$
\begin{aligned}
P_1 e^{i\omega t} &= EI\frac{\partial^3 v}{\partial x^3} + \left((1-\eta)\,\rho A c^2 - R_0\right)\frac{\partial v}{\partial x} + \rho A c\frac{\partial v}{\partial t} \\
N_2 e^{i\omega t} &= EI\frac{\partial^2 v}{\partial x^2} \\
P_2 e^{i\omega t} &= -EI\frac{\partial^3 v}{\partial x^3} - \left((1-\eta)\,\rho A c^2 - R_0\right)\frac{\partial v}{\partial x} - \rho A c\frac{\partial v}{\partial t}
\end{aligned}
$$

Substitute for v from Equation (42) and Equation (46) to give

$$\{F\} = \left([D]_1 + [D]_2 + [D]_3\right)\{B\} \tag{47}$$

where

$$\{F\} = \begin{Bmatrix} P_1 \\ P_2 \\ N_1 \\ N_2 \end{Bmatrix}$$

$$\{B\} = \begin{Bmatrix} B_1 \\ B_2 \\ B_3 \\ B_4 \end{Bmatrix}$$

$$[D]_1 = EI\begin{bmatrix} -i(\alpha_1)^3 & -i(\alpha_2)^3 & -i(\alpha_3)^3 & -i(\alpha_4)^3 \\ i(\alpha_1)^3 e^{i\alpha_1 L} & i(\alpha_2)^3 e^{i\alpha_2 L} & i(\alpha_3)^3 e^{i\alpha_3 L} & i(\alpha_4)^3 e^{i\alpha_4 L} \\ (\alpha_1)^2 & (\alpha_2)^2 & (\alpha_3)^2 & (\alpha_4)^2 \\ -(\alpha_1)^2 e^{i\alpha_1 L} & -(\alpha_2)^2 e^{i\alpha_2 L} & -(\alpha_3)^2 e^{i\alpha_3 L} & -(\alpha_4)^2 e^{i\alpha_4 L} \end{bmatrix}$$

$$[D]_2 = \left((1-\eta)\,\rho A c^2 - R_0\right)\begin{bmatrix} i\alpha_1 & i\alpha_2 & i\alpha_3 & i\alpha_4 \\ -i\alpha_1 e^{i\alpha_1 L} & -i\alpha_2 e^{i\alpha_2 L} & -i\alpha_3 e^{i\alpha_3 L} & -i\alpha_4 e^{i\alpha_4 L} \\ 0 & 0 & 0 & 0 \\ 0 & 0 & 0 & 0 \end{bmatrix}$$

$$[D]_3 = i\omega\rho Ac \begin{bmatrix} 1 & 1 & 1 & 1 \\ -e^{i\alpha_1 L} & -e^{i\alpha_2 L} & -e^{i\alpha_3 L} & -e^{i\alpha_4 L} \\ 0 & 0 & 0 & 0 \\ 0 & 0 & 0 & 0 \end{bmatrix}$$

The unknown coefficients B_i can be expressed, in terms of the maximum end deflections and slopes, as

$$\{V\} = [C]\{B\} \tag{48}$$

where

$$\{V\} = \begin{Bmatrix} V_1 \\ V_2 \\ \theta_1 \\ \theta_2 \end{Bmatrix}$$

$$[C] = \begin{bmatrix} 1 & 1 & 1 & 1 \\ e^{i\alpha_1 L} & e^{i\alpha_2 L} & e^{i\alpha_3 L} & e^{i\alpha_4 L} \\ i\alpha_1 & i\alpha_2 & i\alpha_3 & i\alpha_4 \\ i\alpha_1 e^{i\alpha_1 L} & i\alpha_2 e^{i\alpha_2 L} & i\alpha_3 e^{i\alpha_3 L} & i\alpha_4 e^{i\alpha_4 L} \end{bmatrix}$$

or

$$\{B\} = [C]^{-1}\{V\} \tag{49}$$

The stiffness matrix for a moving beam $[K]_m$ can now be found by substituting Equation (49) into Equation (47) to give

$$\{F\} = ([D]_1 + [D]_2 + [D]_3)[C]^{-1}\{V\} \tag{50}$$

therefore

$$[K]_m = ([D]_1 + [D]_2 + [D]_3)[C]^{-1} \tag{51}$$

The numerical values for this stiffness matrix can be calculated easily in a computer program, which can then be assembled into a global stiffness matrix using

exactly the same procedure as for the stationary beam problem discussed in Chapter 4. The natural frequencies are found when the determinant of the global stiffness matrix is equal to zero.

This method is the exact method hence each span of the moving beam can be represented by one single element. It can analyse problems with any combination of free, simply-supported, clamped and sliding end conditions. The free end condition has not been discussed in previous publications because it was not considered as a practical boundary condition for the bandsaw problem, however, there are applications in other fields of moving material, such as a cantilevered pipe conducting fluid.

6.3 Effects of Boundary Conditions on a High Strain Moving Beam

The bandsaw blade has been assumed to have simply-supported boundary conditions. Anderson (1974) [6] looked at the effects of clamped ends on the moving beam problem and concluded that the support conditions do not have a great influence on the first natural frequency. However, the blade dimensions chosen in Anderson's paper were different from the dimensions of the saw blade used on the Waimak bandsaw. This section, therefore, attempts to compare the natural frequencies of simply-supported end conditions and those of clamped-clamped end conditions for the Waimak bandsaw blade. Blades with similar dimensions to those of the Waimak saw blade were used by Kirbach and Bonac (1978) [37,38] to investigate the effects of tensions and axial speeds on the blades. These results were used to compare with the results obtained by the dynamic stiffness method.

The common parameters in this study were the Young's modulus E, the density

Table 1: First two natural frequencies of a stationary blade with simply-supported and clamped-clamped end conditions.

Length (m)	S-S Beam (Hz)	C-C Beam (Hz)
0.30	125.2	159.7
	288.0	360.8
0.51	71.0	81.6
	150.3	172.5
0.83	43.1	46.8
	88.2	95.8
1.00	35.7	38.2
	72.5	77.7

ρ and the strain parameter η. E can be assumed to be $200 \times 10^9 \mathrm{N/m^2}$. The density is the usual $7800 \mathrm{kg/m^3}$, however, because the width of the blade is the width excluding the teeth, the density was taken as $8200 \mathrm{kg/m^3}$ to take into account the weight of the teeth [38]. The straining device for the Waimak bandsaw was the counterweight mechanism, therefore, $\eta = 1$. The length L, the axial speed c and the initial tension R_0 were chosen as the variables for this study.

6.3.1 Varying Length

The cutting span of the blade does not have a single set length because the upper guide is always adjusted for different log size. This means that the cutting span can possess a range of frequencies depending on the position of the upper guide.

Table 1 lists the first two natural frequencies of a simply-supported beam (S-S) and a clamped-clamped beam (C-C) for various lengths. The width of the beam was 0.22 m and the thickness was 0.00165 m.

These results show that the first two natural frequencies of a S-S beam are always smaller than those of a C-C beam, and the shorter the length, the larger the differences in the natural frequencies. At a typical length of about 0.5 m, the difference in the first natural frequency is about 10 Hz, or a 14% discrepancy, which

Table 2: First two natural frequencies of a blade with different tensions.

Tension (N)	S-S Beam (Hz)	C-C Beam (Hz)	Exp. Results (Hz)
17,169.	39.6 80.5	42.4 86.1	37.2
20,201.	42.9 87.0	45.7 92.6	42.2
26,833.	49.4 99.8	52.2 105.4	47.8

is quite significant.

6.3.2 Varying Tension

Kirbach and Bonac (1978) [37] measured the first transverse natural frequency for a blade with 0.237 m in width, 0.0016 m in thickness and a fixed span length of 0.943 m, at three different tensions. Table 2 shows their experimental results and the calculated results for S-S and C-C beams.

These results also show that the frequencies for a simply-supported beam are closer to the actual frequencies than those for the clamped-clamped beam. The differences in the frequencies of the two types of beam are almost unchanged for the range of tensions under investigation. It seems that the end conditions for the cutting span of the blade are best approximated by the simply-supported boundary conditions. Kirbach and Bonac (1978) [38] suggested that the span length of the blade was given by the distance between the outer edges of the guides instead of the distance between the inner edges of the guides because of the curvature of the blade as illustrate in Figure 65, therefore the measured frequencies were slightly lower than the calculated frequencies. Although, this hypothesis seems to agree with their experimental results, in practice the sharp edges of the guides would be worn off very quickly, hence reducing the effective span length from the length between the outer edges of the guides to the length between the inner edges of the guides.

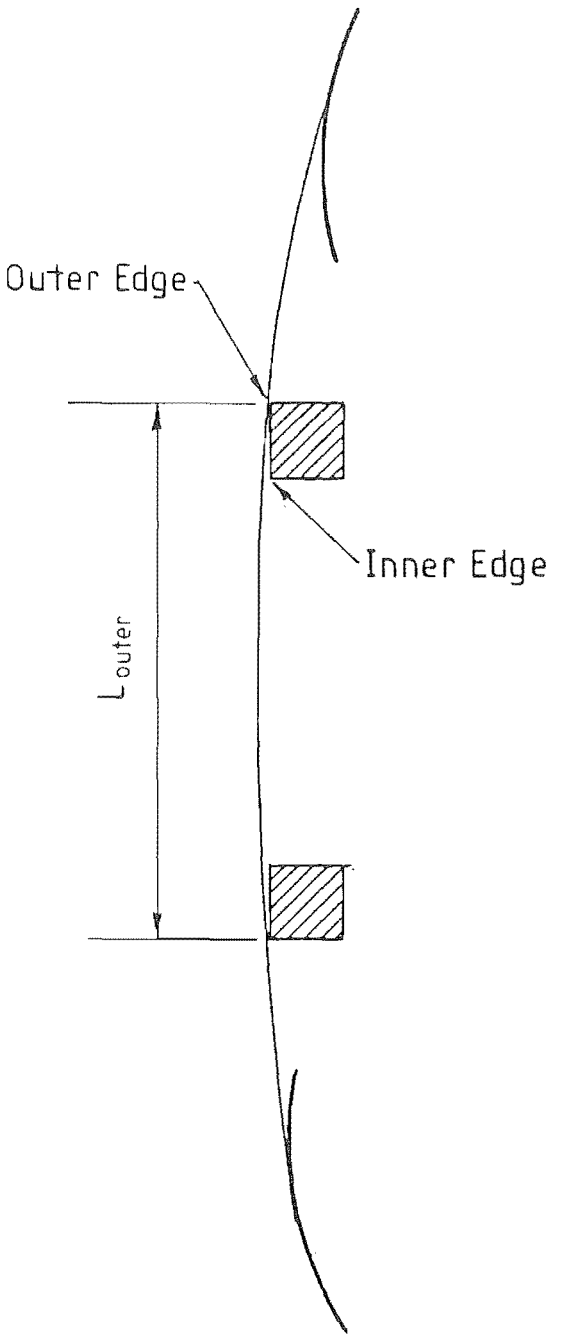

Figure 65: Effective span length in a pressure guide system.

Table 3: First two natural frequencies of a blade with various axial speeds.

Speed (m/s)	Flexible Sol.(Hz)	S-S Beam (Hz)	C-C Beam (Hz)
0	45.5	45.6	48.0
	91.0	92.0	96.8
25	43.7	43.9	46.1
	87.4	88.8	93.4
50	39.3	39.6	41.6
	78.7	80.9	85.2
75	34.3	34.7	36.5
	68.7	71.5	75.3

6.3.3 Varying Axial Speed

Table 3 shows the natural frequencies of a S-S beam and a C-C beam for different transport speeds. The dimensions of the blade were 0.235 m in width, 0.0014 m in thickness and 0.948 m in length, the tension was chosen to be 20,069 N.

The flexible band solution given by Mote (1965) [52] was of the form

$$f = \frac{n}{2L}\left(\frac{R_0}{\rho A}\right)^{1/2}\left(1-(1-\eta)\frac{\rho A c^2}{R_0}\right)\left(1+\eta\frac{\rho A c^2}{R_0}\right)^{-1/2} \tag{52}$$

where f was the natural frequency in Hz, n was the mode of vibration. This solution was a lower bound approximation, hence the results were slightly less than those obtained by the dynamic stiffness method. As the axial speed increased the difference between the natural frequencies of the S-S beam and those of the C-C beam decreased.

Table 4 shows the frequencies of the Waimak bandsaw blade with an axial speed of 38 m/s. At a span length of 1.0 m, the difference between the first natural frequencies is only about 4.4%, but up to 28.7% difference for a span length of 0.3 m.

Table 4: First two natural frequencies of the Waimak saw blade at 38 m/s transport speed.

Length (m)	S-S Beam (Hz)	C-C Beam (Hz)
0.30	115.4	148.5
	281.2	354.7
0.51	63.9	73.8
	141.1	162.9
1.00	31.6	33.0
	65.4	70.3

6.3.4 Conclusion

For a typical bandsaw blade configurations the boundary conditions can alter the calculated natural frequencies considerably. The simply-supported boundary conditions appear to give closer results to the measured data than those obtained with the clamped-clamped conditions.

The simply-supported boundary conditions should be used for the bandsaw blade case, however, for cases where the end conditions are known to be more closely related to the clamped conditions then the dynamic stiffness method should be used to obtain more accurate solutions.

6.4 Multiple Span Beams

The cutting span of a bandsaw blade has been assumed to be a simply-supported beam, however, it should be considered to be a three-span beam with the two end supports being the points where the blade ceases contact with the two pulleys, and the two intermediate supports being the two guides. For a three-span beam with no tension, the modes of vibration are coupled, however, for a beam under high tension the coupling effects may be negligible. This section investigates these coupling effects on the Waimak bandsaw blade, that is, a blade with 0.22 m wide and 0.00165 m thick.

6.4.1 Three Equal Span Lengths

The total length of the beam was taken to be 2.286 m, that is, 0.762 m for each equal span length.

The first four natural frequencies of the stationary three span beam with no tension were 6.4 Hz, 8.2 Hz, 11.9 Hz, 25.5 Hz, and their mode shapes are shown in Figure 66. These results showed that the first natural frequency was the expected first natural frequency of a single span beam because the mode shape for each span was the same as the first mode shape of a single beam. There were also two other frequencies close to this first natural frequency, which were present because of the coupling effects of the three span beam. The fourth frequency was the expected second natural frequency of a single span.

For 15000 N tension the first four natural frequencies became 47.0 Hz, 48.1 Hz, 50.3 Hz and 96.6 Hz. Again there were three close natural frequencies, relating to the first natural frequency of a single span beam. The tension caused the first three natural frequencies to be closer to each other compared to those of a beam without tension. This was because the tension became the major restoring force in the vibration instead of the bending stiffness, therefore if the tension was assumed to be infinitely large then there would be three identical natural frequencies which would be equal to the first natural frequency of a single span beam, that is, the tension uncoupled the modes of vibration of the three span beam.

For a single span beam with 0.762 m in length and axially moving at a speed of 38 m/s, the first two natural frequencies were 41.8 Hz and 88.2 Hz. For the three span beam moving at the same speed, the first four natural frequencies were 41.9 Hz, 42.9Hz, 44.9 Hz and 88.2 Hz. This means that a single span beam can be used to approximate the frequencies of the three span beam, however, there are two other frequencies slightly higher than the first frequency due to the coupling

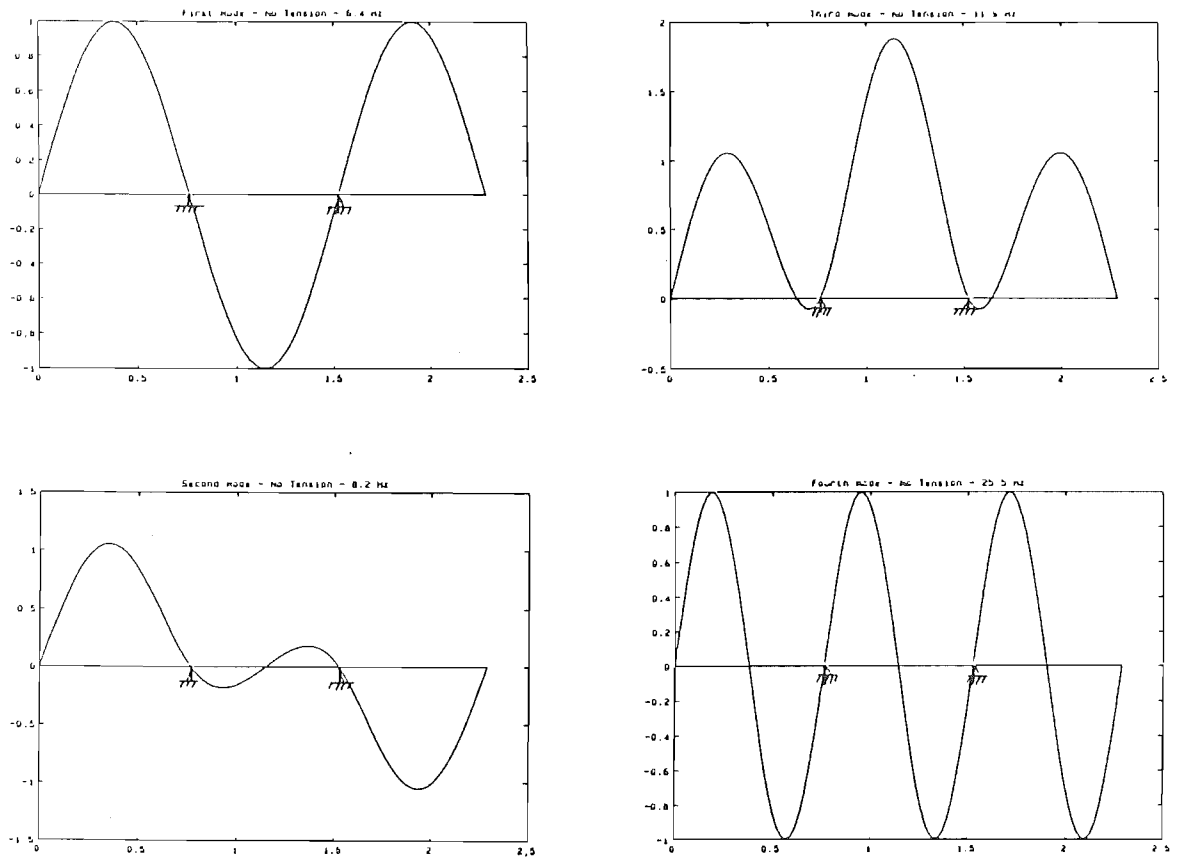

Figure 66: First four modes of a three span beam with no tension.

effects of the three span beam, in fact every frequency of the single span beam will be accompanied by two coupling frequencies.

6.4.2 Long Centre Span

For the bandsaw blade case, the lower guide is fixed in one position, therefore the span length between the bottom pulley and the lower guide always remains the same (0.786 m). The upper guide is moved to adjust for the size of the timber being cut, this means that the span length of the centre span and the upper span are never the same. This section considered the case when the centre span length was 1 m, and the upper span was therefore 0.5 m long.

With no tension, the first four natural frequencies were 5.1 Hz, 8.3 Hz, 15.9 Hz and 21.2 Hz. Figure 67 shows the mode shapes corresponding to these four natural frequencies.

The first two natural frequencies of a simply-supported beam were :

- 3.7 Hz and 14.8 Hz, for 1.0 m in length.
- 6.0 Hz and 23.9 Hz, for 0.786 m in length.
- 14.8 Hz and 59.1 Hz, for 0.5 m in length.

Comparing the results for the three span beam with the results for the three individual beams revealed that:

- The 5.1 Hz of the three span beam corresponded to the first natural frequency, 3.7 Hz, of the centre span. The coupling effects of the other two spans caused an increase in the frequency of the three span beam.
- The 8.3 Hz corresponded to the 6.0 Hz of the 0.786 m span.

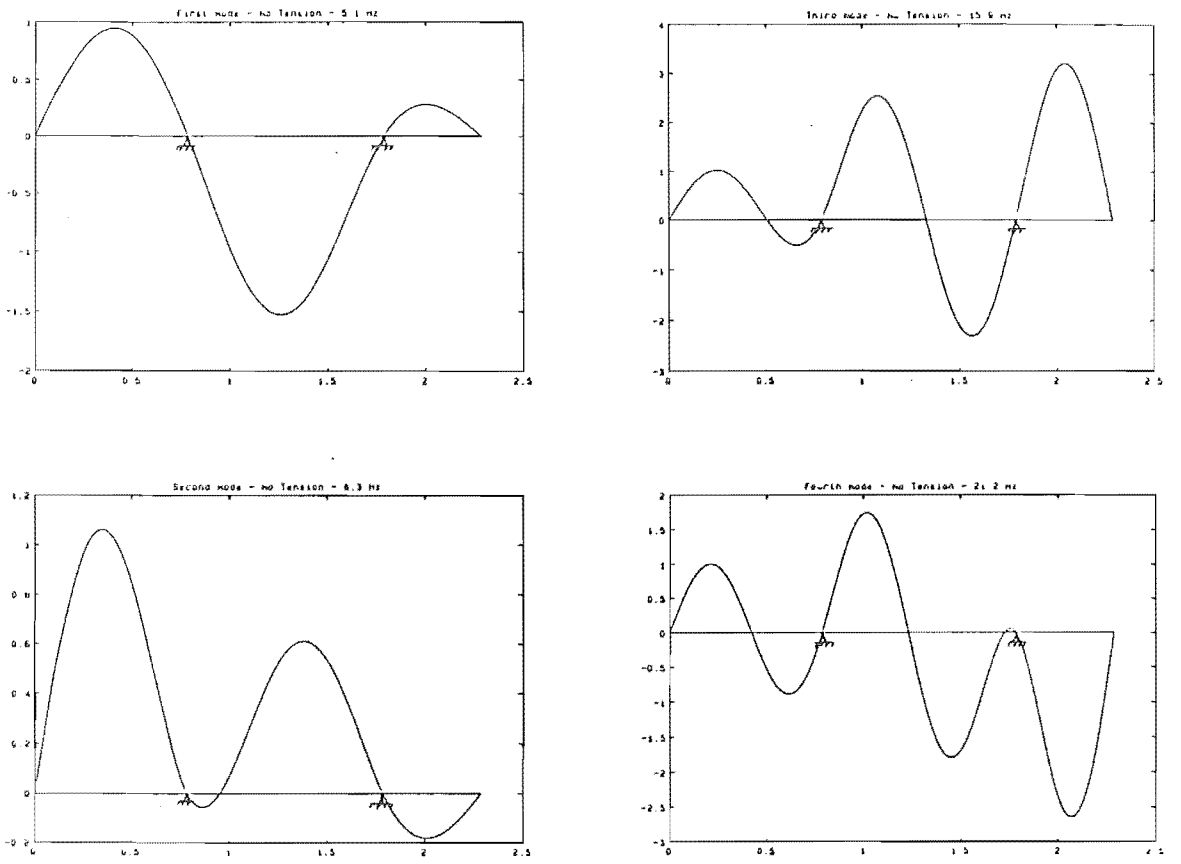

Figure 67: First four natural modes of a three span beam with 0.786 m, 1.0 m, 0.5 m span lengths under no tension.

- The 15.9 Hz corresponded to the 14.8 Hz of both the first natural frequency of the 0.5 m span and the second natural frequency of the 1.0 m centre span.
- The 21.2 Hz of the three span beam seemed to be closest to the 23.9 Hz second natural frequency of the 0.786 m span.

The first four natural frequencies of the three span beam under 15000 N tension were 36.9 Hz, 46.6 Hz, 73.2 Hz and 76.8 Hz. The first two natural frequencies of each individual span were :

- 35.7 Hz and 72.5 Hz, for 1.0 m in length.

- 45.6 Hz and 93.4 Hz, for 0.786 m in length.
- 72.5 Hz and 153.8 Hz, for 0.5 m in length.

The mode shapes of the three span beam are in Figure 68. These mode shapes together with the frequencies of the single span beams indicate that the 36.9 Hz was associated with the first mode of the centre span, the 46.6 Hz with the first mode of the 0.786 m span, the 73.2 Hz with the first mode of the 0.5 m span and the 76.8 Hz with the second mode of the centre span. This also confirms that the 21.2 Hz of the untensioned three span beam was related to the 14.8 Hz second natural frequency of the centre span instead of the 23.9 Hz second mode of the 0.786 m span.

These results showed that the coupling effects always raise the natural frequencies of each beam member, and the tension on the beam reduces the coupling effects. Therefore the natural frequencies of a high tension three span beam could be approximated by obtaining the natural frequencies of each span independently which would be the lower bounds of the actual natural frequencies. There might be more than one actual natural frequencies associated with each approximated frequency.

At 38 m/s axial velocity, the first four natural frequencies of the tensioned three span beam became 32.2 Hz, 41.4 Hz, 66.0 Hz and 70.7 Hz. Again these frequencies could be related to the frequencies of each span. The first two natural frequencies of each individual span were :

- 31.6 Hz and 65.4 Hz, for 1.0 m in length.
- 40.5 Hz and 85.2 Hz, for 0.786 m in length.
- 65.4 Hz and 144.8 Hz, for 0.5 m in length.

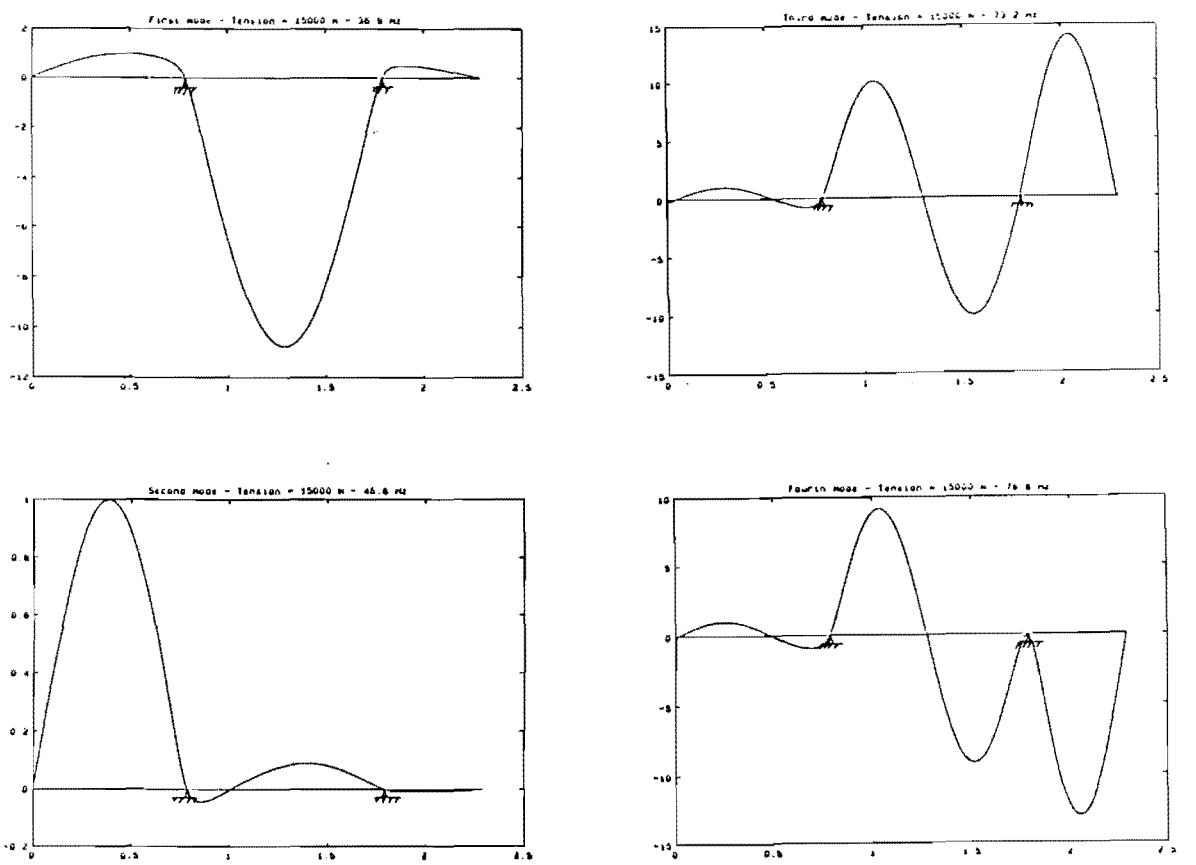

Figure 68: First four natural modes of a three span beam with 0.786 m, 1.0 m, 0.5 m span lengths under 15000 n tension.

6.4.3 Short Centre Span

The characteristics of the coupling effects found in the previous sections were also present in this 0.786 m-0.5 m-1.0 m three span beam.

With no tension, the first four natural frequencies were 4.8 Hz, 7.6 Hz, 15.7 Hz and 22.0 Hz, and the mode shapes are shown in Figure 69. The first three frequencies were slightly less than those of the 0.786 m-1.0 m-0.5 m beam, but the fourth one was higher.

With 15000 N tension, the natural frequencies were 36.3 Hz, 46.5 Hz, 73.0 Hz and 78.3 Hz. Again these were very similar to those of the previous long centre span beam.

At 38 m/s axial velocity, the frequencies were 32.2 Hz, 41.4 Hz, 66.0 Hz and 70.7 Hz. They were almost the same as those obtained for the 0.786 m-1.0 m-0.5 m beam.

6.4.4 Conclusion

The results showed that each natural frequency of a three span beam under high tension is always associated with a principal span, therefore, it is reasonable to use a single span beam for approximating this frequency. The coupling effects increase very slightly the natural frequencies of the single span beam.

6.5 Boundary Excitation of Moving Beams

The dynamic stiffness matrix provides a connection between the generalised forces and the generalised displacements, therefore, a harmonic end force excitation can be analysed by setting up the dynamic stiffness matrix, rearranging it and solving for the instantaneous displacements of the system under investigation.

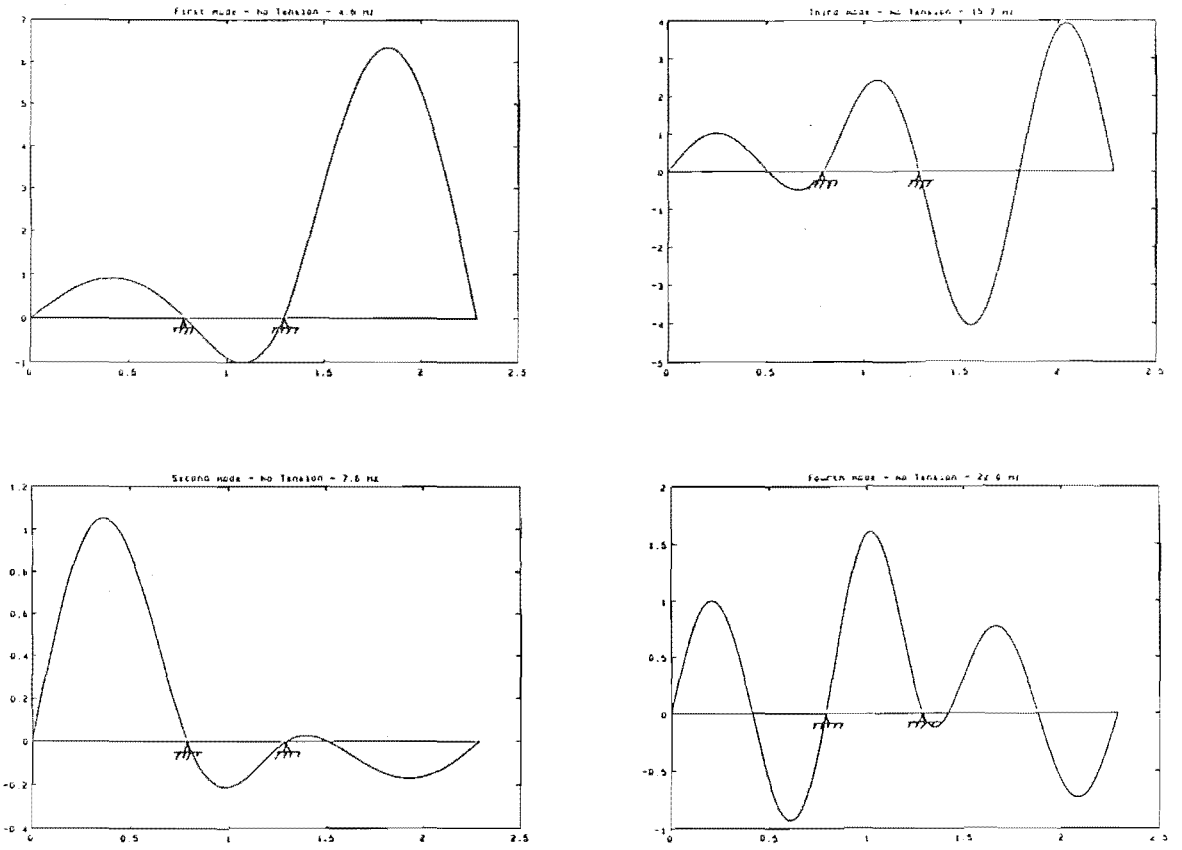

Figure 69: First four natural modes of a three span beam with 0.786 m, 0.5 m, 1.0 m span lengths under no tension.

Initially, it was thought that for a moving beam, the excitation at one end of the beam could produce different results from the excitation at the other end, because the beam was moving away from one end and toward the other. An analysis on this hypothesis showed that the resonance condition for the moving beam problem was the same as the resonance condition on a stationary beam, that is, a large amplitude of vibration occurs when the frequency of the excitation is equal to a natural frequency of the system, regardless the position of the excitation.

Strictly speaking, a moving beam does not have natural frequencies in the classical sense, because there is no single frequency with in phase oscillation. However, there are excitation frequencies which would cause large vibrations from small excitation levels. These frequencies have been referred to in the literature as the natural frequencies of the moving beam. Similarly, the modes of oscilation related to these so called natural frequencies have been called the mode shapes of the moving beam. The first mode of oscillation for a simply-supported moving beam is illustrated in Figure 70. This mode shape had been animated on a computer screen, which appeared as a wave moving in the opposite direction to the travelling direction of the beam.

The experimental results on the bandsaw structure under idling condition (Section 5.7) showed that the bandsaw structure possessed a large number of frequencies in the frequency spectrum, that is, 8 Hz and its harmonics. This means that the blade is likely to be excited by the structure at or near a resonance frequency. Other effects such as damping would prevent excessive amplitude of oscillation of the blade, however, even a small vibration amplitude can result in poor cutting accuracy. An improvement to the cutting performance could be made by eliminating the harmonics of the rotating speed of the pulley.

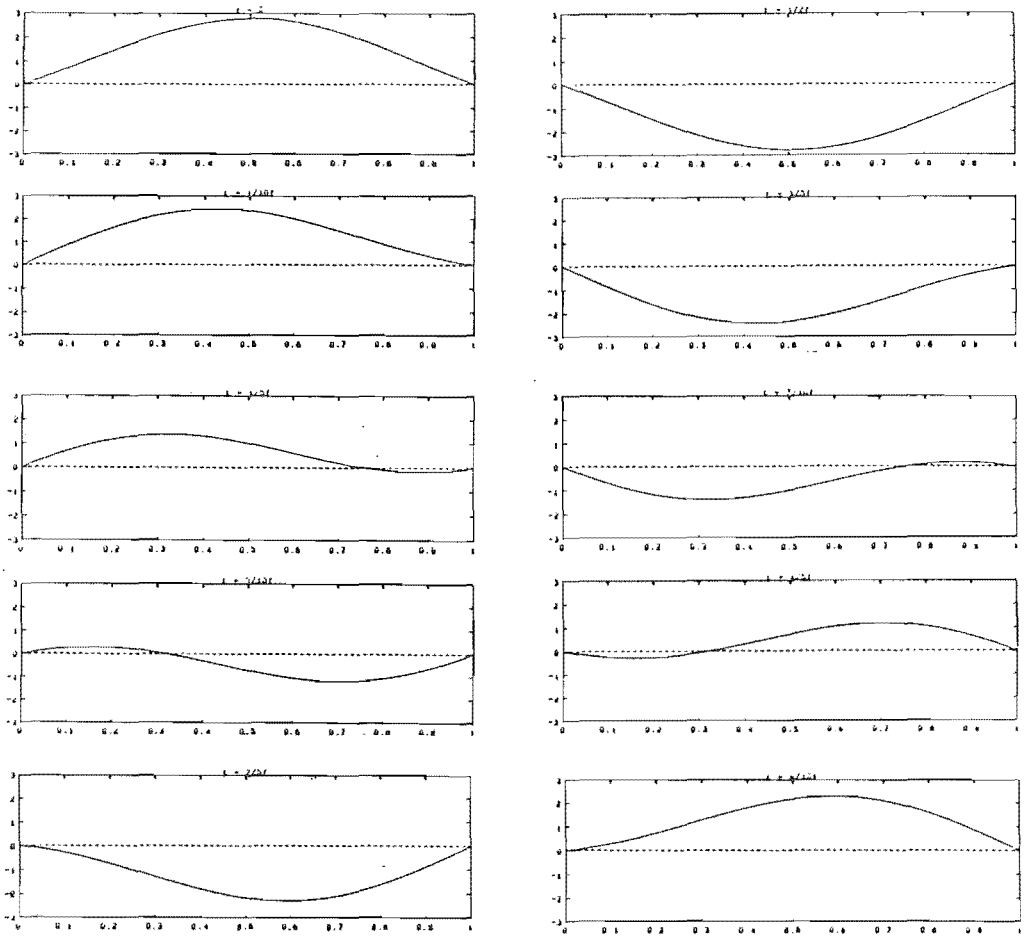

Figure 70: First mode shape of a moving beam.

Chapter 7

A GENERAL PROCEDURE IN THE DYNAMIC ANALYSIS OF RECTANGULAR PLATE

7.1 Introduction

The study of plate vibrations can be found in many vibration text books, notable were the work by Leissa (1969) [45,46] which considered the exact solutions for rectangular plates with various boundary conditions. The use of the exact classical method is, however, restricted to only simple problems, and since modern problems are becoming more complicated, other means of approximating their solutions must be employed.

A moving wide bandsaw blade, under various stress conditions can be modelled as a moving plate under inplane stresses with two opposite edges simply-supported or clamped and the other two edges free. This is a relatively complex problem, and an approximate method must be used to solve it. Only Ulsoy and Mote (1980,

1982) [86,87] studied the vibration of a moving plate using the classical Ritz and the finite element Ritz methods. All other works on the bandsaw blade had modelled the blade as a moving thin beam, which would have been reasonable if the blade were a narrow bandsaw blade or a wide blade with no stress variations across the width. Modern bandsaw blades are often prestressed by rolling, and/or fitted with back-crown, which produces stress variation across the width of the blade, therefore, only the theory of a moving plate can be used to model the wide bandsaw blade accurately.

Future developments on bandsaws will be directed toward automatic control of the cutting process, which would require a much better understanding of the dynamic stability of the blade under various excitations, such as external excitations due to cutting forces, parametric excitations due to stress fluctuations. Therefore, a more general and systematic solution method is required to tackle the complex problems with relative ease.

The aim of this chapter is to introduce a procedure for solving a general plate problem. This procedure is designed to make use of the micro-computer in reducing the hand calculations and if possible some of the algebraic manipulations. It will be extended in the following chapters to handle the more complicated problems associated with the bandsaw blade.

7.2 Formulation - Hamilton's Principle

The conventional method of formulating the equation of motion of a system is based on the Newton's law of motion (Newtonian method). A different method of formulation uses Hamilton's principle, which is perhaps the most advanced variational principle of mechanics. One remarkable advantage of this formulation is that it

is invariant with respect to the coordinate system used. It is, therefore, used extensively in both infinitesimal and finite theories of dynamic elasticity. Hamilton's principle was chosen for the formulation of the plate problems in this thesis.

7.2.1 Hamilton's Principle

References to Hamilton's principle are in [49, page 42], [42, page 233], [98]. Briefly, the mathematical statement of Hamilton's principle is

$$\delta \int_{t_1}^{t_2} (T + W)\, dt = 0 \tag{53}$$

where T is the kinetic energy and W is the virtual work of the noninertial forces. Or in words :

> *The actual path renders the value of the integral in Equation (53) minimum with respect to all possible neighbouring paths that the system may be imagined to take between two instants t_1 and t_2, provided the initial and final configurations of the system are prescribed.*

The virtual work done, W, consists of conservative and nonconservative work done.

$$W = W_c + W_{nc} \tag{54}$$

and

$$W_c = -U \tag{55}$$

where U is the potential energy

Therefore Equation (53) can be rewritten as

$$\int_{t_1}^{t_2} (\delta T - \delta U + \delta W_{nc})\, dt = 0 \tag{56}$$

In the case in which the forces are conservative

$$\int_{t_1}^{t_2} (\delta T - \delta U)\, dt = 0 \tag{57}$$

After the kinetic energy T, the potential energy U, and the non-conservative work done W_{nc} have been determined, the use of Hamilton's principle leads to a scalar integral. The method of the calculus of variations can then be used to evaluate the integral to provide the equations of motions and all necessary boundary conditions of the system under investigation.

The equation of motion and boundary conditions of a stationary plate will be derived as an example to illustrate the use of Hamilton's principle. Other factors such as tension, travelling speed, cutting forces will be considered in the following chapters.

7.2.2 Kinetic and Potential Energy of a Plate

The kinetic energy T of a stationary rectangular plate is

$$T = \frac{1}{2} \int_0^b \int_0^l \rho h \left(\frac{\partial w}{\partial t} \right)^2 dx\, dy \tag{58}$$

where b is the width of the plate, l is the length, h is the thickness, ρ is the density, w is the transverse displacement and hence $\frac{\partial w}{\partial t}$ is the transverse velocity.

The potential energy of the plate caused by bending, U_b, is

$$U_b = \frac{1}{2} \int_0^b \int_0^l D \left\{ \left(\frac{\partial^2 w}{\partial x^2} + \frac{\partial^2 w}{\partial y^2} \right)^2 + 2(1-\nu) \left[\left(\frac{\partial^2 w}{\partial x \partial y} \right)^2 - \frac{\partial^2 w}{\partial x^2} \frac{\partial^2 w}{\partial y^2} \right] \right\} dx\, dy \tag{59}$$

where D is the flexural stiffness, $D = \frac{Eh^3}{12(1-\nu^2)}$, ν is the Poisson's ratio and E is the Young's modulus.

If there are other potential energies present in the plate, such as energies from inplane stresses, then they must be added to the energy expression.

7.2.3 Calculus of Variations

The Hamilton's principle, Equation (57), can now be used to give the equation of motion and the boundary conditions of the plate. Assuming that the operator δ and $\partial/\partial t$, as well as δ and $\partial/\partial x$, are commutative, and that the integrations with respect to t and x are interchangeable, the method of integration by parts can be used to expand Equation (57).

The kinetic energy term can be considered by adding a small variation to Equation (58)

$$\begin{aligned} T+\delta T &= \int_0^b \int_0^l \frac{\rho h}{2}\left[\frac{\partial\left(w+\delta w\right)}{\partial t}\right]^2 dx\,dy \\ &= \int_0^b \int_0^l \frac{\rho h}{2}\left[\left(\frac{\partial w}{\partial t}\right)^2 + 2\frac{\partial w}{\partial t}\frac{\partial\left(\delta w\right)}{\partial t} + \left(\frac{\partial\left(\delta w\right)}{\partial t}\right)^2\right] dx\,dy \end{aligned}$$

Discarding second order term and simplifying gives

$$\delta T = \int_0^b \int_0^l \rho h \frac{\partial w}{\partial t}\frac{\partial\left(\delta w\right)}{\partial t}\,dx\,dy \tag{60}$$

Therefore

$$\begin{aligned} \int_{t_1}^{t_2} \delta T\,dt &= \int_0^b \int_0^l \rho h \int_{t_1}^{t_2} \frac{\partial w}{\partial t}\frac{\partial\left(\delta w\right)}{\partial t}\,dt\,dx\,dy \\ &= \int_0^b \int_0^l \rho h \left[\frac{\partial w}{\partial t}\delta w\Big|_{t_1}^{t_2} - \int_{t_1}^{t_2} \frac{\partial^2 w}{\partial t^2}\delta w\,dt\right] dx\,dy \\ &= -\int_{t_1}^{t_2} \int_0^b \int_0^l \rho h \frac{\partial^2 w}{\partial t^2}\delta w\,dx\,dy\,dt \end{aligned} \tag{61}$$

because δw vanishes at $t = t_1$ and $t = t_2$.

The variation on potential energy, δU, can be treated in a similar manner

$$\begin{aligned} \delta U &= \int_0^b \int_0^l \frac{D}{2}\delta\left[\left(\frac{\partial^2 w}{\partial x^2}\right)^2 + \left(\frac{\partial^2 w}{\partial y^2}\right)^2 + 2\nu\frac{\partial^2 w}{\partial x^2}\frac{\partial^2 w}{\partial y^2} + 2\left(1-\nu\right)\left(\frac{\partial^2 w}{\partial x \partial y}\right)^2\right] dx\,dy \\ &= \int_0^b \int_0^l D\left[\frac{\partial^2 w}{\partial x^2}\frac{\partial^2\left(\delta w\right)}{\partial x^2} + \frac{\partial^2 w}{\partial y^2}\frac{\partial^2\left(\delta w\right)}{\partial y^2} + \right. \\ &\quad \left. \nu\frac{\partial^2 w}{\partial x^2}\frac{\partial^2\left(\delta w\right)}{\partial y^2} + \nu\frac{\partial^2\left(\delta w\right)}{\partial x^2}\frac{\partial^2 w}{\partial y^2} + 2\left(1-\nu\right)\frac{\partial^2 w}{\partial x \partial y}\frac{\partial^2\left(\delta w\right)}{\partial x \partial y}\right] dx\,dy \end{aligned} \tag{62}$$

Integrating Equation (62) by parts and rearranging gives

$$\begin{aligned}\int_{t_1}^{t_2} \delta U\, dt \;=\; & \int_{t_1}^{t_2} D \left\{ \int_0^b \int_0^l \left[\frac{\partial^4 w}{\partial x^4} + 2\frac{\partial^4 w}{\partial x^2 \partial y^2} + \frac{\partial^4 w}{\partial y^4} \right] \delta w\, dx\, dy \right. \\ & + \int_0^b \left[\left(\frac{\partial^2 w}{\partial x^2} + \nu \frac{\partial^2 w}{\partial y^2} \right) \frac{\partial (\delta w)}{\partial x} \bigg|_{x=0}^{l} - \left(\frac{\partial^3 w}{\partial x^3} + \frac{\partial^3 w}{\partial x \partial y^2} \right) \delta w \bigg|_{x=0}^{l} \right. \\ & \left. + (1-\nu) \frac{\partial^2 w}{\partial x \partial y} \frac{\partial (\delta w)}{\partial y} \bigg|_{x=0}^{l} \right] dy \\ & + \int_0^l \left[\left(\frac{\partial^2 w}{\partial y^2} + \nu \frac{\partial^2 w}{\partial x^2} \right) \frac{\partial (\delta w)}{\partial y} \bigg|_{y=0}^{b} - \left(\frac{\partial^3 w}{\partial y^3} + \frac{\partial^3 w}{\partial x^2 \partial y} \right) \delta w \bigg|_{y=0}^{b} \right. \\ & \left. \left. + (1-\nu) \frac{\partial^2 w}{\partial x \partial y} \frac{\partial (\delta w)}{\partial x} \bigg|_{y=0}^{b} \right] dx \right\} dt \end{aligned} \tag{63}$$

Adopting the sign convention as in Figure 71, the edge bending moments and shear forces can be expressed as [35]

$$M_x = -D \left(\frac{\partial^2 w}{\partial x^2} + \nu \frac{\partial^2 w}{\partial y^2} \right) \tag{64}$$

$$M_y = -D \left(\frac{\partial^2 w}{\partial y^2} + \nu \frac{\partial^2 w}{\partial x^2} \right) \tag{65}$$

$$M_{xy} = D(1-\nu) \frac{\partial^2 w}{\partial x \partial y} \tag{66}$$

$$Q_x = -D \left(\frac{\partial^3 w}{\partial x^3} + \frac{\partial^3 w}{\partial x \partial y^2} \right) \tag{67}$$

$$Q_y = -D \left(\frac{\partial^3 w}{\partial y^3} + \frac{\partial^2 w}{\partial x^2 \partial y} \right) \tag{68}$$

Equation (61) and Equation (63) can be substituted into Equation (57), and simplified by using the edge bending moments and shear forces equations above to give

$$\begin{aligned} & \int_{t_1}^{t_2} \left\{ \int_0^b \int_0^l \left[-\rho h \frac{\partial^2 w}{\partial t^2} - D \nabla^4 w \right] \delta w\, dx\, dy \right. \\ & + \int_0^b \left[M_x \frac{\partial (\delta w)}{\partial x} \bigg|_{x=0}^{l} - M_{xy} \frac{\partial (\delta w)}{\partial y} \bigg|_{x=0}^{l} - Q_x \delta w_{x=0}^{l} \right] dy \\ & \left. + \int_0^l \left[M_y \frac{\partial (\delta w)}{\partial y} \bigg|_{y=0}^{b} - M_{xy} \frac{\partial (\delta w)}{\partial x} \bigg|_{y=0}^{b} - Q_y \delta w_{y=0}^{b} \right] dx \right\} dt \;=\; 0 \end{aligned} \tag{69}$$

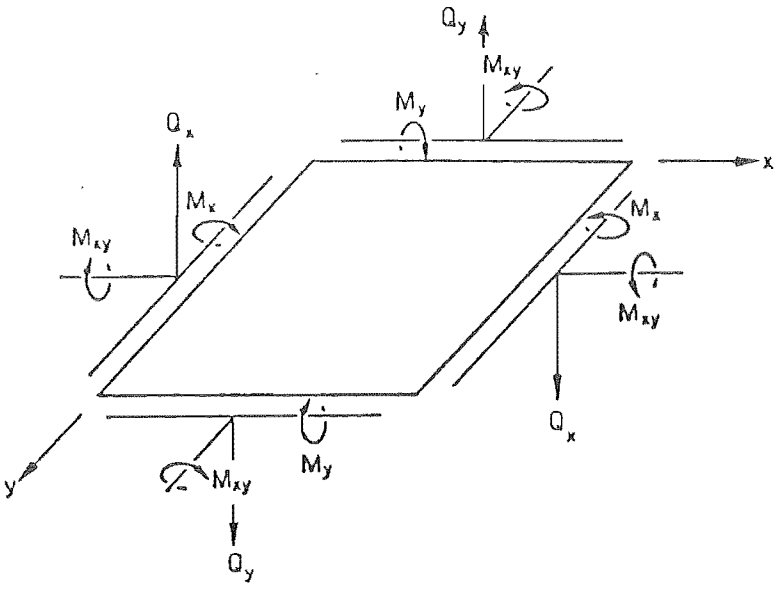

Figure 71: Coordinate directions and sign convention.

where

$$\nabla^4 = \frac{\partial^4}{\partial x^4} + 2\frac{\partial^4}{\partial x^2 \partial y^2} + \frac{\partial^4}{\partial y^4}$$

This equation contains both the equation of motion of the plate and all the necessary boundary conditions on the edges $x = 0$, $x = l$, $y = 0$ and $y = b$.

7.2.4 Equation of Motion and Boundary Conditions

The equation of motion is obtained by simply equating the expression inside the double integral of Equation (69) to zero

$$D\nabla^4 w + \rho h \frac{\partial^2 w}{\partial t^2} = 0 \tag{70}$$

Note that $\delta w = 0$ is the trivial solution, which states that if there is no displacement, there is no vibration.

The expression inside the integral $\int dy$ denotes the boundary conditions along the edges $x = 0$ and $x = l$.

They are

$$M_x = 0 \qquad \text{or} \qquad \frac{\partial(\delta w)}{\partial x} = 0 \tag{71}$$

which means that either the bending moment M_x or the slope in the x-direction must be zero along the two edges.

$$M_{xy} = 0 \qquad \text{or} \qquad \frac{\partial(\delta w)}{\partial y} = 0 \tag{72}$$

which means that either the twisting moment M_{xy} or the slope in the y-direction must be zero along the two edges.

$$Q_x = 0 \qquad \text{or} \qquad \delta w = 0 \tag{73}$$

which means that either the shear force Q_x or the displacement must be zero along the two edges.

Similar boundary conditions along the edges $y = 0$ and $y = b$ can be written down from the expression inside the integral $\int dx$.

These boundary conditions make physical sense, and are the same as those obtained from the Newtonian method.

7.3 Exact Solutions for Plates with Simple Boundary Conditions

Although the exact solutions are restricted to simple boundary conditions, it is important to understand those solutions which fully describe the behaviour of the plate. Approximate solutions for more complicated problems can then be explained and understood by relating to this information.

The types of boundary conditions are abbreviated as SS for simply-supported, C for clamped and F for free, for example, SS-C-SS-F means a rectangular plate with

edge $x = 0$ simply-supported, $y = 0$ clamped, $x = l$ simply-supported, and $y = b$ free.

The equation of motion (Equation (70)) has solutions of the form

$$w = W_n e^{i\omega_n t} \tag{74}$$

where W_n are functions of x and y only and ω_n is the n^{th} angular natural frequency. Substituting this expression into Equation (70) gives

$$\nabla^4 W_n - \lambda^4 W_n = 0 \tag{75}$$

where

$$\lambda^4 = \frac{\rho h \omega_n^2}{D} = \frac{12\left(1-\nu^2\right)\rho\omega_n^2}{Eh^2}$$

Let two opposite edges of the plate parallel to the y-axis be simply-supported, then the shape function W_n takes the form

$$W_n = f(y)\sin\left(\frac{p\pi x}{l}\right) \tag{76}$$

which when substituting into Equation (75) yields

$$\frac{d^4 f(y)}{dy^4} - 2\left(\frac{p\pi}{l}\right)^2 \frac{d^2 f(y)}{dy^2} + \left(\left(\frac{p\pi}{l}\right)^4 - \lambda^4\right) f(y) = 0 \tag{77}$$

Assuming that $\lambda^2 > \left(\frac{p\pi}{l}\right)^2$ the solution has the form

$$f_p(y) = C_{1p}\sin\beta y + C_{2p}\cos\beta y + C_{3p}\sinh\gamma y + C_{4p}\cosh\gamma y \tag{78}$$

where

$$\begin{aligned} \beta^2 &= \lambda^2 - \left(\frac{p\pi}{l}\right)^2 \\ \gamma^2 &= \lambda^2 + \left(\frac{p\pi}{l}\right)^2 \end{aligned}$$

7.3.1 SS-SS-SS-SS Plates

When the two edges $y = 0$ and $y = b$ are simply-supported, the boundary conditions on those edges are $w = 0$ and $M_y = 0$. Because $w = 0$ along those edges, $\frac{\partial w}{\partial x} = 0$, and therefore $\frac{\partial^2 w}{\partial x^2} = 0$. Hence

$$\begin{aligned} w &= 0 \\ \frac{\partial^2 w}{\partial y^2} &= 0 \end{aligned} \tag{79}$$

on $y = 0$ and $y = b$.

Equation (74), Equation (76) and Equation (78) can be substituted into the boundary conditions to give the frequency equation as

$$\sin \beta b = 0 \tag{80}$$

therefore

$$\lambda^2 = \left(\frac{p\pi}{l}\right)^2 + \left(\frac{q\pi}{b}\right)^2 \tag{81}$$

where q is the mode number in the y-direction. This equation can be rearranged to give

$$\omega = \left(\left(\frac{p\pi}{l}\right)^2 + \left(\frac{q\pi}{b}\right)^2\right)\left(\frac{Eh^2}{12\rho(1-\nu^2)}\right)^{1/2} \tag{82}$$

The vibratory forms are

$$W_n = A \sin \frac{p\pi x}{l} \sin \frac{q\pi y}{b} \tag{83}$$

The first four modeshapes of a plate are plotted in Figure 72.

7.3.2 SS-F-SS-F Rectangular Plates

When the two edges $y = 0$ and $y = b$ are free, the boundary conditions on those edges are $M_y = 0$, $M_{xy} = 0$ and $Q_y = 0$. However, three boundary conditions on

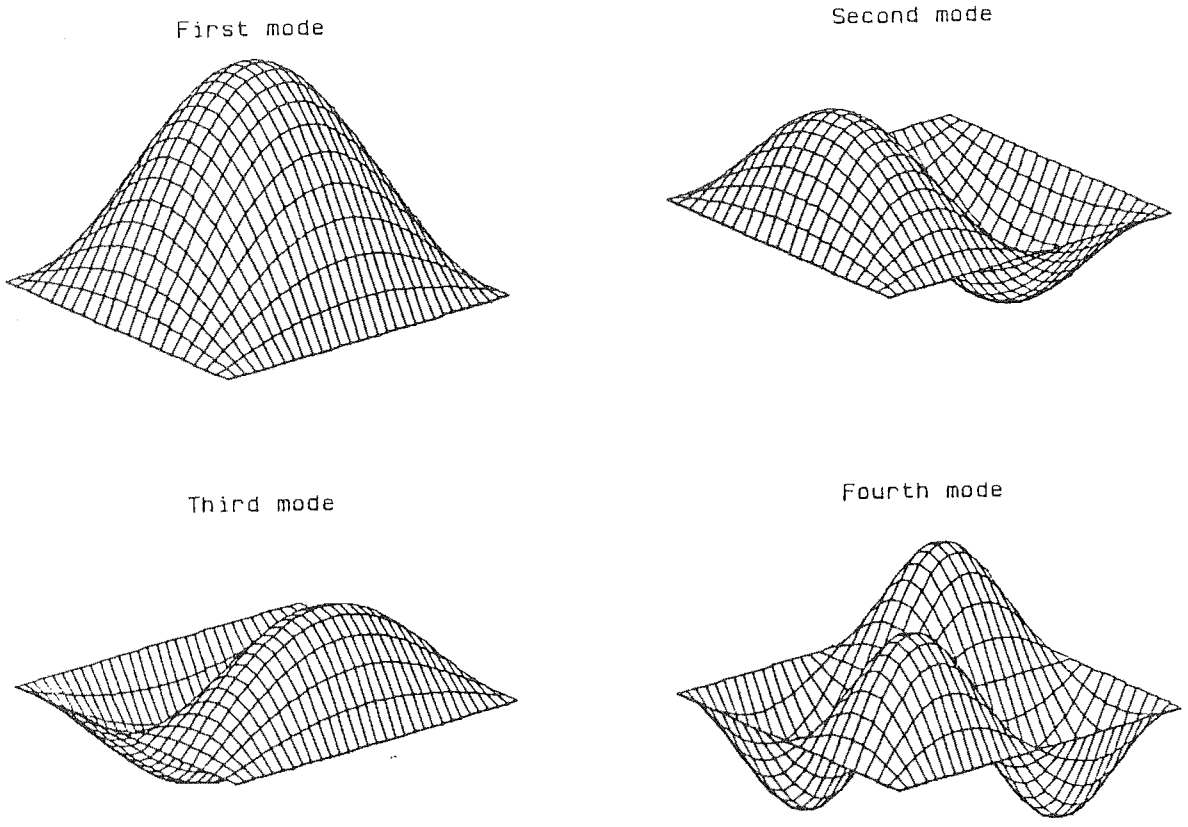

Figure 72: First four modes of a SS-SS-SS-SS rectangular plate.

one edge are too many to be accommodated in the thin plate small deflection theory (though they can be accommodated in the large deflection theory).

It has been shown that M_{xy} can be thought of as vertical forces $-\frac{\partial M_{xy}}{\partial x}$ hence can be combined with Q_y giving one condition $\left(Q_y - \frac{\partial M_{xy}}{\partial x}\right) = 0$. This term is sometimes referred to as the Kirchoff's shear force. Substituting the relevant expressions for M_y, M_{xy} and Q_y in terms of w gives

$$\begin{aligned} \frac{\partial^2 w}{\partial y^2} + \nu \frac{\partial^2 w}{\partial x^2} &= 0 \\ \frac{\partial^3 w}{\partial y^3} + (2-\nu)\frac{\partial^3 w}{\partial x^2 \partial y} &= 0 \end{aligned} \tag{84}$$

on $y = 0$ and $y = b$.

The frequency equation for the SS-F-SS-F plate can be found by substituting Equation (78) into the boundary conditions above. After some lengthy, though not difficult, algebraic manipulation, the frequency equation is given as

$$2\left(1 - \cos\beta b \cosh\gamma b\right) + \left(\frac{\rho_1\rho_4}{\rho_2\rho_3} - \frac{\rho_2\rho_3}{\rho_1\rho_4}\right)\sin\beta b \sinh\gamma b = 0 \tag{85}$$

where

$$\begin{aligned} \rho_1 &= -\beta^2 - \nu\left(\frac{p\pi}{l}\right)^2 \\ \rho_2 &= \gamma^2 - \nu\left(\frac{p\pi}{l}\right)^2 \\ \rho_3 &= -\beta\left[\beta^2 + (2-\nu)\left(\frac{p\pi}{l}\right)^2\right] \\ \rho_4 &= \gamma\left[\gamma^2 - (2-\nu)\left(\frac{p\pi}{l}\right)^2\right] \end{aligned}$$

There is no closed form solutions for this frequency equation, and a numerical roots finding method is needed to obtain the required natural frequencies. The vibratory shapes of the plate are given by Equation (78), and the coefficients can be found arbitrarily by substituting the frequency of interest into the four boundary conditions.

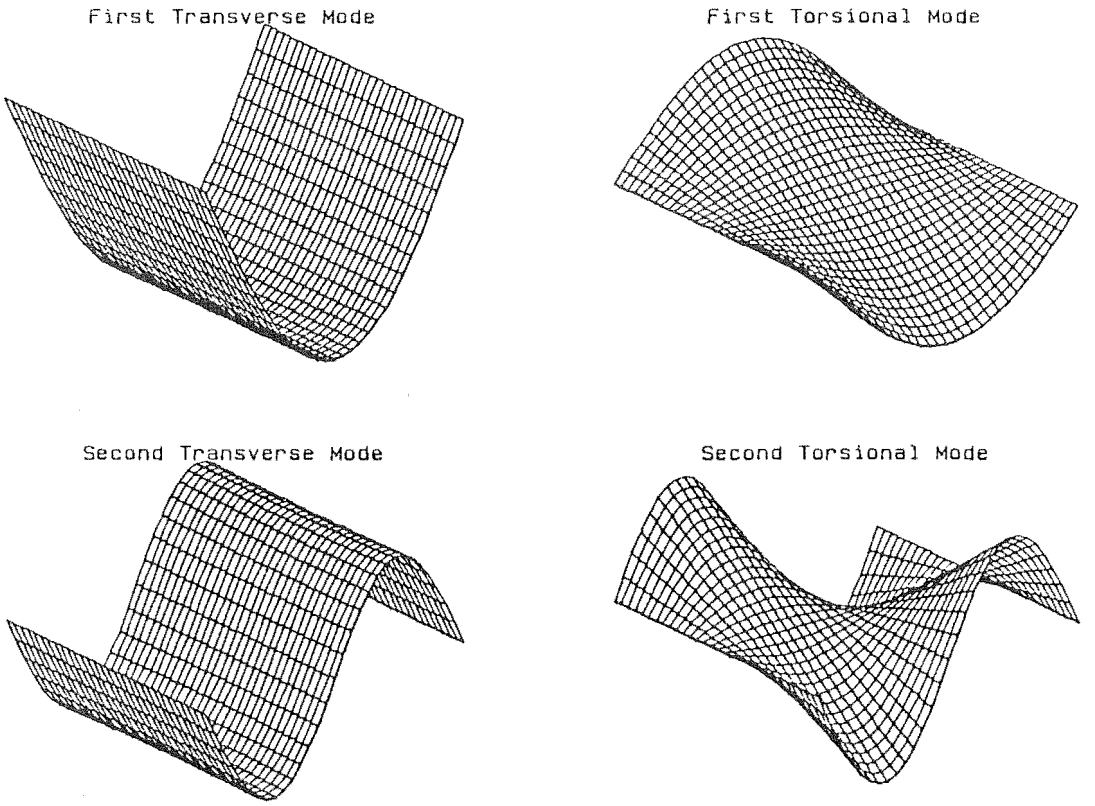

Figure 73: First four modes of a SS-F-SS-F plate.

The first four modeshapes are plotted in Figure 73. Note that when the aspect ratio, l/b, is large, the plate vibration closely resemble beam transverse and torsional vibrations.

7.4 Approximate Solutions - Galerkin Method

7.4.1 Methods of Approximation

The availability of computers allows the solutions of most engineering problems to be approximated by recasting those problems into purely algebraic forms. For the plate problem, which is a continuum problem, the approximation involves a process

called *discretisation.* In such a discretisation, the infinite set of numbers representing the unknown functions is replaced by a finite number of unknown parameters. Some of the common discretisation methods used in plate theory are the *finite difference method*, the *Rayleigh method*, the *Rayleigh-Ritz method*, the *weighted residual method*, and the *finite element method.*

The finite difference method involves a direct discretisation of the differential equation by setting up discrete grid points on the space variable and using Taylor's series expansion to set up the algebraic problems, [99]. It is probably the simplest method, however, its convergence is poor compared with other methods, because a large number of grid points is always necessary to achieve the required accuracy.

The Rayleigh's method is an energy method, where a rough estimation of the mode shape is used to calculate the maximum kinetic and potential energies. Equating the two energies will yield an approximate natural frequency. This method is an upper bound approximation, and the closer the chosen shape function to the true mode shape, the better the result. The Rayleigh-Ritz method extends the Rayleigh's method from one single mode shape to a series of shape functions so that the accuracy of the method can be improved by increasing the number of shape functions in the series. This method is quite popular and can be used successfully in most plate problems [97].

The weighted residual method (WRM) is another very popular method. It uses the trial functions as in the Rayleigh-Ritz method, but instead of substituting into the energy terms, the weighted residual method attempts to approximate the governing equation itself. It is more systematic and more general than the other methods [99]. The finite difference method and the Rayleigh-Ritz method can be thought of as subsets of the weighted residual method. There are many methods of weighted

residual, of which, the Galerkin method is the most widely used because of its computational efficiency.

Instead of using continuous trial functions, as in the weighted residual methods, the finite element method (FEM) proposes to use piecewise trial functions, which enables the method to approximate many problems involving complicated shape functions. This makes the FEM one of the most powerful tools in the field of computational mechanics today. Because of its generality, the FEM does suffer inefficiency and the accuracy of the method is difficult to predict.

The weighted residual method is ideal as the method of solution for the bandsaw blade problem, because if the teeth are neglected, the boundaries are simple, and there exist continuous trial functions for those boundary conditions. It is also well suited for other applications such as stability under parametric excitation [78] and stability under non-conservative forces [43,44].

The Galerkin method was chosen as a discretisation method for all the plate problems dealt with in the remaining chapters. The rest of this chapter is devoted to setting up a general procedure to discretise the equation of motion using the Galerkin method with the help of a computer.

7.4.2 Galerkin Method

Generally speaking, the weighted residual method is used to approximate a set of governing differential equations defined in some region Ω

$$\mathcal{L}(w) = 0 \tag{86}$$

and a set of boundary conditions defined on the boundary Γ

$$\mathcal{B}(w) = 0 \tag{87}$$

where $\mathcal{L}$ and $\mathcal{B}$ are differential operators and w is a variable.

If w is a function of x only, then it can be approximated by

$$w(x) \approx \hat{w}(x) = \sum_{m=1}^{M} a_m \psi_m(x) \tag{88}$$

or if w is a function of x and y (two dimensional) as in the plate problem

$$\hat{w}(x,y) = \sum_{m=1}^{M} \sum_{n=1}^{N} a_{mn} \psi_{mn}(x,y) \tag{89}$$

where a_m, a_{mn} are the coefficients and ψ_m, ψ_{mn} are the *trial functions*. For brevity, assume that the chosen trial functions satisfy all the boundary conditions in Equation (87). Such trial functions are usually referred to as *comparison functions*, whereas *admissible functions* refer to functions which satisfy only the *geometric* boundary conditions (or sometimes referred to as the *essential* boundary conditions) and not the *natural* boundary conditions.

If $\hat{w}$ is substituted into the differential equation, a nonzero residual, R, is obtained from

$$\mathcal{L}(\hat{w}) = R \tag{90}$$

By introducing a set of *weighting functions*, $\{N_r; r = 1, 2, \ldots\}$, R can be forced to be zero over the domain, Ω

$$\int_{\Omega} N_r R \, d\Omega = \int_{\Omega} N_r \mathcal{L}(\hat{w}) \, d\Omega = 0 \tag{91}$$

Equation (91) is the basis for the weighted residual method.

There are a number of methods available for choosing the weighting functions, such as the *point collocation method*, the *subdomain collocation method*, the *least squares method*, and the *Galerkin method*. The Galerkin method is by far the most popular WRM, which makes the obvious choice of taking the trial functions themselves as the weighting functions, that is

$$N_r = \psi_r, \qquad r = 1, 2, \ldots, M \tag{92}$$

or as in the two dimensional case

$$N_{rs} = \psi_{rs}, \qquad \begin{cases} r = 1, 2, \ldots, M \\ s = 1, 2, \ldots, N \end{cases} \tag{93}$$

This leads to a set of $M \times N$ equations to be solved

$$\sum_{r=1}^{M} \sum_{s=1}^{N} \iint_{\Omega} \mathcal{L}(\hat{\omega})\, \psi_{rs}\, d\Omega = 0 \tag{94}$$

When substitute ψ into the above equation, and integrate, a set of algebraic equations is found and can numerically be solved for the required solutions. In the case of dynamic analyses, *eigenvalue problems* are created, for example, in the vibration analysis the natural frequencies are the eigenvalues and the modeshapes are the eigenvectors, and in the buckling analysis the eigenvalues represent the buckling loads and the eigenvectors represent the buckling configurations.

7.5 Plate Solutions Using Galerkin Method

The simple case of SS-SS-SS-SS plate will be used as an example to illustrate the steps involved in obtaining the natural frequencies, and mode shapes using the Galerkin method.

7.5.1 Discretisation of the Plate Equation

By substituting the solutions $w = W(x, y)e^{i\omega t}$ into the equation of motion (70), the governing differential equation, $\mathcal{L}(w)$ can be written as

$$\mathcal{L}(w) = \nabla^4 W - \lambda^4 W = 0 \tag{95}$$

$W(x, y)$ can be approximated by a series of trial functions

$$W \approx \hat{W} = \sum_{m=1}^{M} \sum_{n=1}^{N} a_{mn} \psi_{mn}(x, y) \tag{96}$$

The above expression can be substituted into the Galerkin equation (94) to give

$$\sum_{r=1}^{M}\sum_{s=1}^{N}\int_0^b\int_0^l \psi_{rs}\left\{\sum_{m=1}^{M}\sum_{n=1}^{N} a_{mn}\left(\nabla^4\psi_{mn}-\lambda^4\psi_{mn}\right)\right\}dx\,dy = 0 \tag{97}$$

which can then be integrated and rearranged to give

$$\left\{[K]-\lambda^4[M]\right\}\{X\} = \{0\} \tag{98}$$

It is probably worth noting at this stage that m, n are subscripts associated with the trial functions, and r, s are associated with the weighting functions. Also m and r are related to the x variable while n and s are related to the y variable. The following analyses will adopt the convention that n and s will vary fastest, therefore, the state variable vector $\{X\}$ is

$$\{X\} = \begin{Bmatrix} a_{1,1} \\ a_{1,2} \\ \vdots \\ a_{1,N} \\ a_{2,1} \\ a_{2,2} \\ \vdots \\ a_{M,N-1} \\ a_{M,N} \end{Bmatrix} \tag{99}$$

So an element of $[K]$, referred to as K_{rsmn}, is at row $((r-1)N+s)$, and column $((m-1)N+n)$.

The elements of $[K]$ and $[M]$ are given by

$$K_{rsmn} = \int_0^b\int_0^l \psi_{rs}\nabla^4\psi_{mn}\,dx\,dy \tag{100}$$

and

$$M_{rsmn} = \int_0^b\int_0^l \psi_{rs}\psi_{mn}\,dx\,dy \tag{101}$$

At this stage, the boundary conditions have not entered the analysis. The boundary conditions are considered when selecting the appropriate trial functions, which would satisfy all the boundary conditions explicitly, that is, the trial functions chosen are comparison functions. This is a restriction on the choice of trial functions and in Section 7.7, the *extended Galerkin method* is used to overcome this restriction, so that only admissible functions are required.

7.5.2 SS-SS-SS-SS Plates

For a SS-SS-SS-SS plate, the trial functions are chosen to be

$$\psi_{mn} = \sin\left(\frac{m\pi x}{l}\right)\sin\left(\frac{n\pi y}{b}\right) \tag{102}$$

These functions satisfy all the boundary conditions for SS-SS-SS-SS plate (Equation (79)). In fact, these functions are the exact shape functions for the plate (Equation (83)), therefore, the solutions obtained by the Galerkin method are expected to be those obtained by the exact method.

The trial functions can be differentiated to give

$$\nabla^4\psi_{mn} = \left[\left(\frac{m\pi}{l}\right)^4 + 2\left(\frac{m\pi}{l}\right)^2\left(\frac{n\pi}{b}\right)^2 + \left(\frac{n\pi}{b}\right)^4\right]\sin\left(\frac{m\pi}{l}\right)\sin\left(\frac{n\pi}{b}\right) \tag{103}$$

Each term in the matrices $[M]$ and $[K]$ can be found individually by evaluating the double integrals

$$M_{rsmn} = \int_0^b\int_0^l \psi_{rs}\psi_{mn}\,dx\,dy = \begin{cases} \frac{lb}{4}, & r = m \quad \text{and} \quad s = n \\ 0, & r \neq m \quad \text{or} \quad s \neq n \end{cases} \tag{104}$$

$$K_{rsmn} = \int_0^b\int_0^l \psi_{rs}\nabla^4\psi_{mn}\,dx\,dy = \begin{cases} \frac{lb}{4}\left[\left(\frac{m\pi}{l}\right)^2 + \left(\frac{n\pi}{b}\right)^2\right]^2, & r = m \quad \text{and} \quad s = n \\ 0, & r \neq m \quad \text{or} \quad s \neq n \end{cases} \tag{105}$$

These equations show that both $[K]$ and $[M]$ are diagonal matrices. This is a typical characteristic of the Galerkin method because of the orthogonality property of the chosen trial functions.

The eigenvalues and eigenvectors of Equation (98) can now be found. In this case, the eigenvalues are simply

$$\lambda^4 = \left[\left(\frac{m\pi}{l}\right)^2 + \left(\frac{n\pi}{b}\right)^2\right]^2 \tag{106}$$

or rearrange using λ defined from Equation (75) to give

$$\omega = \left(\left(\frac{m\pi}{l}\right)^2 + \left(\frac{n\pi}{b}\right)^2\right)\left(\frac{D}{\rho h}\right)^{1/2} \tag{107}$$

which is the same as the exact solution in Equation (82).

7.6 Trial Functions for the SS-F-SS-F Plate

The vibratory forms of the SS-F-SS-F plate is not as simple as those of the SS-SS-SS-SS plate, due to the two natural boundary conditions along the two free edges.

The exact shapes can be determined by the exact solutions presented in Section 7.3. The shape functions are separable in x and y coordinates,

$$W(x,y) = \mathcal{X}(x)\,\mathcal{Y}(y) \tag{108}$$

and because the two edges on $x = 0, x = l$ are simply-supported, the shape functions in the x direction take the form

$$\mathcal{X}(x) = \sum_{m=1} \sin\left(\frac{m\pi x}{l}\right) \tag{109}$$

The shape functions in the y direction are quite complicated because they have to satisfy the natural boundary conditions (Equation (84)).

Although, it is possible to use those functions in the Galerkin approximation, they are very cumbersome and inefficient. A more feasible set of functions to use is

the set of eigenfunctions for a free-free beam [97,8]. These eigenfunctions are only admissible functions and do not satisfy all the natural boundary conditions.

One other type of functions which has been successfully applied to plate vibration problems is the *orthogonal polynomials* [9,19]. These polynomials offer an attractive alternative to the classical beam-functions. They were claimed to be more accurate, although there are no other advantages, such as satisfying the natural boundary conditions.

Because there was no comparison between the use of the orthogonal polynomials and the beam-functions as trial functions for the plate problems, the beam eigenfunctions were chosen. This choice also made more physical sense than the polynomials type. The orthogonal polynomials could be used at a later stage to compare with the results presented in this thesis.

Young [97] suggested the functions for a free-free beam as

$$\mathcal{Y}_1 = 1 \tag{110}$$

$$\mathcal{Y}_2 = \sqrt{3}\left(1 - \frac{2y}{b}\right) \tag{111}$$

$$\mathcal{Y}_n = \cosh\frac{\epsilon_n y}{b} + \cos\frac{\epsilon_n y}{b} - \lambda_n\left(\sinh\frac{\epsilon_n y}{b} + \sin\frac{\epsilon_n y}{b}\right),\ n = 3, 4, \ldots \tag{112}$$

where ϵ_n and λ_n can be found from

$$\cos\epsilon_n \cosh\epsilon_n - 1 = 0$$

$$\lambda_n = \frac{\cosh\epsilon_n - \cos\epsilon_n}{\sinh\epsilon_n - \sin\epsilon_n}$$

The equation for ϵ_n must be solved numerically by searching for the roots. $\mathcal{Y}_1$ and $\mathcal{Y}_2$ are the rigid body translation and rotation of the free-free beam respectively. They are included to obtain a complete orthogonal set.

Bassily and Dickinson [8] suggested that the above shape functions were not '*strictly mathematically justifiable and can lead to inaccurate or erroneous results*'. They proposed the use of *degenerated (or relaxed) beam functions.*

The above beam functions for a free-free beam can be rewritten into a simpler form by separating the symmetrical modes from the anti-symmetrical modes as followed

$$\mathcal{Y}_1 = 1 \tag{113}$$

$$\mathcal{Y}_2 = \xi \tag{114}$$

$$\mathcal{Y}_n = \cosh \epsilon_n \xi + \lambda_n \cos \epsilon_n \xi, \quad \text{for } n = 3, 5, \ldots \tag{115}$$

(symmetrical mode)

$$\mathcal{Y}_n = \sinh \epsilon_n \xi + \lambda_n \sin \epsilon_n \xi, \quad \text{for } n = 4, 6, \ldots \tag{116}$$

(antisymmetrical mode)

where

$$\xi = 1 - \frac{2y}{b}$$

and ϵ_n and λ_n can be determined from

$$\tan \epsilon_n + (-1)^{n+1} \epsilon_n = 0, \quad n = 3, 4, \ldots$$

$$\lambda_n = (-1)^n \frac{\sinh \epsilon_n}{\sin \epsilon_n}$$

The concept of the degenerated beam functions involved the relaxation of the unnecessary beam end conditions imposed through the particular choice of λ_n and ϵ_n in accordance with the above relations. Instead, λ_n and/or ϵ_n can be *floated* , hence can be found by the approximation itself.

This idea would improve the accuracy of the higher modes but not as much for the first few modes. Only the first few modes of the plate vibration were of interest, therefore, the usual beam functions were used. The degenerated beam functions could be looked at in future studies, to see if there is actually improvement on the efficiency of the analysis and the accuracy of the results.

The first four values of ϵ_n and λ_n are listed in Table 5.

Table 5: Values of ϵ_n and λ_n.

n	ϵ_n	λ_n
3	2.02875 78381 1043	-4.16583 35079 4104
4	4.49340 94579 0906	-45.80106 48489 7487
5	4.91318 04394 3488	69.42692 66490 5937
6	7.72525 18369 3771	1141.85924 27107 2200

7.7 Extended Galerkin Method for SS-F-SS-F Plates

It is impractical to find a set of trial functions which satisfy all the natural boundary conditions imposed by the two free edges. If possible, admissible functions would provide a simpler option to solve the SS-F-SS-F plate problem.

It is noted that the Rayleigh-Ritz method requires only admissible functions as its trial functions, and the reason for this is because the boundary conditions are already included in the potential energy expression of the plate. This becomes obvious if referring back to the formulation of the plate equation using Hamilton's principle, where both the equation of motion and the boundary conditions were produced from the kinetic and potential energies. This means that the Rayleigh-Ritz method approximates both the equation of motion and the boundary conditions simultaneously, whereas the Galerkin method described previously considered only the equation of motion. One way to extend the Galerkin method is to include the boundary conditions in the approximation, then admissible functions will be allowed as the trial functions of the Galerkin method. This method is sometimes referred to as the *Extended Galerkin method* [99, page 57].

7.7.1 Extended Weighted Residual Method

This method is an extension to the weighted residual method described in Section 7.4.2, which relaxes the requirement that the trial functions must satisfy the boundary conditions $\mathcal{B}(w) = 0$.

If a set of trial functions chosen to approximate the problem does not satisfy some or all of the natural boundary conditions, then the residual in the domain, R_Ω given by

$$R_\Omega = \mathcal{L}(\hat{w}), \qquad \text{in } \Omega \tag{117}$$

is supplemented by a boundary residual R_Γ

$$R_\Gamma = \mathcal{B}(\hat{w}), \qquad \text{on } \Gamma \tag{118}$$

The weighted sum of the residuals on both the domain and the boundary is

$$\int_\Omega N_r R_\Omega d\Omega + \int_\Gamma \bar{N}_r R_\Gamma d\Gamma = 0 \tag{119}$$

hence

$$\int_\Omega N_r \mathcal{L}(\hat{w})\, d\Omega + \int_\Gamma \bar{N}_r \mathcal{B}\left((\hat{w})\right) d\Gamma = 0 \tag{120}$$

where, in general, the weighting functions N_r and $\bar{N}_r$ can be chosen independently.

The first term of the above equation can often be rearranged to

$$\int_\Omega N_r \mathcal{L}(\hat{w})\, d\Omega \equiv \int_\Omega \mathcal{C}(N_r)\, \mathcal{D}(\hat{w})\, d\Omega + \int_\Gamma N_r \mathcal{E}(\hat{w})\, d\Gamma \tag{121}$$

where $\mathcal{C}, \mathcal{D}$ and $\mathcal{E}$ are linear differential operators involving an order of differentiation lower than that of the original operator $\mathcal{L}$. This rearrangement is often referred to as the *weak form* of the weighted residual method.

When Equation (121) is substituted into Equation (120), it may be possible to simplify or even eliminate the two terms in the boundary integral $\int_\Gamma$ by choosing suitable boundary weighting functions $\bar{N}_r$.

When the weighting functions N_r and $\bar{N}_r$ are chosen to be the trial functions or their derivatives, then the extended weighted residual method, described here, is called the extended Galerkin method.

7.7.2 Weak Form of the Plate Equation

The first term in the weighted residual approximation of the plate equation

$$\int_0^b \int_0^l N_{rs} \nabla^4 W \, dx \, dy$$

can be integrated by parts to reduce the order of differentiation

$$\begin{aligned}\int_0^b \int_0^l N_{rs} \nabla^4 W \, dx \, dy &= \int_0^b \int_0^l \nabla^2 N_{rs} \, \nabla^2 W \, dx \, dy \\ &+ \int_0^l \left\{ \left(\frac{\partial^3 W}{\partial y^3} + \frac{\partial^3 W}{\partial x^2 \partial y} \right) N_{rs} \Big|_{y=0}^{b} - \left(\frac{\partial^2 W}{\partial x^2} + \frac{\partial^2 W}{\partial y^2} \right) \frac{\partial N_{rs}}{\partial y} \Big|_{y=0}^{b} \right\} dx \\ &+ \int_0^b \left\{ \left(\frac{\partial^3 W}{\partial x^3} + \frac{\partial^3 W}{\partial x \partial y^2} \right) N_{rs} \Big|_{x=0}^{l} - \left(\frac{\partial^2 W}{\partial x^2} + \frac{\partial^2 W}{\partial y^2} \right) \frac{\partial N_{rs}}{\partial x} \Big|_{x=0}^{l} \right\} dy \quad (122)\end{aligned}$$

where ∇^2 is the Laplace operator

$$\nabla^2 = \frac{\partial^2}{\partial x^2} + \frac{\partial^2}{\partial y^2}$$

When the boundary geometry of the plate is more complicated than the rectangular case, such as the circular plate problem, then the *divergence theorem* should be used instead of the integration by parts [49, page 179].

7.7.3 SS-F-SS-F Plates

The boundary conditions on the two simply-support edges, $x = 0$ and $x = l$, are already satisfied by the trial functions, $\sin\left(\frac{m\pi x}{l}\right)$, hence there is no need to approximate them in the analysis.

The boundary conditions on the two free edges are, however, required in the approximation, because the trial functions do not satisfy them explicitly.

Applying the extended Galerkin method to the plate equation of motion (Equation (75)), and the boundary conditions (Equation (84)) gives

$$\int_0^b \int_0^l \psi_{rs} \left(\nabla^4 W - \lambda^4 W\right) \, dx \, dy + \int_0^l \left\{ \bar{N}_{rs} \left(\frac{\partial^2 W}{\partial y^2} + \nu \frac{\partial^2 W}{\partial x^2} \right) \Bigg|_{y=0}^{b} + \bar{N}'_{rs} \left(\frac{\partial^3 W}{\partial y^3} + (2-\nu) \frac{\partial^3 W}{\partial x^2 \partial y} \right) \Bigg|_{y=0}^{b} \right\} dx = 0 \quad (123)$$

The weak form, Equation (122), can be then substituted into the first term of Equation (123), hence

$$\int_0^b \int_0^l \left(\nabla^2 \psi_{rs} \, \nabla^2 W - \lambda^4 W\right) \, dx \, dy + \int_0^l \left\{ \bar{N}_{rs} \left(\frac{\partial^2 W}{\partial y^2} + \nu \frac{\partial^2 W}{\partial x^2} \right) \Bigg|_{y=0}^{b} - \frac{\partial \psi_{rs}}{\partial y} \left(\frac{\partial^2 W}{\partial y^2} + \frac{\partial^2 W}{\partial x^2} \right) \Bigg|_{y=0}^{b} + \bar{N}'_{rs} \left(\frac{\partial^3 W}{\partial y^3} + (2-\nu) \frac{\partial^3 W}{\partial x^2 \partial y} \right) \Bigg|_{y=0}^{b} + \psi_{rs} \left(\frac{\partial^3 W}{\partial y^3} + \frac{\partial^3 W}{\partial x^2 \partial y} \right) \Bigg|_{y=0}^{b} \right\} dx = 0 \quad (124)$$

Recalled that $\bar{N}_{rs}$ and $\bar{N}'_{rs}$ are independent weighting functions, and by letting

$$\bar{N}_{rs} = \frac{\partial \psi_{rs}}{\partial y}$$
$$\bar{N}'_{rs} = -\psi_{rs}$$

Equation (124) can be simplified to

$$\int_0^b \int_0^l \left(\nabla^2 \psi_{rs} \, \nabla^2 W - \lambda^4 \psi_{rs} W\right) \, dx \, dy - (1-\nu) \int_0^l \left(\frac{\partial \psi_{rs}}{\partial y} \frac{\partial^2 W}{\partial x^2} + \psi_{rs} \frac{\partial^3 W}{\partial x^2 \partial y} \right) \Bigg|_{y=0}^{b} dx = 0 \quad (125)$$

Equation (125) shows that when the trial functions do not satisfy all the natural boundary conditions, the Galerkin equation contains extra terms in the boundary integral.

7.8 A Computer-Oriented Procedure

When the plate problem becomes more complicated, the work involved in obtaining the solutions also becomes more tedious. Because the main purpose of discretising the problem is to allow a computer to carry out this time-consuming task of arithmetic, a systematic procedure is developed in this section to utilize fully the computer capability for solving these problems.

From the previous section, the two steps that involved a lot of computations were the double integrations of each term in the $[M]$ and $[K]$ matrices and the eigenvalue solver.

Both of these mentioned steps can be carried out numerically by using a computer. At present, the use of personal computers (PC) are very popular because of their powerful capabilities and low prices. Developing the solver on a PC was more convenient and will, perhaps, be more useful to others than if done on a main frame computer.

7.8.1 Eigenvalue Solver - PC-MATLAB

PC-MATLAB is an interactive computer program that serves as a convenient *laboratory* for computations involving matrices. It provides easy access to matrix software developed by the *LINPACK* and *EISPACK* projects [20,74]. MATLAB was initially written in Fortran and designed to run on mainframe computers. PC-MATLAB is the second generation of MATLAB for the IBM-PC. It had been completely rewritten in the C language and included many new features which made it a flexible and powerful scientific *spreadsheet* for many types of numeric calculations, not just matrix computations.

A multi-purpose eigenvalue solver is a very complex piece of software [63,74]. PC-MATLAB comes fully equipped with a set of powerful routines for solving eigenvalue problems, the EISPACK routines. These routines, together with the flexible interactive environment, and the way in which MATLAB handles matrices, make it the obvious choice for solving the eigenvalue problems presented in this thesis. Its only shortcoming would be the allowable 100×100 maximum size for a matrix. So far, the matrices involved in this thesis had been smaller than 100×100.

7.8.2 Numerical Integration

The integration step could also be handled by MATLAB using its own interpreted language, which would give a much more compact coding than that written by Fortran to perform the same task. However, the integration procedure required for the Galerkin plate problem is very complicated, a separate computer program would be more feasible. The values calculated could then be imported into MATLAB for the second phase of the analysis, the search for eigenvalues.

The method of numerical integration will be dealt with in Section 7.9.

7.8.3 Computer Language - The C Language

There are many indications that C can be used as a very powerful computer language for scientific purposes, it was therefore chosen as the computer language for developing the program to perform the integration. A few of C's better features, compared with the more conventional languages, such as Fortran, include

- More powerful control structures, such as *while, switch.*
- More versatile data types such as *pointers, structures, unions.* These data types enable the true dynamic memory allocation of variables, which means

that there is no longer a need to set aside a large block of memory while a particular application may require only a small portion of this. This feature is very useful when programming on a PC where memory is more limited than on a mainframe computer.

- Much better file and I/O handling.
- The powerful concept of libraries. This enables a function which has more than one application to be saved in a library and therefore can be accessed at a later date by other programs.
- Compatibility. C is believed to be the most compatible language of all.

One of the best reference available for numerical analyses in C is the "Numerical Recipes in C" [64].

7.8.4 The Procedure

The procedure adopted is as follows:

1. The problem is formulated using Hamilton's principle to provide the equation of motion and all the boundary conditions. The equation of motion of the plate is a partial differential equation in time and two dimensional space domains.

$$\mathcal{L}\left(w\left(x,y,t\right)\right)=0$$

where $\mathcal{L}$ is a partial differential operator.

2. Assume a separable solution of time and space

$$w\left(x,y,t\right)=W\left(x,y\right)T\left(t\right)$$

where $T(t)$ is a function of the time variable, and $W(x,y)$ is a function of the space variables.

3. Choose trial functions to approximate the solutions $W(x, y)$ of the governing equation, by trying to find functions which satisfy all the geometric boundary conditions and as many of the natural boundary conditions as possible. Differentiations of the trial functions with respect to x and y will also be required, depending on the governing equation. These functions are placed in the program once for each different plate geometry. Changes in the natural boundary conditions are taken care of by the extended Galerkin formulation, and not the trial functions themselves.

4. Substitute the governing differential equation into the Galerkin equation. For problems where the trial functions do not satisfy all the natural boundary conditions, the extended Galerkin method is used to approximate the governing equations and the natural boundary conditions simultaneously.

   This step reduces the governing equation to a set of ordinary differential equations, or in the case of linear vibration analysis a set of algebraic equations, which can be expressed in matrix form.

5. Simplify the problem by integrating by parts and choosing appropriate weighting functions to eliminate as many terms in the boundary integration as possible.

6. Rearrange the Galerkin equation so that most of the parameters, such as the flexural rigidity, the density, the thickness, the transport speed, and the magnitude of tension, are not included in the program. These parameters can be defined interactively in MATLAB. The dimensions l and b of the plate, and the profiles of the stresses (as in Chapter 9) are however, needed in the program.

7. Write computer subroutines which use the trial functions and any other differentiations of the trial functions to calculate the terms required for the integrations. Cycling over r, s, m and n, and using the numerical integration routine to compute each element of the matrices given in the matrix equation. The numerical values of those matrices can be saved in a MATLAB-format data file.

8. Enter the MATLAB environment, read the data file, define all the parameters required for the analysis, set up the matrix equation and finally solve for the eigenvalues and eigenvectors of the equation.

7.9 Numerical Integration - Gaussian Quadrature

There are many numerical integration schemes available, of which, the most popular scheme is Gaussian quadrature, therefore it was chosen to perform the integration required in this thesis.

A one dimensional Gaussian quadrature rule is given by

$$I = \int_{-1}^{1} \phi(\xi)\, d\xi \approx N_1\, \phi(\xi_1) + N_2\, \phi(\xi_2) + \cdots + N_n\, \phi(\xi_n) \qquad (126)$$

that is, I is approximated by evaluating $\phi(\xi)$ at each of several locations ξ_i, multiplying each $\phi(\xi_i)$ by an appropriate weight N_i, then adding them together. The sampling points ξ_i, sometimes called the *Gauss points*, and the weights N_i for $i = 1, 2, \cdots, n$ are determined by the Gauss method to provide the greatest accuracy. Numerical values of the Gauss points and weights are given in [14, page 120], or can be calculated using the computer program given in [64, page 136].

Similarly, for a two dimensional case

$$I = \int_{-1}^{1} \int_{-1}^{1} \phi(\xi, \eta)\ d\xi\, d\eta \approx \sum_{i=1}^{m} \sum_{j=1}^{n} N_i N_j\, \phi(\xi_i, \eta_j) \tag{127}$$

Note that the Gauss points and the weights are given for $-1 \leq \xi \leq 1$ and $-1 \leq \eta \leq 1$; for the plate problems in this thesis, the integrations over the area of the plate are for $0 \leq x \leq l$ and $0 \leq y \leq b$, therefore transformations of coordinates are required before they may be integrated, thus

$$\begin{aligned} \int_0^b \int_0^l f(x,y)\ dx\, dy &= \int_{-1}^{1} \int_{-1}^{1} f\left(\frac{l}{2}(\xi+1), \frac{b}{2}(\eta+1)\right) \frac{lb}{4}\, d\xi\, d\eta \\ &\approx \frac{lb}{4} \sum_{i=1}^{m} \sum_{j=1}^{n} N_i N_j\, f\left(\frac{l}{2}(\xi+1), \frac{b}{2}(\eta+1)\right) \end{aligned} \tag{128}$$

In general, a polynomial of degree $2n-1$ is integrated exactly by n Gauss points. For all the calculations in this thesis, eight Gauss points were chosen for each direction, that is, a fifteenth degree polynomial could be integrated exactly.

Chapter 8

MOVING PLATES

8.1 Introduction

A wide bandsaw blade, when stationary, can be analysed using the usual plate model, however, under idling or cutting conditions, it must be represented by a *moving plate*.

The moving plate model belongs to a class of problems referred to as the axially moving material problems. The first investigation into these problems was the study on an axially moving string in 1897 [73]. It was not until 1965 when the first research on the bandsaw vibration was published by Mote [52] which was on the transverse vibration of a moving beam. Since then, research on bandsaw blades has escalated and diverged into many different areas, such as the torsional vibration of a moving beam [5,75], the parametric excitation of a moving beam under fluctuating tension [58]. The first investigation of a moving plate problem was published in 1980 [86,87], which pointed out that the moving plate theory was necessary to model a wide bandsaw blade.

Recent research had been directed toward more complicated subjects, such as,

the coupling between the transverse and torsional vibration of a moving beam [75,95], the coupling between the cutting and non-cutting span of the bandsaw blade [94,88,89], the stability of a moving beam under a periodic edge loading [95]. These studies revealed many interesting phenomena, however they did not consider the moving plate case.

Chapter 7 had discussed a general method of analysing plate problems, and had considered the vibration analysis of stationary plates. This chapter presents a step which extends the theory of stationary plates to cover the moving plate problem.

8.2 The Formulation

The Hamilton's principle discussed in Section 7.2 was used to formulate the equation of motion and the boundary conditions of a moving plate.

An actual saw blade is always subjected to a large tensile force which increases the stiffness of the blade and therefore increases the potential energy of the plate. For brevity, the inclusion of this extra potential energy due to the tensile force is deferred until the next chapter. The potential energy of a moving plate is, therefore, the same as that of a stationary plate, and Equation (59) and (63) are still valid for this case.

The kinetic energy of a moving plate is obtained by finding the velocity of the plate with respect to a stationary spatial coordinates system, (x, y, z). The material coordinates system, (x', y', z'), is moving with a velocity c along the x direction with respect to the stationary coordinates (see Figure 74).

Assume arbitrarily that at time $t = 0$ the two coordinates systems are coincided,

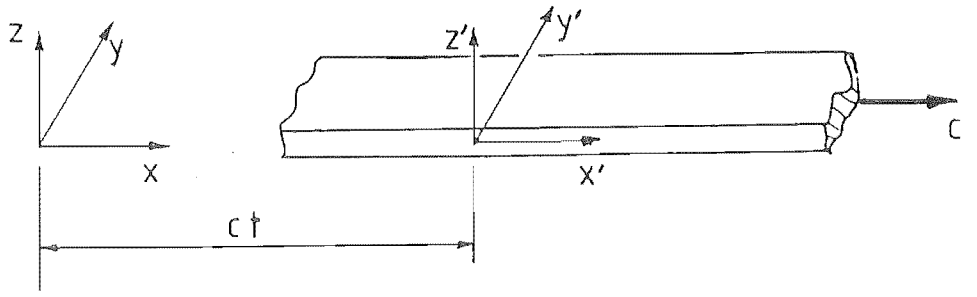

Figure 74: Spatial and material coordinates.

then at time $t = t$

$$\begin{Bmatrix} x \\ y \\ z \end{Bmatrix} \equiv \begin{Bmatrix} x' + ct \\ y' \\ z' \end{Bmatrix} \tag{129}$$

The time dependent lateral displacement of the plate referenced to the material coordinates is $w'(x', y', t)$ or referenced to the spatial coordinates is $w(x, y, t)$. They are, in fact, the same displacement but referred to by a different coordinates system, hence

$$w'(x', y', t) \equiv w(x' + ct, y', t) \tag{130}$$

The lateral velocity of a plate with respect to the moving frame of reference is simply $\frac{\partial w'}{\partial t}$, and from the definition of partial differentiation, this velocity can be expressed as

$$\frac{\partial w'}{\partial t} = \lim_{\Delta t \to 0} \left[\frac{w'(x', y', t + \Delta t) - w'(x', y', t)}{\Delta t} \right] \tag{131}$$

Substituting the expression in Equation (130) into the above equation to give

$$\begin{aligned} \frac{\partial w'}{\partial t} &= \lim_{\Delta t \to 0} \left[\frac{w(x' + c(t + \Delta t), y', t + \Delta t) - w(x', y', t)}{\Delta t} \right] \\ &= \lim_{\Delta t \to 0} \left[\frac{w(x + c\Delta t, y, t + \Delta t) - w(x, y, t)}{\Delta t} \right] \end{aligned} \tag{132}$$

This is actually the definition of a total derivative $\frac{D}{Dt}$ with $\Delta x = c\Delta t$ and

$\triangle y = 0$, hence

$$\begin{aligned} \frac{\partial w'(x', y', t)}{\partial t} &= \frac{Dw(x, y, t)}{Dt} \\ &= \frac{\partial w}{\partial t} + c\frac{\partial w}{\partial x} \end{aligned} \tag{133}$$

The absolute velocity of a vibrating moving plate is

$$\begin{aligned} v &= \left[c^2 + \left(\frac{\partial w'}{\partial t}\right)^2\right]^{1/2} \\ &= \left[c^2 + \left(\frac{\partial w}{\partial t} + c\frac{\partial w}{\partial x}\right)^2\right]^{1/2} \end{aligned} \tag{134}$$

hence the kinetic energy is given by

$$T = \int_0^b \int_0^l \frac{\rho h}{2}\left[c^2 + \left(\frac{\partial w}{\partial t} + c\frac{\partial w}{\partial x}\right)^2\right] dx\, dy \tag{135}$$

When $c = 0$, Equation (135) becomes Equation (58) the kinetic energy of a stationary plate.

Applying the calculus of variations as illustrated in Section 7.2 to the kinetic energy Equation (135) gives

$$\begin{aligned} \int_{t_1}^{t_2} \delta T\, dt &= \int_{t_1}^{t_2}\left\{\int_0^b \int_0^l -\rho h\left(\frac{\partial^2 w}{\partial t^2} + 2c\frac{\partial^2 w}{\partial x \partial t} + c^2\frac{\partial^2 w}{\partial x^2}\right)\delta w\, dx\, dy \right. \\ &\quad \left. + \int_0^b \rho h c\left(\frac{\partial w}{\partial t} + c\frac{\partial w}{\partial x}\right)\delta w\Big|_{x=0}^{l} dy\right\} dt \end{aligned} \tag{136}$$

Substituting Equation (136) and Equation (63) into the Hamilton's equation (Equation (57)) gives the equation of motion of an axially moving plate as

$$D\nabla^4 w + \rho h\left(\frac{\partial^2 w}{\partial t^2} + 2c\frac{\partial^2 w}{\partial x \partial y} + c^2\frac{\partial^2 w}{\partial x^2}\right) = 0 \tag{137}$$

On $x = 0$ and $x = l$, the boundary conditions are

$$w = 0 \quad \text{or} \quad \left(\rho h c\frac{\partial w}{\partial t} + \rho h c^2\frac{\partial w}{\partial x} - Q_x\right) = 0 \tag{138}$$

$$\frac{\partial w}{\partial x} = 0 \quad \text{or} \quad M_x = 0 \tag{139}$$

$$\frac{\partial w}{\partial y} = 0 \quad \text{or} \quad M_{xy} = 0 \tag{140}$$

and on $y = 0$, $y = b$

$$w = 0 \quad \text{or} \quad Q_y = 0 \tag{141}$$

$$\frac{\partial w}{\partial y} = 0 \quad \text{or} \quad M_y = 0 \tag{142}$$

$$\frac{\partial w}{\partial x} = 0 \quad \text{or} \quad M_{xy} = 0 \tag{143}$$

The terms $c^2 \frac{\partial^2 w}{\partial x^2}$ and $2c \frac{\partial^2 w}{\partial x \partial t}$ can be regarded as the centripetal term, and the coriolis term respectively.

8.3 Approximate Solutions for a Moving SS-F-SS-F Plate

8.3.1 Galerkin Equation

The method of solving the moving plate problem is similar to that for the stationary plate in Section 7.7. The extra terms in the boundary conditions do not affect the solution, because the edges along $x = 0$ and $x = l$ are simply-supported, that is, $w = 0$. Therefore, only two extra terms in the equation of motion are to be added to the stationary plate solution. The boundary conditions on the $y = 0, y = b$ edges remain the same as previously.

The trial functions are exactly the same as for those used in the stationary plate case, because there are no changes in the boundary geometry. For the sake of generality, instead of assuming $w(x, y, t) = W(x, y)e^{i\omega t}$, $w(x, y, t) = W(x, y)T(t)$ was used, which when substituted into the Galerkin equation will produce a set of second-order ordinary differential equations, instead of a set of algebraic equations.

Applying the weighting functions, ψ_{rs}, on the two extra terms due to the transport velocity, c, and combining with Equation (125) gives

$$\int_0^b \int_0^l \left\{ \rho h \left(\psi_{rs} W \ddot{T} + 2c\psi_{rs} \frac{\partial W}{\partial x} \dot{T} + c^2 \psi_{rs} \frac{\partial^2 W}{\partial x^2} T \right) + D \nabla^2 \psi_{rs} \nabla^2 W T \right\} dx\, dy$$
$$- (1-\nu) D \int_0^l \left\{ \psi_{rs} \frac{\partial^3 W}{\partial x^2 \partial y}\bigg|_{y=0}^{b} + \frac{\partial \psi_{rs}}{\partial y} \frac{\partial^2 W}{\partial x^2}\bigg|_{y=0}^{b} \right\} T\, dx = 0 \quad (144)$$

Note that the third term in the above equation can be simplified by using integration by parts

$$\begin{aligned} \int_0^b \int_0^l \psi_{rs} \frac{\partial^2 W}{\partial x^2} dx\, dy &= \int_0^b \psi_{rs} \frac{\partial W}{\partial x}\bigg|_{x=0}^{l} dy - \int_0^b \int_0^l \frac{\partial \psi_{rs}}{\partial x} \frac{\partial W}{\partial x} dx\, dy \\ &= - \int_0^b \int_0^l \frac{\partial \psi_{rs}}{\partial x} \frac{\partial W}{\partial x} dx\, dy \end{aligned} \quad (145)$$

since $\psi_{rs} = 0$ at $x = 0$ and $x = l$.

Rearranging Equation (144) into a matrix form, and separating out the parameters D, ρ, h, c from the matrices. These matrices will be evaluated by the numerical integration routine.

$$\rho h [A] \left\{ \ddot{T} \right\} + 2\rho h c [B] \left\{ \dot{T} \right\} + \left(D [C] + \rho h c^2 [D] \right) \{T\} = 0 \quad (146)$$

where the element of $[A], [B], [C]$ and $[D]$ are

$$\begin{aligned} A_{rsmn} &= \int_0^b \int_0^l \psi_{rs} \psi_{mn}\, dx\, dy \\ B_{rsmn} &= \int_0^b \int_0^l \psi_{rs} \frac{\partial \psi_{mn}}{\partial x} dx\, dy \\ C_{rsmn} &= \int_0^b \int_0^l \nabla^2 \psi_{rs} \nabla^2 \psi_{mn}\, dx\, dy \\ &\quad - (1-\nu) \int_0^l \left\{ \psi_{rs} \frac{\partial^3 \psi_{mn}}{\partial x^2 \partial y} + \frac{\partial \psi_{rs}}{\partial y} \frac{\partial^2 \psi_{mn}}{\partial x^2} \right\}\bigg|_{y=0}^{b} dx \\ D_{rsmn} &= \int_0^b \int_0^l - \frac{\partial \psi_{rs}}{\partial x} \frac{\partial \psi_{mn}}{\partial x} dx\, dy \end{aligned}$$

Referring to Section 7.5.1 for the meaning of the subscripts r, s, m, n.

For vibration analyses, $\{T\}$ is assumed to be

$$\{T\} = \{X\}\, e^{\lambda t} \tag{147}$$

where $\{X\}$ represents the generalised coordinates vector as in Equation (99). Substituting this into the second-order differential equation to produce a quadratic eigenvalue problem. The complication here is the existence of a mixed derivative term in the equation of motion, which becomes a first order differential term in the Galerkin equation. A special technique is, therefore, required for solving the quadratic eigenvalue problem.

8.3.2 Quadratic Eigenvalue Problems

For simplicity, Equation (147) combining with Equation (146) can be rearranged to a more general quadratic eigenvalue form

$$\left([M_0] - \lambda\,[M_1] - \lambda^2\,[M_2]\right)\{X\} = \{0\} \tag{148}$$

One method of obtaining the eigenvalues of the equation directly is by using an *inverse iteration method* [47]. Another method available is the *linearisation* of the quadratic eigenvalue problem [2,78], which is perhaps less efficient than the inverse iteration, but much simpler in principle. The linearisation method was chosen for solving the quadratic eigenvalue problems in this thesis.

Equation (148) can be rearranged by shifting the λ^2 term to the right hand side, and pre-multiplying the equation by $[M_2]^{-1}$ to give

$$\left([M_2]^{-1}\,[M_0] - \lambda\,[M_2]^{-1}\,[M_1]\right)\{X\} = \lambda^2\,\{X\} \tag{149}$$

Introducing a new variable $\{Y\} = \lambda\,\{X\}$, and combining with Equation (149) gives

$$\begin{bmatrix} [0] & [I] \\ [M_2]^{-1}\,[M_0] & -[M_2]^{-1}\,[M_1] \end{bmatrix} \begin{Bmatrix} X \\ Y \end{Bmatrix} = \lambda \begin{Bmatrix} X \\ Y \end{Bmatrix} \tag{150}$$

where [0] is a zero matrix, and $[I]$ is an identity matrix, both are the same size as $[M_0]$.

This augmented equation can now be solve for the eigenvalues λ by the usual eigenvalue solver such as the one provided by PC-MATLAB.

Note that the number of eigenvalues found by this method is twice the number of the eigenvalues found for the stationary plate. This is because λ contain the eigenvalues of the linearisised equation, whereas, the stationary plate eigenvalues are λ^2, which are, in fact, $\pm\lambda$.

Chapter 9

STRESSES IN BANDSAW BLADES

9.1 Introduction

The bandsaw blade is subjected to large in-plane stresses for a number of reasons, some of the reasons are intended by the designer, while some are produced from the interactions of the saw blade with other parts of the machine during its operation.

In 1972 Pahlitzsch and Puttkammer [60] and later in 1985 Allen [3] investigated the cause of stresses occurring in bandsaw blades. A recent improvement on the dynamic behaviour of a saw blade was achieved by introducing a higher stress level than that in the conventional blades. The improved bandsaw is sometimes referred to as a high-strain bandsaw. This development has pushed the stress to the limit of the elastic strength of the material, hence reducing the life expectancy of the blade. A result of excessive stress in the saw blade is the development of cracks in the gullets of the saw teeth.

This subject of stressing bandsaw blades is still not fully understood because

all the work carried out so far has been from observation in production, or from experiments or based on basic theories of strength of materials. A plane-stress finite element analysis of the blade in the region of the tooth and the gullet would have been quite useful, unfortunately, it was out of the scope of this thesis.

The dynamic behaviour of a stressed wide bandsaw blade is also inadequately understood, therefore, this chapter extends the plate theory presented in the previous chapters to include the effects of in-plane stresses, and investigates various patterns of stress occurring in bandsaw blades.

9.2 General Formulation and Method of Solutions

9.2.1 Formulation

Inplane-stresses of a plate consist of a direct stress in the x direction σ_x, a direct stress in the y direction σ_y and a shear stress τ_{xy}. Since the thickness of a saw blade is constant, a more convenient unit of measurement for the stresses are forces per unit length, that is, $N_x = \sigma_x h, N_y = \sigma_y h, N_{xy} = \tau_{xy} h$, where h is the thickness.

These forces per unit length raise the potential energy of the plate, therefore, they have to be included into the potential energy of the previous plate model. The total potential energy of the plate, U, can then be expressed as

$$U = U_b + V \tag{151}$$

where U_b is the potential energy caused by bending, which was given by Equation (59), and V is the potential energy caused by the in-plane forces

$$V = \int_0^b \int_0^l \frac{1}{2} \left\{ N_x \left(\frac{\partial w}{\partial x} \right)^2 + 2N_{xy} \frac{\partial w}{\partial x} \frac{\partial w}{\partial y} + N_y \left(\frac{\partial w}{\partial y} \right)^2 \right\} dx\, dy \tag{152}$$

The variation of this term can be written down and integrated by parts using the method described in Section 7.2 to give

$$\begin{aligned}\int_{t_1}^{t_2} \delta V \, dt \;=\; & \int_{t_1}^{t_2} \left\{ \int_0^b \int_0^l - \left[\frac{\partial}{\partial x}\left(N_x \frac{\partial w}{\partial x} \right) + \frac{\partial}{\partial y}\left(N_y \frac{\partial w}{\partial y} \right) + \frac{\partial}{\partial x}\left(N_{xy} \frac{\partial w}{\partial y} \right) \right. \right. \\ & \left. + \frac{\partial}{\partial y}\left(N_{xy} \frac{\partial w}{\partial x} \right) \right] dx \, dy + \int_0^b \left[N_x \frac{\partial w}{\partial x} + N_{xy} \frac{\partial w}{\partial y} \right] \delta w \Big|_{x=0}^{l} dy \\ & \left. + \int_0^l \left[N_y \frac{\partial w}{\partial y} + N_{xy} \frac{\partial w}{\partial x} \right] \delta w \Big|_{y=0}^{b} dx \right\} dt \end{aligned} \tag{153}$$

The equation of motion and the boundary conditions can be found by combining Equation (153) with Equation (63) and Equation (61) for the stationary plate case or Equation (136) for the moving plate case.

For a stationary plate, the equation of motion is

$$D\nabla^4 w + \rho h \frac{\partial^2 w}{\partial t^2} = \frac{\partial}{\partial x}\left(N_x \frac{\partial w}{\partial x} \right) + \frac{\partial}{\partial x}\left(N_{xy} \frac{\partial w}{\partial y} \right) + \frac{\partial}{\partial y}\left(N_{xy} \frac{\partial w}{\partial x} \right) + \frac{\partial}{\partial y}\left(N_y \frac{\partial w}{\partial y} \right) \tag{154}$$

and the boundary conditions on $x = 0$ and $x = l$ are

$$M_x = 0 \qquad \text{or} \qquad \frac{\partial w}{\partial x} = 0 \tag{155}$$

$$M_{xy} = 0 \qquad \text{or} \qquad \frac{\partial w}{\partial y} = 0 \tag{156}$$

$$\left(N_x \frac{\partial w}{\partial x} + N_{xy} \frac{\partial w}{\partial y} + Q_x \right) = 0 \qquad \text{or} \qquad w = 0 \tag{157}$$

and on $y = 0$ and $y = b$ are

$$M_y = 0 \qquad \text{or} \qquad \frac{\partial w}{\partial y} = 0 \tag{158}$$

$$M_{xy} = 0 \qquad \text{or} \qquad \frac{\partial w}{\partial x} = 0 \tag{159}$$

$$\left(N_y \frac{\partial w}{\partial y} + N_{xy} \frac{\partial w}{\partial x} + Q_y \right) = 0 \qquad \text{or} \qquad w = 0 \tag{160}$$

Similarly, for a moving plate the equation of motion is

$$D\nabla^4 w + \rho h\left(\frac{\partial^2 w}{\partial t^2} + 2c\frac{\partial^2 w}{\partial x \partial y} + c^2\frac{\partial^2 w}{\partial x^2}\right) = \frac{\partial}{\partial x}\left(N_x\frac{\partial w}{\partial x}\right) + \frac{\partial}{\partial x}\left(N_{xy}\frac{\partial w}{\partial y}\right) + \frac{\partial}{\partial y}\left(N_{xy}\frac{\partial w}{\partial x}\right) + \frac{\partial}{\partial y}\left(N_y\frac{\partial w}{\partial y}\right) \quad (161)$$

and the boundary conditions on $x = 0$ and $x = l$ are

$$M_x = 0 \qquad \text{or} \qquad \frac{\partial w}{\partial x} = 0 \quad (162)$$

$$M_{xy} = 0 \qquad \text{or} \qquad \frac{\partial w}{\partial y} = 0 \quad (163)$$

$$\left(\rho hc\frac{\partial w}{\partial t} + \rho hc^2\frac{\partial w}{\partial x} - N_x\frac{\partial w}{\partial x} - N_{xy}\frac{\partial w}{\partial y} - Q_x\right) = 0$$

$$\text{or} \qquad w = 0 \quad (164)$$

and on $y = 0$ and $y = b$ are

$$M_y = 0 \qquad \text{or} \qquad \frac{\partial w}{\partial y} = 0 \quad (165)$$

$$M_{xy} = 0 \qquad \text{or} \qquad \frac{\partial w}{\partial x} = 0 \quad (166)$$

$$\left(N_y\frac{\partial w}{\partial y} + N_{xy}\frac{\partial w}{\partial x} + Q_y\right) = 0 \qquad \text{or} \qquad w = 0 \quad (167)$$

9.2.2 Method of Solutions

The trial functions for the SS-F-SS-F plate in Section 7.6 are still valid for both the stationary and the moving plate problem in this chapter, and the Galerkin equations can be constructed the same way as described previously.

There are four extra terms in the boundary conditions due to the in-plane stresses, which can be simplified by combining with the terms in the equation of motion using the weak-form of the Galerkin method discussed in Section 7.7.2 . By this method, the stress terms in the equation of motion are first integrated using

the method of integration by parts, then the terms in the boundary integral can be combined or even cancelled out with the four terms in the boundary conditions. That is

$$\int_0^b \int_0^l \psi_{rs} \left[\frac{\partial}{\partial x}\left(N_x \frac{\partial w}{\partial x} \right) + \frac{\partial}{\partial x}\left(N_{xy} \frac{\partial w}{\partial y} \right) + \frac{\partial}{\partial y}\left(N_{xy} \frac{\partial w}{\partial x} \right) + \frac{\partial}{\partial y}\left(N_y \frac{\partial w}{\partial y} \right) \right] dx\, dy =$$
$$\int_0^b \left\{ \psi_{rs} \left(N_x \frac{\partial w}{\partial x} + N_{xy} \frac{\partial w}{\partial y} \right) \Big|_{x=0}^{l} - \int_0^l \frac{\partial \psi_{rs}}{\partial x} \left(N_x \frac{\partial w}{\partial x} + N_{xy} \frac{\partial w}{\partial y} \right) dx \right\} dy +$$
$$\int_0^l \left\{ \psi_{rs} \left(N_{xy} \frac{\partial w}{\partial x} + N_y \frac{\partial w}{\partial y} \right) \Big|_{y=0}^{b} - \int_0^b \frac{\partial \psi_{rs}}{\partial y} \left(N_{xy} \frac{\partial w}{\partial x} + N_y \frac{\partial w}{\partial y} \right) dy \right\} dx \quad (168)$$

where ψ_{rs} is the trial functions, and the weighting functions of the Galerkin method.

Again, the boundary integral on $x = 0, x = l$ is equal to zero because of zero displacement ($\psi_{rs} = 0$). The boundary integral on $y = 0, y = b$ is of the same form as the boundary conditions, therefore, it can be cancelled out by selecting the appropriate weighting functions for the boundary conditions. This leads to the general Galerkin equation for a moving plate under in-plane stresses as

$$\int_0^b \int_0^l \left\{ \rho h \left[\psi_{rs} W \ddot{T} + 2c\psi_{rs} \frac{\partial W}{\partial x} \dot{T} - c^2 \frac{\partial \psi_{rs}}{\partial x} \frac{\partial W}{\partial x} T \right] + \left[D \nabla^2 \psi_{rs} \nabla^2 W + \frac{\partial \psi_{rs}}{\partial x} \left(N_x \frac{\partial W}{\partial x} + N_{xy} \frac{\partial W}{\partial y} \right) + \frac{\partial \psi_{rs}}{\partial y} \left(N_{xy} \frac{\partial W}{\partial x} + N_y \frac{\partial W}{\partial y} \right) \right] T \right\} dx\, dy$$
$$- (1 - \nu) \int_0^l \left\{ \left(\psi_{rs} \frac{\partial^3 W}{\partial x^2 \partial y} + \frac{\partial \psi_{rs}}{\partial y} \frac{\partial^2 W}{\partial x 2} \right) \Big|_{y=0}^{b} \right\} T\, dx = 0 \quad (169)$$

For a stationary plate, the Galerkin equation is the same as Equation (169) with $c = 0$.

9.3 Stresses due to the Static Tension

The lateral stiffness of the saw blade is very low, therefore, a large tension is required to stiffen the blade during idling and cutting conditions. The mechanism of applying the tension, the straining device, has been discussed in Chapter 2.

9.3.1 Stress Characteristics

This static tension can be assumed to be uniformly distributed across the width of the blade. It is velocity dependent, because an increase in the transport velocity of the blade would cause an increase in the centripetal acceleration, which is required to keep the band in tight contact with the pulley surface. This centripetal acceleration is provided by the straining mechanism. For the counter weight mechanism, the pressure between the pulley and the blade is always kept constant, hence, the total tension on the blade is

$$N_x = \frac{R_0}{b} + \rho h c^2 \tag{170}$$

where R_0 is the static initial tension force (N). However, the unit of measurement for N_x is force per unit width (N/m), therefore, a new variable q_0 was introduced to represent the magnitude of N_x instead of R_0, where

$$q_0 = \frac{R_0}{b}$$

For other types of straining device, such as the air-strain mechanism, the extra tension required to take up the centripetal effect may be less than $\rho h c^2$, a constant η was, therefore, introduced to represent this effect

$$N_x = q_0 + \eta \rho h c^2 \tag{171}$$

where $0 \leq \eta \leq 1$. $\eta = 1$ represents the counter weight mechanism, $\eta = 0$ represents the rigid pulley support. For an air-strain mechanism η can only be obtained from

Table 6: First two natural frequencies of a plate under various stress levels.

Stress (N/mm^2)	Experimental Frequencies (Hz)	Frequencies for 2×2 Functions (Hz)	Frequencies for 3×3 Functions (Hz)
45.3	37.2	39.6	39.6
	43.4	45.3	45.3
53.3	42.2	43.0	43.0
	47.7	48.2	48.2
70.8	47.8	49.4	49.4
	54.1	54.1	54.1

experimental results. Typical values of η are close to 1 [86].

The static tensioning of the blade does not affect N_y and N_{xy}, hence

$$N_y = N_{xy} = 0$$

The Waimak bandsaw uses a tension level of, approximately, 15000N in force, that is, a stress of 41 N/mm^2, or a force per unit width 68000 N/m.

Kirbach and Bonac experiments [37] used stress levels 45.3, 53.3, 70.8 N/mm^2 for similar blade dimensions to those of the Waimak saw blade.

9.3.2 Stationary Plates under Tension

The first two natural frequencies for a plate, 0.237 m wide, 0.0016 m thick and 0.943 m long, are presented in Table 6 together with the experimental results of Kirbach and Bonac [37]. For brevity, the number of modes assumed for a trial function was denoted by $M \times N$, where M is the number of modes in the x direction and N is the number of modes in the y direction. Therefore, a 2×2 trial function would produce 4×4 matrices in the Galerkin equation and hence four eigenvalues, a 3×3 trial function would produce nine eigenvalues.

The first two natural frequencies for the plate, calculated with the 2×2 trial function were the same as those calculated with the 3×3 trial function, however, the higher natural frequencies of the 3×3 function calculation would be more accurate

Table 7: First two natural frequencies of the Waimak saw blade at various lengths and transport speed.

Speed	Frequencies (Hz)		
2-4 (m/s)	l = 0.3 m	l = 0.5 m	l = 1.0 m
0	125.6	72.6	35.7
	147.4	86.0	42.5
25	121.3	69.3	33.8
	143.3	83.0	40.8
38	116.3	65.6	31.8
	138.5	79.6	39.0
50	110.7	61.6	29.6
	133.0	75.7	36.9
75	98.0	53.1	25.1
	120.0	67.0	32.2

than those obtained with the 2×2 function. Table 6 shows that the theoretical results were very close to the experimental results.

The first natural frequencies were associated with the first transverse mode of the plate and the second natural frequencies were associated with the first torsional mode of the plate.

These results showed that the natural frequency of the first torsional mode was close to the natural frequency of the first transverse mode of the bandsaw blade, therefore, it was difficult to predict which mode of vibrations would be the principal mode of the blade.

9.3.3 Moving Plate under Tension

Table 7 shows the calculated frequencies for the Waimak saw blade for three different span lengths.

The first transverse natural frequencies were the same as those calculated from the moving beam theory in Chapter 6. The first torsional frequencies were the second frequencies of the plate, which also decreased as the transport speed increases. The

Table 8: First two natural frequencies of a blade at various transport speeds.

Speed (m/s)	Experimental Frequencies (Hz)	Frequencies for 2×2 Functions (Hz)	Frequencies for 3×3 Functions (Hz)
0	40.	45.9 49.7	45.9 49.7
25	37.5	44.2 48.2	44.2 48.2
50	34.	40.4 44.5	40.0 44.2
75	29.	36.0 40.2	35.1 39.3

effect of varying transport speed on a short blade was greater than that on a longer blade.

The first two natural frequencies for a plate with a thickness of 0.0014 m, a width of 0.235 m, a length of 0.948 m and subjected to a tension of 61 N/mm^2 were also calculated for various transport speeds and presented in Table 8 and Figure 75.

The calculated results were about 6 Hz higher than the experimental results of Kirbach and Bonac [38]. This discrepancy was probably due to the difference in actual span length of the blade and the measured length as explained in Chapter 6. As expected, both natural frequencies decreased with increasing transport speed.

Note that at high transport speed, the calculations with the 3×3 trial function gave frequencies that were in better agreement with those found experimentally than did those with the 2×2 function[1].

As pointed out in Chapter 7, the moving beam theory was adequate for a wide saw blade with a uniform stress distribution across the width, such as the results presented in this section. The following sections will consider non-uniform stress distribution on bandsaw blades, which obviously cannot be determined by the beam theory.

[1]Galerkin method is an upperbound method, therefore, the lower the result the more accurate it is.

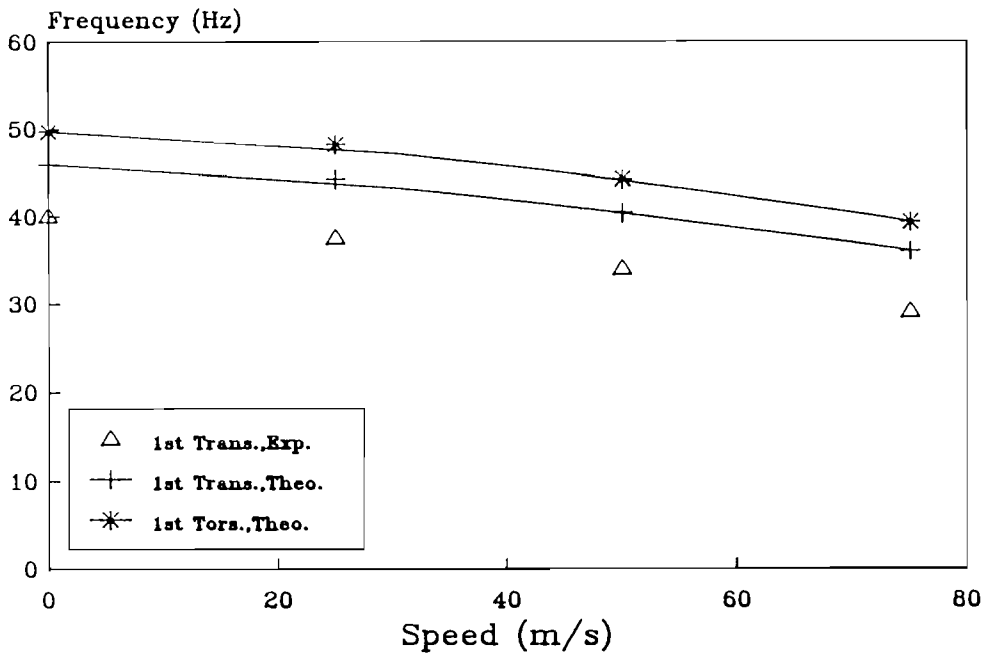

Figure 75: Natural frequency versus transport speed.

9.4 Stresses due to Wheel-tilting and Back-crowning

Wheel-tilting and back-crowning, as described in Chapter 2, can be assumed to induce linear stress variations across the width of the blade. The main purpose of this is to provide a higher tension on the cutting edge than that on the back edge, which is desirable for the stability of the blade during cutting [71]. Allen [3] stated that another reason for back-crowning is to compensate for the temperature gradient between the cutting edge and the back edge of the blade during cutting.

9.4.1 Stress Characteristics

To represent the linear stress variation across the blade, N_x can be modify to

$$N_x = \left(d + e\frac{y}{b}\right) q_0 + \eta\rho hc^2 \tag{172}$$

where d and e are parameters which characterise the distribution of N_x.

- For a uniform tension, $d = 1$ and $e = 0$.
- For a triangularly distributed load, $d = 1$ and $e = -1$.
- For a pure bending, $d = 1$ and $e = -2$.

Again, the other in-plane stresses are not affected by the wheel-tilting and/or back-crowning, hence

$$N_y = N_{xy} = 0$$

It is very difficult to measure the amount of wheel-tilting accurately, therefore the values of d and e cannot be given from the angle of tilt. A more accurate way of determining d and e is to measure directly the stresses at the cutting edge and at the back edge. This method is satisfactory for experimental studies but not feasible in practice.

The magnitude of back-crown is indicated by the diameter D of a circular arc along the back edge of the blade, or conventionally, the maximum distance δ between a straight edge and the circular arc of the back edge over a specified length L (Figure 76). A typical value for back-crown is 0.4 mm in a length of 1.524 m. Although, the effects of fitting back-crown to the saw blade are well understood, there is no published theoretical study of those effects; to enable them to be accurately predicted by theoretical calculations.

Allen [3] provided a formula for calculating the stress induced by back-crown, which is

$$\sigma_{BC} = \pm\frac{Eb}{D} = \pm\frac{4\delta Eb}{L^2} \tag{173}$$

where E is the Young's modulus and b is the width of the blade.

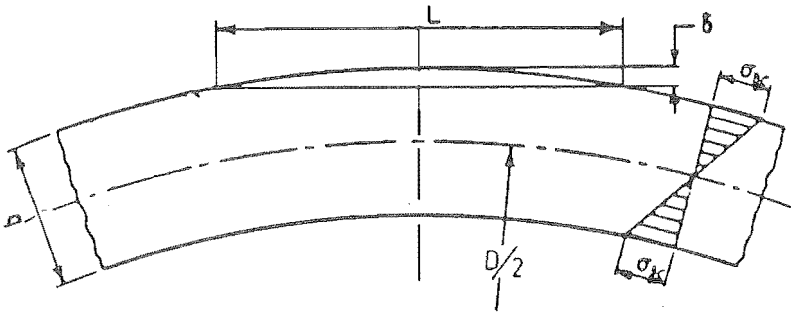

Figure 76: Stress due to back-crown.

9.4.2 Wheel-tilting

Kirbach and Bonac [37] presented the first two natural frequencies of a blade at various amounts of wheel-tilting and various tensions. The amount of tilt was given by the stress ratio γ between the back edge and the cutting edge, that is, $\gamma = 1$ for uniform stress, and $\gamma = 0$ for zero stress on the back edge.

If q_0 in Equation (172) represents the initial static force per unit width, then the two parameters d and e could be found by

$$d = \frac{2}{1+\gamma}, e = \frac{2(\gamma - 1)}{1+\gamma} \tag{174}$$

Tables 9, 10, and 11 list the experimental results of Kirbach and Bonac, and the theoretical results obtained in the present investigation at three different stress levels. These values were also plotted in Figures 77, 78, and 79.

These results show that the theoretical calculations were closely correlated to the experimental results found by Kirbach and Bonac. Wheel-tilting results in a decrease in the first transverse natural frequency and an increase in the first torsional frequency of a blade. While a small amount of wheel-tilting may improve the performance of the blade, too much tilt would have a destabilising effect on the blade because of the low first transverse natural frequency.

Table 9: First two natural frequencies for various stress ratios, at 45.2 N/mm^2 static stress.

Stress Ratio γ	Experimental Frequencies (Hz)	Theoretical Frequencies (Hz)
1.	37.2	39.6
	43.5	45.2
0.8	37.7	39.3
	43.5	45.5
0.6	38.0	38.4
	45.0	46.2
0.4	38.0	36.8
	48.0	47.5
0.2	37.7	34.0
	54.0	49.5
0.	37.5	29.4
	60.0	52.2

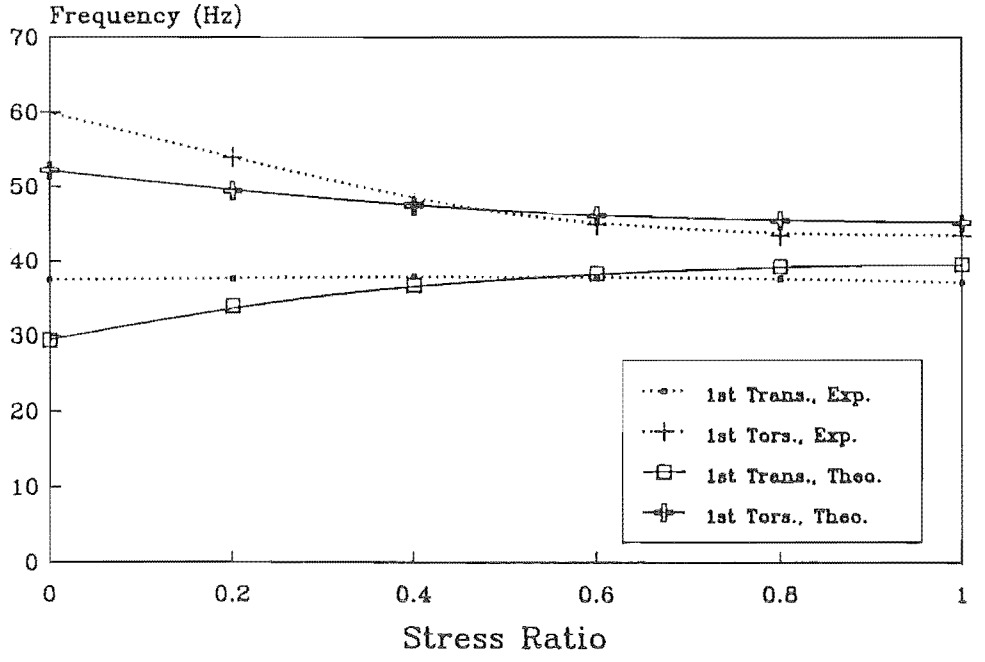

Figure 77: Natural frequency versus stress ratio, at 45.2 N/mm^2 stress level.

Table 10: First two natural frequencies for various stress ratios, at 53.3 N/mm^2 static stress.

Stress Ratio γ	Experimental Frequencies (Hz)	Theoretical Frequencies (Hz)
1.	42.6	42.9
	47.5	48.2
0.8	42.8	42.6
	49.0	48.5
0.6	43.0	41.5
	50.2	49.4
0.4	42.5	39.6
	52.6	51.0
0.2	41.0	36.5
	54.0	53.1
0.	37.0	31.4
	55.5	56.2

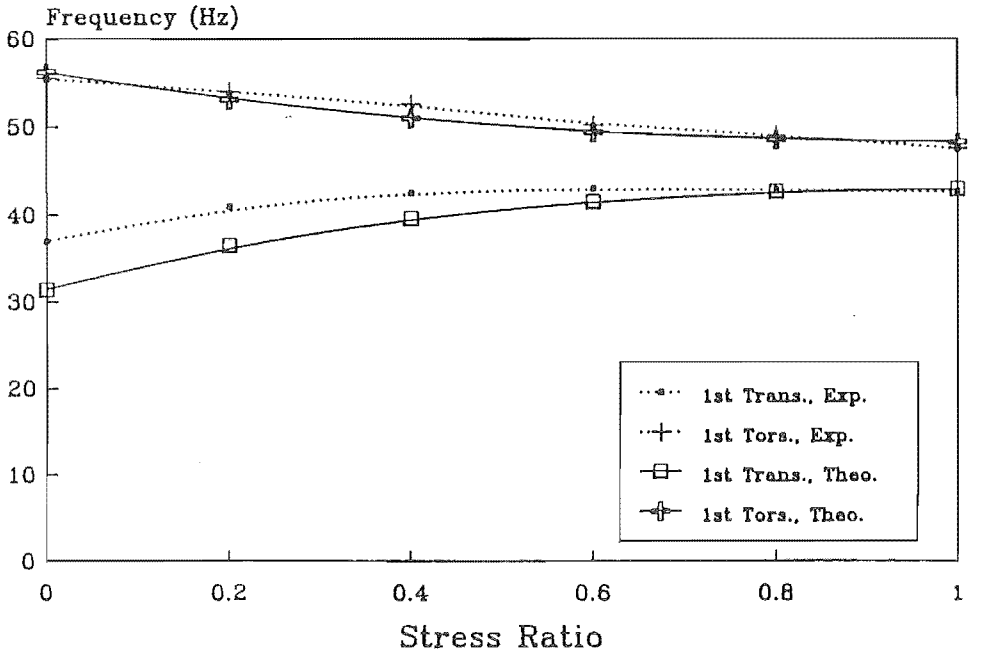

Figure 78: Natural frequency versus stress ratio, at 53.3 N/mm^2 stress level.

Table 11: First two natural frequencies for various stress ratios, at 70.8 N/mm^2 static stress.

Stress Ratio γ	Experimental Frequencies (Hz)	Theoretical Frequencies (Hz)
1.	47.5	49.4
	54.0	54.1
0.8	47.5	49.0
	54.0	54.5
0.6	46.5	47.5
	54.2	55.8
0.4	45.0	45.1
	55.0	57.7
0.2	42.5	41.3
	57.0	60.3
0.	39.0	35.1
	60.0	63.9

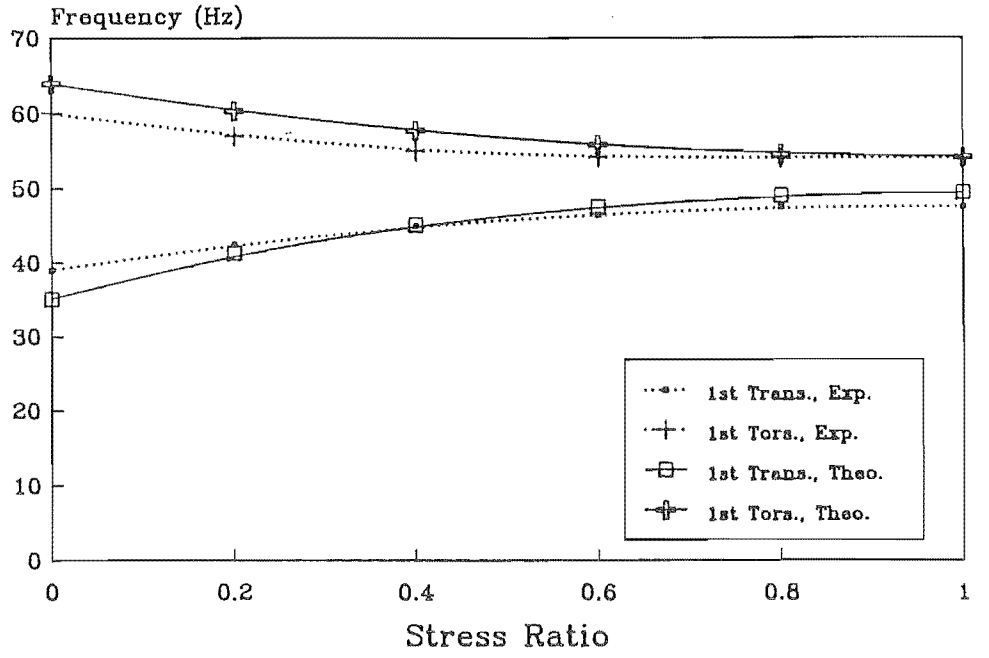

Figure 79: Natural frequency versus stress ratio, at 70.8 N/mm^2 stress level.

Table 12: First two natural frequencies of a blade with no back-crown, at various transport speeds.

Speed (m/s)	Experimental Frequencies (Hz)	Theoretical Frequencies (Hz)
0.	29.0	30.0
	32.5	31.6
32.	28.0	29.1
	32.0	30.8
43.	26.0	28.5
	31.0	30.2
53.	25.5	27.8
	28.0	29.5

9.4.3 Back-crowning

Tanaka et.al. presented the first two natural frequencies of three blades, one with no back-crown and two fitted with back-crown having 352 m and 144 m diameter. The blade had a width of 0.127 m, a thickness of 0.0009 m and a span length of 2.16 m. The static tension on the blade was at 1600 kg, that is, q_0 =123590 N/m.

Equation (173) was used to calculate the stress induced from a back-crown, which was then used to find the stress ratio between the cutting edge and the back edge. For the blade fitted with 352 m diameter back-crown, the stress ratio γ was 0.3111. The stress induced from the 144 m back-crown was actually larger than the static tensile stress, therefore γ was negative ($\gamma = -0.12$). For all practical purposes, γ was assumed to be zero.

Table 12, 13 and 14 lists the first two natural frequencies of the three blades at various transport speeds. Figure 80 and 81 plots these results for the first natural frequencies and the second natural frequencies respectively.

For the blades with no back-crown and with a 352 m back-crown, the theoretical results agreed well with the experimental results. For the blade with a 144 m back-crown, the discrepancy between the theoretical and experimental results was greater than the two previously mentioned cases. It appeared that the magnitude of the

Table 13: First two natural frequencies of a blade with 352 m back-crown, at various transport speeds.

Speed (m/s)	Experimental Frequencies (Hz)	Theoretical Frequencies (Hz)
0.	27.0	25.9
	34.0	35.0
32.	25.0	24.9
	33.0	34.3
43.	24.0	24.2
	31.0	33.7
53.	22.0	23.5
	30.0	33.1

Table 14: First two natural frequencies of a blade with 144 m back-crown, at various transport speeds.

Speed (m/s)	Experimental Frequencies (Hz)	Theoretical Frequencies (Hz)
0.	25.0	20.7
	37.0	38.3
32.	24.0	19.5
	35.0	37.6
43.	22.0	18.6
	34.5	37.1
53.	20.0	17.8
	33.0	36.5

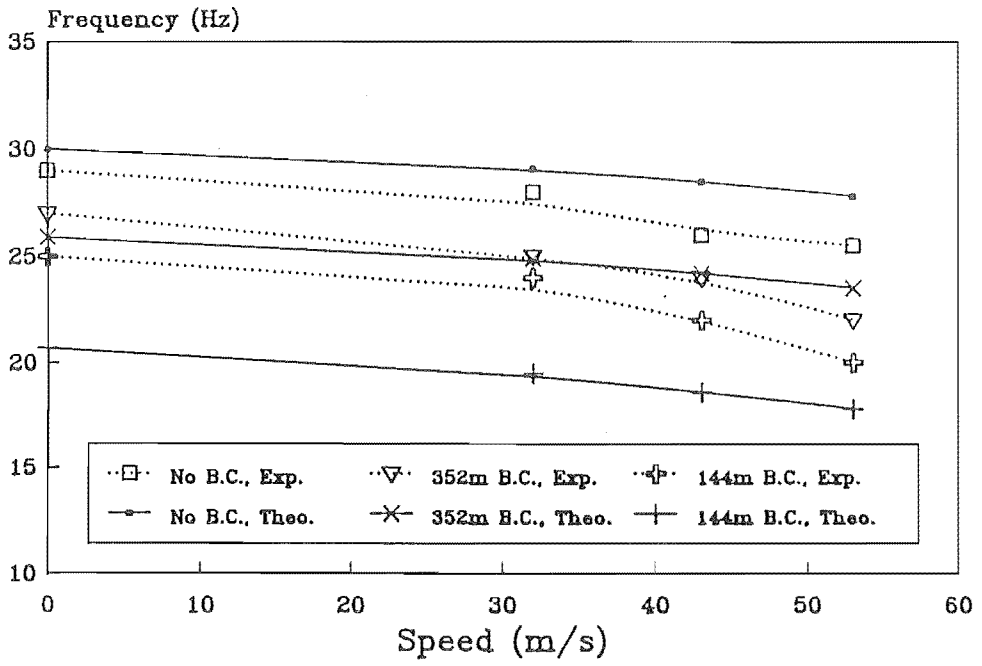

Figure 80: First natural frequencies versus transport speed, for blades with various back-crowns.

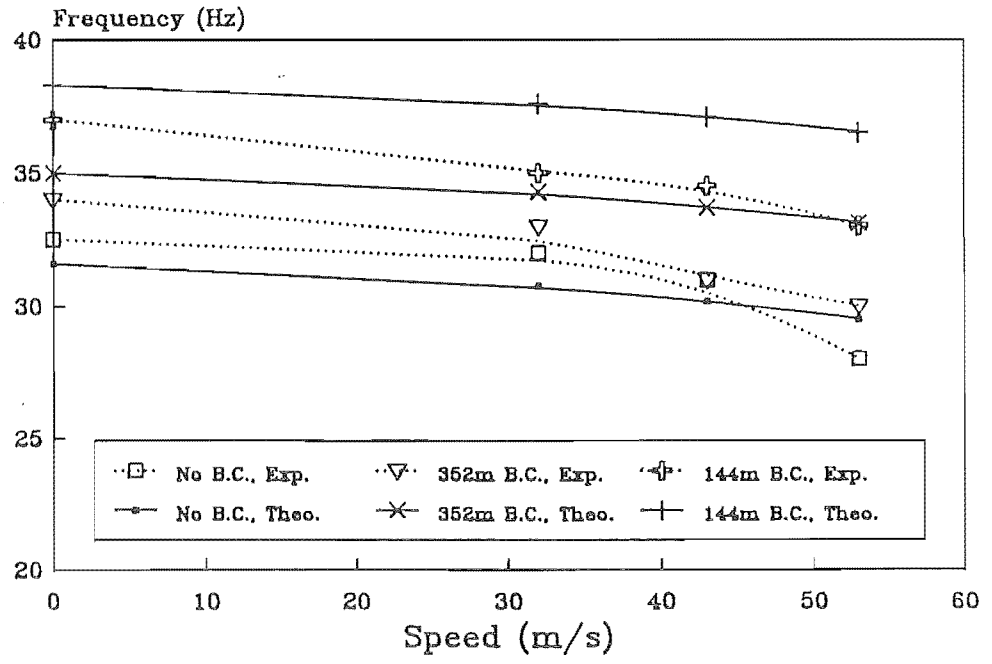

Figure 81: Second natural frequencies versus transport speed, for blades with various back-crowns.

stress induced by the back-crown was less than that calculated with Equation (173). It was not clear whether the inaccuracy of the results was from Equation (173) or from the measurement of the back-crown. However, in general, the assumption that back-crowning produces linearly distributed stresses across the width of the blade appeared to be correct, and its effects were to decrease the first transverse frequency and to increase the first torsional frequency of the blade.

To test the validity of Equation (173) for estimating the stresses induced by back-crowns, experimental measurements of the stresses across the width of the blades fitted with various back-crowns have to be carried out and compare with those obtained by Equation (173). This subject is left for future investigation.

9.5 Stresses due to Prestressing

It was found experimentally that, by stretching the central area of a blade in relation to the two longitudinal edges, a saw blade with a better performance was produced. This stretching process has been referred to in the literature as tensioning or prestressing. In this thesis, the stretching process will only be referred to as prestressing.

There is no published theoretical study to determine the optimum prestress value for a particular blade. The Saw Doctors performing the prestressing process can only use their experience in estimating the amount of prestress.

Three main reasons for prestressing a bandsaw blade are

- To counteract the expansion which take place during the cutting operations.
- To stiffen the cutting edge so that it resists the cut.
- To ensure that the saw runs in a constant position on the pulleys.

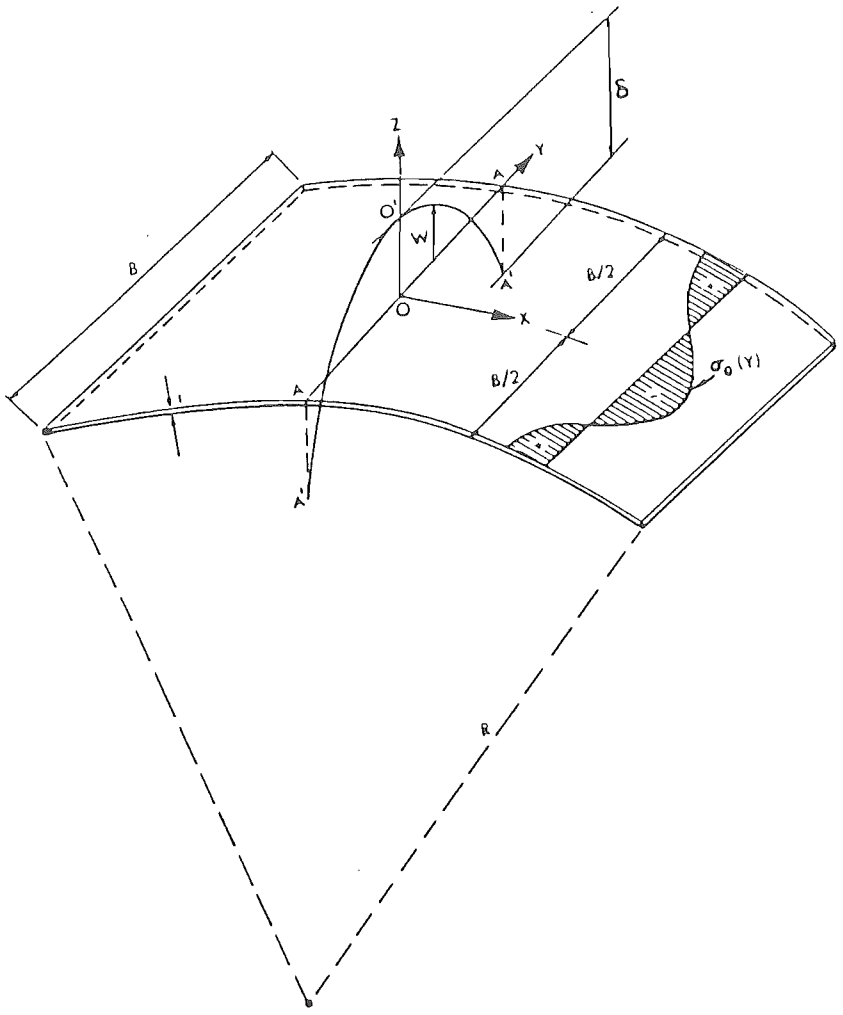

Figure 82: Bent bandsaw blade and transverse deflected shape.

9.5.1 Stress Characteristics

It was explained that the prestressing process improves the performance of the blade because it sets up residual stresses in the blade. It is very difficult to measure the residual stresses accurately, and in the past, Saw Doctors have controlled the level of prestress by measuring the *light gap* δ when the blade is bent over a given radius [25] (see Figure 82). This light gap is measured by using *tension gauges*, and these are graded in numbers, for example, 26, 28, 44, the numbers being the diameter (in feet) of a circular arc (see Figure 83).

It was found experimentally that a parabolic distribution of the residual stress

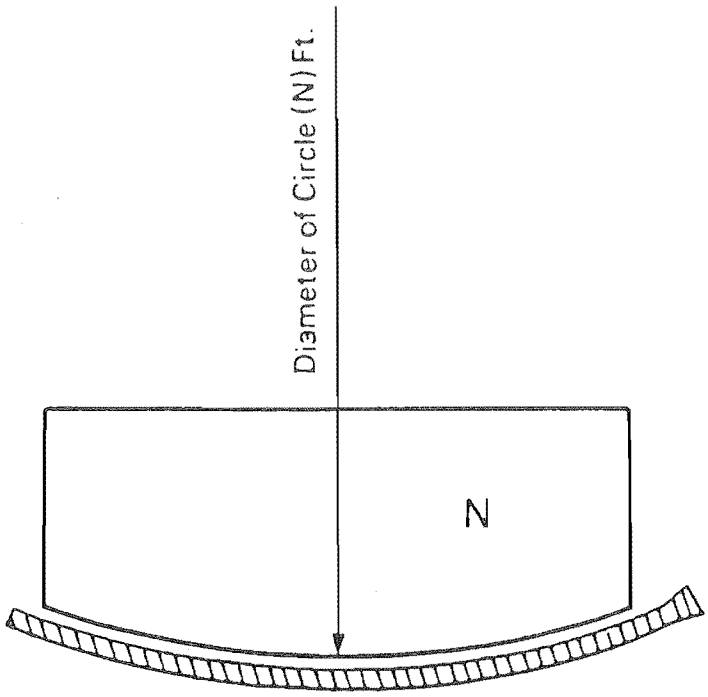

Figure 83: Tension gauge index number.

across the width of the blade gives better sawing accuracy than any other stress distribution [4].

A theoretical calculation of the light gap δ, given the radius of curvature R, the width b, the thickness h, and the residual stress distribution $\sigma_x(y)$, was presented by Foschi [25], which considered the differential equation

$$\frac{d^4w}{dy^4} + \frac{12\left(1-\nu^2\right)}{R^2h^2}w = -\frac{12\left(1-\nu^2\right)}{ERh^2}\sigma_x \tag{175}$$

This equation is closely related to that of the *anticlastic* curvature of flat plates.

For a parabolic residual stress

$$\sigma_x\left(y\right) = -\sigma_c + 12\sigma_c\left(\frac{y}{b} - \frac{1}{2}\right)^2 \tag{176}$$

where σ_c is the magnitude of the compressive stress at the centre of the blade. At the edges $y = 0, y = b$, Equation (176) gives a tensile stress of $\sigma_t = 2\sigma_c$.

The solution of Equation (175) can now be used to express the light-gap, δ, for this parabolic stress as

$$\frac{\delta}{h} = \left[\nu C + 24\frac{\beta}{C}\right]\left[\alpha_1\left(1 - \cosh\gamma\cos\gamma\right) - \alpha_2\sinh\gamma\sin\gamma\right] + 3\frac{\beta}{C} \qquad (177)$$

where

$$C = \frac{b^2}{Rh}$$

$$\beta = \frac{\sigma_c}{E}\left(\frac{b}{h}\right)^2$$

$$\gamma = \sqrt[4]{\frac{3}{16}\left(1-\nu^2\right)C^2}$$

$$\alpha_1 = \frac{\sinh\gamma\cos\gamma - \cosh\gamma\sin\gamma}{\sqrt{3\left(1-\nu^2\right)}C\left(\sinh 2\gamma + \sin 2\gamma\right)}$$

$$\alpha_2 = \frac{\sinh\gamma\cos\gamma + \cosh\gamma\sin\gamma}{\sqrt{3\left(1-\nu^2\right)}C\left(\sinh 2\gamma + \sin 2\gamma\right)}$$

δ can also be obtained from Figure 84 for any particular C and β.

Foschi also pointed out that a particular transverse deflected shape may not represent a unique residual stress distribution, hence concluded that the light gap technique cannot be considered as a reliable estimator of the residual stresses. Nevertheless, this technique is, at present, the only means of non-destructive test for measuring the prestress.

In this thesis, the prestress on the blade is assumed to produce a parabolic residual stress distribution, and the magnitude of the stress can be approximated from Figure 84, given the magnitude of the light gap, δ, the radius of curvature, R, and the dimensions of the blade.

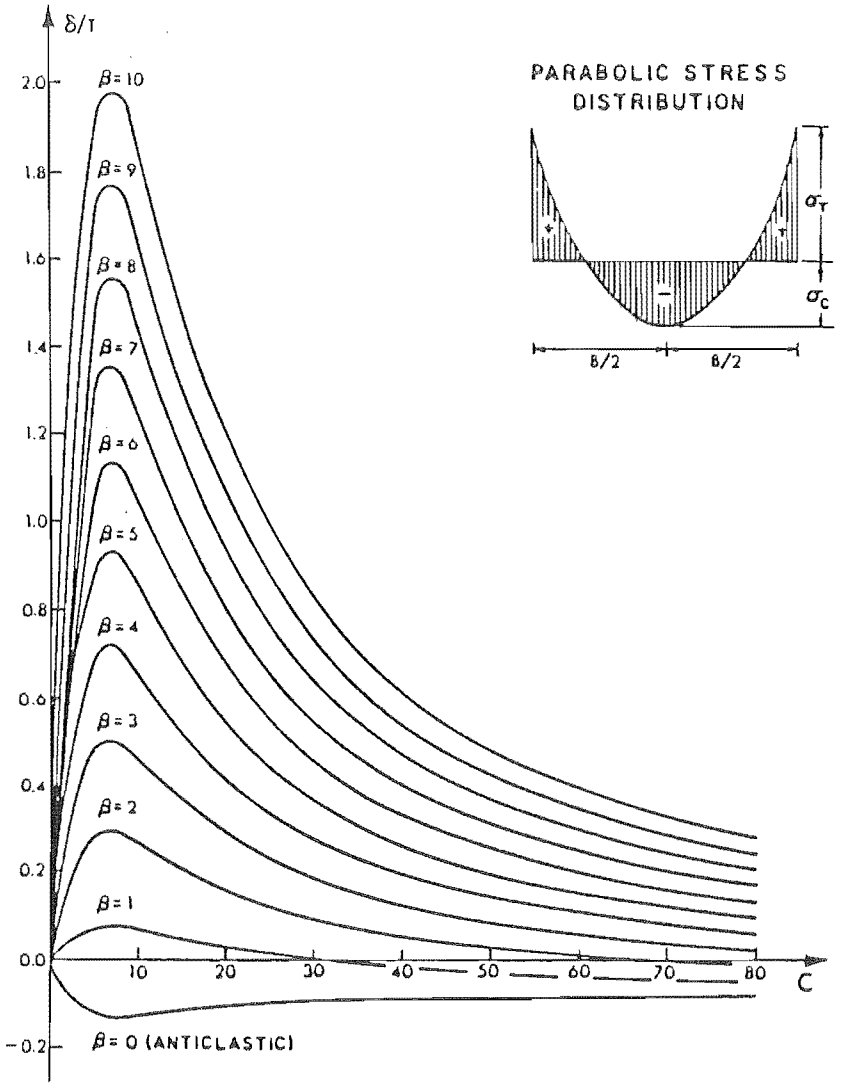

Figure 84: Light gap for parabolic residual stresses.

Kirbach and Bonac [37], and Tanaka et.al. [80] had shown experimentally that the prestress on bandsaw blades results in a slight decrease of the first lateral natural frequency and a marked increase of the first torsional natural frequency. Ulsoy and Mote [86] had also verified these effects theoretically, by applying a parabolic in-plane stress, N_x to their plate model. However, there was no discussion of the magnitudes of the prestress used. It is very important to find out if the magnitude of a prestress could be estimated from the tension gauge number, and whether or not this prestress value could be used to obtain accurately the natural frequencies of the saw blade.

The parabolic prestress could be incorporated into the plate problem presented in this thesis by letting the in-plane stress N_x be

$$N_x = q_s \left[d + e\left(\frac{y}{b}\right) + f\left(\frac{y}{b}\right)^2 \right] + \eta\rho hc^2 \tag{178}$$

where q_s is a magnitude in force per unit width, and d, e, f are parameters which define the stress distribution. If $f = 0$ this equation becomes Equation (172). For the prestress in Equation (176), $d = 2, e = -12, f = 12$ and $q_s = h\sigma_c$.

Other stresses such as the static tensile stress or the stresses due to wheel tilting and/or back crowning, can be superimposed on the prestress distribution, for example, a prestressed blade, which is statically strained to q_0, would have a distribution of

$$N_x = q_s \left[\left(2 + \frac{q_0}{q_s}\right) - 12\left(\frac{y}{b}\right) + 12\left(\frac{y}{b}\right)^2 \right] + \eta\rho hc^2$$

The other two in-plane stresses are no longer zero and can be found by considering the compatibility conditions, the equilibrium conditions and the boundary conditions of the plate. These conditions for a two dimensional stress state are given in text books on the theory of elasticity, such as [84, page 57-69].

The equilibrium conditions are

$$\frac{\partial \sigma_x}{\partial x} + \frac{\partial \tau_{xy}}{\partial y} = 0, \qquad \frac{\partial \sigma_y}{\partial y} + \frac{\partial \tau_{xy}}{\partial x} = 0 \tag{179}$$

The compatibility conditions are

$$\left(\frac{\partial^2}{\partial x^2} + \frac{\partial^2}{\partial y^2}\right)(\sigma_x + \sigma_y) = 0 \tag{180}$$

and the boundary conditions for this case are $\sigma_y = \tau_{xy} = 0$ at $y = 0$ and $y = b$.

It is common to choose a class of stress fields which identically satisfy the equilibrium equations. This is achieved by using the Airy stress functions $\phi(x, y)$, which are related to the stresses as follows

$$\sigma_x = \frac{\partial^2 \phi}{\partial y^2}, \qquad \sigma_y = \frac{\partial^2 \phi}{\partial x^2}, \qquad \tau_{xy} = -\frac{\partial^2 \phi}{\partial x \partial y} \tag{181}$$

Substitution of these expressions into the compatibility equation, Equation (180), yields

$$\frac{\partial^4 \phi}{\partial x^4} + 2\frac{\partial^4 \phi}{\partial x^2 \partial y^2} + \frac{\partial^4 \phi}{\partial y^4} = \nabla^4 \phi = 0 \tag{182}$$

A simple class of solutions to Equation (182) are those which can be written as polynomial expressions in x and y directions. In most practical cases, polynomial functions can provide the exact solutions for the stress state of the plate [83], unfortunately, in this prestressed saw blade case, it was impossible for the polynomial functions to satisfy all the boundary conditions. That is, if σ_x was a quadratic function along the $x = 0, x = l$ edges, then τ_{xy} would not be equal to zero along the $y = 0, y = b$ edges. A more general class of functions, such as trigonometric functions, should be used for accurate representation of stresses of the blade. However, it was impractical to further complicate the dynamic problem of the saw blade at this stage, because the parabolic stress distribution due to prestress was only an approximation. The subject of exact stresses induced from the prestressing process is left for future study.

Table 15: First two natural frequencies of K&B prestressed blade at various static tensions.

Static Stress (N/mm^2)	Experimental Frequencies (Hz)	Theoretical Frequencies (Hz)
45.2	37.5	39.4
	46.5	53.3
53.3	42.5	42.8
	52.4	55.9
70.8	47.5	49.3
	57.0	61.0

In this thesis, assume that $\sigma_y = \tau_{xy} = 0$, that is $N_y = N_{xy} = 0$, then obtain the natural frequencies of the blade under quadratic stress σ_x and compare with the experimental results published by Kirbach and Bonac [37], and Tanaka et.al. [80] to see if Figure 84 could be used to estimate the magnitude of the prestress.

9.5.2 Kirbach and Bonac Experimental Results

The experiment was carried out on a blade with a width of 0.237 m, a thickness of 0.0016m and a length of 0.943 m. The blade was prestressed to '*a profile that is considered in the industry as optimum for good cutting performance*', unfortunately, the magnitude of the prestress was not given in the publication. Simmonds [71, page 24] recommended that for a blade with similar dimensions, the amount of prestress should be about 52 gauge, that is, $2R$=15.85 m.

From Figure 84, the magnitude of the prestress was q_s = 46400 N/m. The experimental and theoretical results are listed in Table 15.

Comparison between these results and those in Table 6 showed that the prestress increased the first torsional frequencies, but did not alter the first transverse natural frequencies. The theoretical results appeared to produce the correct effects of prestress on the blade, however, the calculated torsional frequencies were higher than the measured frequencies. This meant that q_s should be less than 46400 N/m,

Table 16: First two natural frequencies of the Tanaka's blade with no prestress, at various static tensions.

Static Tension (×9.81 N)	Experimental Frequencies (Hz)	Theoretical Frequencies (Hz)
1030	24.0	24.0
	27.3	26.1
1257	26.0	26.6
	30.0	28.4
1600	30.0	30.0
	32.4	31.6
1943	32.5	33.0
	35.0	34.5
2170	34.5	34.9
	37.0	36.3

however, it could very well be that the prestress on the blade was not at 52 foot gauge, therefore, no conclusion can be drawn about the Foschi's calculation of the prestress level at this stage.

9.5.3 Tanaka et.al. Experimental Results

Tanaka et.al. provided the results for a 0.0009 × 0.127 × 2.16 m blade at two different levels of prestress, $R = 7.7$ m and $R = 4.35$ m, and from Figure 84 the prestress levels were $q_s = 27000$ N/m for $R = 7.7$ m and $q_s = 28800$ N/m for $R = 4.35$ m.

The experimental and theoretical results for a blade with no prestress, $R = 7.7$ m prestress and $R = 4.35$ m prestress, are listed in Table 16,17,18 for various static tensions.

These results showed excellent agreement between the experimental and the theoretical natural frequencies. The magnitude of the prestress for $R = 4.35$ m seemed to be slightly lower than that found in practice.

As the magnitude of the prestress increased, the experimental first transverse

Table 17: First two natural frequencies of the Tanaka's blade with $r = 7.7$ m prestress, at various static tensions.

Static Tension (×9.81 N)	Experimental Frequencies (Hz)	Theoretical Frequencies (Hz)
1257	26.0	26.6
	31.5	31.0
1600	29.5	29.9
	34.5	34.0
1943	32.5	33.0
	37.0	36.7

Table 18: First two natural frequencies of the Tanaka's blade with $r = 4.35$ m Prestress, at various static tensions.

Static Tension (×9.81 N)	Experimental Frequencies (Hz)	Theoretical Frequencies (Hz)
1030	22.5	24.0
	32.5	29.1
1257	24.5	26.6
	34.8	31.2
1600	27.8	29.9
	37.3	34.1
1943	31.0	33.0
	39.3	36.9
2170	32.5	34.9
	41.7	38.8

frequencies decreased slightly, however, the theoretical frequencies remained the same for all three cases. The first torsional frequencies increased as the magnitude of the prestress increased, for both the experimental and the theoretical results. The effects of the prestress at a low static tension were greater than those at a higher static tension.

9.5.4 Conclusion

The results in this section showed that the approximate parabolic stress distribution in the longitudinal direction of the blade appeared to produce similar behaviour to that of a prestressed saw blade. The magnitude of the prestress calculated from Foschi's theory provided acceptable starting point for the cases considered in this thesis.

However, there were still many uncertainties on the subject of prestressing, and further experimental work needs to be carried out to answer the following questions:

- What is the actual residual stress distribution in the x direction of a prestressed saw blade ?
- Is there any residual stress in the y direction ?
- What happens to the stress distribution when the blade is placed on the pulleys and statically stretched ?
- Is there a better residual stress profile than the parabolic type ?

9.6 Stresses Induced by Cutting Forces

This is an area of research which has been neglected in the past, perhaps because of the difficulties in obtaining experimental results. Ulsoy and Mote (1980,1982) [86,87]

regarded the edge forces on the plate, due to cutting, as very small and concluded that they were not the cause of instability of the blade. Wu (1986) [96], and Wu and Mote (1986) [95] have considered the effects of cutting forces on a moving beam and shown that these cutting forces coupled the transverse vibration with the torsional vibration. Attempts to study the vibration of the saw blades during cutting have been made experimentally [81,17], but there appeared to be a lack of direction and of conclusive results. It is important that both theoretical and experimental studies are considered together so that results from one can be verified or explained by results from the other.

The experimental studies of the saw blade behaviour during cutting was beyond the scope of the present investigation, but it is hoped that such studies can be made in the future to support the theoretical results found presented here.

9.6.1 Cutting Forces

There are three main forces applied on the blade during sawing :

- Perpendicular in-plane force, F_f, on the cutting edge of the blade, due to the work piece being fed onto the blade. The reaction forces are from the tilting of the top wheel, and the friction between the band and the outer surface of the pulley.

- Tangential force, F_c on the cutting edge, due to the resistance of the timber to the cutting effects of the saw teeth.

- Perpendicular transverse force, F_t, may arise from the interaction between the blade and the work piece.

Pahlitzsch and Puttkammer [60] concluded that the feed force, F_f, and the transverse force, F_t, could be neglected because they were very small compared to the

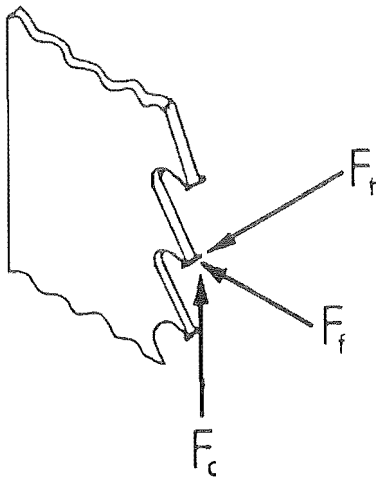

Figure 85: Cutting forces on the blade.

static tension. Wu [96,95], in his theoretical analysis, took the feed force into account and showed that it coupled the transverse mode with the torsional mode due to the reaction from the end moments, however, he did not mention the magnitude of the feed force.

It has been observed on one bandsaw that the saw blade was pulled forward during cutting, instead of being pushed back due to the feed force. This effect can be explained by considering the magnitude of the feed force, and the mechanism of cutting wood.

The feed speed is dependent on the type of timber and the depth of cut. Timbers can be graded by densities (at an approximate 15% moisture content) or more accurately, by hardness and texture [71, page 114]. The feed rates are also divided into basic ranges from less than 0.127 m/s to above 1 m/s, with typical feed speeds of approximately 0.5 m/s.

The blade speed is dependent on the type and size of bandsaw. For the Waimak bandsaw, the rotating speed is about 8 Hz (50 rad/s) and the pulley diameter is about 1.5 m, hence the blade speed is about 38 m/s. At a very high feed speed

of 1 m/s, the slope at which a single tooth passing over the timber is 38:1, that is almost vertical. The feed force, F_f is, therefore, about one thirty-eighth of the force F_c tangential to the blade, hence F_f is very small compared with F_c.

The mechanism of cutting wood has not been thoroughly studied, but an analogy to that of cutting metal shows that if there is a high positive rake angle, then it is possible for the work piece to pull the saw blade during cutting [68, page 58]. A typical rake angle for a bandsaw blade is about 28 degrees, which should not produce the grabbing effect, however, it is possible that a higher rake angle had been employed on the bandsaw where the grabbing effect was observed.

The above considerations suggest that the main effects of the cutting process on the saw blade is the tangential cutting force F_c. In this thesis, F_f and F_t were assumed to be negligible compared with F_c.

9.6.2 Stress Characteristics

The tangential cutting force, F_c can be taken into account by considering the stress state of the blade.

Because the saw guides are always close to the work piece during cutting, F_c is best represented by a distributed load rather than a point load. For simplicity, let the load be uniformly distributed along the edge $y = b$, with a magnitude of q_c force per metre. The boundary conditions are, therefore, at $y = 0, \sigma_y = \tau_{xy} = 0$ and at $y = b, \sigma_y = 0, \tau_{xy} = q_c$.

From the compatibility, equilibrium, boundary conditions and the usage of polynomial stress functions, the stress state for a blade under a uniform tangential edge load along the edge $y = b$ is given by

$$\begin{aligned} \sigma_x &= -\frac{2q_c}{hb^2}\left(x - \frac{l}{2}\right)y \\ \sigma_y &= 0 \end{aligned}$$

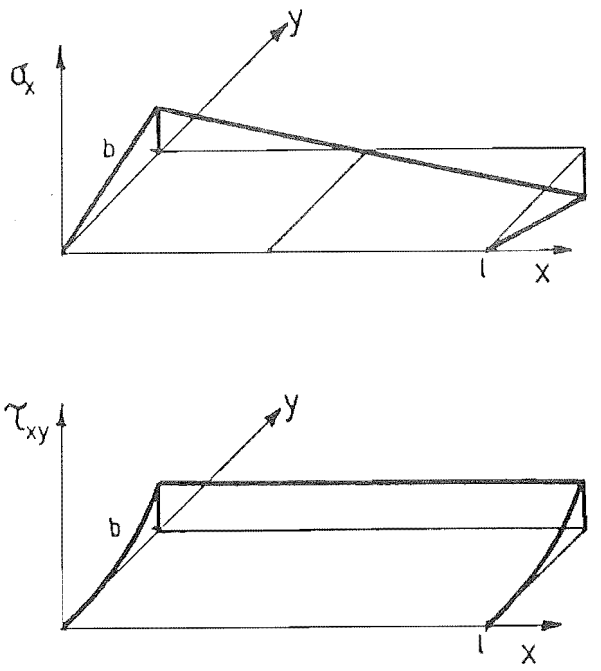

Figure 86: Distribution of σ_x and τ_{xy}.

$$\tau_{xy} = \frac{q_c}{hb^2} y^2$$

Figure 86 plots the distribution of the stresses.

A linear stress distribution along the x direction, due to static tension and back-crown, can be superimposed on the above stress and the results can be multiplied by h to give

$$N_x = q_0 \left(d + e\frac{y}{b} \right) - q_c \frac{l}{b} \left(2\frac{x}{l} - 1 \right) \frac{y}{b} \tag{183}$$

$$N_y = 0 \tag{184}$$

$$N_{xy} = q_c \left(\frac{y}{b} \right)^2 \tag{185}$$

Note that a parabolic stress along the x direction would not satisfy the compatibility conditions, therefore, this investigation only considered the tangential force on a blade with no prestress.

9.6.3 Magnitude of Cutting Forces

The magnitude of cutting forces has not been conclusively found, because, as discussed in Chapter 6, the mechanism of cutting wood has not been very well understood.

A recent publication on this area of research was a progress report on an ongoing project by Grönlund (1988) [26], which experimentally investigated the magnitude of cutting forces in relation to various parameters, such as cutting speed, chip thickness, rake angle, clearance angle, edge sharpness, density of wood, moisture content, hardness, and direction of the cut with respect to the fibre direction and the year ring direction. An equation to calculate the main cutting force was given, which was based on a non-linear regression analysis of the various measurements of the cutting force, unfortunately there are errors in the equation which make it impossible to use. It was mentioned that more work had to be done on improving this statistical model.

In this investigation, the main interest was focused on the dynamic behaviour of the blade, therefore an approximate value of the main cutting force was sufficient. A typical value for the tangential cutting force q_c was about 1000 N/m.

9.6.4 Results for a Stationary Blade

Although, there are no practical problems associated with the stationary blade under a tangential edge force, the following results provide a better understanding of the effects of the tangential force on a plate, and they may also be experimentally verified with relative ease.

A blade, with dimensions of $0.22 \times 0.00165 \times 0.8$ m and with a static tension of 15000 N, was used as a sample calculation to illustrate the effects of the tangential cutting force.

Table 19: First four natural frequencies of a stationary blade subjected to various tangential loads.

Tangential Load (N/m)	Frequencies for 3×3 Functions (Hz)	Frequencies for 4×4 Functions (Hz)
0	44.8	44.8
	53.2	53.1
	91.8	91.8
	108.4	107.9
10000	43.8	43.8
	52.8	52.7
	90.6	90.5
	108.0	107.4
30000	32.6	30.4
	50.4	50.1
	81.2	77.4
	105.5	104.5
40000	10.0	-
	48.3	47.4
	74.5	65.4
	104.3	103.0

The first four natural frequencies were calculated for various q_c. The results are listed in Table 19 and plotted in Figure 87. The values obtained with the 4×4 trial function Galerkin solution gave more accurate results than the 3×3 function, however, for q_c less than about 20000 N/m the first four natural frequencies were practically the same for both calculations. The mode shapes of the blade subjected to 30000 N/m tangential load are shown in Figure 88.

The blade was statically buckled at a tangential load of about 40000 N/m. This value seemed to be reasonable since the strain on the blade was equivalent to a load of 68182 N/m, that is, the tangential load had a of similar order of magnitude to the straining load for divergent buckling to occur. This value was very high compared with the typical cutting load.

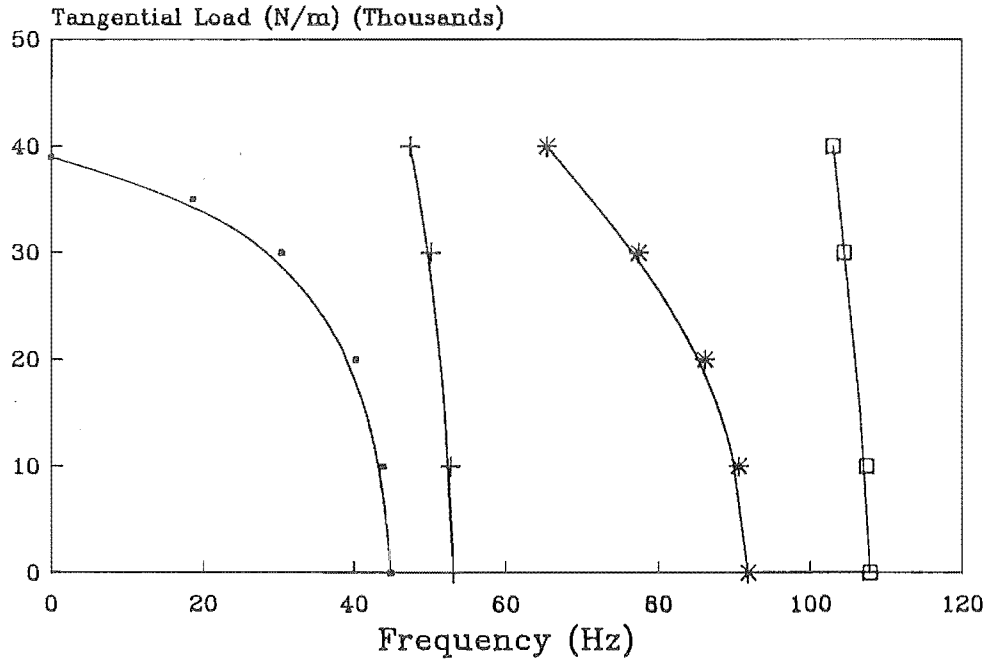

Figure 87: Natural frequency versus tangential edge load, for a stationary blade.

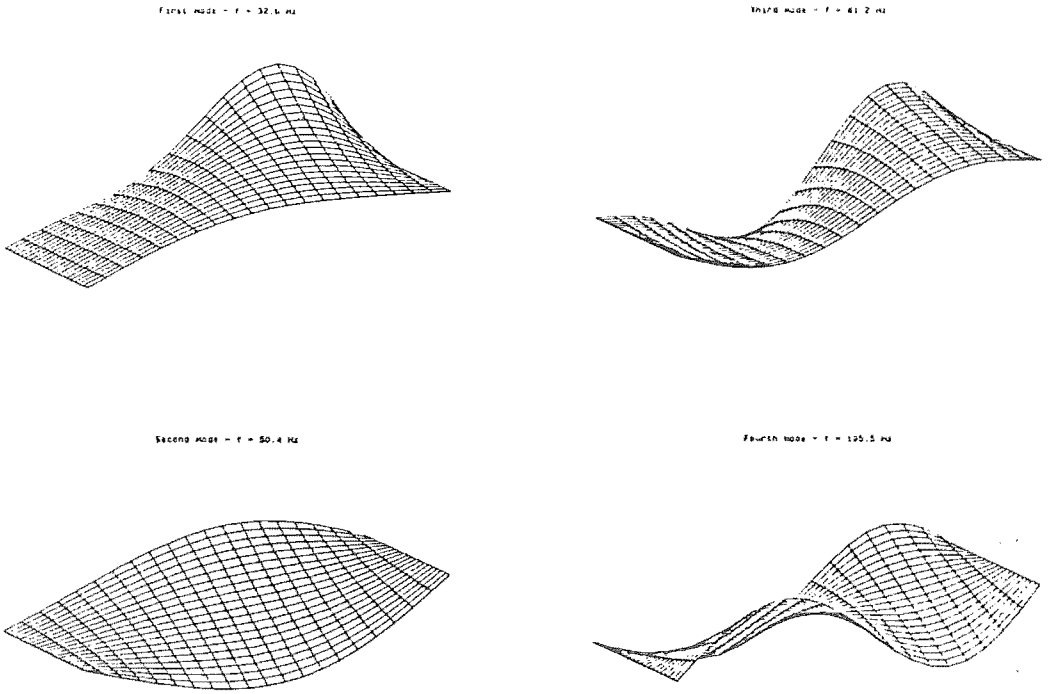

Figure 88: First four modes of a stationary blade subjected to 30000 N/m tangential load (3×3 trial function).

Table 20: First four natural frequencies of a blade with 38 m/s transport speed, subjected to various tangential loads.

Tangential Load (N/m)	Frequencies for 3×3 Functions (Hz)	Frequencies for 4×4 Functions (Hz)
0	40.0	39.9
	48.9	48.7
	87.0	84.1
	103.5	100.5
10000	38.9	38.8
	48.7	48.5
	86.3	83.0
	103.3	100.0
30000	28.0	25.7
	47.1	46.6
	80.6	73.2
	101.5	97.3
40000	8.4	-
	45.6	44.9
	75.7	63.8
	100.5	95.7

9.6.5 Results for a Moving Blade

The first four natural frequencies of the same blade as in the previous section, with an axial speed of 38 m/s are given in Table 20, and plotted in Figure 89.

The overall effect of the transport speed was a 12% reduction in the natural frequencies of the blade. Therefore, the buckling load was also decreased, however, this reduction was insignificant compared with the magnitude of the buckling load.

9.6.6 Conclusion

For a typical bandsaw blade configuration, the effects of axial speed on the divergent buckling load was minimal, therefore, a stationary blade would provide a reasonably accurate description of the divergent buckling effect.

The magnitude of the buckling load was much greater than that of a typical

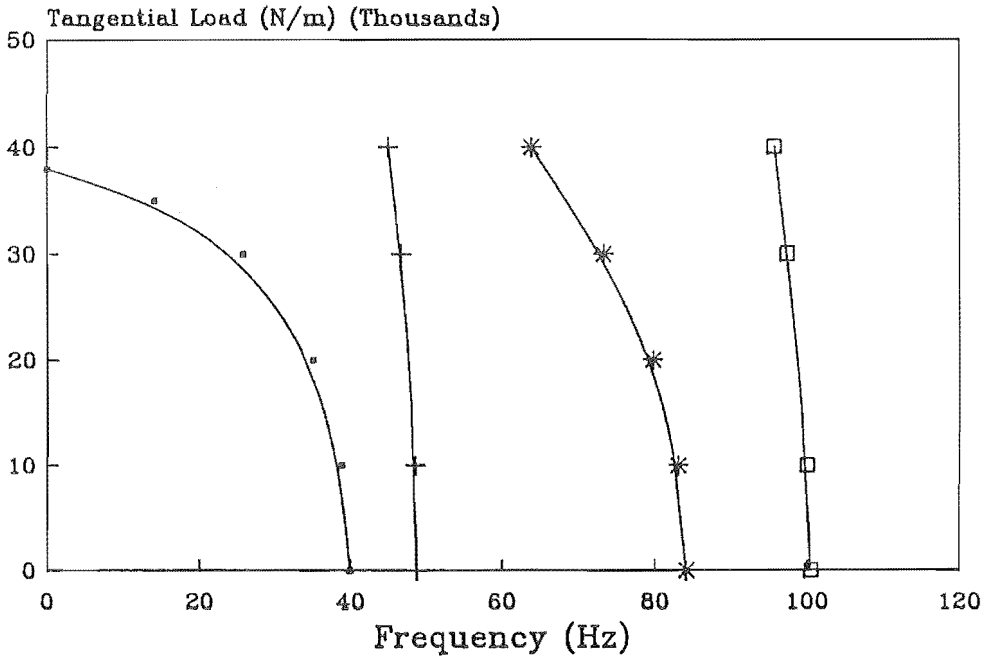

Figure 89: Natural frequency versus tangential load, for a blade with 38 m/s transport speed.

cutting load, however, this is to be expected because otherwise the present bandsaw operation would be considered unsafe.

It seems unlikely that the magnitude of the cutting load could be as high as that of the buckling load. However, the divergent buckling of the blade due to tangential cutting force cannot be ruled out as a possible cause of the blade instability, because the magnitude of the cutting load, which causes the blade to become unstable, has not been measured.

It becomes obvious at this stage that a full experimental investigation of the unstable behaviour of the bandsaw blade is necessary to verify many uncertainties in this field of work.

The theory presented in this thesis provides a powerful technique for the analysis of bandsaw blades under in-plane stresses. Until the parameters associated with the cutting process are determined, this theory should become an important tool in the

design of bandsaw blades with better performance.

Chapter 10

STABILITY OF BANDSAW BLADE UNDER PARAMETRIC EXCITATIONS

10.1 Introduction

The subject undertaken in this chapter belongs to a modern branch of the theory of elasticity, the *theory of dynamic stability of elastic systems.* The counterpart of this theory is the theory of *static stability,* where a static load may result in *divergent buckling* of the system. The dynamic stability problems involve loads which are dependent on time (dynamic loads), such as periodic loads. A low level dynamic load can cause the system to have large vibrations. This phenomenon is referred to as the *parametric resonance* of the system, and the dynamic load is called the *parametric excitation.*

For the bandsaw blade problem, parametric excitations are present and must be considered as possible causes of the saw blade vibration during idling and cutting

conditions. Naguleswaran and Williams (1968) [58] have considered the effects of periodic fluctuations in tension on the transverse vibration of a moving beam, due to pulleys eccentricity, joints and flaws in the band and on the pulley surfaces. Ariaratnam and Asokanthan (1988) [7] considered the same phenomenon but for the torsional oscillations of a moving beam. Wu and Mote (1986) [95] addressed the in-plane normal periodic edge load on the moving beam. However, there has not been a published study of parametric excitations of a moving plate; this would be more suited for the analysis of wide bandsaw blades.

The objectives of this chapter are:

- To introduce a powerful and simple method for the analysis of a moving plate subjected to parametric excitations.
- To re-examine the effects of periodic fluctuations in tension on the behaviours of a bandsaw blade
- To investigate the effects of periodic tangential cutting force on the behaviours of a bandsaw blade.

10.2 Method of Analysis

10.2.1 Introduction

A dynamical system under parametric excitation is governed by a set of differential equations with periodic coefficients. If the degrees of freedom are finite, then the governing equations of motion are a set of second order ordinary differential equations

$$[M]\left\{\ddot{X}\right\} + [G(t)]\left\{\dot{X}\right\} + [K(t)]\{X\} = 0 \tag{186}$$

where the elements of $[G(t)]$ and $[K(t)]$ are periodic in t. This set of equations is sometimes referred to as a set of Hill's equations, and when the periodicity is sinusoidal (simple harmonic), it is then called a set of Mathieu's equations.

The primary objective is to determine whether the trivial solution of Equation (186), $\{X\} = 0$, is stable or unstable.

The most advanced and general theory in this area is the theory of bifurcation, which aims at '*an understanding of the mechanisms by which forms are generated in nature*' and at '*a classification and unifying description of generic pattern-forming processes independent of system details*' [27]. This theory is still being developed by mathematicians and physicists, and at present, there are few applications in the field of engineering.

The method of Liapunov is often mentioned in the theory of bifurcation, which proposes to obtain the stability information without having to find explicit solutions for the equations of motion. Kozin and Milstead (1979) applied the Lyapunov's method to solve the stability of a moving elastic strip subjected to a random parametric excitation. However, it appeared that this method involved more complicated mathematics than that typically used to solve engineering problems. This method still has a great potential in the study of bifurcation problems, but more applications and simplifications are needed before it can replace the more conventional methods.

These more conventional methods include the Linstep's purturbation method, the Hsu's asymtotic method [34], the multiple scales method [59], the averaging method [7], the harmonic balance method [12,50,77] and the direct numerical integration method. These methods, except for the harmonic balance method, are small parameter methods, that is, only small parametric excitations are applicable.

Sometimes referred to as the Bolotin's method, the harmonic balance method was developed by Bolotin (1964) [12]. He found that the direct evaluation of this method

was impractical and developed a simpler approximation. The latter method, unfortunately, omitted the case of combination parametric resonances[1]. Takahashi (1981) [77] realised this restriction and removed it by simply solving the first Bolotin's formulation, with the help of modern computational techniques. This method was used to solve plate problems with combinations of simply-supported and clamped boundary conditions, subjected to a periodic in-plane stress [78].

The bandsaw blade problem is closely related to the study by Takahashi (1988) [78], therefore, the harmonic balance method was chosen for the investigation of the stability of a moving bandsaw blade subjected to parametric excitations.

10.2.2 Harmonic Balance Method

Parametric excitations in the bandsaw blades can be assumed to be sinusoidal, for example, the tension fluctuations are from the rotation of the pulleys. This means that the governing equations can be discretised and arranged to a set of coupled Mathieu's equations of the form

$$[M]\left\{\ddot{T}\right\} + \left([K_0] + q_p\,[K_p]\cos\Omega t\right)\{T\} = \{0\} \tag{187}$$

or in the case of a moving plate

$$[M]\left\{\ddot{T}\right\} + [G]\left\{\dot{T}\right\} + \left([K_0] + q_p\,[K_p]\cos\Omega t\right)\{T\} = \{0\} \tag{188}$$

where $\{T\}$ is the generalised coordinate vector, $[M]$, $[G]$ and $[K_0]$ are time independent matrices, q_p denotes the magnitude of the parametric excitation, $[K_p]$ is the stiffness matrix in connection with this parametric excitation and Ω is the angular frequency of the excitation.

[1]There are simple parametric resonances and combination parametric resonances. A simple resonance associates with one single mode of vibration, whereas, a combination resonance involves the coupling of two or more modes of vibration

The solutions for Equation (188) are periodic with a frequency of Ω, and the Fourier expansion is [12, page 214]

$$\{T\} = e^{\lambda t}\left\{\frac{1}{2}\{b_0\} + \sum_{k=1}\left(\{a_k\}\sin k\Omega t + \{b_k\}\cos k\Omega t\right)\right\} \tag{189}$$

where $\{b_0\}, \{a_k\}, \{b_k\}$ are the time-independent coefficient vectors.

The usual solutions for vibration problems are of the form $\{b\}e^{i\omega t}$, which are included in the above Fourier expansion. However, $e^{\lambda t}$ was used instead of $e^{i\omega t}$, hence the imaginary part of λ is the natural frequency, the real part of λ represents the damping factor and if it is positive, the system is unstable (positive damping).

Equation (189) is differentiated with respect to time t, and substituted into the governing differential equations, Equation (187) or Equation (188). The harmonic balance method is now used to obtain a set of algebraic equations. In this method, the trigonometric identities,

$$\cos A\cos B = \frac{1}{2}\left(\cos\left(A-B\right) + \cos\left(A+B\right)\right)$$

and

$$\sin A\cos B = \frac{1}{2}\left(\sin\left(A-B\right) + \sin\left(A+B\right)\right)$$

are used to rearrange the governing equations. The coefficients of $e^{\lambda t}$, $e^{\lambda t}\sin\left(k\Omega t\right)$, and $e^{\lambda t}\cos\left(k\Omega t\right)$ can then be collected and equated to zero [72].

Applying the harmonic balance method to Equation (187), gives

$$\frac{1}{2}\lambda^2[M]\{b_0\} + \frac{1}{2}[K_0]\{b_0\} - \frac{1}{2}q_p[K_p]\{b_1\} = 0 \tag{190}$$

$$\lambda^2[M]\{a_k\} - 2k\lambda\Omega[M]\{b_k\} + \left([K_0] - k^2\Omega^2[M]\right)\{a_k\} - \frac{1}{2}q_p[K_p]\left(\{a_{k-1}\} + \{a_{k+1}\}\right) = 0 \tag{191}$$

$$\lambda^2[M]\{b_k\} + 2k\lambda\Omega[M]\{a_k\} + \left([K_0] - k^2\Omega^2[M]\right)\{b_k\} - \frac{1}{2}q_p[K_p]\left(\{b_{k-1}\} + \{b_{k+1}\}\right) = 0 \tag{192}$$

For the moving plate equation (Equation (188)), this method gives

$$\frac{1}{2}\lambda^2[M]\{b_0\} + \frac{1}{2}\lambda[G]\{b_0\} + \frac{1}{2}[K_0]\{b_0\} - \frac{1}{2}q_p[K_p]\{b_1\} = 0 \quad (193)$$

$$\lambda^2[M]\{a_k\} - 2k\lambda\Omega[M]\{b_k\} + \left([K_0] - k^2\Omega^2[M]\right)\{a_k\} + \lambda[G]\{a_k\} - k\Omega[G]\{b_k\} - \frac{1}{2}q_p[K_p](\{a_{k-1}\} + \{a_{k+1}\}) = 0 \quad (194)$$

$$\lambda^2[M]\{b_k\} + 2k\lambda\Omega[M]\{a_k\} + \left([K_0] - k^2\Omega^2[M]\right)\{b_k\} + \lambda[G]\{b_k\} + k\Omega[G]\{a_k\} - \frac{1}{2}q_p[K_p](\{b_{k-1}\} + \{b_{k+1}\}) = 0 \quad (195)$$

where $k = 1, 2, 3, \ldots$ and $a_0 = 0$.

These equations can be rearranged into the form

$$\left([M_0] - \lambda[M_1] - \lambda^2[M_2]\right)\{X\} = \{0\} \quad (196)$$

Mickens (1984) [50] stated that, in most cases of practical interest, the method of harmonic balance need not be carried out beyond the first approximation, that is, $k = 1$.

In this thesis, the Fourier expansion was taken to two sinusoidal terms, $k = 1, 2$, hence

$$\{X\} = \begin{Bmatrix} \{b_0\} \\ \{a_1\} \\ \{a_2\} \\ \{b_1\} \\ \{b_2\} \end{Bmatrix} \quad (197)$$

The size of the state vector is five times larger than that of the state vector for a usual vibration problem.

By separating the zeroth, first and second powers of λ, the matrices in Equation (196) can be expressed in matrix forms.

For the case when $[G] = 0$ (Equation (187))

$$[M_0] = \begin{bmatrix} [K_0] & 0 & 0 & -q_p[K_p] & 0 \\ 0 & [K_1] & -\frac{1}{2}q_p[K_p] & 0 & 0 \\ 0 & -\frac{1}{2}q_p[K_p] & [K_2] & 0 & 0 \\ -\frac{1}{2}q_p[K_p] & 0 & 0 & [K_1] & -\frac{1}{2}q_p[K_p] \\ 0 & 0 & 0 & -\frac{1}{2}q_p[K_p] & [K_2] \end{bmatrix} \tag{198}$$

where

$$[K_1] = [K_0] - \Omega^2[M], \qquad [K_2] = [K_0] - 4\Omega^2[M]$$

$$[M_1] = \begin{bmatrix} 0 & 0 & 0 & 0 & 0 \\ 0 & 0 & 0 & 2\Omega[M] & 0 \\ 0 & 0 & 0 & 0 & 4\Omega[M] \\ 0 & -2\Omega[M] & 0 & 0 & 0 \\ 0 & 0 & -4\Omega[M] & 0 & 0 \end{bmatrix} \tag{199}$$

$$[M_2] = \begin{bmatrix} -[M] & 0 & 0 & 0 & 0 \\ 0 & -[M] & 0 & 0 & 0 \\ 0 & 0 & -[M] & 0 & 0 \\ 0 & 0 & 0 & -[M] & 0 \\ 0 & 0 & 0 & 0 & -[M] \end{bmatrix} \tag{200}$$

For the moving plate case (Equation (188))

$$[M_0] = \begin{bmatrix} [K_0] & 0 & 0 & -q_p[K_p] & 0 \\ 0 & [K_1] & -\frac{1}{2}q_p[K_p] & -\Omega[G] & 0 \\ 0 & -\frac{1}{2}q_p[K_p] & [K_2] & 0 & -2\Omega[G] \\ -\frac{1}{2}q_p[K_p] & \Omega[G] & 0 & [K_1] & -\frac{1}{2}q_p[K_p] \\ 0 & 0 & 2\Omega[G] & -\frac{1}{2}q_p[K_p] & [K_2] \end{bmatrix} \tag{201}$$

$$[M_1] = \begin{bmatrix} -[G] & 0 & 0 & 0 & 0 \\ 0 & -[G] & 0 & 2\Omega[M] & 0 \\ 0 & 0 & -[G] & 0 & 4\Omega[M] \\ 0 & -2\Omega[M] & 0 & -[G] & 0 \\ 0 & 0 & -4\Omega[M] & 0 & -[G] \end{bmatrix} \tag{202}$$

$$[M_2] = \begin{bmatrix} -[M] & 0 & 0 & 0 & 0 \\ 0 & -[M] & 0 & 0 & 0 \\ 0 & 0 & -[M] & 0 & 0 \\ 0 & 0 & 0 & -[M] & 0 \\ 0 & 0 & 0 & 0 & -[M] \end{bmatrix} \tag{203}$$

Equation (196) is a quadratic eigenvalue problem and the method of obtaining the eigenvalues and the eigenvectors is the same as the method described in Section 8.3.2.

The conditions for which the system becomes unstable under parametric excitations can be best represented on a stability chart, or sometimes referred to as a Strutt diagram, where the instability regions in the frequency-amplitude space of the excitation are plotted.

Takahashi's method for plotting the unstable regions seemed to be by inspection of the real part of the eigenvalues for a range of excitation frequencies and amplitudes.

Recently, a variation of the harmonic balance method, the *incremental harmonic balance method*, has been developed to solve several problems in nonlinear dynamics [24,62]. This method is more suited for computational work than the classical harmonic balance method, however, insight into the method of solution is lost, because the problem of solving the governing differential equations is replaced by that

of solving a a simpler set of equations involving increments in the motion, exciting force, and/or frequency of excitation. This method can perhaps be used in the future, to see if it is more efficient than the classical harmonic balance method.

10.3 Periodic Tension Fluctuation

In this section, the in-plane load N_y, N_{xy} are assumed to be zero, and N_x to be linearly distributed, hence, the model covers the case of backcrowning and wheel tilting but not in the case of prestressing. However a prestressed saw blade can still be investigated with the same method, by choosing the appropriate in-plane stress distributions.

When the tension on the blade possesses a periodic fluctuation, the magnitude of the in-plane load, q_0, can be extended to $q_0 + q_p \cos \Omega t$, where q_p is the magnitude of the periodic load (parametric load) and Ω is the frequency of the parametric excitation.

10.3.1 Stationary Blades

The linearly distributed in-plane load, N_x, with periodic fluctuation is

$$N_x = q_0 \left(d + e\frac{y}{b} \right) + q_p \cos \Omega t \tag{204}$$

This in-plane load can be substituted into the equation of motion (Equation (154)), discretised using the Galerkin method (Equation (169) with $c = 0$), and finally rearranged into the form of Equation (187), where the elements of the matrix $[M], [K_0], [K_p]$ are given by

$$\begin{aligned} M_{rsmn} &= \int_0^b \int_0^l \rho h \psi_{rs} \psi_{mn} \, dx \, dy \\ (K_0)_{rsmn} &= \int_0^b \int_0^l D \nabla^2 \psi_{rs} \nabla^2 \psi_{mn} + q_0 \left(d + e\frac{y}{b} \right) \frac{\partial \psi_{rs}}{\partial x} \frac{\partial \psi_{mn}}{\partial x} \, dx \, dy \end{aligned} \tag{205}$$

$$- (1-\nu) \int_0^l \left\{ \psi_{rs} \frac{\partial^3 \psi_{mn}}{\partial x^2 \partial y} + \frac{\partial \psi_{rs}}{\partial y} \frac{\partial^2 \psi_{mn}}{\partial x^2} \right\} \Bigg|_{y=0}^{b} dx \qquad (206)$$

$$(K_p)_{rsmn} = - \int_0^b \int_0^l \frac{\partial \psi_{rs}}{\partial x} \frac{\partial \psi_{mn}}{\partial x} \, dx \, dy \qquad (207)$$

where ψ are the trial functions. The subscripts r, s, m, n are as explained in Section 7.5.1.

The harmonic balance method, Equations (196,198,199,200), can now be used to obtain the instability regions for various excitation frequencies and amplitudes.

Numerical results were obtained for a blade with dimensions 0.22×0.00165×0.8 m, and with a uniform tension of 15000 N. The natural frequencies of this blade were:

- $f_1 = 44.8$ Hz for the first transverse mode.
- $f_2 = 53.2$ Hz for the first torsional mode.
- $f_3 = 91.8$ Hz for the second transverse mode.
- $f_4 = 108.4$ Hz for the second torsional mode.

The mode shapes were plotted in Figure 73.

For the first transverse mode (1×1 trial function in the Galerkin solution), the instability regions, obtained from a one-term Fourier expansion in the harmonic balance step, were plotted on a Strutt diagram as shown in Figure 90.

The Strutt diagram shows that the primary region of instability was at an excitation frequency of twice the natural frequency of the blade, referred to as the $2f_1$ simple parametric resonance. There was also a secondary region of instability at $\Omega = f_1$, referred to as the f_1 simple parametric resonance.

Figure 91 shows the same instability problem with two-term Fourier expansion in the harmonic balance step. The primary instability region was the same as obtained from the one-term Fourier expansion calculation, whereas the width of the f_1 simple

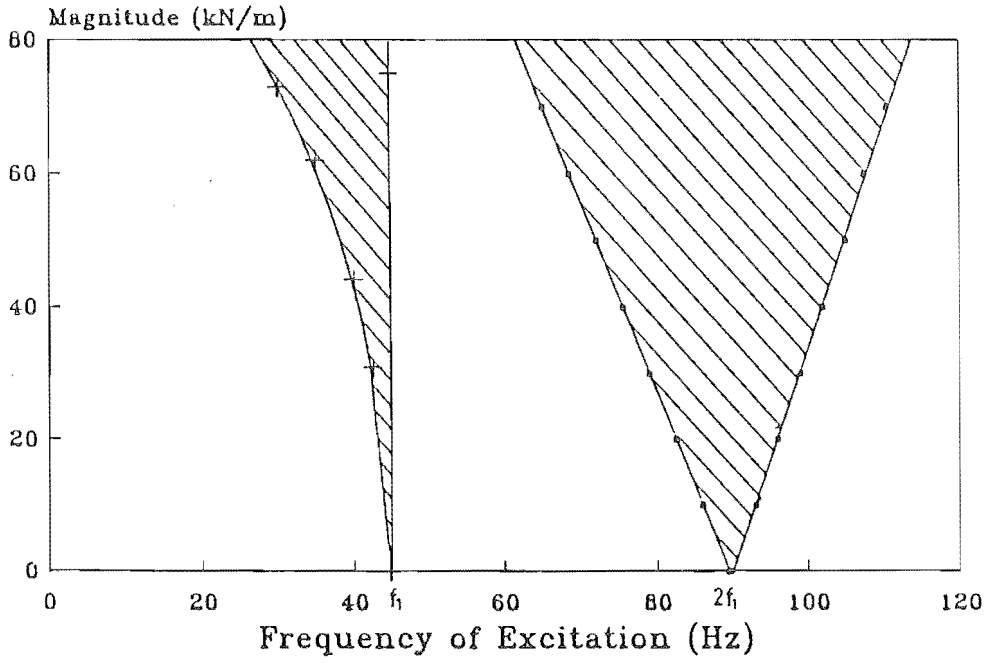

Figure 90: Instability regions for the first transverse mode of a stationary blade subjected to fluctuating tensions, with a one-term Fourier expansion.

parametric resonance region was much narrower than that from the one-term Fourier calculation. There were regions of instability associated with $2/3f_1$ and $1/2f_1$, which are sometimes referred to as the sub-harmonic resonances of the first mode.

These results showed that an increase in the number of terms, taken for the Fourier expansion of the harmonic balance method, would result in an increase in the number of the sub-harmonic resonance regions. However, the width of these regions would be narrow. In practice, these sub-harmonic resonance regions are likely to be insignificant due to the presence of damping, except when the amplitudes of the excitation are very high.

Similar Strutt diagrams can be obtained for the other modes, and the primary instability regions will always be the $2f_n$ simple parametric resonance regions.

Figure 92 shows a Strutt diagram obtained for a 2×2 trial function Galerkin solution. This diagram showed that for a blade subjected to fluctuating tension,

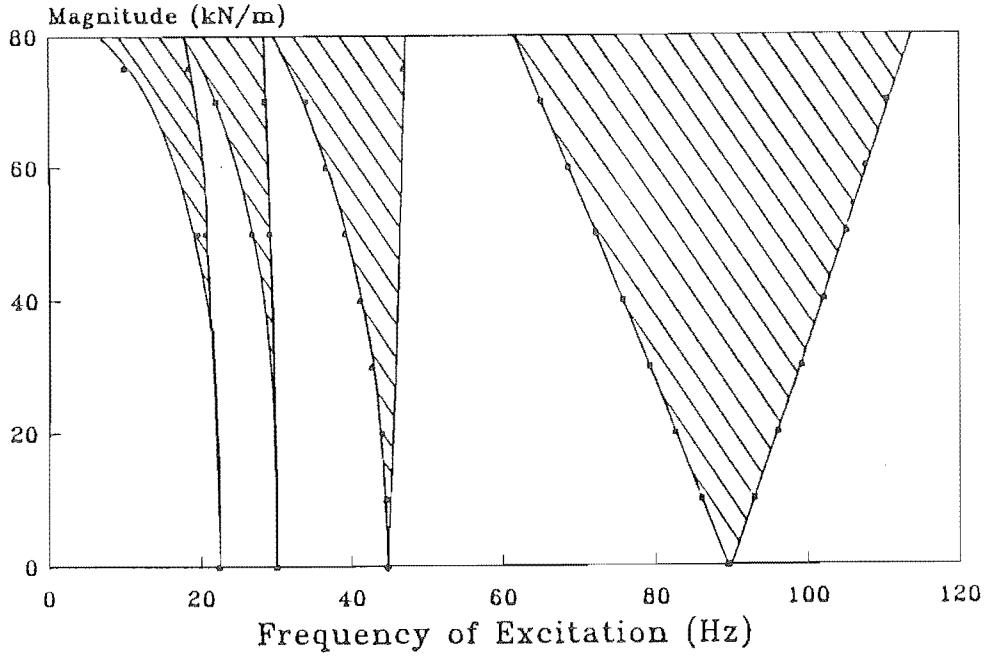

Figure 91: Instability regions for the first transverse mode of a stationary blade subjected to fluctuating tensions, with a two-term Fourier expansion.

combination parametric resonances were not possible, and each $2f_n$ simple parametric resonance could be calculated independently and then be superimposed on the same Strutt diagram to represent the regions of instability of the blade.

Parametric resonances only occur through the non-zero terms in the matrix $[K_p]$, and for this case, $[K_p]$ was diagonal, hence only the simple parametric resonances were possible.

10.3.2 Moving Blade

The in-plane load for a moving plate is the same as for a stationary plate with an extra term added to take into account the effect of the straining device

$$N_x = q_0\left(d + e\frac{y}{b}\right) + q_p \cos\Omega t + \eta\rho h c^2 \tag{208}$$

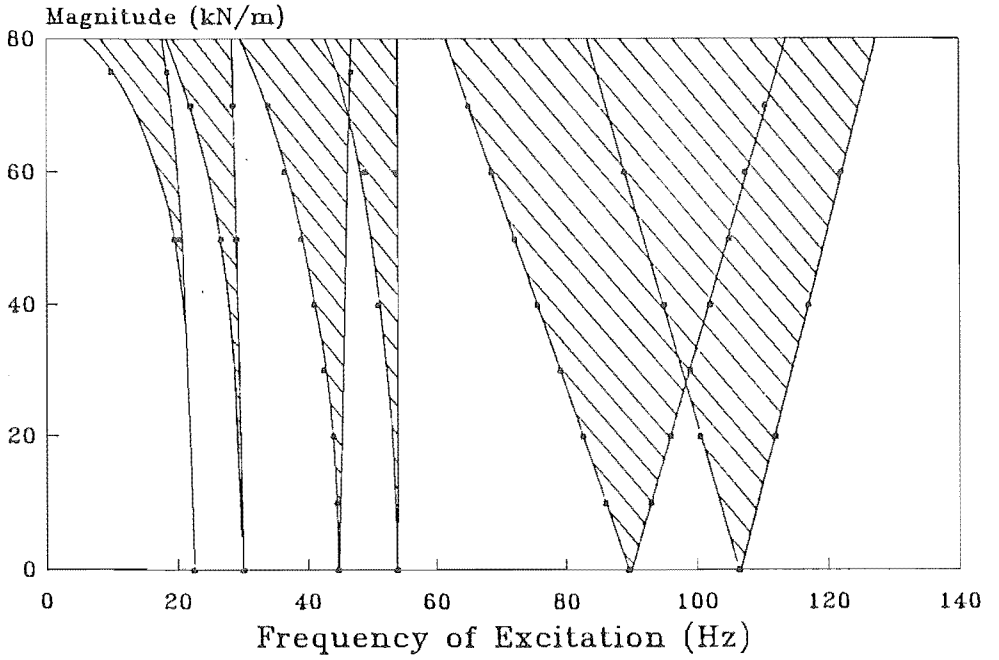

Figure 92: Instability regions for a 2×2 trial function Galerkin solution of a stationary blade subjected to fluctuating tensions, with a two-term Fourier expansion.

Applying the Galerkin method to the governing differential equation and re-arranging it to the form of Equation (188) where the coefficients of the matrices are

$$M_{rsmn} = \int_0^b \int_0^l \rho h \psi_{rs} \psi_{mn} \, dx \, dy \tag{209}$$

$$G_{rsmn} = \int_0^b \int_0^l 2\rho h c \psi_{rs} \frac{\partial \psi_{mn}}{\partial x} \, dx \, dy \tag{210}$$

$$\begin{aligned} (K_0)_{rsmn} = & \int_0^b \int_0^l \left\{ D\nabla^2\psi_{rs}\nabla^2\psi_{mn} + q_0 \left(d + e\frac{y}{b}\right) \frac{\partial \psi_{rs}}{\partial x}\frac{\partial \psi_{mn}}{\partial x} \right. \\ & \left. - (1-\eta)\,\rho h c^2 \frac{\partial \psi_{rs}}{\partial x}\frac{\partial \psi_{mn}}{\partial x} \right\} dx\, dy \\ & - (1-\nu) \int_0^l \left\{ \psi_{rs} \frac{\partial^3 \psi_{mn}}{\partial x^2 \partial y} + \frac{\partial \psi_{rs}}{\partial y}\frac{\partial^2 \psi_{mn}}{\partial x^2} \right\} \Bigg|_{y=0}^{b} dx \end{aligned} \tag{211}$$

$$(K_p)_{rsmn} = -\int_0^b \int_0^l \frac{\partial \psi_{rs}}{\partial x}\frac{\partial \psi_{mn}}{\partial x} \, dx \, dy \tag{212}$$

The harmonic balance method can again be used on Equation (188) to give the

quadratic eigenvalue Equation (196) with the matrices $[M_0], [M_1], [M_2]$ as given by Equations (201, 202, 203).

The effects of transport speed are the inclusion of the centripetal term and the Coriolis term in the governing equation.

The centripetal term is the $-(1-\eta)\rho hc^2 \frac{\partial \psi_{rs}}{\partial x} \frac{\partial \psi_{mn}}{\partial x}$ in the matrix $[K_0]$. Therefore, when $\eta = 1$, as for the counterweight straining mechanism, the centripetal term does not affect the saw blade. However, if it was present ($\eta \neq 1$), this term would have a destabilising effect on the blade, by increasing the size of the instability regions [58].

The Coriolis term is included in the matrix $[G]$, and an inspection of this matrix would help in understanding the results. $[G]$ is a skew symmetric matrix, and for a 2×2 trial function Galerkin solution, it is of the form

$$[G] = \begin{bmatrix} 0 & 0 & G_{13} & 0 \\ 0 & 0 & 0 & G_{24} \\ G_{31} & 0 & 0 & 0 \\ 0 & G_{42} & 0 & 0 \end{bmatrix} \tag{213}$$

This matrix showed that the 1×1 or 1×2 trial function Galerkin solution could not account for the Coriolis term, because $[G] = [0]$. The mimimum requirement was a 2×1 function Galerkin solution, which could accurately predict the first natural frequency of a moving blade.

Figure 93 shows the Strutt diagram for a moving blade, with a transport speed of 40 m/s. As the the transport speed increased, the first natural frequency of the blade decreased, therefore, the $2f_1$ parametric resonance region also shifted down the frequency axis. There were other regions of instability at higher amplitudes of parametric excitation.

Naguleswaran and Williams (1968) [58], and Wu and Mote (1986) [95] showed

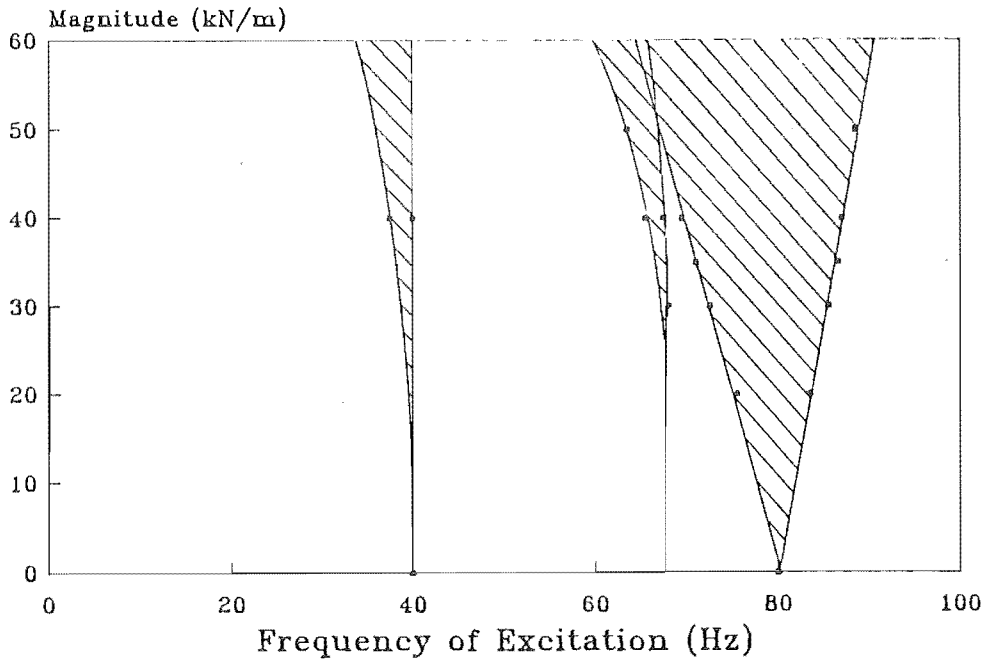

Figure 93: Instability regions for a 2×1 trial function Galerkin solution of a moving blade, with $c = 40$ m/s, subjected to fluctuating tensions, with a two-term Fourier expansion.

that the Coriolis term stabilised the blade by reducing the width of the instability regions. This effect is shown in Figure 94, where the slope of the boundaries of the $2f_1$ parametric resonance region are plotted against the transport speeds. As the transport speed increased, the slope of the instability boundary increased, that is, the area of the instability region decreased. However, Figure 93 shows that at large amplitudes of tension fluctuation, other regions of instability appeared close to the primary region of instability, therefore, the width of this region was actually larger than expected. These extra regions of instability had not been discussed in previous publications, perhaps, because their methods of analysis were only for small amplitudes, whereas in this thesis, the harmonic balance method was used, which could be applied to large amplitudes of parametric excitation.

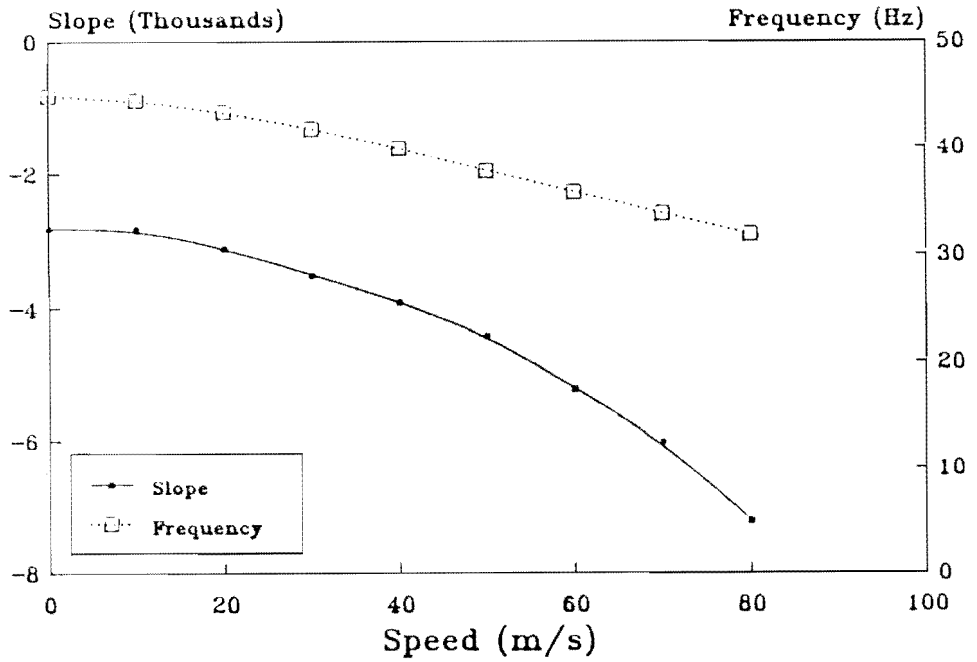

Figure 94: Inclination of the left boundary of the $2f_1$ simple parametric resonance region versus transport speeds, c.

10.4 Periodic Tangential Cutting Forces

Wu and Mote (1986) [95] stated that '*cutting forces in bandsaws possess periodic, in-plane edge loading components potentially inducing combination parametric instabilities*'. However, they only discussed the in-plane normal periodic load due to the feeding force of the timber into the blade. They concluded that simple torsional parametric resonances and combination transverse-torsional parametric resonances could be excited, but simple transverse, combination transverse-transverse, or combination torsional-torsional parametric resonances could not.

As discussed in Section 9.6, the perpendicular component of the cutting force may be much smaller than the tangential component. This section will, therefore, look at the parametric instabilities of the blade due to a periodic tangential component of the cutting force.

The most significant periodicity of the tangential cutting force is from the frequency of the teeth impacting the timber, hence, the angular frequency of the parametric excitation Ω is equal to the blade axial speed c times the number of teeth per unit length of the blade N, $\Omega = cN$. However, Ω is usually very high (760 Hz for the Waimak saw blade), and therefore out of the range of parametric resonances.

10.4.1 Stationary Blades

There has not been any application involving a stationary plate subjected to a periodic tangential edge force, however, a study of this would provide more insight into the moving plate problem.

In this section, only the cutting force q_c was assumed to possess periodicity, therefore, the in-plane loads were given as

$$N_x = q_0\left(d + e\frac{y}{b}\right) - (q_c + q_{cp}\cos\Omega t)\,\frac{l}{b}\left(2\frac{x}{l} - 1\right)\frac{y}{b} \tag{214}$$

$$N_y = 0 \tag{215}$$

$$N_{xy} = (q_c + q_{cp}\cos\Omega t)\left(\frac{y}{b}\right)^2 \tag{216}$$

where q_{cp} was the magnitude of the periodic component of the cutting force, and Ω was the frequency of the parametric excitation.

The Galerkin method could now be used to discretise the equation of motion to the form of Equation (187) where

$$M_{rsmn} = \int_0^b \int_0^l \rho h \psi_{rs}\psi_{mn}\,dx\,dy \tag{217}$$

$$\begin{aligned}(K_0)_{rsmn} = {} & \int_0^b \int_0^l D\nabla^2\psi_{rs}\nabla^2\psi_{mn} + q_0\left(d + e\frac{y}{b}\right)\frac{\partial\psi_{rs}}{\partial x}\frac{\partial\psi_{mn}}{\partial x}\,dx\,dy \\ & + q_c\left\{\left(\frac{y}{b}\right)^2\left(\frac{\partial\psi_{rs}}{\partial y}\frac{\partial\psi_{mn}}{\partial x} + \frac{\partial\psi_{rs}}{\partial x}\frac{\partial\psi_{mn}}{\partial y}\right)\right. \\ & \left. - \frac{l}{b}\frac{y}{b}\left(2\frac{x}{l} - 1\right)\frac{\partial\psi_{rs}}{\partial x}\frac{\partial\psi_{mn}}{\partial x}\right\}\,dx\,dy\end{aligned}$$

$$- (1-\nu) \int_0^l \left\{ \psi_{rs} \frac{\partial^3 \psi_{mn}}{\partial x^2 \partial y} + \frac{\partial \psi_{rs}}{\partial y} \frac{\partial^2 \psi_{mn}}{\partial x^2} \right\} \Bigg|_{y=0}^{b} dx \tag{218}$$

$$(K_p)_{rsmn} = - \int_0^b \int_0^l \left\{ \frac{l}{b} \frac{y}{b} \left(2\frac{x}{l} - 1 \right) \frac{\partial \psi_{rs}}{\partial x} \frac{\partial \psi_{mn}}{\partial x} - \left(\frac{y}{b} \right)^2 \left(\frac{\partial \psi_{rs}}{\partial y} \frac{\partial \psi_{mn}}{\partial x} + \frac{\partial \psi_{rs}}{\partial x} \frac{\partial \psi_{mn}}{\partial y} \right) \right\} dx\, dy \tag{219}$$

The numerical values in this section were calculated for a blade with the same tension and dimensions as that in the previous section.

The matrix $[K_p]$ for a 2×2 mode Galerkin solution had the form

$$[K_p] = \begin{bmatrix} 0 & 0 & (K_p)_{13} & (K_p)_{14} \\ 0 & 0 & (K_p)_{23} & (K_p)_{24} \\ (K_p)_{31} & (K_p)_{32} & 0 & 0 \\ (K_p)_{41} & (K_p)_{42} & 0 & 0 \end{bmatrix} \tag{220}$$

The non-zero elements of $[K_p]$ showed that the major parametric resonances were the $(f_1 + f_3)$, $(f_2 + f_3)$, $(f_1 + f_4)$, and $(f_2 + f_4)$ combination resonances. These instability regions are shown in Figure 95, assuming that the nominal cutting force q_c was equal to zero. In practical cases, the magnitude of q_c would be small and hence would not significantly affect the blade (Section 9.6).

The order of importance of the combination parametric resonances are:

1. The combination first transverse-second torsional parametric resonance $(f_1 + f_4)$.

2. The combination first transverse-second transverse parametric resonance $(f_1 + f_3)$.

3. The combination first torsional-second torsional parametric resonance $(f_2 + f_4)$.

4. The combination first torsional-second transverse parametric resonance $(f_2 + f_3)$.

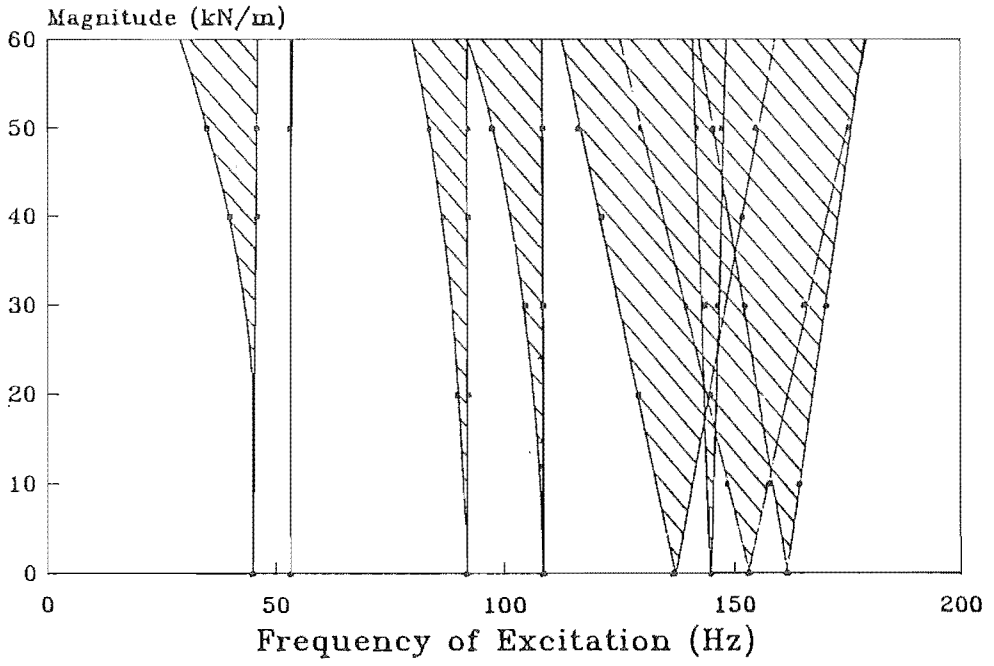

Figure 95: Instability regions for a 2×2 trial function Galerkin solution of a stationary blade subjected to periodic tangential cutting forces, with a two-term Fourier expansion.

These instability regions could also be obtained independently by considering appropriate subsets of $[M]$, $[K_0]$ and $[K_p]$, which would be more feasible than investigating the total configuration.

10.4.2 Moving Blades

For moving plates, extra terms were added into the matrices to give the governing Equation (188). The components of the matrices in Equation (188) are

$$M_{rsmn} = \int_0^b \int_0^l \rho h \psi_{rs} \psi_{mn} \, dx \, dy \tag{221}$$

$$G_{rsmn} = \int_0^b \int_0^l 2\rho h c \psi_{rs} \frac{\partial \psi_{mn}}{\partial x} \, dx \, dy \tag{222}$$

$$\begin{aligned}(K_0)_{rsmn} = & \int_0^b \int_0^l \left\{ D\nabla^2\psi_{rs}\nabla^2\psi_{mn} + q_0 \left(d + e\frac{y}{b}\right) \frac{\partial \psi_{rs}}{\partial x}\frac{\partial \psi_{mn}}{\partial x} \, dx \, dy \right. \\ & \left. + q_c \left\{ \left(\frac{y}{b}\right)^2 \left(\frac{\partial \psi_{rs}}{\partial y}\frac{\partial \psi_{mn}}{\partial x} + \frac{\partial \psi_{rs}}{\partial x}\frac{\partial \psi_{mn}}{\partial y} \right) \right.\end{aligned}$$

$$- \frac{l}{b}\frac{y}{b}\left(2\frac{x}{l}-1\right)\frac{\partial\psi_{rs}}{\partial x}\frac{\partial\psi_{mn}}{\partial x}\Bigg\} - (1-\eta)\,\rho hc^2\frac{\partial\psi_{rs}}{\partial x}\frac{\partial\psi_{mn}}{\partial x}\Bigg\}\,dx\,dy$$

$$- (1-\nu)\int_0^l\left\{\psi_{rs}\frac{\partial^3\psi_{mn}}{\partial x^2\partial y} + \frac{\partial\psi_{rs}}{\partial y}\frac{\partial^2\psi_{mn}}{\partial x^2}\right\}\Bigg|_{y=0}^{b} dx \qquad (223)$$

$$(K_p)_{rsmn} = -\int_0^b\int_0^l\left\{\frac{l}{b}\frac{y}{b}\left(2\frac{x}{l}-1\right)\frac{\partial\psi_{rs}}{\partial x}\frac{\partial\psi_{mn}}{\partial x}\right.$$

$$\left. - \left(\frac{y}{b}\right)^2\left(\frac{\partial\psi_{rs}}{\partial y}\frac{\partial\psi_{mn}}{\partial x} + \frac{\partial\psi_{rs}}{\partial x}\frac{\partial\psi_{mn}}{\partial y}\right)\right\}dx\,dy \qquad (224)$$

The major parametric resonances for the periodic cutting force problem were the combination parametric resonances, therefore, the matrix $[G]$ had to accommodate all the frequencies of interest. For example, to investigate the $f_1 + f_3$ combination parametric resonance, the Galerkin aprroximation had to be able to calculate f_1 and f_3 accurately for any transport speed c. A 2×1 mode Galerkin solution could not determine f_3 accurately, therefore, a 3×1 mode Galerkin solution was necessary for this case.

Figure 96 shows the $f_1 + f_3$ combination parametric resonance region for a blade moving at a transport speed of 40 m/s. This diagram showed that the boundaries of the instability region were not straight, and there was another unstable region at a higher amplitude range of the excitation, which was the $\frac{2}{3}f_1 + f_3$ combination parametric resonance.

The effect of the Coriolis term in the low amplitude range could again be represented by plotting the boundary slopes against the transport speeds. Figure 97 shows this effect for q_p less than 20000 N/m. The Coriolis term also stabilised the blade subjected to a periodic tangential cutting force in the low amplitude range.

This study showed that the periodic tangential load on the blade produced various combination parametric resonances, which provided another possibility for the instability of bandsaw blades during cutting.

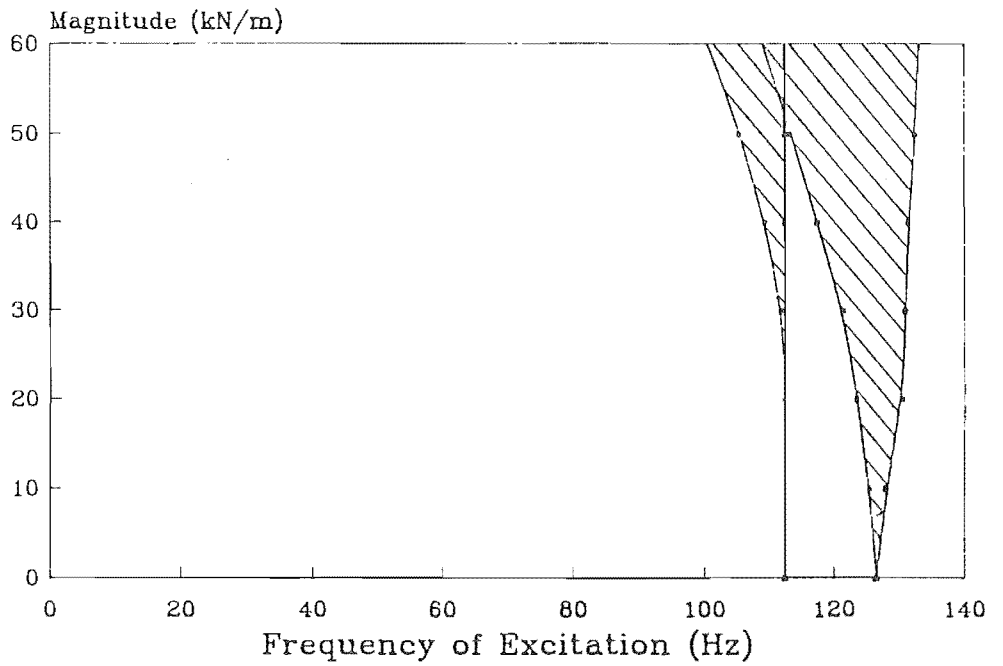

Figure 96: Instability regions for a 2×2 trial function Galerkin solution of a moving blade, subjected to periodic tangential cutting forces, with a two-term Fourier expansion.

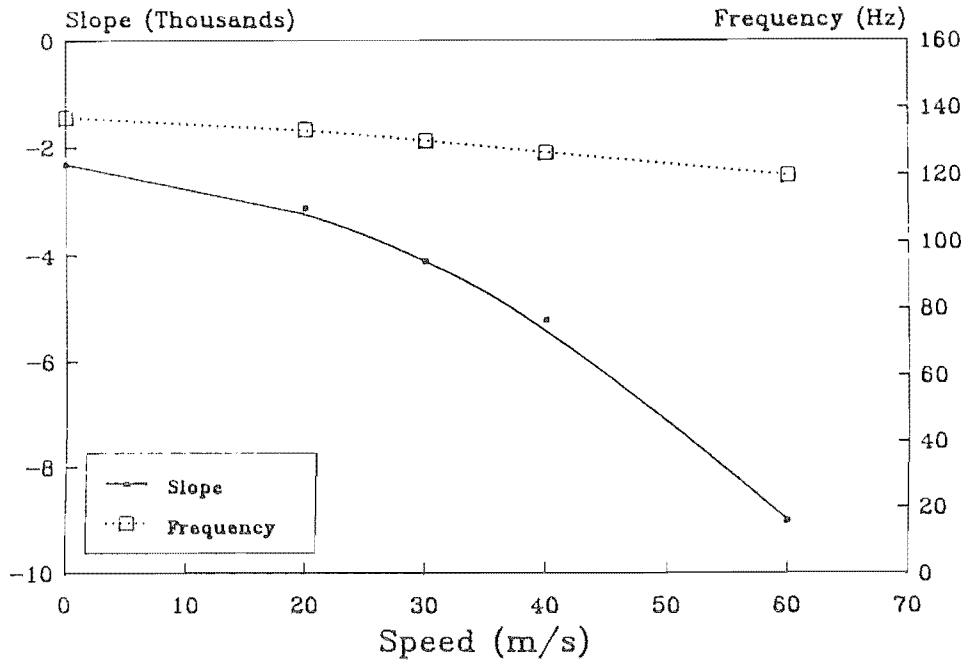

Figure 97: Inclination of the left boundary of the $f_1 + f_3$ combination parametric resonance region versus transport speeds, c.

Chapter 11

STABILITY OF BANDSAW BLADES UNDER NONCONSERVATIVE CUTTING FORCES

11.1 Nonconservative Problems

Elastic stability of nonconservative problems is yet another branch of the theory of elasticity. The foundation of this subject was developed by Bolotin, who published a book in Russian in 1961; it was translated to English in 1963 [11].

To illustrate the difference between conservative problems and nonconservative problems, the behaviour of a cantilevered beam subjected to a unidirectional longitudinal force is compared with that of a cantilevered beam subjected to a *follower* force.

A cantilevered beam, subjected to a unidirectional compression, represents the

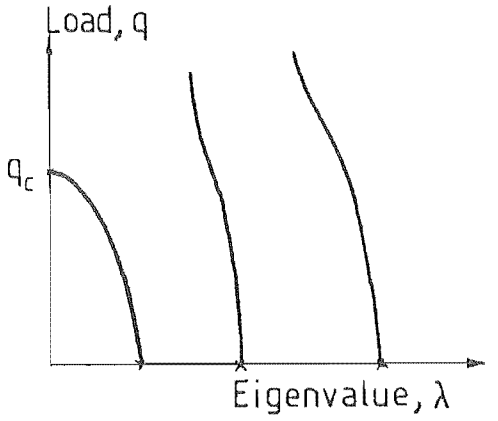

Figure 98: Load versus frequency for a beam under unidirectional force.

classic Euler buckling problem. As the magnitude of the compressive force increases, the fundamental natural frequency of the beam decreases. The load at which the natural frequency becomes zero is the buckling load. This type of buckling is referred to as the *divergent buckling* or the *static instability*, which can be presented on a plot of load versus natural frequency (Figure 98), or on a root-locus diagram, where the complex roots of the equation of motion are traced as the load increases (Figure 99). The equation of motion is usually manipulated to a matrix equation, and the complex roots are its eigenvalues. For most stability problems, the imaginary part of the eigenvalues, the natural frequencies, always come in pairs of positive and negative values.

Figure 100 shows the action of a follower force on a cantilevered beam.

As the magnitude of the follower force increases, the fundamental natural frequency increases. The Euler buckling analysis would, therefore, predict that the follower force stabilises the beam because the fundamental frequency would never be equal to zero. However, a more advanced theory of elastic stability, the *dynamic method*, would show that this system possesses a dynamic instability at a certain magnitude of follower force. The dynamic instability can also be presented on a

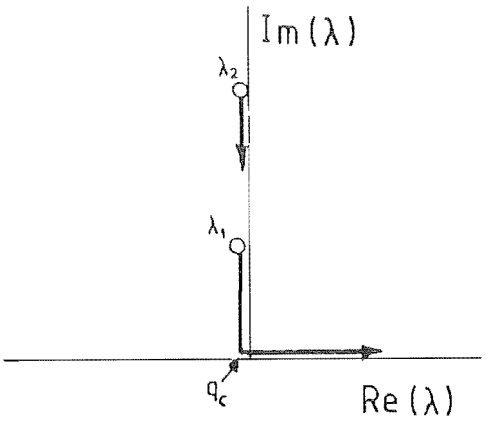

Figure 99: Root-locus diagram for a beam under unidirectional force.

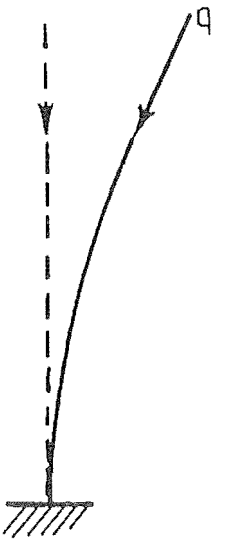

Figure 100: Follower force on a cantilevered beam.

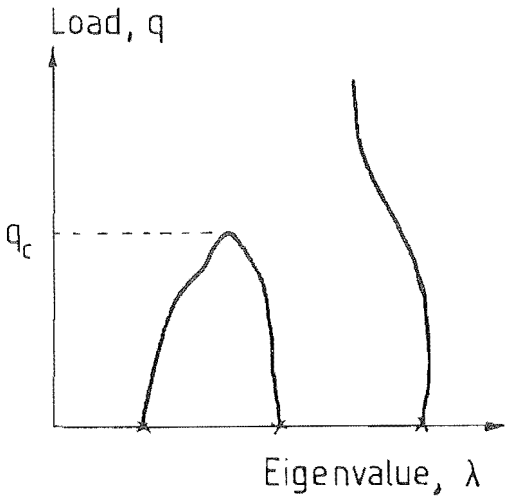

Figure 101: Load versus frequency for a beam under follower force.

plot of the amplitude of the load versus the natural frequency (Figure 101), or on a root-locus diagram (Figure 102).

As discussed in Chapter 10, a dynamic instability occurs when the real part of one or more eigenvalues become positive. On the load versus frequency plot, the dynamic buckling load is the load at which an eigencurve reaches a maximum. On the root-locus diagram, a dynamic buckling occurs when two natural frequencies approach each other on the imaginary axis, which then turn 90 degrees and move away from each other as the load increases beyond the buckling load.

The reason, as explained by Bolotin, that the Euler method cannot predict the dynamic instability of the follower force is because the Euler method is only applicable for conservative problems. The follower force problem is a nonconservative problem.

The definition of a conservative force field is [49, page 32]

> *a field in which the work done in moving a particle from point 1 to point 2 depends only on the position* r_1 *and* r_2 *and is independent of the path of integration (Figure 103).*

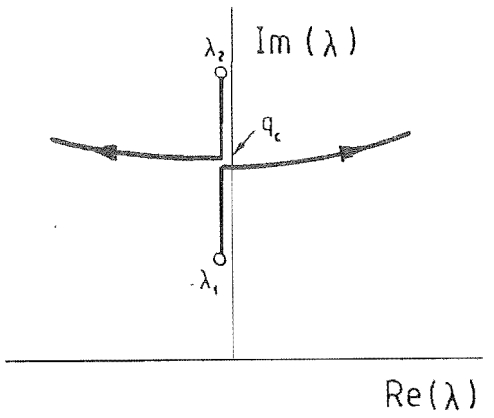

Figure 102: Root-locus diagram for a beam under follower force.

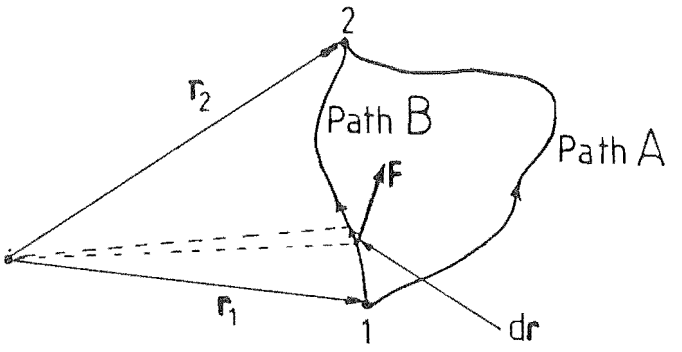

Figure 103: Conservative force field.

$$W_{12c} = \underbrace{\int_{r_1}^{r_2} \mathbf{F}\cdot d\mathbf{r}}_{\text{path A}} = \underbrace{\int_{r_1}^{r_2} \mathbf{F}\cdot d\mathbf{r}}_{\text{path B}} \tag{225}$$

The follower force problem can be shown to be nonconservative from the dependency of the work done by the force on the manner in which the beam attains its final state. Figure 104 shows three ways in which the beam can reach a state defined by a transverse deflection d and an angle of rotation ϕ of the end section. In case (a), rotation through an angle ϕ with a subsequent displacement, the work done by

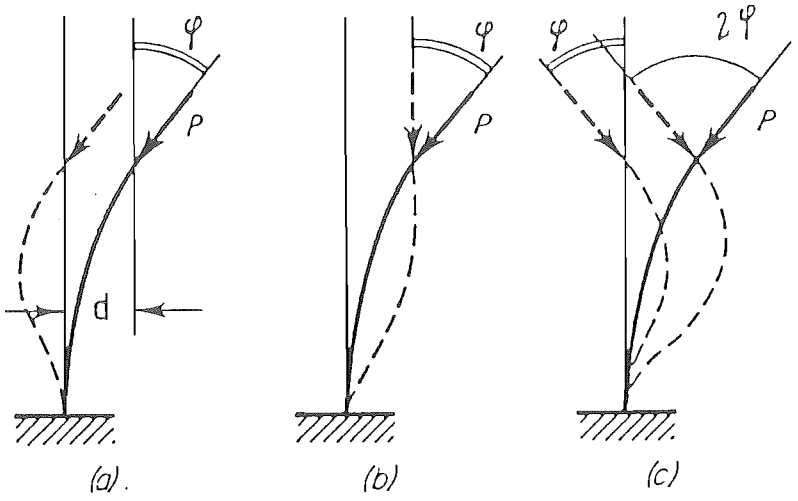

Figure 104: Three ways in which a beam attains its final state.

the force F is negative; in case (b), displacement with a subsequence rotation, the work done is zero, and in case (c), rotation through an angle $-\phi$, a displacement and a final rotation through an angle 2ϕ, the work done is positive. This is one feature inherent in all nonconservative problems.

11.2 Nonconservative Cutting Forces on Bandsaw Blades

The cutting forces on a bandsaw blade are typically small [86], and, in the past, were not considered to be the cause of instability of the bandsaw blade. Section 9.6 showed that for a typical bandsaw blade under a (unidirectional) tangential load, the static buckling load was about 40 times the cutting load under normal conditions. Chapter 10 had considered the possibility that the instability was caused by the periodic component of the tangential cutting force, however, the periodicity of the cutting force had not been established. The dynamic instability due to a nonconservative tangential cutting force was another possibility that had not been

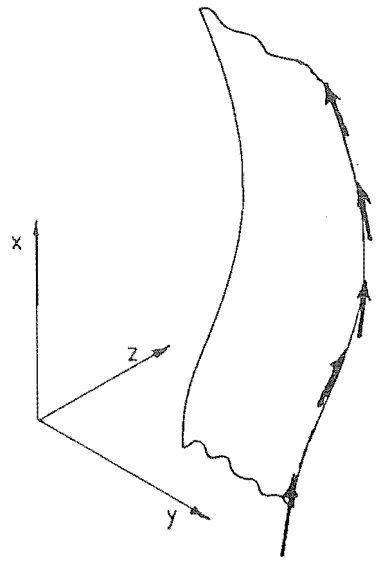

Figure 105: Follower tangential force on a saw blade.

considered previously.

The tangential cutting force on bandsaw blades can be shown to possess a non-conservative property, by looking at the characteristics of the cutting process. There are various cutting forces present in the cutting process, however, the largest force is the one which opposes the motion of the saw tooth. It is obvious that this force will always be *tangential* to the slope of the cutting edge of the blade as in Figure 105, that is, a follower tangential force[1].

Of course, if the blade is assumed to have small displacements, then the component of the follower force perpendicular to the blade is small compared with the component parallel to the equilibrium configuration of the blade. This is the assumption in the study of blades under tangential edge loads in Section 9.6. This chapter excludes this assumption to see if the follower tangential cutting force can alter the vibrational characteristics of the blade.

[1]The term *tangential force* refers to the in-plane force parallel to a longitudinal edge of the *equilibrium configuration* of the blade, whereas, the term *follower tangential force* refers to the in-plane force tangential to a longitudinal edge of the *vibrational configuration* of the blade.

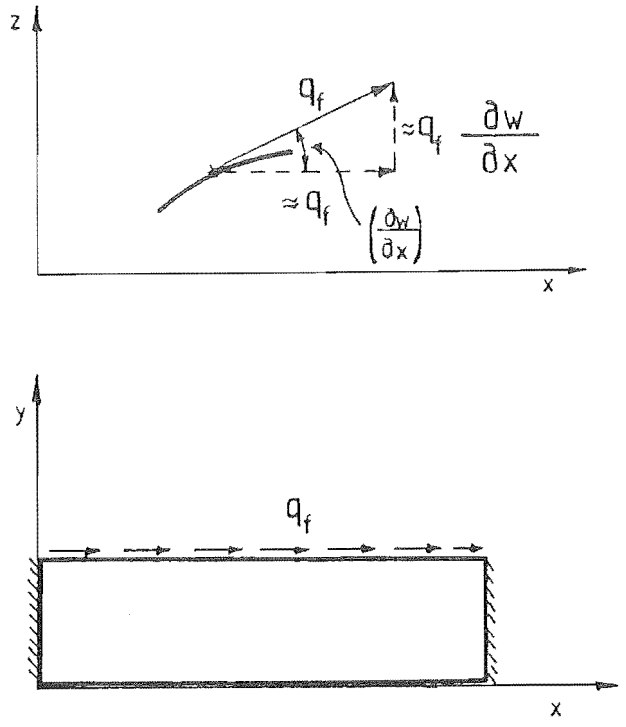

Figure 106: Components of the follower force.

11.3 Formulation of Nonconservative Problems

The Hamilton's principle, described in Chapter 7 (Equation (53)), can be used to formulate nonconservative problems, through the inclusion of the nonconservative work done term.

The kinetic energy and the potential energy due to bending and due to in-plane stresses are the same as those given in the previous chapters. The nonconservative work done can be found by considering the tangential cutting force. For simplicity, assume that the force is uniform along the cutting edge of the blade, with a magnitude of q_f force per unit length. The two components of this follower tangential load are q_f in the x direction (parallel to the plane of the plate) and $q_f \frac{\partial w(x,b)}{\partial x}$ perpendicular to the plane of plate, where $\frac{\partial w(x,b)}{\partial x}$ is the slope of the plate on the cutting edge $y = b$.

The component of the force parallel to the x-axis is conservative and has been included in the in-plane stresses in Section 9.6. The contribution of the nonconservativeness to the system is from the nonconservative work done by the perpendicular component of this force. The variation of the nonconservative work done is given by

$$\delta W_{nc} = \int_0^l q_f \frac{\partial w}{\partial x} \delta w \Big|_{y=b} dx \tag{226}$$

$$= \int_0^b \int_0^l q_f \frac{\partial w}{\partial x} \bar{\delta}(y-b)\, \delta w \, dx \, dy \tag{227}$$

where $\bar{\delta}(y-b)$ is a dirac delta function, which is equal to zero, except when $y = b$.

This work done can be added into in the Hamilton's equation together with the other energy terms (Section 9.6). The equation of motion is then given as

$$D\nabla^4 w + \rho h \left(\frac{\partial^2 w}{\partial t^2} + 2c\frac{\partial^2 w}{\partial x \partial t} + c^2 \frac{\partial^2 w}{\partial x^2} \right) =$$
$$\frac{\partial}{\partial x}\left(N_x \frac{\partial w}{\partial x} \right) + \frac{\partial}{\partial x}\left(N_{xy} \frac{\partial w}{\partial y} \right) + \frac{\partial}{\partial y}\left(N_{xy} \frac{\partial w}{\partial x} \right) + q_f \frac{\partial w}{\partial x} \bar{\delta}(y-b) \tag{228}$$

where

$$N_x = q_0 \left(d + e\frac{y}{b} \right) - q_f \frac{l}{b}\frac{y}{b}\left(2\frac{x}{l} - 1 \right) + \eta \rho h c^2$$
$$N_{xy} = q_f \left(\frac{y}{b} \right)^2$$

the boundary conditions are the same as for the conservative case (Equation (161)).

11.4 Method of Analysis

The method of analysis is the same as that for the conservative problems. Essentially, the presence of a nonconservative force produces a non-self-adjoint boundary value problem. A direct analysis of the non-self-adjoint problem is extremely difficult, and an approximation method must be used in obtaining the solution. The most effective approximation method for this case is the Galerkin method [11, page 58], even

though the convergence of this method when applied to non-self-adjoint problems has not been conclusively proven. However, it has been confirmed by experiments and exact calculations that the form of loss of stability in the nonconservative cases, can be successfully approximated by the first few modes of the natural oscillations. The convergence of the Galerkin method can also be tested by a gradual increase in the number of modes used in approximating the problem, and examining their effects on the solution. If an increase in the number of modes does not alter the solution by much, then it is likely that the solution has converged.

Abrahamsson and Sällström (1989) [1] applied a two-sided Ostrowski matrix iteration to the eigenproblems of nonconservative continuous systems. For continuous beam systems, this method uses the exact solutions obtained from the dynamic stiffness method, (Chapter 4) to solve the nonconservative cases, instead of using predefined shape functions. However, this method does not offer any advantages to the continuous plate problems because the exact solutions are difficult to obtain.

Leipholz and Pfendt (1982,1983) [43,44] studied the stability of rectangular plates subjected to uniformly distributed follower forces, using the Galerkin method. These studies closely resembled the bandsaw blade problem, and their method of analysis was similar to the method used previously in this thesis. In fact, there was no special technique required for the nonconservative problem, as long as there was an eigen-solver which could handle non-self-adjoint problems; the PC-MATLAB eigen-solver could.

More recently, Higuchi and Dowell (1989) [32] presented a study of a completely free plate subjected to a nonconservative follower force, using the Rayleigh-Ritz method. Even though, the method of discretisation differed from that in Leipholz and Pfendt work, the treatment of the nonconservative element of the problem was the same. These papers showed the same phenomena of dynamic instabilities as

those discussed by Bolotin. In the plate problem, these instabilities are sometimes referred to as *flutters.*

Experimental verifications of these dynamic instabilities would be valuable. Unfortunately, they have not been cited in the literature, perhaps, because the non-conservative forces are difficult to simulate.

The first step in the analysis is to discretise the partial differential equation of motion and the boundary conditions of the plate, to a set of second order ordinary differential equations by using the Galerkin method

$$[M]\left\{\ddot{T}\right\} + [G]\left\{\dot{T}\right\} + [K]\{T\} = \{0\} \tag{229}$$

where the elements of the matrices are given by

$$M_{rsmn} = \int_0^b \int_0^l \rho h \psi_{rs} \psi_{mn}\, dx\, dy \tag{230}$$

$$G_{rsmn} = \int_0^b \int_0^l 2\rho h c \psi_{rs} \frac{\partial \psi_{mn}}{\partial x}\, dx\, dy \tag{231}$$

$$\begin{aligned} K_{rsmn} = \int_0^b \int_0^l \Bigg\{ & D\nabla^2\psi_{rs}\nabla^2\psi_{mn} + q_0\left(d + e\frac{y}{b}\right)\frac{\partial \psi_{rs}}{\partial x}\frac{\partial \psi_{mn}}{\partial x} \\ & + q_f\left[\left(\frac{y}{b}\right)^2\left(\frac{\partial \psi_{rs}}{\partial y}\frac{\partial \psi_{mn}}{\partial x} + \frac{\partial \psi_{rs}}{\partial x}\frac{\partial \psi_{mn}}{\partial y}\right) - \frac{l}{b}\frac{y}{b}\left(2\frac{x}{l} - 1\right)\frac{\partial \psi_{rs}}{\partial x}\frac{\partial \psi_{mn}}{\partial x}\right] \\ & - (1-\eta)\rho h c^2 \frac{\partial \psi_{rs}}{\partial x}\frac{\partial \psi_{mn}}{\partial x}\Bigg\}\, dx\, dy \\ & - (1-\nu)\int_0^l \left\{\left(\psi_{rs}\frac{\partial^3 \psi_{mn}}{\partial x^2 \partial y} + \frac{\partial \psi_{rs}}{\partial y}\frac{\partial^2 \psi_{mn}}{\partial x^2}\right)\Bigg|_{y=0}^{b} - q_f \psi_{rs}\frac{\partial \psi_{mn}}{\partial x}\Bigg|_{y=b}\right\} dx \end{aligned} \tag{232}$$

The solution is of the form

$$\{T\} = \{X\}\, e^{\lambda t} \tag{233}$$

Substitution of this equation into Equation (229) will lead to a quadratic eigenvalue problem, which can again be solved by using the method described in Section 8.3.2. The eigenvalues (λ's) can be plotted against the magnitude of the force q_f. Instabilities occur at the turning points (maxima) of the eigen curves.

Table 21: First four frequencies (Hz) of a stationary blade subjected to a follower tangential load.

q_f	3×3 Functions	4×4 Functions	5×5 Functions
0	$44.8i$	$44.8i$	$44.7i$
	$53.2i$	$53.1i$	$53.1i$
	$91.8i$	$91.8i$	$91.8i$
	$108.4i$	$107.9i$	$107.9i$
30000	$42.7i$	$42.8i$	$42.8i$
	$62.4i$	$65.0i$	$65.3i$
	$82.2i$	$79.1i$	$79.1i$
	$111.4i$	$113.8i$	$117.7i$

11.5 Results and Discussion

The numerical results in this section have been calculated for a blade with the same dimensions and tension as that of Section 9.6 and Chapter 10.

11.5.1 Stationary Blades

Table 21 lists the first four natural frequencies of the blade at various magnitudes of follower tangential edge load q_f. The results were calculated with a 3×3, 4×4, and 5×5 trial functions in the Galerkin discretisation, which showed that the 3×3 function approximation could produce accurately the first four eigenvalues for $q_f \leq 20000$ N/m , while the results calculated with a 4×4 function approximation were practically the same as those calculated with a 5×5 function solution. Although, these results were not proof of convergence for the Galerkin method in nonconservative problems, they suggested that, for this application, the Galerkin method appeared to converge to a unique set of solutions as the number of trial functions increased.

Figure 107 shows the eigencurves for the 4×4 function calculations.

The nonconservative nature of the tangential load stabilised the first mode of

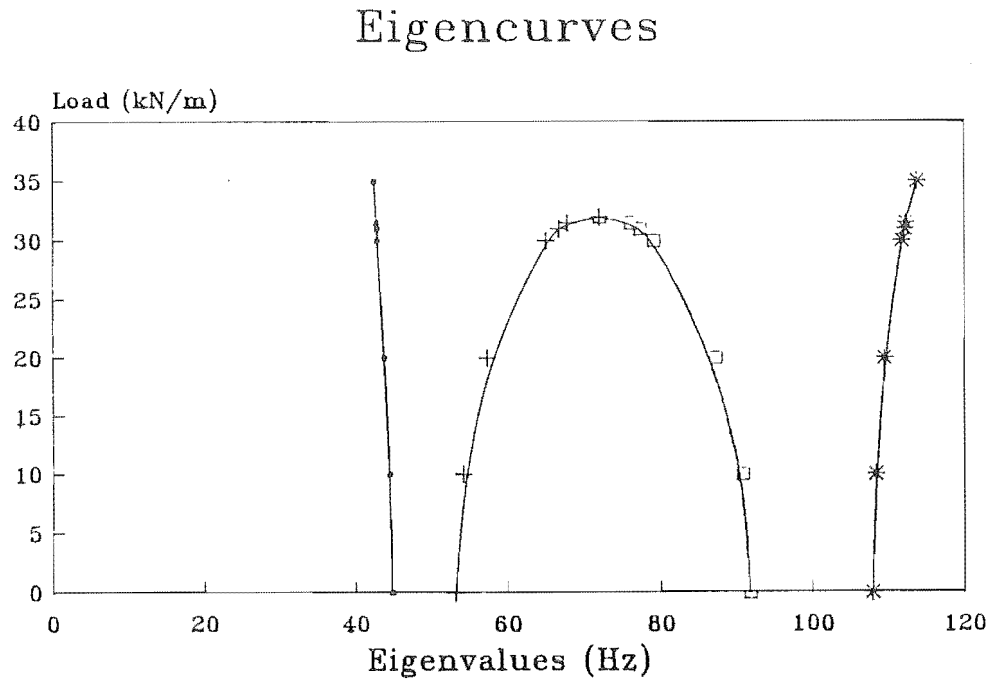

Figure 107: Eigencurves for a stationary blade subjected to a follower tangential edge load.

vibration, because at 30000 N/m tangential load, the first frequency for the conservative case was 30.4 Hz (Table 19), whereas for the nonconservative case, it was 42.8 Hz.

The interesting dynamic instability, discussed by Bolotin et.al., occurred when the second (first torsional) natural frequency approached the third (second transverse) natural frequency as q_f increased to approximately 32000 N/m. Even though, this flutter load was very high compared with the usual cutting load, and was of the same order of magnitude as the conservative buckling load ($\approx$40000 N/m), the form of loss of stability was very different from that found in the conservative case. This type of instability on the bandsaw blade due to a tangential cutting force has not been discussed previously, therefore, experimental studies are required to verify the theoretical results presented in this chapter. However, these results were as expected for the nonconservative case.

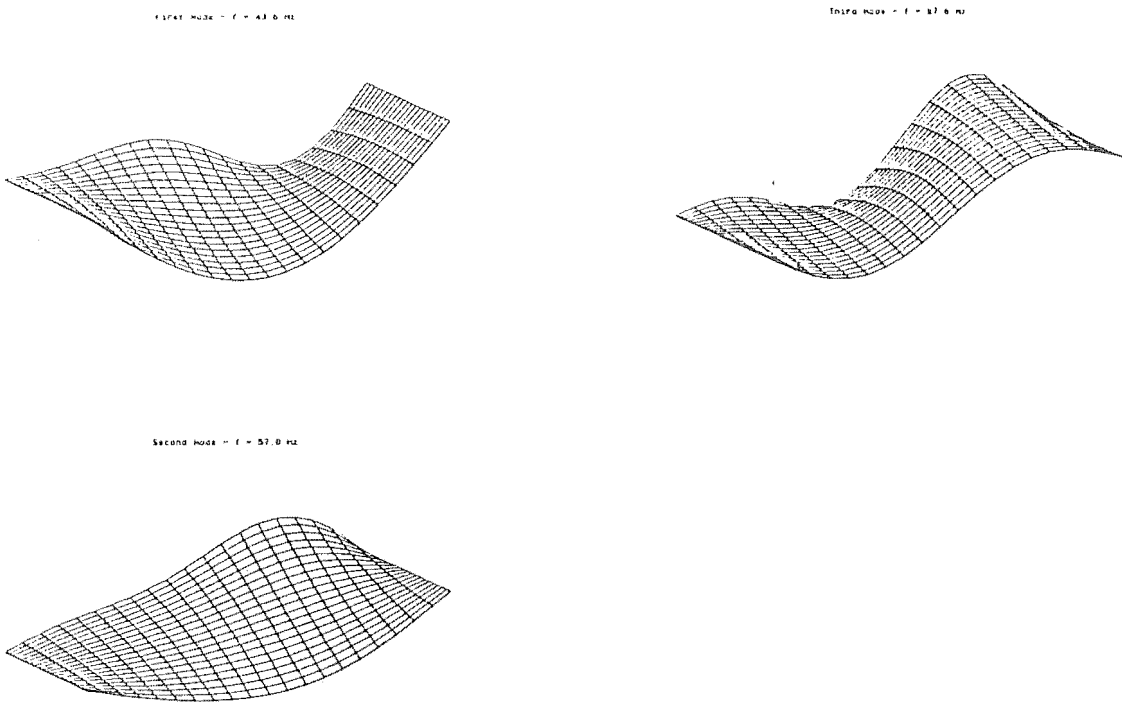

Figure 108: First three modes of a blade subjected to 20000 N/m follower tangential load, with a 3×3 trial function Galerkin solution.

The first three mode shapes of the blade, subjected to 20000 N/m follower tangential load, are in Figure 108, which illustrates the effect of a follower tangential load on the blade. Figure 109 shows the first mode and the unstable mode of the blade at 36200 N/m load. The unstable mode was the combination of the first torsional mode and the second transverse mode.

11.5.2 Moving Blades

Table 22 shows the first four eigenvalues[2] of a blade subjected to three different follower tangential loads q_f, for various transport speeds c.

[2]The eigenvalues have been divided by 2π so that the imaginary parts represent the natural frequencies in Hz, therefore, the actual damping factors are 2π times the real part of the listed numerical values.

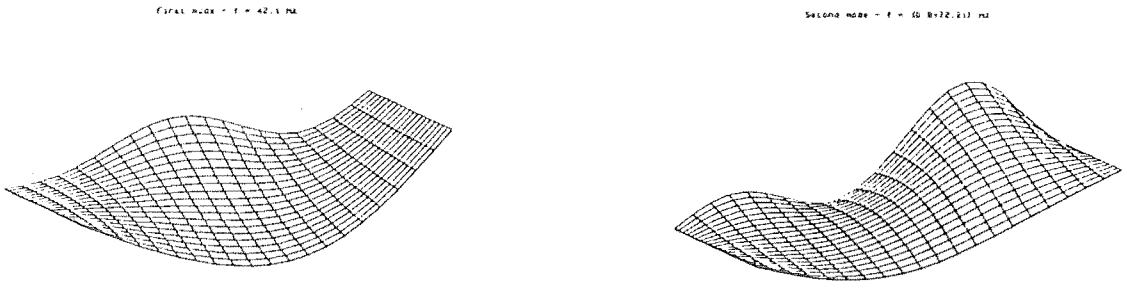

Figure 109: The first mode and the unstable mode of a blade subjected to 36200 N/m follower tangential load, with a 3×3 trial function Galerkin solution.

Table 22: First four eigenvalues of a blade subjected to three different follower tangential loads q_f, at various transport speed c, with 4×4 trial function Galerkin solutions.

c (m/s)	q_f =0 N/m	q_f =20000 N/m	q_f =35000 N/m
0.	$0.0 + 44.8i$	$0.0 + 43.7i$	$0.0 + 42.4i$
	$0.0 + 53.1i$	$0.0 + 57.3i$	$-8.0 + 71.9i$
	$0.0 + 91.8i$	$0.0 + 87.3i$	$+8.0 + 71.9i$
	$0.0 + 107.9i$	$0.0 + 109.5i$	$0.0 + 113.8i$
-20.	$0.0 + 43.2i$	$-2.0 + 42.5i$	$-3.5 + 41.7i$
	$0.0 + 51.9i$	$-4.5 + 54.8i$	$-14.0 + 61.5i$
	$0.0 + 89.5i$	$-1.6 + 85.7i$	$+2.0 + 76.9i$
	$0.0 + 105.7i$	$-2.4 + 107.1i$	$-3.8 + 110.5i$
-40.	$0.0 + 39.5i$	$-3.2 + 39.5i$	$-5.4 + 39.8i$
	$0.0 + 48.3i$	$-7.5 + 49.1i$	$-17.9 + 49.8i$
	$0.0 + 83.4i$	$-2.8 + 80.9i$	$-2.5 + 75.6i$
	$0.0 + 99.7i$	$-4.5 + 100.0i$	$-6.6 + 101.3i$
-70.	$0.0 + 32.7i$	$-3.6 + 33.6i$	$-5.1 + 34.7i$
	$0.0 + 41.5i$	$-9.5 + 39.8i$	$-20.6 + 35.7i$
	$0.0 + 71.9i$	$-3.3 + 71.1i$	$-5.0 + 68.9i$
	$0.0 + 87.8i$	$-5.7 + 87.1i$	$-8.3 + 86.7i$

These results show a very interesting phenomenon, which is the presence of damping in the natural frequencies of the moving blade subjected to follower tangential loads. If the transport speed c is positive, that is, the blade travels in the same direction as the tangential load, then the real part of the eigenvalues are positive, fortunately, this case is not possible in practice.

The dynamically unstable mode, found in the stationary blade analysis, also occurred in this moving blade case, but at a higher q_f, because of the damping. The behaviour of the eigenvalues with a gradual increase in q_f can be best represented on a root-locus diagram. Figure 110 shows the root-locus diagram of a blade with c =40 m/s, and a 4×4 function Galerkin solution. The third eigenvalue was the one responsible for the dynamic instability of the moving blade, while the second eigenvalue was stabilised by the follower tangential force (large damping factor).

Because the nature of the cutting forces had not been well established, no specific conclusion could be made about the stability of bandsaw blades during cutting. However, this chapter illustrated a mechanism for the dynamic instability of the blade due to a follower tangential cutting force. Because these results are presented for the first time, their validity is questionable, however, they appeared to agree with all the work published in the field of nonconservative problems, and they also make physical sense.

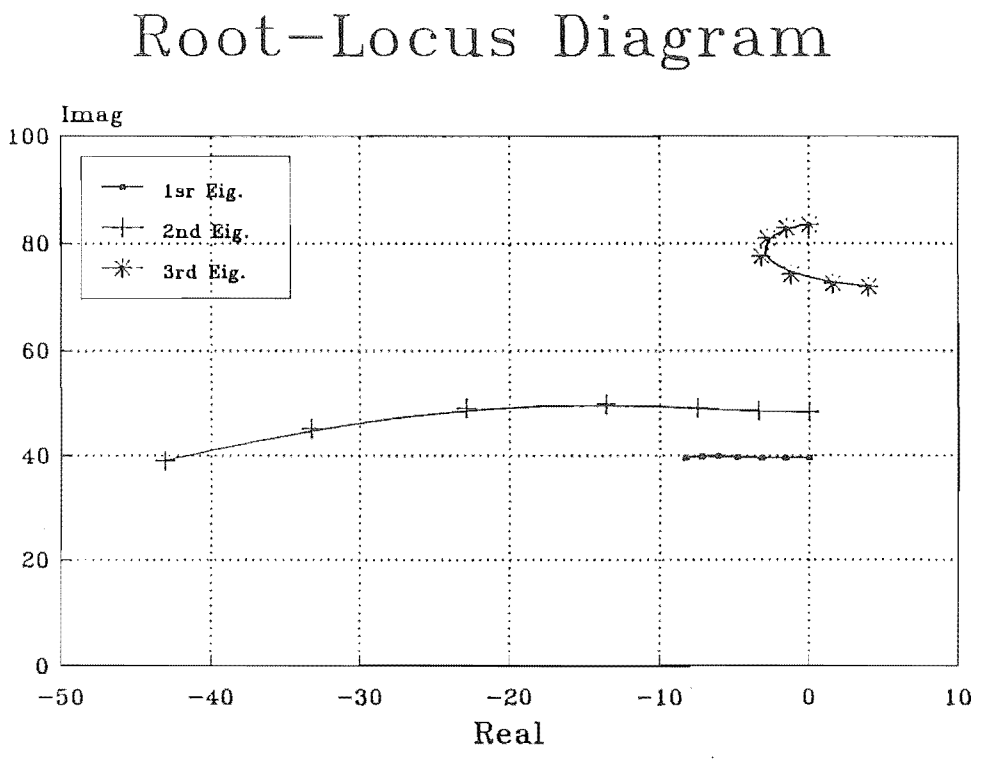

Figure 110: Root-locus diagram for the the first three eigenvalues of a blade, at c =40 m/s.

Chapter 12

CONCLUSION

12.1 Summary

The work presented in this thesis can be summarised as follows:

12.1.1 Analysis of Structural Vibrations

The *dynamic stiffness method* was used in developing a computer program to solve general three dimensional structure problems, consisting of thin beams, thick beams, concentrated masses, gyroscopic rotors, springs, and viscous dampers.

A unique feature of this program was the inclusion of gyroscopic rotors, and viscous dampers. This feature involved the use of complex arithmetic, and the search for complex natural frequencies. The Muller's method was successfully employed in the search for the real and complex natural frequencies of the systems under investigation. In general, the Muller's method should have converged to a root closest to the starting values, unfortunately, it was not always the case.

The modeshape of the system at a given frequency could be plotted by the computer program, which had provided a useful tool for visualising the vibrational

characteristics of the system.

This program had been used to study the Waimak bandsaw structural vibrations.

12.1.2 Structural Vibration of the Waimak Bandsaw

Experimental and theoretical analysis of the Waimak bandsaw revealed the following vibrational characteristics:

- The structure of the bandsaw below the base contributed two low natural frequencies of vibration at 30 Hz and 36 Hz. The dynamics of the shaft were the major contribution to these two frequencies. If it were necessary to shift these frequencies, an alteration to the shaft dimensions would be required. It was not, however, a practical consideration for the existing bandsaws, but on a new bandsaw design, this information may be of use.

- The structure above the base contributed two low natural frequencies at 9 Hz and 21 Hz. The major contribution to the 9 Hz was a torsional mode of the main column, and to the 21 Hz it was to-and-fro transverse vibration of the main column. Because the rotating speed of the pulley was about 8 Hz, the 9 Hz torsional natural frequency was undesirable, and therefore, it should be increased by adding extra stiffeners to the web of the main column. This alteration could be easily accomplished on the existing bandsaws. The 20 Hz frequency could also be increased by bracing the main column to the foundation in the direction of the vibration. It was noted that the Waimak bandsaw had previously been braced to the foundation, however, the brace was positioned near the central axis of the torsional mode, hence it had a minimal effect on the 9 Hz vibration.

- The top pulley oscillated vertically at 3.8 Hz natural frequency, due to the flexibility of the straining device. A large amplitude of oscillation corresponding to this 3.8 Hz frequency had been observed during starting-up, and during cutting, which would cause large tension fluctuations on the bandsaw blade. An increase in the frequency of oscillation would result in a decrease in the amplitude, and this could be accomplished by reducing the leverage ratio of the counterweight lever arm. However, an investigation would be necessary to optimise the leverage ratio of the counterweight arm.

- The gyroscopic effects of the rotating pulleys did not affect the structural natural frequencies at the present bandsaw operating speed.

- Under idling conditions, the bandsaw structure vibrated at 8 Hz and its harmonics. Mechanical looseness offered the best explanation for the presence of those harmonics.

12.1.3 Boundary Conditions of Moving Bandsaw Blades

This thesis has shown that it was possible to solve the moving beam problem by using the dynamic stiffness method. The explicit form of the dynamic stiffness matrix was difficult to obtain, however, a numerical scheme has been successfully applied to the formulation of the moving beam dynamic stiffness matrix.

This method had been used to investigate three cases: the differences between simply-supported and clamped-clamped end conditions, the coupling effects of intermediate supports, and the forced lateral vibrations of moving beams.

For a typical bandsaw blade configuration, the natural frequencies of the simply-supported end conditions were lower than those of the clamped-clamped end conditions, up to 14% difference was found for the fundamental frequency of a blade

0.3 m in length. As the axial speed of the moving beam increased the difference in the natural frequency decreased. Comparisons between the calculated results and the experimental results showed that simply-supported conditions provided a better representation of the bandsaw blade end conditions than the clamped-clamped conditions.

For an untensioned three-span bandsaw blade, the coupling effects between the spans were quite significant. For a saw blade under a typical level of tension, coupling was small and the natural frequencies of each span could be calculated individually. The coupling effects increased the single span natural frequencies only slightly. As the axial speed of the beam increased, the coupling effects decreased.

Although, the '*mode shapes*' of a moving beam were dependent on the direction of axial motion of the beam, the resonance frequencies were not. A large amplitude of transverse vibration would occur when the frequency of the transverse excitation was close to the natural frequency of the moving beam, regardless the position of the excitation.

12.1.4 Analysis of Plate

A procedure for solving plate problems, based on the Galerkin approximation, has been developed in this thesis. Firstly, Hamilton's principle was used to obtain the equation of motion and all the boundary conditions of a plate problem. Then, the equation of motion and the boundary conditions were discretised into a set of second order differential equations, or in the case of linear vibration, a set of algebraic equations. Gaussian quadrature rule was used to perform the integration required in the discretisation step, hence reducing most of the unnecessary hand-calculations. The program PC-MATLAB was then used in the final step of finding the eigenvalues and the eigenvectors of the governing equation.

This procedure has been extended to cover a wide range of applications, from simple vibration problems to dynamic instability problems. The moving plate case has also been solved by using this Galerkin approximation procedure.

12.1.5 Stresses in Bandsaw Blade

In-plane stresses are very important in bandsaw blades, because they can alter the saw blade performance considerably. This thesis considered the vibration of saw blades subjected to: a uniform stress, a linear stress due to backcrowning and wheeltilting, a parabolic stress due to prestressing, and stresses induced by uniform tangential cutting forces.

For the uniform tension, the plate solutions were close to the solutions of a beam under longitudinal tension. An advantage of the plate solutions over the beam solutions was that it combined both the transverse and the torsional mode of vibration, hence it would take care of coupling effects automatically. The solutions for a moving plate under uniform tension were also close to those for a moving beam.

This thesis had shown that the effects of the wheel-tilting can be represented by a linear stress distribution. Wheel-tilting results in a decrease of the first transverse frequency and an increase of the first torsional frequency. A small amount of wheel-tilting would improve the performance of the blade, however, too much tilt would destabilise the blade because of the low first transverse frequency.

The backcrowning process appeared to set up a linear residual stress distribution across the width of the blade, and its effects were, therefore, similar to those obtained from the wheel-tilting operation. An approximate equation had been used to calculate the magnitude of the residual stress induced from back-crowning. It showed good agreement with the experimental results, however, more work is needed to test the validity of this approximate solution for a wider range of backcrowning.

The main objective of prestressing was to set up a parabolic residual stress across the width of the blade. The light-gap measurement technique had been used to measure the amount of prestress, however, Foschi had concluded that this method was unreliable. This thesis investigated the effects of parabolic residual stress on bandsaw blade as an approximation to the prestressing process. The effects found were an increase in the first torsional frequency and a slight decrease in the first transverse frequency, which agreed with the experimental results. Strictly speaking, the parabolic residual stress in the longitudinal direction alone was not adequate, because it would induce additional stresses in other directions. However, these stresses were very difficult to incorporate into the polynomial stress functions considered in this thesis, they were, therefore omitted, but should be included in a more complete study of stresses occurring in bandsaw blade.

A uniform tangential force along one edge was used to consider the effects of the main cutting force on a bandsaw blade. The buckling force was found to be approximately forty times larger than the typical cutting force. For a moving blade the buckling force decreased, but the decrease was insignificant compared to its magnitude. Because the magnitude of the main cutting force at the onset of instability has not been measured, it was impossible to draw any conclusions about the type of instability occurring in the bandsaw blade. However, the results in this thesis suggested that the divergent buckling due to tangential cutting force seemed unlikely to occur in practice.

12.1.6 Parametric Excitations on Bandsaw Blades

In this thesis, the harmonic balance method has been applied to the parametric excitations of a bandsaw blade. Two cases of parametric excitation have been examined: the periodic fluctuations in tension, and the periodic tangential cutting force.

For the periodic fluctuations in tension, no combination parametric resonance was possible. The major regions of dynamic instability were the $2f_n$ simple parametric resonance regions, which had been predicted from the beam model. For a moving blade, a Coriolis term, and a centripetal term were added to the equation of motion for a stationary blade. However, the centripetal term was eliminated because the straining device was a counterweight mechanism, therefore, only the Coriolis term was included. The Coriolis term stabilised the parametric resonances of the blade by reducing the width of the instability regions. At large amplitudes of excitation, other regions of instability were present, which increased the areas of instability. These additional instability regions had not been presented previously, perhaps, because the methods of investigation had been for small amplitudes of excitation only. The harmonic balance method allowed large amplitudes of excitation to be investigated.

The periodic tangential cutting force on the blade produced interesting combination parametric resonances, while the simple parametric resonances became insignificant. The important parametric resonances were the combination first transverse-second torsional, first transverse-second transverse, first torsional-second torsional, and first torsional-second transverse parametric resonance. For a typical bandsaw blade configuration, these regions of dynamic instability were close to each other, and therefore, at a certain magnitude of excitation, they merged together to produce a large region of instability. Conclusions similar to those for the stationary blade have been drawn for the moving blade case.

12.1.7 Nonconservative Cutting Forces on Bandsaw Blades

The tangential cutting force had been shown to possess a nonconservative property. The theoretical investigation into the nonconservative problems has revealed another

interesting type of dynamic instability. As the magnitude of the tangential load increased, the first transverse natural frequency decreased slightly, the first torsional frequency increased, and the second transverse frequency decreased. When the first torsional frequency approached the second transverse frequency, they became dynamically unstable, because one of the eigenvalues contained a positive real part. The magnitude of the buckling load in this case was less than that in the conservative problem, however, it was still very high compared with a typical cutting load.

For the moving blade case, damping was produced by the nonconservative load, because all the eigenvalues possessed negative real parts. The magnitude of the buckling load was, therefore, increased as the transport speed of the blade increased, and the frequency which was responsible for the instability was the second transverse frequency.

12.2 Future Work

The work presented in this thesis has covered a wide range of disciplines in the bandsaw vibration field. Therefore, it is necessary, in the future, to direct efforts to more specific areas of interest, so that greater confidence can be associated with the results of the present analyses.

The following suggestions are arranged in the order of their importance.

12.2.1 Mechanism of Cutting Wood

The mechanism of cutting wood is believed to be the most important topic in wood machining at present. It will provide useful information for studying the behaviour of the present saw blades as well as for developing new methods of cutting wood.

An experimental study would be best carried out in a laboratory environment.

A testing machine should consider the following items:

- Isolation of one tooth cutting action.
- Variety of tooth profiles.
- High speed photography.
- Accurate measurements of various cutting forces.
- Precise adjustment of the cutting speed, and the depth of cut.

A theoretical consideration can, perhaps, follow by modelling the cutting action, or the energies transferred during the cutting process.

12.2.2 In-Plane Stress Measurement Techniques

As indicated in this thesis, the present methods of measuring residual stresses in a bandsaw blade are not reliable, a better non-destructive technique would, therefore, be very valuable. It would assist the Saw Doctors in optimizing the performance of the saw blade, as well as the researchers in finding better ways of improving the blade.

This development, perhaps, will not be perfected in the near future. In the mean time, experimental investigation on the accuracy of the present techniques would be quite feasible. For example, the measurements of prestress using the light-gap technique could be compared with the direct measurements from using strain gauges.

12.2.3 Parameters Relating to the Instability of Saw Blades during Cutting

The instability of bandsaw blades during cutting is the most critical factor in limiting the rate of production, it is, therefore, necessary to investigate the cause of this instability. The mechanism of cutting wood and the measurement of cutting forces should be the prerequisite for this instability investigation. The theoretical method presented in this thesis should be adequate for the verification of the experimental results.

12.2.4 Straining Devices

In-plane stresses play a major part in the stability of bandsaw blades, of which, the static tension provides the highest stress level. The straining device is, therefore, a very important part of the bandsaw. Modern bandsaws have used air or hydraulic straining mechanisms, instead of the counterweight mechanism. However, the advantages of these modern straining devices have not been discussed, and from the theoretical point of view, they are less favourable than the previous counterweight mechanism (due to the presence of the centripetal term in the equation of motion).

Perhaps, an active control of bandsaw vibrations can be achieved through the straining device.

Acknowledgements

I would like to thank *Professor H. McCallion*, my supervisor and the Head of the Mechanical Engineering Department, for his assistance and guidance throughout this research. I am also grateful to *Dr. R.J. Astley* and *Mr. B. Donohue* for their interest and assistance.

Acknowledgement is also due to: *Mr. G. McGill*, for proof-reading this thesis and for making many valuable constructive criticisms; *Mr. M. Minard*, for assisting with the experimental work; *Mr. P. Smith*, for helping with the computer facility; and to all my postgraduate colleages, in particular *Dr. M. Aitken*, for discussing and giving helpful advice on this research.

Appreciation is extended to: the *University Grants Committee*, for their financial assistance; the *Southern Industrial Development Division*, for the use of their equipment; the *Waimakariri Sawmill*, for allowing access to their bandsaw; and the *Southern Cross Engineering Company*, for providing invaluable information on the design of their bandsaws.

I also wish to thank all my family, whose encouragement was very much appreciated. Last, but not least, I am indebted to my fiancée, *Thu Hong*, for her continued patience and encouragement throughout this research.

References

[1] T.J.S.Abrahamsson and J.H.Sällström 1989 *International Journal for Numerical Methods in Engineering* **28**, 1827-1837. Eigensolutions of non-conservative continuous mechanical systems computed by use of a matrix iteration method.

[2] D.Afolabi 1987 *Computers and Structures* **26**, 1039-1040. Linearisation of the quadratic eigenvalue problem.

[3] F.E.Allen 1985 *Proceedings of the Eigth International Wood Machining Seminar, Forest Products Laboratory, University of California*, 384-404. High-strain theory and application.

[4] F.E.Allen 1973 *Australian Forest Industries Journal* **39**, 30-35. Quality control in the timber industry.

[5] D.W.Alspaugh 1967 *Journal of the Franklin Institute* **283**, 328-338. Torsional vibration of a moving band.

[6] D.L.Anderson 1974 *Natural Frequency of Lateral Vibrations of a Multiple Span Moving Band Saw.* Vancouver: Western Forest Products Laboratory.

[7] S.T.Ariaratnam and S.F.Asokanthan 1988 *Journal of Vibration, Acoustics, Stress, and Reliability in Design, Transactions of the ASME* **110**, 350-355. Torsional oscillations in moving bands.

[8] S.F.Bassily and S.M.Dickinson 1975 *Journal of Applied Mechanics, Transactions of the ASME* **42**, 858-863. On the use of beam functions involving free edges.

[9] R.B.Bhat 1985 *Journal of Sound and Vibration* **102**, 493-499. Natural frequencies of rectangular plates using characteristic orthogonal polynomials in Rayleigh-Ritz method.

[10] R.E.D.Bishop and D.C.Johnson 1960 *The Mechanics of Vibration.* Cambridge: Cambridge University Press.

[11] V.V.Bolotin 1963 *Nonconservative Problems of the Theory of Elastic Stability.* Oxford: Pergamon Press.

[12] V.V.Bolotin 1964 *The Dynamic Stability of Elastic Systems.* San Francisco: Holden-Day.

[13] R.L.Burden,J.D.Faires and A.C.Reynolds 1981 *Numerical Analysis.* Boston: Prindle, Weber & Schmidt.

[14] R.D.Cook 1981 *Concepts and Applications of Finite Element Analysis.* New York: John Wiley & Sons, Inc.

[15] G.R.Cowper 1966 *Journal of Applied Mechanics, Transactions of the ASME* **33**, 335-340. The Shear Coefficient in Timoshenko's Beam Theory.

[16] C.D'Angelo III,N.T.Alvarado,K.W.Wang and C.D.Mote,Jr. 1985 *Shock and Vibration Digest* **17**, 11-23. Current research on circular saw and band saw stability.

[17] A.K.Das 1982 *Proceedings of the Seventh International Wood Machining Seminar, Forest Product Labratory, University of California*, 175-182. Analysis of

dynamic stability of bandsaw systems.

[18] S.G.J. de Cock 1987 *Transactions of the Institution of Professional Engineers New Zealand* **14**, 152-162. The role of experimental vibration analysis in product development and machine diagnostics.

[19] S.M.Dickinson and A.D.Blasio 1986 *Journal of Sound and Vibration* **108**, 51-62. On the use of orthogonal polynomials in the Rayleigh-Ritz method for the study of the flexural vibration and buckling of isotropic and orthotropic rectangular plates.

[20] J.J.Dongarra et.al. 1979 *LINPACK Users' Guide.* Philadelphia: Society for Industrial & Applied Mathematics.

[21] E.Downham 1957 *The Engineer*, 588-591. Theory of shaft whirling. No.III-Influence of rotor inertia.

[22] E.Downham 1957 *The Engineer*, 624-628. Theory of shaft whirling. No.IV-The influence of asymmetry in bearing constraints on the whirling of a shaft and rotor.

[23] D.J.Ewins 1984 *Modal Testing:Theory and Practice.* Letchworth: Research Studies Press Ltd.

[24] A.A.Ferri 1986 *Journal of Applied Mechanics, Transactions of the ASME* **53**, 455-457. On the equivalence of the incremental harmonic balance method and the harmonic balance-Newton Raphson method.

[25] R.O.Foschi 1975 *Wood Science and Technology* **9**, 243-255. The light-gap technique as a tool for measuring residual stresses in bandsaw blades.

[26] A.Grönlund 1988 *Proceedings of the Ninth International Wood Machining Seminar, Forest Products Laboratory, University of California*, 342-350. Measuring and modelling of cutting forces-progress report on an ongoing project.

[27] W.Güttinger 1987 *International Series of Numerical Mathematics* **79**, 98-113. Bifurcation theory in physics: recent trends and problems.

[28] W.G.Halvorsen 1977 *Sound and Vibration* **11**, 8-20. Impulse technique for structural frequency response testing.

[29] R.D.Henshell, et.al. 1965 *Proceedings of the Institute of Electrical Engineers* **112**, 2133-2139. Natural frequencies and mode shapes of vibration of transformer cores.

[30] Hewlett-Packard 1982 *The Fundamentals of Signal Analysis.* Application Note 243, U.S.A.

[31] Hewlett-Packard 1983 *Dynamic Signal Analyzer Applications, Effective Machinery Maintenance Using Vibration Analysis.* Application Note 243-1, U.S.A.

[32] K.Higuchi and E.H.Dowell 1989 *Journal of Sound and Vibration* **132**, 115-128. Dynamic stability of a completely free plate subjected to a controlled non-conservative follower force.

[33] W.P.Howson 1985 *Software for Engineering Problems.* Adey, 27-36. A compact method for computing the eigenvalues and eigenvectors of plane frames.

[34] C.S.Hsu 1963 *Journal of Applied Mechanics, Transactions of the ASME* **30**, 367-372. On the parametric excitation of a dynamic system having multiple degrees of freedom.

[35] L.G.Jaeger 1964 *Elementary Theory of Elastic Plates.* Oxford: Pergamon Press, Ltd.

[36] Y.I.Kim and B.Tabarrok 1972 *Journal of the Franklin Institute* **294** 381-399. On the nonlinear vibration of travelling strings.

[37] E.Kirbach and T.Bonac 1978 *Wood and Fiber* **9**, 245-251. The effect of tensioning and wheel tilting on the torsional and lateral fundamental frequencies of bandsaw blades.

[38] E.Kirbach and T.Bonac 1978 *Wood and Fiber* **10**, 19-27. An experimental study on the lateral natural frequency of bandsaw blades.

[39] F.Kozin and R.M.Milstead 1979 *Journal of Applied Mechanics, Transactions of the ASME* **46**, 404-410. The stability of a moving elastic strip subjected to random parametric excitation.

[40] G.Kron 1939 *Tensor Analysis of Networks.* New York: John Wiley.

[41] G.Kron 1963 *Diakoptics.* London: Macdonald.

[42] H.L.Langhaar 1962 *Energy Methods in Applied Mechanics.* New York: John Wiley & Sons, Inc.

[43] H.H.E.Leipholz and F.Pfendt 1982 *Computer Methods in Applied Mechanics and Engineering* **30**, 19-52. On the stability of rectangular, completely supported plates with uncoupling boundary conditions subjected to uniformly distributed follower forces.

[44] H.H.E.Leipholz and F.Pfendt 1983 *Computer Methods in Applied Mechanics and Engineering* **37**, 341-365. Application of extended equations of Galerkin

to stability problems of rectangular plates with free edges and subjected to uniformly distributed follower forces.

[45] A.W.Leissa 1969 *Vibration of plates.* NASA SP-160.

[46] A.W.Leissa 1973 *Journal of Sound and Vibration* **31**, 257-259. The free vibration of rectangular plates.

[47] A.Y.T.Leung 1988 *Journal of Sound and Vibration* **124**, 249-267. Inverse iteration for the quadratic eigenvalue problem.

[48] H.McCallion 1973 *Vibration of Linear Mechanical Systems.* London: Longman Group Limited.

[49] L.Meirovitch 1967 *Analytical Methods in Vibrations.* New York: The Macmillan Company.

[50] R.E.Mickens 1984 *Journal of Sound and Vibration* **94**, 456-460. Comments on the method of harmonic balance.

[51] C.Moler,J.Little and S.Bangert 1987 *PC-MATLAB User's Guide.* The Math Works, Inc.

[52] C.D.Mote,Jr. 1965 *Journal of the Franklin Institute* **279**, 430-444. A study of bandsaw vibrations.

[53] C.D.Mote,Jr. and S.Naguleswaran 1966 *Journal of Engineering for Industry, Transactions of the ASME* **88** 151-156. Theoretical and experimental band saw vibrations.

[54] C.D.Mote,Jr. 1966 *Journal of Applied Mechanics, Transactions of the ASME* **33**, 463-464. On the nonlinear oscillation of an axially moving string.

[55] C.D.Mote,Jr. 1968 *International Journal of Mechanical Science* **10**, 281-295. Divergence buckling of an edge-loaded axially moving band.

[56] C.D.Mote,Jr. 1968 *Journal of the Franklin Institute* **285**, 329-346. Dynamic stability of an axially moving band.

[57] C.D.Mote,Jr. and A.L.Thurman 1971 *Journal of Applied Mechanics, Transactions of the ASME* **38**, 279-280. Oscillation modes of an axially moving material.

[58] S.Naguleswaran and C.J.H.Williams 1968 *International Journal of Mechanical Science* **10**, 239-250. Lateral vibration of bandsaw blades, pulley belts and the like.

[59] A.H.Nayfeh and D.T.Mook 1979 *Nonlinear Oscillations.* New York: Wiley-Interscience.

[60] G.Pahlitzsch and K.Puttkammer 1972 *Holz als Roh- und Werkstoff* **30**, 165-174. The loading of bandsaw blades: Stresses and and strength factors.

[61] N.S.Palmer and H.McCallion 1973 *The Institution of Mechanical Engineers, Applied Mechanics Group* **187**, 63-70. Natural frequencies and mode-shapes of systems of generally interconnected shafts.

[62] C.Pierre and E.H.Dowell 1985 *Journal of Applied Mechanics, Transactions of the ASME* **52**, 693-697. A study of the dynamic instability of plates by an extended incremental harmonic balance method.

[63] W.H.Press,B.P.Flannery,S.A.Teukolsky and W.T.Vetterling 1986 *Numerical Recipes: the Art of Scientific Computing.* Cambridge: Cambridge University Press.

[64] W.H.Press,B.P.Flannery,S.A.Teukolsky and W.T.Vetterling 1988 *Numerical Recipes in C: the Art of Scientific Computing.* Cambridge: Cambridge University Press.

[65] N.F.Rieger and H.McCallion 1965 *International Journal of Mechanical Science* **7**, 253-261. The natural frequencies of portal frames-I.

[66] N.F.Rieger and H.McCallion 1965 *International Journal of Mechanical Science* **7**, 263-276. The natural frequencies of portal frames-II.

[67] R.J.Roark and W.C.Young 1975 *Formulas for Stress and Strain.* Tokyo: McGraw-Hill Kogakusha.

[68] A.D.Roberts and S.C.Lapidge 1977 *Manufacturing Proccesses.* New York: McGraw-Hill, Inc.

[69] R.H.Russell and J.C.Deel 1977 *Sound and Vibration* **11**, 22-38. Modal Analysis: Trouble-shooting to product design.

[70] J.M.M.Silva and N.M.M.Maia 1988 *Journal of Sound and Vibration* **124**, 13-26. Single mode identification techniques for use with small microcomputer.

[71] A.Simmond 1980 *Wide Bandsaws, the Art of Saw Doctoring.* London: Stobart & Son Ltd.

[72] S.K.Sinha 1988 *Journal of Sound and Vibration* **128**, 505-507. Comments on "Dynamic stability of a rectangular plate subjected to distributed in-plane dynamic force".

[73] R.Skutch 1897 *Annalen der Physik und Chemie* **61**, 190-195. Ueber die Bewegung eines gespannten Fadens, welcher gezwungen ist, durch zwei feste Punkte

mit einer konstanten Geschwindigkeit zu gehen und zwischen denselben in Transversal-Schwingungen von geringer Amplitude versetzt wird.

[74] B.T.Smith et.al. 1974 *Matrix Eigensystem Routines-EISPACK Guide.* Berlin: Springer.

[75] A.I.Soler 1968 *Journal of the Franklin Institute* **286**, 295-307. Vibrations and stability of a moving band.

[76] R.Szilard 1974 *Theory and Analysis of Plates.* Englewood Cliffs, New Jersey: Prentice-Hall, Inc.

[77] K.Takahashi 1981 *Journal of Sound and Vibration* **78**, 519-529. An approach to investigate the instability of the multiple-degree-of-freedom parametric dynamic systems.

[78] K.Takahashi and Y.Konishi 1988 *Journal of Sound and Vibration* **123**, 115-127. Dynamic stability of a rectangular plate subjected to distributed in-plane dynamic force.

[79] C.A.Tan and C.D.Mote,Jr. 1988 *Proceedings of the Ninth International Wood Machining Seminar, Forest Product Laboratory, University of California*, pg 266-285. Vibration analysis of a guided axially moving band.

[80] C.Tanaka,Y.Shiota,A.Takahashi and M.Nakamura 1981 *Wood Science and Technology* **15**, 145-159. Experimental studies on bandsaw blade vibration.

[81] C.Tanaka,Y.Shiota and A.Takahashi 1983 *Mokuzai Gakkaishi* **29**, 308-314. Bandsaw blade vibration during sawing.

[82] A.L.Thurman and C.D.Mote,Jr. 1969 *Journal of Applied Mechanics, Transactions of the ASME* **36**, 83-91. Free, periodic nonlinear oscillation of an axially

moving strip.

[83] S.P.Timoshenko and J.N.Goodier 1970 *Theory of Elasticity.* New York: McGraw-Hill.

[84] A.C.Ugural and S.K.Fenster 1981 *Advanced Strength and Applied Elasticity.* London: Edward Arnold.

[85] A.G.Ulsoy and C.D.Mote,Jr. 1978 *Shock and Vibration Digest* **10**, 3-15. Band saw vibration and stability.

[86] A.G.Ulsoy and C.D.Mote,Jr. 1980 *Wood Science* **13**, 1-10. Analysis of bandsaw vibration.

[87] A.G.Ulsoy and C.D.Mote,Jr. 1982 *Journal of Engineering for Industry, Transactions of the ASME* **104**, 71-78. Vibration of wide band saw blades.

[88] K.W.Wang and C.D.Mote 1986 *Journal of Sound and Vibration* **109**, 237-258. Vibration coupling analysis of band/wheel mechanical systems.

[89] K.W.Wang and C.D.Mote 1987 *Journal of Sound and Vibration* **115**, 203-216. Band/wheel system vibration under impulsive boundary excitation.

[90] P.M.Ware 1977 *Ph.D. Thesis, University of Canterbury.* An investigation into the behaviour of rotating shaft systems incorporating oil film bearings and gyroscopic effects.

[91] Wilkie Brothers Foundation *Fundamentals of Band Machining.* Albany, New York, Delmar.

[92] F.W.Williams and W.H.Wittrick 1970 *International Journal of Mechanical Science* **12**, 781-791. An automatic computational procedure for calculating natural frequencies of skeletal structures.

[93] Ed M.Williston 1978 *Saws: Design, Selection, Operation, Maintenance.* San Francisco: Miller Freeman Publications.

[94] W.Z.Wu and C.D.Mote,Jr. 1984 *Forest Products Journal* **34**, 12-21. Analysis of vibration in a bandsaw system.

[95] W.Z.Wu and C.D.Mote,Jr. 1986 *Journal of Sound and Vibration* **110**, 27-39. Parametric excitation of an axially moving band by periodic edge loading.

[96] W.Z.Wu 1986 *Proceedings of the Fourth International Modal Analysis Conference, Union College, Schenectady, New York*, 1621-1627. Modal analysis of a moving band under cutting loads.

[97] D.Young 1950 *Journal of Applied Mechanics, Transactions of the ASME* **17**, 448-453. Vibration of rectangular plates by the Ritz method.

[98] Yi-Yuan Yu 1964 *The Journal of the Acoustical Society of America* **36**, 111-120. Generalized Hamilton's principle and variational equation of motion in nonlinear elasticity theory, with application to plate theory.

[99] O.C.Zienkiewicz and K.Morgan 1983 *Finite Elements and Approximation.* New York: John Wiley & Sons, Inc.

Appendix A

DYNAMIC STIFFNESS MATRIX OF THICK BEAMS

Referring to Figure 18 for the positive sign convention, the relationships between the end forces and the end displacements are

$$\begin{Bmatrix} P_1 \\ P_2 \\ N_1 \\ N_2 \end{Bmatrix} = \begin{bmatrix} K_{11} & K_{12} & K_{13} & K_{14} \\ K_{21} & K_{22} & K_{23} & K_{24} \\ K_{31} & K_{32} & K_{33} & K_{34} \\ K_{41} & K_{42} & K_{43} & K_{44} \end{bmatrix} \begin{Bmatrix} V_1 \\ V_2 \\ \Theta_1 \\ \Theta_2 \end{Bmatrix}$$

That is

$$\{F\} = [K]\{V\}$$

where $[K]$ is the dynamic stiffness matrix of thick beams.

The elements of the dynamic stiffness matrix are

$$K_{11} = K_{22} = -\epsilon_1\epsilon_2 C\left(\frac{\gamma_2}{\beta}\cos\alpha L\sinh\beta L + \frac{\gamma_1}{\alpha}\sin\alpha L\cosh\beta L\right)$$

$$K_{12} = K_{21} = \epsilon_1\epsilon_2 C\left(\frac{\gamma_1}{\alpha}\sin\alpha L + \frac{\gamma_2}{\beta}\sinh\beta L\right)$$

$$-K_{31} = -K_{13} = K_{24} = K_{42} = \gamma_1\gamma_2 C\left\{\left(\frac{\gamma_1}{\alpha^2} + \frac{\gamma_2}{\beta^2}\right)\sin\alpha L \sinh\beta L + \frac{\gamma_2 - \gamma_1}{\alpha\beta}\left(\cos\alpha L \cosh\beta L - 1\right)\right\}$$

$$-K_{32} = -K_{23} = K_{14} = K_{41} = \epsilon_1\epsilon_2 C\left(\cos\alpha L - \cosh\beta L\right)$$

$$K_{33} = K_{44} = \epsilon_1 C\left(\frac{\gamma_1}{\alpha}\cos\alpha L \sinh\beta L - \frac{\gamma_2}{\beta}\sin\alpha L \cosh\beta L\right)$$

$$K_{34} = K_{43} = \epsilon_1 C\left(\frac{\gamma_2}{\beta}\sin\alpha L - \frac{\gamma_1}{\alpha}\sinh\beta L\right)$$

where

$$2\alpha^2 = \rho\omega^2\left(\frac{1}{kG} + \frac{1}{E}\right) + \sqrt{\rho^2\omega^4\left(\frac{1}{kG} - \frac{1}{E}\right)^2 + \frac{4\rho A\omega^2}{EI}}$$

$$2\beta^2 = -\rho\omega^2\left(\frac{1}{kG} + \frac{1}{E}\right) + \sqrt{\rho^2\omega^4\left(\frac{1}{kG} - \frac{1}{E}\right)^2 + \frac{4\rho A\omega^2}{EI}}$$

$$\gamma_1 = \alpha^2 - \frac{\rho\omega^2}{kG}$$

$$\gamma_2 = \beta^2 + \frac{\rho\omega^2}{kG}$$

$$\epsilon_1 = \alpha^2 + \beta^2$$

$$\epsilon_2 = \frac{\gamma_1\gamma_2}{\alpha\beta}$$

$$C = \frac{EI}{-\left(\left(\frac{\gamma_2}{\beta}\right)^2 - \left(\frac{\gamma_1}{\alpha}\right)^2\right)\sin\alpha L \sinh\beta L + 2\epsilon_2\left(\cos\alpha L \cosh\beta L - 1\right)}$$

Appendix B

EQUATION OF MOTION FOR A MOVING BEAM

The kinetic energy T of a moving beam is

$$T = \frac{1}{2}\int_0^L \rho A\left[c^2 + \left(\frac{\partial v}{\partial t} + c\frac{\partial v}{\partial x}\right)^2\right] dx$$

The potential energy U of a beam under a longitudinal force R is

$$U = \frac{1}{2}\int_0^L \left\{EI\left(\frac{\partial^2 v}{\partial x^2}\right)^2 + R\left(\frac{\partial v}{\partial x}\right)^2\right\} dx$$

The tension R is given by

$$R = R_0 + \eta\rho A c^2$$

where R_0 is the initial tension, and η is a constant depending on the type of the straining device. For the counterweight mechanism, $\eta = 1$.

The energy terms can be substituted into the Hamilton's principle

$$\begin{aligned}\int_{t_1}^{t_2} (\delta T - \delta U)\, dt &= \int_{t_1}^{t_2}\int_0^L \left\{\rho A\left(\frac{\partial v}{\partial t} + c\frac{\partial v}{\partial x}\right)\left(\frac{\partial(\delta v)}{\partial t} + c\frac{\partial(\delta v)}{\partial x}\right)\right. \\ &\quad \left. - EI\frac{\partial^2 v}{\partial x^2}\frac{\partial^2(\delta v)}{\partial x^2} - R\frac{\partial v}{\partial x}\frac{\partial(\delta v)}{\partial x}\right\} dx\, dt \\ &= 0.\end{aligned}$$

Integrating the above equation by parts gives

$$\int_{t_1}^{t_2}\left\{\int_0^L\left[-\rho A\left(\frac{\partial^2 v}{\partial t^2}+c\frac{\partial^2 v}{\partial x\partial t}\right)-\rho Ac\left(\frac{\partial^2 v}{\partial x\partial t}+c\frac{\partial^2 v}{\partial x^2}\right)\right.\right.$$
$$\left.-EI\frac{\partial^4 v}{\partial x^4}+R\frac{\partial^2 v}{\partial x 2}\right]\delta v\,dx-EI\,\frac{\partial^2 v}{\partial x^2}\,\frac{\partial\,(\delta v)}{\partial x}\Bigg|_0^L$$
$$\left.\left[\rho Ac\left(\frac{\partial v}{\partial t}+c\frac{\partial v}{\partial x}\right)+EI\frac{\partial^3 v}{\partial x^3}-R\frac{\partial v}{\partial x}\right]\delta v\Bigg|_0^L\right\}\,dt \;=\; 0$$

Therefore, the equation of motion is

$$EI\frac{\partial^4 v}{\partial x^4}+\rho A\frac{\partial^2 v}{\partial t^2}+2\rho Ac\frac{\partial^2 v}{\partial x\partial t}+\left(\left(1-\eta\right)\rho Ac^2-R_0\right)\frac{\partial^2 v}{\partial x^2}=0$$

and the boundary conditions are

$$v=0 \quad \text{or} \quad EI\frac{\partial^3 v}{\partial x^3}+\left(\left(1-\eta\right)\rho Ac^2-R_0\right)\frac{\partial v}{\partial x}+\rho Ac\frac{\partial v}{\partial t}=0$$
$$\frac{\partial v}{\partial x}=0 \quad \text{or} \quad EI\frac{\partial^2 v}{\partial x^2}=0$$